

University of Nottingham
UK | CHINA | MALAYSIA

Faculty of Engineering

Department of Architecture and Built Environment

Regulation of Power Generated from Thermoelectric Generators

Ssennoga Twaha

(Bsc. Eng, Msc. Eng)

February 2018

Thesis submitted in fulfillment of the requirement leading to the award of Doctorate of Philosophy in Sustainable Energy Technology

Table of content

Table of content ii
List of Figures vi
List of Tables xii
List of Publications xiii
Statement of Originality xv
Acknowledgement xvi
Table of Abbreviations xvii
Abstract xix
Chapter 1. Introduction 1
1.1. Background of TEGs and summary of the thesis 1
1.2. Structure of the thesis 5
Chapter 2. The working principles and past works on thermoelectric technology and power conditioning 6
2.1. Background 7
2.2. Description of TEMs and the concept of Seebeck effect 10
2.2.1. The concept of Seebeck effect 10
2.2.2. Analysis of important parameters of TEMs 16
2.3. Different materials used for TEG/TEC 19
2.3.1. Selection criteria for TEG/TEC material 19
2.3.2. Recent advances on TEG material 21
2.4. Application of thermoelectric devices 25
2.4.1. Application of TEG for heat recovery from the vehicle 25
2.4.2. Cooling applications of thermoelectric devices 29
2.4.3. Hybrid systems 30
2.4.4. Application of TEDs for power generation 33
2.4.4.1. Thermoelectric applications for power generation 33
2.4.4.2. Power generation with TEG using non-waste heat 34
2.5. Thermoelectric modelling methods 36
2.5.1. The simplified thermoelectric models 39
2.5.1.1. Standard simplified thermoelectric models 39
2.5.1.2. Improved simplified thermoelectric models 40
2.5.2. Complex thermoelectric models 40
2.5.2.1. Analytical thermoelectric models 42
2.5.2.2. Electrical analogy thermoelectric models 42
2.5.2.3. Numerical thermoelectric models 42
2.6. Different structures of TEG units/Modules 43
2.6.1. The basic structure of TEG module 43
2.6.2. The modified structures of TEG module 44
2.6.3. Progress on TEG module structural improvement 44
2.6.4. Progress of TEG system improvement 48
2.7. Methods of efficiency improvement of thermoelectric devices 51
2.7.1. Impedance matching 52

2.7.2. Adjusting the boundary temperature and the TEG units 53
2.7.3. TEG power conditioning using DC-DC converters 54
2.7.3.1. Use of dc-dc converter with MPPT 56
2.7.3.2. TEG output power regulation with dc-dc C´uk converter 58
2.7.3.3. MPPT control with C´uk dc-dc converter 59
2.7.3.4. Distributed multi-section multilevel dc-dc conversion networks 60
2.7.4. Power conditioning using temperature sensor based MPPT 61
2.7.5. Other methods for TEDs performance improvement 62
2.8. Observations and recommendations for further research on TEDs 63
2.9. Summary 66
Chapter 3. Research Objectives and Methodology 68
3.1. Problem statement 68
3.2. Aims and objectives of the research 68
3.3. Scope 69
3.4. Modelling of TEG/converter system 70
3.5. Experimental work methodology 71
Chapter 4. Conditioning of TEG power using dc-dc converters 72
4.1. Introduction 72
4.2. Power conditioning and efficiency improvement of TEG 72
4.3. DC/DC converters performance features 74
4.4. The proposed TEG power conditioning system 76
4.4.1. TEG modelling 76
4.4.2. Principle of operation of a dc-dc converter 80
4.5. Results and discussion 83
4.5.1. Steady state model performance 84
4.5.2. Verification of simulation results 86
4.6. Summary 88
Chapter 5. Modelling of TEG/dc-dc converter system with IC MPPT 89
5.1. Research background 89
5.2. The proposed TEG power conditioning system 90
5.2.1. The structure and modelling of TEG device 90
5.2.2. The dc-dc converter with MPPT system 91
5.3. IC algorithm 92
5.4. Results and discussion 94
5.4.1. Verification of simulation results 100
5.4.2. Performance comparison of IC and P&O techniques 102
5.4.3. Converter output without MPPT 103
5.4.4. Variation of voltage with TEG modules 106
5.5. Summary 107
Chapter 6. Parameter Analysis of TEG/dc-dc converter system with MPPT and variable load 109
6.1. Background 109
6.2. The dc-dc converter model parameters 110

6.3. Results and discussion....115
6.3.1. Results for the increasing step hot side temperature.... 116
6.3.1.1 Converter parameters with the MPPT mode 116
6.3.1.2. Converter parameters with direct PWM signal 120
6.3.2. Results for the increasing random hot side temperature 124
6.3.3. Effect of converter components on the accuracy of results 127
6.4. Summary....130
Chapter 7. Modelling of TEG/dc-dc converter system with ESC MPPT 131
7.1. Background....131
7.2. TEGs with different materials....132
7.3. Principle of operation MPPT techniques....138
7.3.1. ESC MPPT technique.... 138
7.3.2. P&O MPPT technique.... 141
7.4. Results and discussion....147
7.4.1. Results of ESC MPPT method.... 147
7.4.2. Results of P&O MPPT method 149
7.4.3. Comparison of ESC and P&O MPPT techniques 152
7.4.4. Validation: Comparison of Simulink and COMSOL TEG models 157
7.5. Performance Comparison of ESC and IC methods....164
7.5.1. Voltages, current and power curves of ESC and IC techniques 164
7.5.2. Comparison of the ESC and IC methods.... 165
7.6. Summary....167
Chapter 8. Application of distributed dc-dc converter Architecture 169
8.1. The concept and the design of DCA for regulation of TEG output 169
8.1.1. The concept of distributed dc-dc converters.... 169
8.1.2. Distributed versus centralized dc-dc converters 171
8.1.3. The design of distributed dc-dc converters for TEG system 174
8.1.4. Factor considered while selecting the converter topology 178
8.2. Demonstration of DCA design for TEG system....179
8.3. Simulation of DCA with TEG system....179
8.4. Experimental study on DCA with TEG system....190
8.5. Experimental test with the hotplate based TEG system....193
8.5.1. Experimental design of the TEG rig and dc-dc converters..... 193
8.5.2. Results: Analysis of parameters affecting TEG perormance 199
8.5.2.1. Effect of switching time for different components..... 199
8.5.2.2. Effect of the ambient temperature..... 203
8.5.3. TEG and the converter output..... 204
8.5.4. Output voltages and currents under loading conditions..... 208
8.5.4.1. Output with resistors connected to TEGs..... 208
8.5.4.2. Output with resistors connected through dc-dc converters . 213
8.5.5. Challenges and limitations of the experiment 214
8.6. Summary....214
Chapter 9. Conclusion and future work....216
9.1. Conclusion....216

9.2. Future work 219
References.....220
Appendices 236
Appendix 1..... 236

List of Figures

Figure 2.1. Power generation and cooling/heating thermoelectric heat engines (Zheng, Liu, Yan, et al. 2014) 11
Figure 2.2. The movement of electrons and holes in p- and n-type materials13
Figure 2.3. Heat transfer mechanism and Seebeck effect for the TEM 14
Figure 2.4. The domestic TCS (Zheng, Liu, Boukhanouf, et al. 2014) 31
Figure 2.5. A schematic view of a TEC 38
Figure 2.6. Heat flux convention in a thermoelectric leg 39
Figure 2.7. TEG setting for Power generation (Niu et al. 2015) 44
Figure 2.8. Traditional thermoelectric couple configuration with segmented elements 45
Figure 2.9. Alternative thermoelectric couple configuration with segmented elements of different total element thickness 45
Figure 2.10. Schematic diagram of each module installation on TEGs (In et al. 2015) 49
Figure 2.11. Normalized thermopower from all thermal conditions tested and its rate of change relative to the electrical load 53
Figure 2.12. TEG power conditioning system MPPT controller (Kim et al. 2008) 57
Figure 2.13. Basic C´uk converter 58
Figure 2.14. Power conditioning system based on C´uk converter with MPPT 59
Figure 2.15. General topology of TEG based dc-dc conversion network (Li et al. 2011)..... 60
Figure 4.1. The relationship between the TEG, converter and load parameters 74
Figure 4.2. Block diagram of the proposed TEG Power conditioning system 76
Figure 4.3. The simplified TEG model from the previous study (Li 2011) 79
Figure 4.4.The modified simplified TEG model 80
Figure 4.5. A classical boost converter equivalent circuit 80
Figure 4.6. The working principle of a boost converter 81
Figure 4.7. Boost converter circuit implemented in Simulink: with direct PWM signal 82
Figure 4.8. The proposed TEG Power conditioning system..... 83
Figure 4.9. Hot side temperature input of the TEG module..... 84
Figure 4.10. Average input, output voltage of the converter and open circuit voltage of TEG for a single TEG modules..... 85
Figure 4.11. Average input and output voltage of the converter at different temperature for ten TEG modules 85
Figure 4.12. Average input and output power of the converter for a single TEG module 86
Figure 4.13. Input power to the converter under the matching conditions 87

Figure 4.14. Conversion efficiency of the converters at different hot side temperatures 88
Figure 5.1. Block diagram of the proposed TEG power conditioning system 90
Figure 5.2. Basic flow chart of IC method (Ishaque et al. 2014b) 93
Figure 5.3. The proposed TEG Power conditioning system modelled in Simulink 94
Figure 5.4. The hot side temperature input to the TEG system 95
Figure 5.5. TEG block parameter adjustment in the simulation model 96
Figure 5.6. The instantaneous values of voltage for the systems 97
Figure 5.7. Values of power from TEG as well as to and from the converter 98
Figure 5.8. The average input and output voltages of the converter at different temperatures for ten TEG modules 99
Figure 5.9. The average input, output voltages of the converter and open circuit voltages of the TEG at different temperatures and T_c=30°C for a single TEG module 99
Figure 5.10. Average input and output powers of the converter and TEG output power at different hot side temperatures and T_c=30°C for a single TEG module 100
Figure 5.11. Converter input and output voltages and TEG open circuit voltages with P&O method at T_c=30°C (Li 2011) 101
Figure 5.12. Input and output power of converter compared to the output power of TEG with P&O method at T_c=30°C (Li 2011) 102
Figure 5.13. MPPT matching efficiency at different hot side temperatures and at T_c=30°C 103
Figure 5.14. Theoretical conversion ratio of boost converter 104
Figure 5.15. Conversion ratio of a boost converter obtained from the simulation 104
Figure 5.16. Output voltages of the converter at different values of D 105
Figure 5.17. The relationship between the converter input voltage and the hot side temperature at different number of TEG modules 106
Figure 5.18. The MVMF at different temperature 107
Figure 6.1. The TEG-converter simulation model 111
Figure 6.2. Increasing step hot side temperature 115
Figure 6.3. Increasing random hot side temperature 116
Figure 6.4. Variation of input voltage of the converter with resistance at different hot side temperatures 117
Figure 6.5. Variation of output voltage of the converter with resistance at different hot side temperatures 117
Figure 6.6. Variation of output power converter with resistance at different hot side temperature 118
Figure 6.7. Variations of output power, voltage and current with load resistance at different hot side temperature 119
Figure 6.8. Variation of converter output voltage with hot side temperature and duty cycle at Rload = 1.1 Ω 120

Figure 6.9. Variation of converter output power with hot side temperature and duty cycle at Rload = 1.1Ω..... 121
Figure 6.10. Comparison of output power at different values of D and hot side temperature 122
Figure 6.11. Comparison of MPPT and direct PWM mode output power ... 123
Figure 6.12. Voltage conversion ratio at D=0.1 for different converter loads at different hot side temperatures 123
Figure 6.13. Voltages and output current for MPPT based model with Random increasing hot side temperature at Rload =1.1Ω..... 124
Figure 6.14. Voltages and output current for MPPT based model with Random increasing hot side temperature at Rload =4Ω 125
Figure 6.15. Voltages and output current for direct PWM based model with Random increasing hot side temperature at D =0.1 and Rload =4Ω 126
Figure 6.16. Voltage and output current for direct PWM based model with Random increasing hot side temperature at D =0.5 and Rload =4Ω 126
Figure 6.17. Ripple voltage at ESR = $1x10^{-9}\Omega$..... 127
Figure 6.18. Ripple voltage at ESR = $1x10^{-6}\Omega$..... 128
Figure 6.19. Ripple voltage at ESR = $1x10^{-6}\ \Omega$ when Rload = 1Ω..... 128
Figure 6.20. Ripple voltage at ESR = 1Ω when Rload = 1Ω 129
Figure 6.21. Effect of increasing the switching frequency from 5 kHz to 20 kHz on the input and output voltage..... 129
Figure 7.1. Principle of operation of a TEGs: part (C) is modified from (Electropaedia n.d.) 132
Figure 7.2. Seebeck coefficient of Bi_2Te_3 TEG 134
Figure 7.3. Variation of thermal conductivity with temperature for the Bi_2Te_3 material of TEG..... 136
Figure 7.4. Variation of electrical conductivity with temperature for the Bi_2Te_3 material of TEG..... 137
Figure 7.5. Classical ESC scheme (Heydari-doostabad et al. 2013) 138
Figure 7.6. Classical ESC estimator (Heydari-doostabad et al. 2013) 140
Figure 7.7. The block diagram of the applied ESC circuit 140
Figure 7.8. Block diagram of TEG/dc-dc converter system with ESC MPPT 141
Figure 7.9. Flow chart of conventional P&O method (Ishaque & Salam 2013) 143
Figure 7.10. Block diagram of TEG/dc-dc converter system with P&O MPPT 144
Figure 7.11. The Simulink model of TEG/dc-dc boost converter system 145
Figure 7.12. The simulink P&O block..... 145
Figure 7.13. The simulated boost converter circuit 146
Figure 7.14. The output voltages of the ESC MPPT model for a single TEG 148
Figure 7.15. The output power of the ESC based model for a single TEG . 148

Figure 7.16. The voltage, current and output power of ESC MPPT model for a single TEG 149
Figure 7.17. The output voltages of the P&O MPPT model for a single TEG 150
Figure 7.18. The output power of the P&O based model for a single TEG . 151
Figure 7.19. The output voltage, current and output power of P&O MPPT model for a single TEG 151
Figure 7.20. The comparison between the output voltages of ESC and P&O based models 152
Figure 7.21. The comparison of output power of ESC and P&O based models 153
Figure 7.22. The output power difference between ESC and P&O based models 154
Figure 7.23. Output of ESC and P&O near the optimum point..... 155
Figure 7.24. Percentage increase of the output of the converter due to the application of ESC MPPT method 156
Figure 7.25. Output voltage of Bi_2Te_3 TEG 158
Figure 7.26. Output power of Bi_2Te_3 TEG (From simulink) 159
Figure 7.27. Comparison of output power of TEG for different materials.... 160
Figure 7.28. Comparison of output power of Simulink and PbTe based COMSOL models..... 161
Figure 7.29. Comparison of output power of Simulink and Bi_2Te_3 based COMSOL models..... 162
Figure 7.30. The plot of the simulation time for the COMSOL models at different temperature 163
Figure 7.31. Output voltages, currents and power of IC method for different temperature 164
Figure 7.32. Output voltages, currents and power of ESC method for different temperature 165
Figure 7.33. Comparison of output voltages of ESC and IC methods..... 166
Figure 7.34. Comparison of output power of both methods 166
Figure 8.1. Design option 1: The DCA design when TEG devices are within the same location (the same heat and cooling blocks or otherwise) and the converters are confined in the same location..... 175
Figure 8.2. Design option 2: The DCA design when TEG devices are within two locations and the converters are kept in two different locations..... 175
Figure 8.3. Design option 3: The DCA design when TEG devices are within two locations (the same heat and cooling blocks or otherwise) and the converters are confined in the same location 176
Figure 8.4. Simulation of different dc-dc converter topologies supplied by the same voltage source..... 180
Figure 8.5. Simulation of DCA applied to TEG system 181
Figure 8.6. Voltages from DCA applied to TEG system at the same input voltages 183

Figure 8.7. Currents from distributed dc-dc converter architecture applied to TEG system at the same input voltages 184
Figure 8.8. Converter input voltages at the same TEG voltage of 7.4V 185
Figure 8.9. Converter input currents at the same TEG voltage of 7.4V 185
Figure 8.10. Converter input power at the same TEG voltage of 7.4V for Buck and SEPIC topologies..... 186
Figure 8.11. Converter input power at the same TEG voltage of 7.4V for Boost, Buck-boost and C´UK topologies..... 187
Figure 8.12. Converter output powers at the same TEG voltage of 7.4V.... 188
Figure 8.13. The I-V characteristics curves: (a) Boost; (b) Buck-boost; (c) Buck; (d) C´UK..... 189
Figure 8.14. The I-V characteristics curve for the SEPIC converter topology 190
Figure 8.15. The ADM00664 integrated switch PWM Boost converter 192
Figure 8.16. TPS63060EVM-619 evaluation Module for a Buck-Boost Converter..... 192
Figure 8.17. The Block diagram for the experimental setup of the TEG system 194
Figure 8.18. Parts of the actual experimental rig and the associated components in the laboratory..... 196
Figure 8.19. Demonstration of the Heat exchanger system, thermocouple points, heat isolation and the electrical connections 197
Figure 8.20. The dimensions of layout of the cooling block on top of the hotplate 198
Figure 8.21. Temperature readings of the thermocouples, when both the hotplate and the chiller are switched off at the same time (at 15:58:16) 200
Figure 8.22. Temperature readings of the thermocouples, when the hotplate and the chiller are switched off at different times 202
Figure 8.23. OCVs when hotplate is off while the chiller is left on until 16:59:21 202
Figure 8.24. Effect of ambient temperature on thermocouple readings 203
Figure 8.25. The OCVs for TEGs with the effect of external temperature... 204
Figure 8.26. The OCVs for TEGs with the effect of thermocouple malfunctioning 205
Figure 8.27. Illustration of the relationship between the OCVs and terminal voltages of TEGs and the effect of manual combination of TEGs in series 206
Figure 8.28. Input volatges and output OCVs of the boost and buck-boost converters when the hotplate temperature is increased to 185°C..... 207
Figure 8.29. Output parameters of the TEGs for a 10Ω load connected on each TEG after the hotplate temperature is increased to 170°C: (a) Output voltage (b) Output current urrent..... 209
Figure 8.30. Output parameters of the TEGs for a 10Ω load connected on each TEG when the hotplate temperature is increased to 185°C: (a) Output voltage (b) Output current urrent..... 211

Figure 8.31. The output parameters of the TEGs for a 15Ω load connected on each TEG when the hotplate temperature is increased to 185°C: (a) Output voltage (b) Output current urrent..... 212
Figure 8.32. Voltages with a 15Ω load connected to each of the six TEG devices through a dc-dc converter at 185°C hotplate temperature 213

List of Tables

Table 2.1.The characteristic of available TEGs materials (Hamid Elsheikh et al. 2014) 21
Table 2.2. The most commonly used alloys for thermoelectric application ... 23
Table 2.3. Comparison of different TEGs systems in terms of performance. 51
Table 2.4. The qualities and implications of applying different dc-dc converters on TEGs..... 55
Table 4.1. Specifications of the TEG module..... 77
Table 7.1. Material properties for lead Telluride – PbTe 134
Table 7.2. List of electronic components for the boost converter design 146
Table 7.3. Simulation time for the COMSOL TEG model..... 162
Table 7.4. The computation times for ESC and IC techniques 167
Table 8.1. Specifications for integrated switch PWM boost converter evaluation module..... 191
Table 8.2. Specifications for a TPS63060EVM-619 buck-boost converter evaluation module..... 193

List of Publications

Publications related to the thesis

1. Twaha S, Zhu J, Maraaba L, Huang K, Li B, Yan Y. Maximum Power Point Tracking Control of a Thermoelectric Generation System Using the Extremum Seeking Control Method. Energies. 2017;10(12):1-18. doi:10.3390/en10122016.
2. Twaha S, Zhu J, Li B, Yan Y, Huang K. Parameter analysis of thermoelectric generator/dc-dc converter system with maximum power point tracking. Energy Sustain Dev. 2017;41:49-60. doi:10.1016/j.esd.2017.08.005.
3. Twaha S, Zhu J, Yan Y. Performance comparison of thermoelectric generators with Extremum seeking control and incremental conductance MPPT methods. In: 16 Th International **Conference** on Sustainable Energy Technologies (SET207), Bologna-Italy. Bologna: University Eprint; 2017. http://eprints.nottingham.ac.uk/id/eprint/44647.
4. Twaha S, Zhu J, Yan Y, Li B, Huang K. Performance analysis of thermoelectric generator using dc-dc converter with incremental conductance based maximum power point tracking. Energy Sustain Dev. 2017;37:86-98. doi:10.1016/j.esd.2017.01.003.
5. Twaha S, Zhu J, Yan Y. Power conditioning of thermoelectric generated power using dc-dc converters: a case study of a boost converter. In: Nottingham ePrints, ed. International Heat Transfer **Symposium** 2016, University of Nottingham-UK. Nottingham; 2016. http://eprints.nottingham.ac.uk/id/eprint/34193.
6. Twaha S, Zhu J, Yan Y, Li B. A comprehensive review of thermoelectric technology: Materials, applications, modelling and performance improvement. Renew Sustain Energy Rev. 2016;65. doi:10.1016/j.rser.2016.07.034.

Other Publications

1. Li B, Huang K, Yan Y, Li Y, Twaha S, Zhu J. Heat transfer enhancement of a modularised thermoelectric power generator for passenger vehicles. *Appl Energy*. 2017;205:868–879. doi:10.1016/j.apenergy.2017.08.092.
2. Huang K, Li B, Yan Y, Li Y, Twaha S, Zhu J. A comprehensive study on a novel concentric cylindrical thermoelectric power generation system. *Appl Therm Eng*. 2017;117:501-510. doi:10.1016/j.applthermaleng.2017.02.060.

Statement of Originality

I declare that this thesis has never been submitted to any institution in partial or complete form for the award of any diploma, degree, master or PhD. The work contained herein is the original contribution of the author of this thesis during his period of study at the university of Nottingham, UK. For any referenced work, the due citation and acknowledgement has been given to the original author/s of that specific work.

SSENNOGA TWAHA

Acknowledgement

The great thanks are due to ALLAH, the Almighty the Creator, the Sustainer and the Magnificent for enabling me to compile this thesis at this material time.

Sincere gratitude is due to the Islamic Development Bank (IDB) organization in Jeddah Saudi Arabia for the PhD scholarship at the University of Nottingham and Master of Engineering Electrical Power at Universiti Teknologi Malaysia (UTM). I also acknowledge part of the PhD scholarship from the University of Nottingham.

I would like to extend a vote of thanks to the individuals or specific groups for their generous contributions and support towards the completion of my PhD;

I would like to extend my sincere gratitude to my internal and external examiners for their willingness to assess my work.

I categorically thank my supervisors for their enormous support rendered at any specific time during the study period. I cannot forget to single out Dr. Jie Zhu for his full availability, without hesitation whenever he is needed for support. Special appreciation is due to Prof. Yuying Yan who endeavoured to ensure that I am always happy and on course of my studies as well as his willingness to foresee and tame any dispute that might arise during the period of the study. Dr. Bo Li deserves a distinct indebtedness for always giving short but very useful and technical tips that have been very helpful for the success of research.

I thank all my colleagues, fellow PhD researchers in the department, technicians and my family who were always willing to give support whenever it is necessary.

Table of Abbreviations

DCA	Distributed converter architecture
ESC	Extremum seeking control
ESR	Equivalent Series resistance
MTBF	Mean time between failure
MTFF	Mean time to first failure
MVMF	Module voltage multiplicity factor
OCV	Open circuit voltage
SEPIC	Single-Ended Primary-Inductor Converter
TEC	Thermoelectric cooling
TEM	Thermoelectric module
VCR	Voltage conversion ratios
CCHP	Combined cooling, heating and power
COP	Coefficient of performance
CTED	Composite thermoelectric device
DSSC	Dye sensitized solar cells
EMF	Electromotive force
EV	Electric vehicles
FC	Fuel cell
FEM	Finite elements method
IC	Incremental conductance
ICE	Internal combustion engine
MPPT	Maximum power point tracking
P&O	Perturb and observe
PM	Power matching
PWM	Pulse width modulated
SEM	Scanning electron microscopy
TCS	Thermoelectric cogeneration system
TED	Thermoelectric device

TEG	Thermoelectric generator
ZT	Figure of merit
EMI	Electromagnetic interference
EVM	TPS63060EVM-619 evaluation module
GHG	Greenhouse gas
FORTRAN	FORmula TRANslation
HPTEG	Heat Pipe thermoelectric
HVAC	Heating, ventilation, and air conditioning
IGBT	Insulated-gate bipolar transistors
MEMS	Micro electromechanical systems
MOSFET	Metal–oxide–semiconductor field-effect transistors
MTTF	Mean time to failure
PID	Proportional-integral-derivative
RF	Radio frequency
SiC	Silicon Carbide
TEH	Thermoelectric Heating
TRNSYS	Transient System Simulation
TPV	Thermo-photovoltaic
T_c	Cold side temperature
T_h	Hot side temperature

Abstract

In recent years, the efficiency of thermoelectric devices has improved greatly due thermoelectric material and device geometrical improvements. However, the efficiency of TEG is still low, being a subject of further research for more improvement. Hence, the main objective of the research carried out in this thesis is to analyse the performance of dc-dc converters with or without MPPT in conditioning the power generated from TEG. In light of this objective, the following case studies have been carried out.

The initial study has analysed the performance of a TEG/dc-dc boost converter system. Results indicate that the converter is able to stabilise and boost the voltage and higher efficiencies are achieved at different hot side temperatures.

The next study proposes the use of MPPT algorithm to harvest maximum power from TEG system. Hence, the analysis of the performance of TEG/dc-dc converter with MPPT enabled by Incremental conductance (IC) method is done. The results indicate that the IC based MPPT approach is able to track the maximum power point but with relatively lower efficiencies than the Perturb and Observe (P&O) based MPPT method. method.

Another study has analysed the parameters for the performance of TEG/dc-dc converter system in different modes with a variable load. The TEG system is subjected to different hot side temperatures, including increasing step, increasing random and constant cold side temperature profiles. The study has demonstrated how the proper selection of converter components is a necessity to avoid converter losses as well interferences on the load connected to TEG/dc-dc converter system.

Furthermore, another study compares the performance of extremum seeking control (ESC) and P&O MPPT algorithms applied to TEG system. The TEG model is validated with results from multiphysics (COMSOL) modelling

software. To assess the effect of temperature dependency of TEG parameters, two TEG materials have been chosen; bismuth telluride (Bi_2Te_3) with temperature dependent Seebeck effect (S), electrical conductivity (σ) and thermal conductivity (k); and lead telluride (PbTe) with non-temperature dependent S, σ and k. Results indicate that ESC MPPT method outperforms the P&O technique in terms extracting maximum power and the simulation speed. Results also indicate that ESC outperforms the IC technique in terms of extracting maximum power and the speed of computation. ESC method is faster than the IC method.

In the final study, the application of the concept and the design of a distributed dc-dc converter architecture (DCA) on TEG system is deliberated. The distributed or cascaded converter architecture involves the use of non-isolated per-TEG dc-dc converter connected to the load. Alternatively, for some specific loads, especially in automotive applications, soft-switched, isolated bi-directional dc-dc converters can be used instead of non-isolated converters because these integrated converters enable bi-directional power flow control capability. Simulations and experimental studies have been carried out to demonstrate and prove the necessity of the DCA design application on TEG systems. In addition, some of the factors affecting the performance of TEG systems are correspondingly analysed.

Chapter 1. Introduction

This chapter introduces the topic addressed in this thesis as well as the summary of the thesis.

1.1. Background of TEGs and summary of the thesis

The variable energy demands, availability of intermittent renewable energy resources, and the possibility of integrating storage and energy production systems give rise to the necessity of defining criteria and strategies to improve efficiency and energy supply, in total consideration of the environmental and economic sustainability (Boukettaya & Krichen 2014). Thermoelectric technology is one of those technologies which aims to improve the energy sustainability and maximum utilization. Thermoelectric devices are used in several applications. A number of currently available and applicable low-grade waste heat recovery methods adopt TEMs including district/water heating, direct power generation and others (Ebrahimi et al. 2014). TEMs offer low cost electricity without moving parts or production of environmentally deleterious wastes (Seetawan et al. 2014). Biomass cooking stoves which are commonly applied in developing countries with limited access to electricity, can be operated with TEG devices to generate low level electricity for home use, such as for mobile phone charging (Najjar & Kseibi 2017)(Yap et al. 2017). In this regard, a TEG based biomass cooking stove was developed and deployed for electricity generation, in the off grid areas (Mal et al. 2016).

The conversion efficiency of thermoelectric generators is determined by the value of figure of merit (ZT) for the thermoelectric materials. The higher the value of ZT, the higher the Efficiency of TEG devices. Over a long period, the value of ZT has stagnated at low levels, mainly ZT of less than one. Therefore, TEGs have relatively low efficiency for electric power generation (Qiu & Hayden 2012). Thus, thermoelectric devices have been mainly limited to cogeneration

systems, for example with photovoltaic (PV) systems. The automobile industry has been identified as one of the target industries for the reduction of greenhouse gas (GHG) emissions, hence numerous researches have been carried out in this area (Orr et al. 2014). In the automotive industry, thermoelectric devices have the potential to replace mechanical alternators for electricity generation in vehicles, which typically account for 2.4% of input fuel (Rattner & Garimella 2011). However, intensified research is necessary to overcome the challenges faced by thermoelectric devices before meaningful applications are realized in the automotive sector.

Although, thermoelectric devices are faced with a multitude of challenges, research shows that thermoelectric technology has received much attention and that several methods have been employed to address these challenges. The ways of combating these challenges can generally be grouped into two categories. The first category comprises of those techniques that pertain the adjustment of the device structures and the associated device parameters, which are called *Device-level TEG improvement methods*. The second category involves proper harvesting and utilization of the power generated by applying TEG devices, which is referred to as *External TEG improvement techniques*. Device level TEG improvement methods involve modification of the structure of TEG module for example by geometrical modifications, TEG material improvements such as hybridizing of TEG materials where some TEGs are made of three segments, each with different material type etc. External TEG improvement methods include TEG system improvement by; impedance matching, adjusting the boundary temperature conditions, variation of the number of TEG units and the use of output power conditioning methods, particularly the application of dc-dc converters.

In particular, to improve the performance of the overall TEG system, several power conditioning methods have been proposed and analysed in recent years. The dc-dc converters are known to have the potential to provide a more

stable power output and improve the efficiency of the Photovoltaic (PV) systems as awell as the TEG systems since both systems have similar performance characteristics. However, to facilitate better performance improvement, several Maximum power point tracking (MPPT) methods can be applied to extract maximum power from TEG system as they do in PV systems. Therefore, more research is necessary to test the performance of several converter topologies with the available MPPT techniques on TEG system, especially those which are already tested on PV systems. Hence, the main objective of the research carried out in this thesis is to analyse the performance of dc-dc converters with or without MPPT in conditioning the power generated from TEG.

The initial study has analysed the performance of a TEG/dc-dc boost converter system. The simplified model has been used as the basis of TEG design. Results indicate that the converter is able to stabilise and boost the voltage and higher efficiencies are achieved at different hot side temperatures.

The next study proposes the use of MPPT algorithm to harvest maximum power from TEG system. Hence, the analysis of the performance of TEG/dc-dc converter with MPPT enabled by Incremental conductance (IC) method is done. The results indicate that the IC based MPPT approach is able to track the maximum power point but with relatively lower efficiencies than the Perturb and Observe (P&O) based MPPT method. The matching efficiencies for the 200°C – 300°C temperature range is 99.92 – 99.95% and 99.46- 99.97% for P&O and IC methods respectively. However IC based method is noted with higher voltage gain and converter efficiencies than the P&O based MPPT method. Therefore, the dc-dc converters are able to improve the steady state performance of TEG system as well as boosting the voltage to the desired level, hence improving the overall performance of the TEG system.

Another study has analysed the parameters for the performance of TEG/dc-dc converter system in different modes with a variable load. The TEG system is subjected to different hot side temperatures, including increasing step, increasing random and constant cold side temperature profiles. Results indicate that a dc-dc converter with MPPT based model is able to extract maximum power from TEG better than the direct pulse width modulated (PWM) based model. From the study, for maximum power point to be achieved, it has been established that the TEG/dc-dc converter system has to be operated at a certain optimum load which is determined at a point where the overall converter resistance is equivalent to the internal resistance of TEG module. The study has demonstrated how the proper selection of converter components is a necessity to avoid converter losses as well interferences on the load connected to TEG/dc-dc converter system.

Furthermore, another study compares the performance of extremum seeking control (ESC) and P&O MPPT algorithms applied to TEG system. The MPPT is applied to guarantee maximum power extraction from the TEG system. The TEG model is validated with results from multiphysics (COMSOL) modelling software. To assess the effect of temperature dependency of TEG parameters, two TEG materials have been chosen; bismuth telluride (Bi_2Te_3) with temperature dependent Seebeck effect (S), electrical conductivity (σ) and thermal conductivity (k); and lead telluride (PbTe) with non-temperature dependent S, σ and k. Results indicate that ESC MPPT method outperforms the P&O technique. Results also indicate that ESC outperforms the IC technique in terms of extracting maximum power and the speed of computation. ESC method is faster than the IC method.

In the final study, the application of the concept and the design of a distributed dc-dc converter architecture (DCA) on TEG system is deliberated. The DCA design involves using several enabling components such as different converter topologies, sensors, relays, microprocessors etc. A robust computer algorithm

is also vital if the idea of voltage compensation to the loads with the reserve TEGs is to be successful. The simulations and experimental studies have been carried out to demonstrate and prove the necessity of the DCA design application on TEG systems. In addition, during the experiment, some of the factors that affect the performance of TEG systems have been analysed including the effect of the time of switching on/off of different components, the effect of thermocouple mulfunctioning as well as the impact of variation of the hot temperature. Consequently, appropriate tuning of TEG system parameters is necessary to improve the performance of TEG system.

1.2. Structure of the thesis

The thesis is made of nine chapters. Chapter 1 has stated the introduction to the research topic with the related terms in the research title clearly explained. Chapter 2 deals with the literature review about the TEG and the dc-dc converter. Chapter 3 discusses the objectives, problem and methodology for the research work conducted during the whole period of study. Chapter 4 describes the work about conditioning of thermoelectric generated power using dc-dc boost converters. Chapter 5 details the performance analysis of TEG system using dc-dc converters with incremental conductance (IC) MPPT technique. The parameter analysis of TEG/dc-dc converters system with MPPT and the variable loads has been discussed in chapter 6. The modelling of TEG/dc-dc converter system with extremum seeking control (ESC) MPPT is elaborated in chapter 7 whereas the concept and design of distributed dc-dc converter architecture (DCA) is deliberated in chapter 8.The conclusions as well as the future work are described in chapter 9.

Chapter 2. The working principles and past works on thermoelectric technology and power conditioning

Thermoelectric technology is regarded as alternative and environmentally friendly technology for harvesting and recovering heat which is directly converted into electrical energy using TEG. Conversely, Peltier coolers and heaters are utilized to convert electrical energy into heat energy for cooling and heating purposes The main challenge behind the thermoelectric technology is the low efficiency of these devices mainly due to low figure of merit (ZT) of the materials used in making them as well as improper setting of the thermoelectric systems. The objective of this work is to carry out a comprehensive literature review of thermoelectric technology encompassing the materials, applications, modelling techniques and performance improvement. The literature review covers a wide range of topics related to thermoelectric technology subject area including the output power conditioning techniques such as dc-dc converters. The review reveals some important critical aspects regarding thermoelectric device application and performance improvement. It is observed that the intensified research into thermoelectric technology has led to an outstanding increase in ZT, rendering the use thermoelectric devices in diversified application a reality. It is noted that the thermoelectric material research and device geometrical adjustment contributes to the device performance improvement whereas the use of advanced mathematical models have facilitated the appropriate segmentation of TEMs with different materials and integrated thermoelectric device designs. Thermoelectric devices are observed to have booming applications in cooling, heating, electric power generation as well as hybrid applications. With the generation of electric energy using TEG, heat source is not only provided by waste heat but also by other energy sources like solar, geothermal, biomass, infra-red radiation, have gained increased utilization in thermoelectric based systems. However, the main challenge remains in striking the balance between the conflicting parameters; ZT and power factor, when designing and optimizing advanced thermoelectric materials. Hence more research is necessary to overcome this and other

challenge so that the performance thermoelectric devices can be improved further.

2.1. Background

The changes in climate have driven the need for increasing research into alternative sources of energy. Those rapid changes in climate are mainly attributed to the use of fossil fuels for transport and energy generation. Due to climatic challenges, several countries around the world have pledged to reduce primary energy consumption through an increase of efficiency in production, distribution and end-use, limit carbon dioxide emissions and increase the utilization of renewable energy sources (Morini et al. 2013). The rapid development of power electronics technologies has enabled the realization of high energy-efficient systems such as electric vehicles (Tie & Tan 2013). The U.S. Energy Administration in 2011 estimated that almost two-thirds of total demand for petroleum is from the transportation sector. With an assumption that daily production of petroleum holds steady at 63.5 million barrels, global oil reserves are conventionally predicted to last approximately fifty years (Varnhagen et al. 2011). In the French industry, 75% of the final energy is used for thermal purposes such as furnaces, reactors, boilers and dryers. However, around 30% of this heat is assumed to be wasted in form of discharged hot exhaust gas, cooling water and heated product (Haddad et al. 2014). Therefore, the recovery and utilization of the waste heat is believed to have the potential to contribute some amount of energy to the energy needs of the society.

Research and development have been promoted on TEMs which convert heat energy directly into electrical energy. Thermoelectric devices are semiconductor devices that have the ability to either generate a voltage when exposed to a temperature gradient, exploiting the Seebeck effect, or produce a temperature gradient when supplied by electricity, exploiting the Peltier effect

(Montecucco et al. 2012). Heat energy can be harvested or recovered using two direct electricity generation strategies: thermoelectricity and pyroelectricity. Whereas thermoelectricity is the generation of electricity using thermoelectric harvesting systems which exploit the Seebeck effect for conversion of heat energy i.e., generation of electricity due to difference in temperature of two dissimilar conductors or semiconductors connected together at two junctions, pyroelectricity exploits specific materials whose structures are modified when heat is applied on them and in turn the polarization of the material is changed, thus creating electric potential (Akhtar & Husain 2015).

TEMs offer low cost electricity, and green energy technology without the use of moving parts or production of environmentally deleterious wastes (Seetawan et al. 2014). However, the optimal performance of TEMs depends on several factors like material selection and operation strategy. A study has used an irreversible model to analyse the performance of a TEG with external and internal irreversibilities, providing some significant instructions for their optimal operation including the information about optimal device design parameters, efficiency, maximum power output, etc. (Chen & Wu 2000). Most of the research by 2005 had concentrated on electronics cooling applications especially on the variation of the geometric features such as shapes, sizes, and orientations to the flow in heat transfer systems but in later years, research on thermoelectric technology has gained a lot of momentum (Goldstein et al. 2010).

Although energy-related GHG emissions from fossil fuel combustion account for 70% of total emissions including those from heat supply and electricity generation, a relatively large portion is generated from the transportation industry (Bazmi & Zahedi 2011). Although electric vehicles (EV) powered by renewable energies are seen as a potential solution to curtail GHG from transport industry (Hannan et al. 2014), thermoelectric technology is also continuously introduced in low carbon vehicles to extract waste energy from

various points of the vehicle. For a typical gasoline-engine vehicle, about 40% of the fuel energy is discharged from the exhaust pipe; about 30% is lost into the cooling system, clutch, gearbox and differential (Royale & Simic 2015). Hence, energy harvesting systems which recover this heat energy to convert it into electricity with the use of TEGs are being studied and introduced (X. Liu et al. 2015)(Noori et al. 2015).

There are several challenges surrounding thermoelectric technology which call for more research to address them. The assembly of TEG devices is still particularly challenging, and consequently these devices have been applied only in niche applications (Weishu Liu, Jie, et al. 2015). With regard to thermoelectric materials, there is a problem of wide lattice thermal conductivity whereby nanostructuring has been considered as an effective approach to enhance the thermoelectric performance of materials by reducing their lattice thermal conductivity (Zolriasatein et al. 2015). The introduction of large concentrations of lattice vacancies in silicon nano-films is noted for creating more than a 20-fold reduction in thermal conductivity, while Seebeck coefficient and electrical conductivity are largely maintained (Bennett et al. 2015). With such a challenge in mind, the impact of the substrate on the efficiency of thin film thermoelectric technology is assessed (Alvarez-Quintana 2015). It is found that as the thickness ratio between the substrate and thin film increases, the parameter ZT sharply tends to zero; this effect causes a serious problem to overcome by the thin film thermoelectric technology, more especially at nanoscale. Frequency dependency of ZT is another challenge especially in cylindrical thermoelectric nano devices. A study indicates that regarding the relative values of the particles' mean-free path and the characteristic size of the system, the performances of the thermoelectric devices are reduced in those situations (Sellitto 2014). However, it is found that non-local effects may be used as aiding tools to have less marked reductions in those performances.

With thermoelectric Coolers (TEC), cooling hot-spots with high heat flux is becoming one of the most important technical challenges in integrated circuit industry, calling for more aggressive thermal solutions, than those required for uniform heating, to mitigate this problem (Yang et al. 2007). One efficient method of hotspot thermal management is to use super lattice TEC which can provide on demand and localized cooling. A detailed 3-D thermal model of a stacked electronic package is developed to investigate the efficacy of TEC in hotspot cooling for 3-D technology where thermal contact resistances between dies, inside the TEC module, and between TEC and heat spreader are shown to have a crucial effect on the TEC performance (Redmond et al. 2013). Regarding TEGs, product development requires solving a couple of challenges in material development and systems engineering to enable new thermoelectric materials and material performance improvements for development of TEGs in numerous applications (Leblanc 2014).

The objective of this chapter is to present a comprehensive literature review of thermoelectric technology encompassing the materials, applications, modelling techniques and performance improvement. A brief background of the TEG devices and materials has been covered first followed by the applications of these technologies. Moreover, the background of application of dc-dc converters for TEG systems is also discussed in addition to shading light on the use of MPPT techniques for maximum power harvesting using TEG devices.

2.2. Description of TEMs and the concept of Seebeck effect

2.2.1. The concept of Seebeck effect

TEMs can be used for either cooling or power generation, as shown in Figure 2.1. A TEG is a solid state device that can convert heat directly into electrical energy when a temperature difference is placed across it (Yu et al. 2015b). The TEM consists of arrays of N and P-type semiconductors in which, by applying

a heat source on one side and a cooler/heat sink to the other side, electric power is produced and vice versa. Electric power can be converted to cooling or heating by reversing the current direction (Zheng, Liu, Yan, et al. 2014).

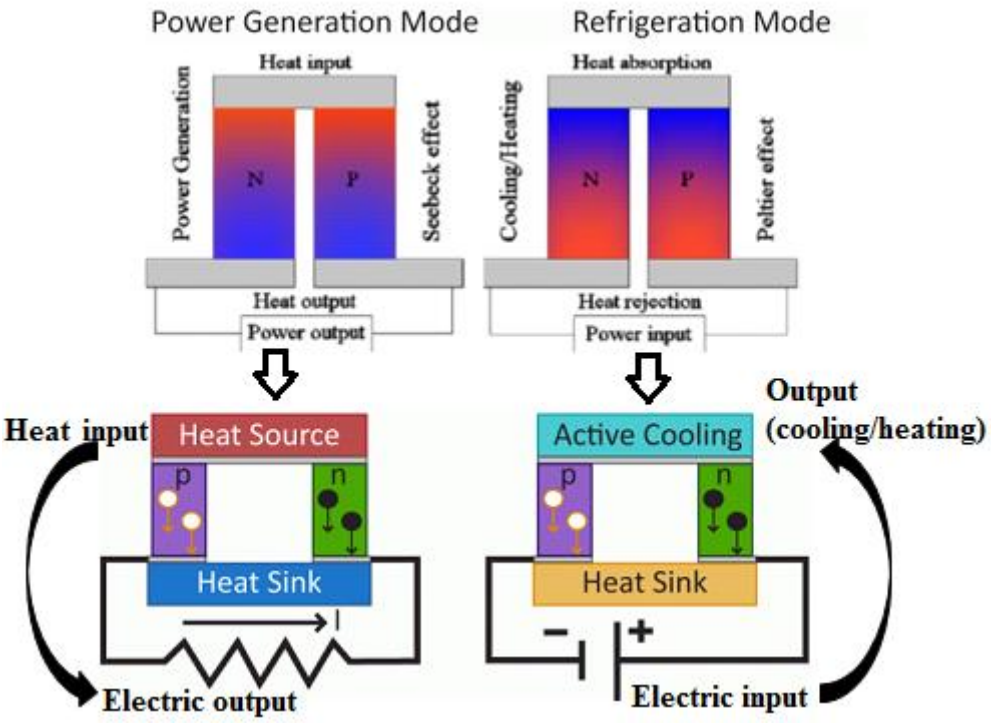


Figure 2.1. Power generation and cooling/heating thermoelectric heat engines (Zheng, Liu, Yan, et al. 2014)

While choosing TEGs for application in varying conditions, it is necessary to select an appropriate semiconductor with acceptable performance in the temperature range of that condition (Niu et al. 2015).

The figure of merit (Z) is a parameter generally used to gauge the performance of a thermoelectric material;

$$Z = \frac{\alpha_{p,n}^2 \sigma_{p,n}}{\lambda_{p,n}} \qquad (2.1)$$

Where $\alpha_{p,n}$ is the Seebeck coefficient of n-type or p-type material (V/K). $\sigma_{p,n}$ is the electrical conductivity of the material (p-type or n-type) in Siemens per meter (S/m) whereas $\lambda_{p,n}$ is the thermal conductivity (W/(m.K)) (Niu et al. 2015).

In general, for obtaining maximum efficiency, the important characteristic for thermoelectric material is the dimensionless performance measurement paremeter called figure of merit ZT (Zheng, Liu, Yan, et al. 2014);

$$ZT = \frac{\sigma \alpha^2 T}{\lambda} \qquad (2.2)$$

Where α, σ, T and λ are the Seebeck coefficient, electrical conductivity, absolute temperature (K) and thermal conductivity, respectively. In order to get high thermoelectric efficiency, the figure of merit should be large.

In a thermoelectric material, there are free electrons or holes which carry both charge and heat. The electric potential (voltage) produced by a temperature difference is known as the Seebeck effect and the proportionality constant is called the Seebeck coefficient. If the free charges are positive (the material is p-type), positive charge will build up on the cold end which will have a positive potential. Similarly, negative free charges (n-type material) will produce a negative potential at the cold end (Bell 2008). Figure 2.2 illustrates the movement of electrons and holes in p- and n-type materials respectively due to Seebeck effect.

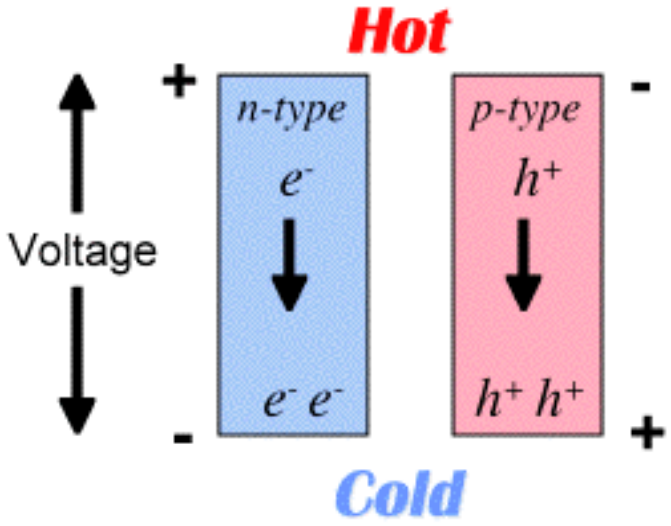


Figure 2.2. The movement of electrons and holes in p- and n-type materials

The features of heat transfer are calculated using the mechanism of the Seebeck effect as shown in Figure 2.3. The compressed air heated by a heater with flow rate F_H, heat transfer coefficient h_1 and at inlet temperature T_i flows through the heat pipe to provide the high/hot temperature side of the TEM. Similarly, the jet air at with flow rate F_C, heat transfer coefficient h_2 and at temperature T_j provides cooling to create the cold side of the module. The waste heat energy is transferred to the heat absorber with temperature $T_{i,s}$ by heat convection while the internal heat sink absorbs some of the waste heat energy, and the thermal grease with thermal conductivity k_{tg} guides the heat to the hot side of TEG with $T_{TEG,H}$ temperature. The heat collection and heat dissipation distinctly at the hot and cold sides of TEG create the temperature difference between both sides of the module to generate electricity due to Seebeck effect. Simultaneously, the internal Joule heating happens in the TEG due to the internal electric resistance R_{int}. More details of the heat transfer mechanism are found in (Tzeng et al. 2014).

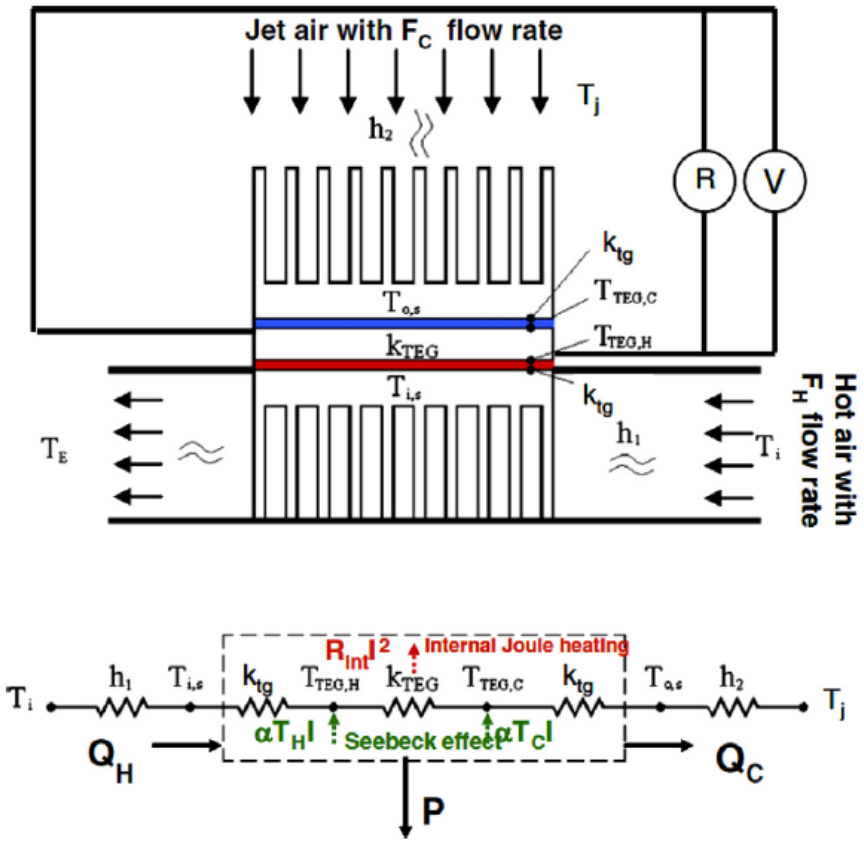


Figure 2.3. Heat transfer mechanism and Seebeck effect for the TEM

The derivation of heat conduction equation is based on the internal energy generation of the TEM (Tzeng et al. 2014);

$$\frac{\partial^2 T}{\partial x^2} + \frac{\dot{q}}{k_{TEG}} = 0 \qquad (2.3)$$

Where x is any thickness of the TEG material, $\dot{q}$ is heat energy generated per unit volume and K_{TEG} is the thermal conductivity of the TEG.

Assuming the low and high temperature sides are taken to be same, the boundary conditions are expressed as $T(0) = T_{i,s}$ at $x = 0$ and $T(\delta) = T_{o,s}$ at $x = \delta$.

The total generated power can be calculated as;

$$P = Q_H - Q_c = \alpha I\left(T_{i,s} - T_{o,s}\right) - \delta A_{TEG}\dot{q} \qquad (2.4)$$

Putting the Seebeck effect into consideration, the thermal power Q_H and Q_C from the high and low temperature sides can respectively be computed as;

$$Q_H = \frac{k_{TEG}A_{TEG}}{\delta}\left(T_{i,s} - T_{o,s}\right) + \alpha T_{i,s} I - \frac{1}{2}R_{int}I^2 \qquad (2.5)$$

$$\mathrm{Q_C} = \frac{\mathrm{k_{TEG}A_{TEG}}}{\delta}\left(\mathrm{T_{i,s}} - \mathrm{T_{o,s}}\right) + \alpha \mathrm{T_{o,s}} \mathrm{I} - \frac{1}{2}\mathrm{R_{int}I^2} \qquad (2.6)$$

Where δ is the thickness of the TEG and I is the current. In this case, A_{TEG} has two meanings; first as the area of the heat sink for the high temperature side, and as the area of the TEM for the low temperature side (Tzeng et al. 2014).

The maximum electric power generated from the TEG is expressed as (In et al. 2015);

$$P_{max} = \frac{k_{TEG}A_{TEG}}{\delta} * \frac{\left[(\gamma+\lambda+1) - \sqrt{(\gamma+\lambda+1)^2 - 4\alpha^*\lambda\left(T_i - T_j\right)}\right]}{4\alpha^*} \qquad (2.7)$$

Where, λ is the biot number of the TEG, γ is the heat transfer ratio of the heat absorber to the heat sink and α^* is the Seebeck parameter of the TEG.

In another form;

$$P_{max} = \frac{E_m^2}{4R_m} \qquad (2.8)$$

Where E_m is the electromotive force (EMF) generated by Seebeck effect. P_{max} occurs when the resistance of R-L circuit (RL) equals to TEG module internal resistance R_{int}.

For the physical properties of thermoelectric materials, some previous studies assumed that they are temperature-independent, however, it has been demonstrated experimentally that the physical properties of the thermoelectric

materials are temperature dependent (Bell 2008). This dependence can be very significant and strongly affect the TEG performance (Yu et al. 2015a). The physical properties of Bi_2Te_3 material are calculated as;

$$\alpha = -6.034 * 10^{-5} + 6.270 * 10^{-7}T - 1.571 * 10^{-9}T^2 + 1.260 * 10^{-12}T^3 (V\,K^{-1}) \quad (2.9)$$

$$\delta = -7.188 * 10^{-7} + 6.926 * 10^{-9}T - 3.573 * 10^{-12}T^2 (\Omega\, m) \quad (2.10)$$

$$k = 2.244 + 6.067 * 10^{-5}T - 2.308 * 10^{-6}T^2 + 4.439 * 10^{-9}T^3 (W\, m^{-1}\, K^{-1}) \quad (2.11)$$

The heat transfer coefficient is also expressed as;

$$h = \frac{Q_{max}}{A_B(T_i - T_o)} \quad (2.12)$$

Where A_B is the heat sink base area.

2.2.2. Analysis of important parameters of TEMs

The parameters that affect the performance of thermoelectric devices can be physical or nonphysical. The most important optimization parameters for TEG include thermoelectric element leg length, leg area ratio between n- and p-type legs, fill fraction, load resistance and module spacing. The effect of various leg geometries on thermo-mechanical and power generation performance of thermoelectric devices are investigated by modelling leg geometries and analysed using finite element method (Erturun et al. 2014). Thermal stresses in the legs, power outputs, temperature distributions and conversion efficiencies are evaluated and the results show that significant differences in sizes and distributions of the thermal stresses in the legs occur due to varying leg geometries. The different output parameters for TEG device are identified as power generation, thermal efficiency, current, thermal and electric fields, etc. (Rabari et al. 2014).

It is also noted that the influences of the effective Seebeck coefficient and carrier density variations on the performance of thermoelectric system are generally neglected, resulting in an overestimation of the power generator performance under strong-ionization temperature region (Wu & Yu 2014). Therefore, researchers suggested and proved the use of finite element tool to solve such complexity, whereby the characteristics of TEG and their relationship to its performance can be well analysed. Additionally, the behaviour of power generation from TEG exposed to a transient heat source on the hot side and natural convection on the cold side are studied (Nguyen & Pochiraju 2013). It is stressed that modelling TEGs under these conditions is complicated compared to thermoelectric coolers because of the non-linearities and the unknown electric currents in a closed-loop circuit. Therefore a transient thermoelectric model which comprises Seebeck, Thomson, Peltier, and Joule effects using finite difference techniques is suggested and the incorporation of Thomson effect plays a significant role in precisely predicting the generated power. Fateh et al. used a finite difference model to investigate the interdependencies among these optimization parameters for thermoelectric elements included with an exhaust gas heat exchanger (Fateh et al. 2014). Different researchers look at the optimum parameters differently depending on the method used in the parameter analysis. The influence of geometric features on TEG device characteristics is done using multi-objective evolutionary algorithms (Ibrahim et al. 2014). The parameters assessing geometric features include pin length size and shape factor while operating parameters include external load and temperature ratio parameter. The influences of the thermal conductivity ratio, the external load parameter, the conductance ratio and the figure of merit on the output power, the efficiency, and the entropy generation rate are predicted for various device parameters (Sahin & Yilbas 2013). A technical solution for recycling blast furnace slag flashing water heat based on TEG is also presented (Meng et al. 2014). The effects of key parameters like the thermoelectric element length, slag washing water temperature, the

packing factor of the TEM and heat exchanger flow passage length on the performance of the TEG device are examined.

While studying the optimum design of thermoelectric devices, dimensionless groups are used to properly define and represent important parameters of the thermoelectric device (Lee 2013). According to this study, the optimum design comprises the optimum parameters such as efficiency, current, power, geometry or number of thermocouples, and thermal resistances of heat sinks. The geometry effects on thermoelectric properties of silicon nanowires based on electronic band structures are also investigated where it is found that thermoelectric properties significantly depend on nanowire geometry such as different sizes, shapes, and orientations (Liang et al. 2010). As nanowire size decreases, thermoelectric properties of nanowires can be enhanced and as a result, triangular nanowires with side length of 1 nm have the best results of ZT and it can be improved to 1.5 for n-type and 0.85 for p-type nanowire. The study on thermoelectric properties of Ge Nanowires (NWs) which is based on electronic band structures also reveals that thermoelectric properties vary significantly depending on the band structure of the Ge NWs of different sizes, cross-sectional shapes, and orientations (Huang et al. 2010). Moreover, the thermodynamics and thermal stress analysis of TEG is also done to assess the influence of pin geometry on device performance (Al-Merbati et al. 2013). With finite element method, it is established that thermal efficiency increases for certain geometric configuration of TEG device and the maximum thermal stress in the pin decreases slightly representing improved life expectancy of TEG.

The power density (power generated per unit surface area) of TEG strongly depends on the TEG module spacing. The optimization of the TEG module spacing and its spreader thickness, for TEG modules attached to a rectangular chimney plate for venting hot flue gases is also done (Jang & Tsai 2013). Therefore, finding the optimal module spacing for the TEG system used in waste heat recovery is crucial to ensure optimum power generation from the

system. The predicted numerical data obtained using finite difference method and a simplified conjugate-gradient method has demonstrated a good power vs. current curve. It is important to note that heat transfer in the TEG is one of the performance measures that need to be investigated before using TEG. Some methods like the longitudinal vortex generators have been used to improve heat transfer performance as well as power output and thermal conversion efficiency (Ma et al. 2015).

2.3. Different materials used for TEG/TEC

The material used in the construction of a TEG or a TEC plays an important role in controlling the performance of these devices. There are many features that describe the performance of these materials to make them suitable for use in TEG device manufacture. In this section, various TEG/TEC materials will be discussed and the selection criteria of these materials for use in thermoelectric power generation as well as for cooling are clarified. The material used for the TEg module (TEG1-12611-6.0) considered in this study is not specified by the manufacturer but the hybrid version of this TEG module which is TEG1-PB-12611-6.0 is made from Bi_2Te_3 and PbTe materials (TECTEG MFR n.d.).

2.3.1. Selection criteria for TEG/TEC material

To achieve the best performance from the TEM, there are some properties of the material that characterise a good TEM. Many researchers have carried out a number of works to determine the effect of these properties on the performance of thermoelectric devices. For example three different methods for predicting the Seebeck coefficient of TEC module are used to determine the properties and performance of a TEC (Chen et al. 2015). One method is based on experimental measurements while other two are formulated based on mathematical models. Basically, all the methods are able to provide useful tools for designing and constructing a TEG system. Some of the thermal and

electrical properties of thermoelectric materials that make the selection criteria for the TEG/TEC material are described below.

Thermal conductivity of the material

The electronic thermal conductivity of thermoelectric material is determined by holes and electrons transporting heat (k_e) as well as phonons travelling through the lattice (k_1). Majorly, ke is related to electrical conductivity by Weidman–Franz law (Snyder & Toberer 2008);

$$\mathrm{k} = \mathrm{k_e} + \mathrm{k_1} \tag{2.13}$$

$$\mathrm{k_e} = \mathrm{L\sigma T} = \mathrm{ne\mu} \tag{2.14}$$

Where L is defined as the Lorenz factor equivalent to 2.4 × 10-8 J2 K–2 C–2, for free electrons.

In order to get high thermoelectric efficiency, the figure of merit should be large. Table 2.1 outlines the available materials for thermoelectric applications categorized according to temperature range along with ZT of the material. As high ZT requires low thermal conductivity but high electrical conductivity, the Weidman–Franz law reveals an in-built materials conflict for attaining high thermoelectric efficiency. For materials with very high electrical conductivity (metals) or very low k_l, the Seebeck coefficient alone primarily determines ZT, as can be seen in equation (2.15), where (kl/ke) << 1 (Snyder & Toberer 2008);

$$ZT = \frac{\alpha^2/L}{1+\frac{k_1}{k_e}} \tag{2.15}$$

Power factor

Another parameter of relative importance is the *power factor* which only focuses on the material performance of electrons when thermal conductivity at the two end reservoirs can be ruled out.

$$Power\ factor = \sigma S^2 \quad (2.16)$$

The difficulty of maximizing ZT and power factor lies in the fact that the above parameters are generally interdependent. Therefore, it is a challenge to develop advanced thermoelectric materials with an optimization of these conflicting properties to increase ZT and power factor. Current thermoelectric devices are considered to be;

- inefficient when ZT is about 1.
- able to recover waste heat when ZT = 2.
- able to match a refrigerator when ZT = 4/5 (Bell 2008).

For a long time, the best ZT has been one for Bi_2Te_3, which translates to efficiencies of about 5-7% for most applications but falls off rapidly with hot side temperatures of over 230^{o}C (Fairbanks 2008).

Table 2.1.The characteristic of available TEGs materials (Hamid Elsheikh et al. 2014)

Temperature (^{o}C)	Type	TEG Material	ZT (Maximum)
<150	p	Bi_2Te_3	0.8
	n	Bi_2Te_3	0.8
150 - 500	p	Zn_4Sb_3	-
	p,n	PbTe	0.7 – 0.8
	p	TeAgGeSb(TAGS)	1.2
500 - 700	p	$CeFe_4Sb_{12}$	1.1
	n	CoSb3	0.8
700 – 900	p, n	SiGe	0.6 – 1.0
	p	LaTe	0.4

2.3.2. Recent advances on TEG material

For materials with ZT>1, it is discovered that most of them have a common feature of having lattice thermal conductivities that are lower than other materials with low ZT (Snyder & Toberer 2008). With reduced lattice thermal

conductivity, the thermoelectric efficiency and ZT improve in addition to allowing re-optimization of the carrier concentration, leading to more ZT improvement. Alternatively, to achieve practical thermoelectric materials with ZT of more than 2, enhancement of the Seebeck coefficient without reducing the electrical conductivity is also possible by using two-dimensional electron gas that enables realization of practical thermoelectric materials without the use of toxic heavy elements (Ohta et al. 2007). For instance alloying Bi_2Te_3 with Sb_2Te_3 and Bi_2Se_3 allows fine tuning of the carrier concentration with a decrease in lattice thermal conductivity. The most commonly studied alloys are the p-type compositions which are near $(Sb0.8Bi0.2)2Te_3$ whereas n-type compositions are close to Bi_2 (Te0.8Se0.2)3. While investigating the thermoelectric materials for waste heat recovery with advanced heat exchangers, Crane and Jackson (Crane & Jackson 2004) analysed a heat exchanger integrated with Bi_2Te_3 TEMs. They proved that power losses from an air fan and a fluid pump result in the optimal configuration at intermediate cooling air and hot fluid flow. However, heat exchangers with Bi_2Te_3 thermoelectrics can achieve net power densities over 40 W/l. A two-dimensional numerical model of a TEG system using nanostructured thermoelectric semiconductor materials with BiSbTe and Bi_2Te_3 is developed (Rabari et al. 2014). A TEG with p-type nanostructured material of BiSbTe and n-type Bi_2Te_3 with 0.1 vol.% Silicon Carbide (SiC) nanoparticles is considered for evaluation of performance. The results indicate that the amount of current generated increases as the temperature differences, which increases the output power.

For mid-temperature power generation (500–900 K), materials based on group-IV tellurides are typically used, such as PbTe, GeTe or SnTe. Alloys, particularly with $AgSbTe_2$, have led to several reports of ZT > 1 for both n-type and p-type materials. The p-type alloy (GeTe) 0.85 (AgSbTe2)0.15, commonly

referred to as TAGS, having maximum ZT>1.2, has been successfully used in durable TEGs.

For high temperature TEGs (>900 K), silicon–germanium alloys have been used for both n- and p-type legs. The ZT of these materials is somehow low, mainly for the p-type material because of the relatively high lattice thermal conductivity of the diamond structure. Table 2.2 summarises the most commonly used alloys for thermoelectric application due advancement in material research.

Table 2.2. The most commonly used alloys for thermoelectric application

Material Name	Molecular Formula	Description	Application
Antimony (III) Telluride powder	Sb_2Te_3	99.9% trace metals basis and 325 mesh	
Antimony (III) selenide	Sb_2Se_3	99.9% trace metals basis	
Bismuth (III) selenide	Bi2Se3		
Bismuth (III) selenide granular (melted)	Bi_2Se_3	99.9% trace metals basis	
Bismuth (III) Telluride powder	Bi_2Te_3	99.9% trace metals basis and 325 mesh - Bi_2Te_3 alloys have the highest ZT for n- and p-type thermoelectric systems	-Near room temperature (Refrigeration - waste heat recovery up to 200 °C
Silver (I) terruride	Ag_2Te		
Lead (II) telluride	PbTe	99.9% trace metals basis	
Lead (II) selenide	PbSe		
Bismuth Antimonide	BiSb	crystalline thermoelectric material with a cage-like crystal structure known as a skudderite (American Elements n.d.).	Potential for new semiconductor chips, thermoelectric devices

The compound zinc antimony Zn_4Sb_3 has also been reported as one of the most efficient thermoelectric materials known with high efficiency obtained through its extraordinarily low thermal conductivity and with the electronic structure of a heavily doped semiconductor (Snyder et al. 2004). Research discovered Zn_4Sb_3 as a thermoelectric material with high ZT between 450K and 670 K (ZT =1.3 at 670 K), mainly because of its low thermal conductivity (Mozharivskyj et al. 2004). Park et al. stress that the integration of CeO_2 and Dy_2O_3 to Zinc oxide (ZnO) leads to a notable increase in the electrical conductivity. The power factor is approximately fifty-six times larger than that of ZnO (0.08E-4 $Wm^{-1}K^{-2}$ at 800 ^oC). The addition of a slightly smaller quantity of Dy_2O_3 is very effective for improving the thermoelectric properties of ZnO (Park et al. 2013).

For cooling below room temperature, alloys of BiSb have been used in the n-type legs, coupled with p-type legs of $(Bi,Sb)_2(Te,Se)_3$. It has been noted that the poor mechanical properties of BiSb allow for improved low temperature materials. Using micro electromechanical systems (MEMS), several different metals and thermoelectric materials are fabricated in a three-dimensional structure to form a TEG (Snyder et al. 2003). It consists of 126 n-type and p-type $(Bi,Sb)_2Te_3$ thermoelectric elements. The device showed good performance in terms of thermal control when operated as a cooler (TEC), and portable power when operated as a TEG.

The oriented thermoelectric p-Sb_2Te_3 and n-Bi_2Te_3 thin films having special nanostructures have also been synthesized by a simple vacuum thermal evaporation technique and the n- and p-type elements set in parallel and series circuits to form a prototype (Tan et al. 2011). The conductivity and Seebeck coefficient which act as electric transport properties and the thermal transportation of the oriented films have been analysed to have optimized properties. The results verified that introducing nanostructures into films is an effective choice to obtain more efficient micro thermoelectric device because

the cooling and electric output power obtained are more than that of the common films.

2.4. Application of thermoelectric devices

Thermoelectric device applications are concerned with environmentally friendly refrigeration and power generation in industrial utilities, transportation tools, military devices, space applications and medical services (Zheng et al. 2012). TEGs have also found application in biomass gasifiers to further improve the recovery of heat (Ma et al. 2014). Thermoelectric devices are either used for cooling or heating purposes or for power generation from either low heat recovery applications or as stand-alone heat to electric energy conversion systems such as a battery charger powered by TEG modules (Eakburanawat & Boonyaroonate 2006). However, methods of delivering maximum power to the battery for a range of temperature gradients across the TEM have to be used (Kinsella et al. 2014).

2.4.1. Application of TEG for heat recovery from the vehicle

Thermoelectric technology presents solution for energy reuse in vehicles driven by internal combustion engine (ICE) especially in the exhaust pipe and the radiator. TEGs are placed at different points of the vehicle to generate energy from waste heat. If the waste energy from the vehicle is appropriately utilized, the consumption of diesel fuel is reduced because it eliminates the need for the generator used for battery charging and other low energy needs in the vehicle (Zachár et al. n.d.). Most of the waste heat energy from the vehicle is recovered from the exhaust pipe than in the radiator, and the most suggested positon is after the catalyst where high temperature is found. It is therefore noted that if the thermoelectric technology advances, in a near future it will be possible to decrease the fuel consumption to 10%.

Various parameters for the TEG in the vehicle are predicted, where the maximum possible exhaust power that can be extracted is defined as (Karri et al. 2011);

$$\dot{W_{e,max}} = \dot{m_e}(C_{p_{e,i}}T_{e,i} - C_{p_{e_{f,i}}}T_{f,i}) \quad (2.17)$$

Where $\dot{W_{e,max}}$ is the total possible exhaust power that can be extracted, $C_{p_{e,i}}$ is the specific heat of the exhaust evaluated at $T_{e,i}$, $T_{e,i}$is the exhaust inlet temperature into the TEG, $C_{p_{e_{f,i}}}$ is the specific heat of the exhaust evaluated at $T_{f,i}$, and $T_{f,i}$ is the coolant inlet temperature into the TEG.

The actual exhaust energy extracted is defined by;

$$\dot{W_e} = \dot{m_e}(C_{p_{e,i}}T_{e,i} - C_{p_{e,o}}T_{e,o}) \quad (2.18)$$

Where $\dot{W_e}$ is the exhaust energy extracted; $C_{p_{e,o}}$ is the specific heat of the exhaust evaluated at $T_{e,o}$ and $T_{e,o}$ is the exhaust outlet temperature from the TEG.

Several researches have been conducted regarding the generation of useful electric power from waste heat using TEG. The case study is carried out on two vehicle models (Karri et al. 2011); HZQW and HZ20M model. The power generated from TEG for HZQW and HZ20M, at a vehicle speed of 117.2 km/h is reported to be 453 W and 140 W respectively. The efficiency of the TEG which is the ratio of power generated by the TEG to exhaust energy extracted is found to be 8.53% and 2.25% for the HZQW and HZ20M vehicle models respectively. The increase in efficiency for the HZQW model is attributed to HZQW's ability to reject less heat and therefore use lower coolant flow rate. Based on this study, a lower parasitic loss and hence higher TEG power is registered although relatively low fuel gains are observed mainly because of the high efficiency the electrical generator used in the experiment. If attempts

are made to further reduce the parasitic loss from the TEG, the output power of TEG device can equally be increased.

The performance features of the TEG were analysed through a prototype vehicle, where an energy harvesting system was constructed to extract electrical energy from the automotive exhaust pipe using TEG (X Liu et al. 2015). The characteristics of the system include cold side temperature, hot side temperature, power output, open circuit voltage and maximum power. The maximum powers obtained are 183.24W, 600W and 944 W and the corresponding efficiencies were reported as 0.9%, 1.28% and 1.85% for the TEG system test, road test and revolving drum test respectively. Because it is not easy to put in place an independent cooling system, a revolving drum test table with the fan system is used to keep the prototype vehicle stationary while at the same time regulating the fan speed. It is noted that the fabricated TEG device is able to recover a significant amount of energy from waste heat. However, the main challenge is in improving the exhaust pipe to decrease the effect of thermal contact followed by increased hot side temperature, thereby increasing the generated power from TEG.

A mathematical model of a TEG device embedded on vehicles' exhaust pipe is analysed with Fourier's law and the Seebeck effect (Wang et al. 2013). It is indicated that the TEG power output and efficiency increase significantly by adjusting the convection heat transfer coefficient of the high temperature-side instead of low temperature side. Additionally, the maximum TEG power and efficiency appear when internal resistance is lower than external resistance. However, with the increment of ZT, the maximum value moves towards the direction of an increasing ratio of external resistance to internal resistance. Meanwhile, raising the ratio of external resistance to internal resistance equally increases the maximum output power of TEG. In particular, a new idea is presented to improve TEG performance using the reformed experimental design. Moreover, with the usage of phase change materials made possible to

strengthen the heat transfer property of the hot temperature side of TEG, the power output and efficiency of TEG can be improved by applying suitable phase change materials.

An energy harvesting system is also constructed by using test benches to analyse the performance of the TEG module (X. Liu et al. 2015). The analysis of the maximum power output and the results from the experiments demonstrate enhanced TEG efficiency with 183.24 W maximum power output at engine revolution of 3200 r/min. The cold side temperature, cold side flow rate and applied pressure are found to have a significant effect on the maximum power output. It is also observed that Bi2Te3-based TEMs have the potential to extract low-grade temperature waste heat energy from automotive exhaust pipes.

In a separate move, the effectiveness of thermoelectric device in cooling and pre-heating as well as waste heat recovery is examined on the Li-family battery system for electric vehicle (Suh et al. 2014). A thermoelectric device is found to be able to contribute meaningfully to the sound operation of the battery, enhanced the reliability and the overall performance of EV. In a unique application, the study is conducted where TEG devices are used to recover heat energy from a table lamp (Weng & Huang 2014). The cold side of the TEG is subjected to cooling by a natural convection heat sink and the power generation rate is predicted based on the hot side and cold side thermal conductance of the open circuit system. A relatively larger maximum power generation rate is observed with a slightly smaller optimal electric load. This is ascribed to the residual electric resistances in the circuit rather than the internal resistance of the external load and TEG device. It is indicated from this study that there is an undesirable role played by the insulating layer which reduces the TEG efficiency. However, it is concluded that thermoelectric conversion is capable of recovering waste heat, because thermoelectric device performance

can be improved for example through appropriate selection of TEMs and proper handling of thermal contacts.

2.4.2. Cooling applications of thermoelectric devices

TECs are commonly known as Peltier coolers. These are well suited for such applications where conventional air-cooling system is not adequate to remove the heat fluxes at an appropriately high rate. The general design criteria for these TECs include high reliability, flexibility in packaging and integration and low weight (Hamid Elsheikh et al. 2014). Additionally, the application of a Peltier cell for electric generation is assessed based on its output power and efficiency where it is demonstrated that Peltier cell is promising for recovering waste heat (Casano & Piva 2011). The cooling applications using thermoelectric devices are mainly found in three categories including; thermoelectric air conditioners (TEACs), refrigerators and air conditioners as well as for cooling electronic devices.

1. **Cooling electronic devices**: In electronic cooling application, a TEC is used to transport heat from a surface that has a temperature higher than the ambient temperature. The role of a TEC is to maintain the junction temperature of an electronic device below a certain temperature by removing heat from the device (Chein & Huang 2004).
2. **Refrigerators**: In refrigeration application, Peltier cooling appliances provide rapid cooling. For example a solar Peltier refrigerator is capable of reducing the temperature from 27 ^{o}C to 5 ^{o}C in about 44 min. A thermoelectric refrigeration system has the merits of being light, rugged, reliable and noiseless. Thermoelectric refrigeration devices are at low cost in mass production if charge carriers in the thermoelectric material are used rather than a refrigerant as the heat dissipation carrier.
3. **Thermoelectric air conditioners (TEACs)**: These are environmentally friendly, simple and reliable; they offer convenient installation and

switching between the cooling and heating modes can be easily achieved by reversing the input current. However, these systems are still very expensive at present. TEACs operation silently and are portable, but with somehow lower COP that limits their application for domestic cooling (Hamid Elsheikh et al. 2014). However, as air conditioners, TEACs have a large promising market for small enclosures, such as submarine cabins and cars, where reliability and safety are indispensable and the power consumption is relatively low.

2.4.3. Hybrid systems

In the hybrid thermoelectric systems, part of the recovered or harvested heat is used for electric generation while the other part is used for other purposes like water heating. The performance analysis has been done for a thermoelectric cogeneration system (TCS) which generates electricity and preheats water for home use (Zheng, Liu, Boukhanouf, et al. 2014). The main source of heat for the thermoelectric cogeneration is a boiler exhaust waste heat. Water is used for cooling the cold side of the TEG and is circulated through a compact heat exchanger for both electricity generation and domestic water heating. The system also uses solar energy from a solar collector mounted on the roof of a building to supply heat on the hot side which is added to the heat from the exhaust pipe of the boiler. Figure 2.4 illustrates the TCS system. It has been noted that the overall efficiency is increased but with some challenges met during heat transfer to and from the TEG. Although thermoelectric technology has been mainly applied for heat recovery, here it can be observed that the technology is now applicable to harvesting energy from solar systems. Such applications are more likely to result into more rigorous research into thermoelectric technology to advocate for higher efficiencies of the thermoelectric devices.

Similarly, an integrated TEG-cooling system is numerically studied with finite element method in which it is discovered that when the lengths of TEG and TEC vary, the highest reductions in system performances are 12.45% and 18.67%, respectively (Chen et al. 2014). It is reported that the system performances for different TEC lengths are significantly different from the performance of TEG for different TEG lengths. However, the results provide useful insights into the design of integrated TEG–TEC systems.

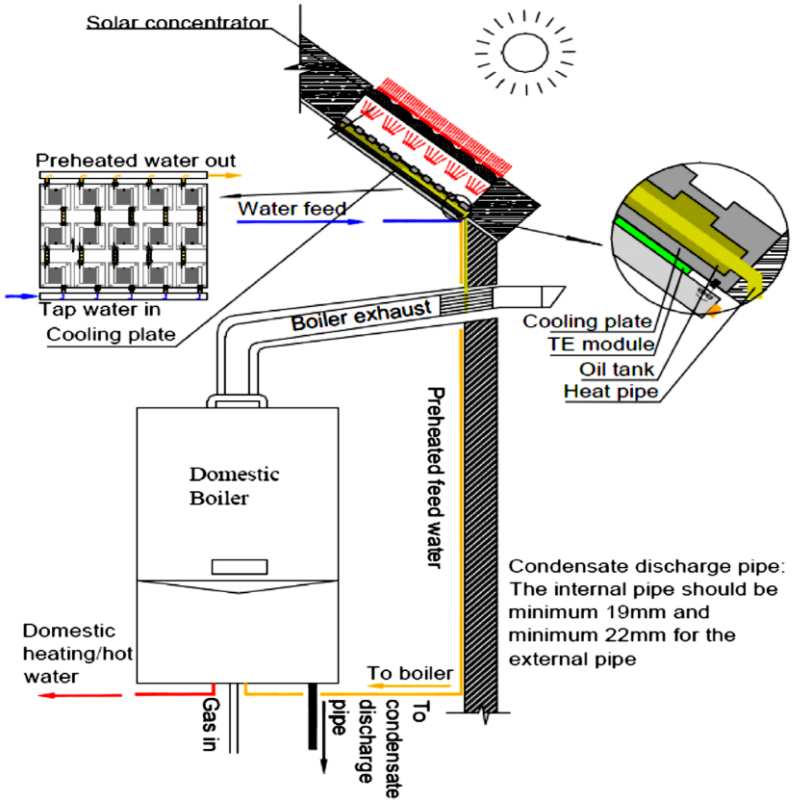


Figure 2.4. The domestic TCS (Zheng, Liu, Boukhanouf, et al. 2014)

Bekir et al. (Yilbas & Sahin 2014) investigated a system that comprises of a TEG and a refrigerator where the effect of location of the TEG in the refrigerator cycle on the coefficient of performance (COP) of the system is analysed. By introducing the dimensionless parameters such as temperature ratio, heat transfer ratio, capacitance ratio to mention but a few, the influence of the

operating conditions on the COP are studied. It is discovered that the placement of the TEG between the condenser and evaporator reduces the COP while TEG's location between condenser and its ambient increases the COP. This finding verifies why hybrid thermoelectric systems are useful because in an area where one device say TEG cannot perform better, another device say TEC can demonstrate an optimum performance. Therefore, if both devices are applied in the system, the overall harvested energy and hence system efficiency is likely to increase with hybrid systems. On a serious note however, the operating parameters affect the overall performance of the whole system with notable improvement in system performance within some range of the parameters.

Furthermore, an evaluation is done for a combined cooling, heating and power (CCHP) system, with the use of TEG and condensing heat exchanger to recover the exhaust gas waste heat from a 16 kW ICE (Wang et al. 2014). The results reveal that the primary energy efficiency of the system can go up to 94.4% with a cost saving ratio and primary energy saving ratio of 0.417 and 0.304, respectively. CCHP for long has been used with relatively good performance since the rejected heat is utilized for heating. However, with the application of TEG on CCHP, higher system performance is expected since even the mild waste heat is utilized for power generation.

From this section, we can observe that with the introduction of thermoelectric technology into heat transfer systems, the overall system performance increases because a significant amount of waste heat is recovered. As well, it can be noted that although solar energy has been utilized by using solar cells, solar PV as well as solar collectors, with the hybridization of the energy systems, the use of TEGs in the system improves the energy extraction and therefore increases the energy supply however little it may be.

2.4.4. Application of TEDs for power generation

Although thermoelectric technology is used for other heat energy conversion purposes, the emphasis in this section is solely highlighting the generation of electric power from heat using TEG. This is because for most of the TEG applications, the harvested or recovered heat is mainly converted into electrical energy. Recent developments of TEGs have mainly put emphasis on stand-alone power generation technology for biomedical, aerospace, military and remote power applications. Below is the list of some of TEG applications.

- Condition monitoring in industrial environments
- Smart metering
- Environmental monitoring in remote locations
- Structural monitoring
- The transport sector in vehicles, aircraft, and spacecraft (in hostile environments). Customized military and aerospace applications dominate the market.

2.4.4.1. Thermoelectric applications for power generation

Thermoelectric applications for electricity generation are divided into two main categories; low and high power generation applications.

1. **Low power generation**: TEGs are being developed as autonomous power sources to compete with batteries which are the most dominant source of stored energy in applications like body-mounted devices in the range of 5 μW to 1W and with 5 years life time. For example Citizen and Seiko are now manufacturing wristwatch with that of Seiko having efficiency of about 0.1%, open circuit voltage of 300mV at 1.5K temperature gradient (Hamid Elsheikh et al. 2014).
2. **High power generation**: some manufacturers including Volvo, Volkswagen, BMW and Ford are developing TEG systems with

generated power of about 1 kW. A TEG having a ZT of 1.25 and about 10% efficiency could be employed to recover 35– 40% of the power from the exhaust manifold at an average temperature of 250 ^{o} C where a considerable amount of power can be generated to contribute to up 16% increase in efficiency (Yu et al. 2015b).

2.4.4.2. Power generation with TEG using non-waste heat

Although TEG devices have found applications majorly in the waste heat recovery, they have also been used to generate electric power from other alternative sources of energy. For example TEGs are used to generate electricity from biomass, geothermal energy and solar energy to form stand-alone energy harvesting systems. Some of the progressive works on this development are reported here.

With the geothermal as a source of heat, electric power is generated using TEG modules (Bitschi 2009). The tools for evaluating TEG devices are developed in which the modelling is done on two levels. In the large scale level, a number of TEG modules are integrated in a heat transfer unit and a cross-flow heat exchanger is used. For the lower size level, the modules are modelled in 3D where the non-linearities and irreversibilities are simulated with the finite element method (FEM). The results show that selection of the geometric parameters should be a compromise between the highest power output and best efficiency as these quantities demonstrate opposing tendencies. Based on this study, it can be observed that geothermal energy can also be used as a heat source with low temperature and low energy density to generate electrical power using TEG which can be used in niche applications. This saves the use of wasteful technology like turbines with moving parts on already a low temperature heat source.

Another application of TEG is the generation of electricity using solar concentrators. Kossyvakis et al. note that the implementation of TEG in solar energy conversion systems, as an alternative method for exploiting the solar potential has attracted increasing attention (Kossyvakis et al. 2015a). They performed an analytical study on thermoelectric-based solar conversion unit using ANSYS software. They predicted electrical output from the system under various operating conditions, achieving maximum power output of 33.7 W. Similarly, a solar parabolic concentrator coupled to a TEM is used to generate electricity by using a BiTe-based TEM installed on the receiver plate (Lertsatitthanakorn et al. 2014). At maximum heat flux, a TEM has the ability to produce output power of 1.32 W at 0.42 m^3/min air flow rate which corresponds to a conversion efficiency of 2.89%. Therefore, a higher flow rate is suggested subject to the level of efficiency of the heat sink used in order to achieve higher power from TEG.

In a unique application, thermo-photovoltaic (TPV) cells are used to provide input heat to the TEG to generate electricity. TPV cells are capable of converting infra-red radiation into electricity. The TPV and TEG are cascaded, with TPV acting as a heat stream to supply the TEG which later converts heat into electricity (Qiu & Hayden 2012). Through analysing the electrical characteristics of the TPV cells and the TEG under various operating conditions, the results indicate that the cascading power generation is practicable and has the potential for some applications. Furthermore, a stand-alone biomass power plant that uses TEG to generate electrical energy from biomass is designed and tested (Bianchini et al. 2014). The test facility is intended to give a great deal of information about the integration of TEG devices with biomass power plant and to show the feasibility of having a stand-alone biomass power plant where the electrical energy generated is consumed directly by the load. Another study reports the estimation of power generated using TEG by harvesting heat from biomass fired thermal oil heater (Barma et

al. 2015). The TEGs are placed between flue gas duct and fresh air duct of an industrial thermal oil heatern where the results indicate that the estimated annual electrical power generation from this system is about 181,209 kWh.

Miranda et al. carried out a feasibility study on the use of TEC in an air conditioner for EV (Miranda et al. 2013). TECs were used as load, high power lithium-ion batteries as an energy storage device and dye sensitized solar cells (DSSCs) as energy source to form a solid-state air conditioner model. The dynamic performance simulation demonstrates that a solid-state air conditioning system is feasible in providing green energy from DSSCs through the use of TEC unlike traditional vapour compression air conditioning systems that consume substantial amount of energy which reduces the driving performance of an electric vehicle.

2.5. Thermoelectric modelling methods

Thermoelectric effect is the direct conversion of temperature difference into electric voltage and vice versa (wikipedia n.d.). The term "thermoelectric effect" embraces three separate effects: the Seebeck, Peltier, and Thomson. The Peltier, Seebeck and Thomson effects are thermodynamically reversible, whereas Joule heating is not. Joule heating occurs when an electric current flows through a resistance or a conductor and induces a temperature gradient in a microfluidic device (Ge et al. 2015). If it occurs in graphene or nanowire/nanotube element under a high current density, Joule heating affects mainly the electronic transport properties and henceforth is an important aspect of device design (Ravi Chandran 2015).

With the application of current through a thermoelectric element, thermal energy is generated or absorbed at the junction due to Peltier effect. The exchange of Peltier heat between the semiconductor and a metal (both the n- and p-type) is demonstrated in Figure 2.5 (a). Figure 2.5 (b) shows a

dimensional view of a TEC. The Seebeck coefficient is proportional to the temperature and this effect is different at different places along the thermoelectric material. The thermoelectric element is a combination of a series of many small Peltier junctions (as shown in dotted lines in Figure 2.5 a), each of which separately produces or absorbs heat. This is the Thomson power developed per unit volume. For Thomson effect, heat is evolved or absorbed when the current is passed through a thermoelectric element with a temperature gradient. Therefore, this effect is equally proportional to the temperature gradient and the electric current.

The Thomson coefficient τ is expressed as;

$$\tau = T\frac{d\alpha}{dT} \qquad (2.19)$$

Based on equation (2.19), the Thomson coefficient cannot be applied in situations where Seebeck coefficient is constant and calculated with the average temperature.

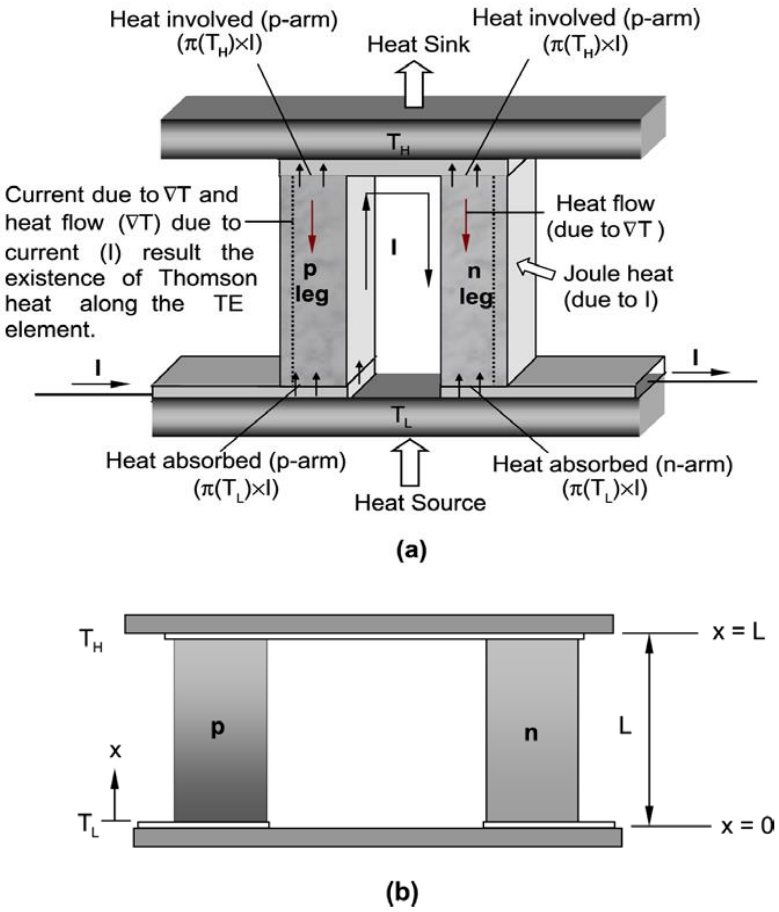


Figure 2.5. A schematic view of a TEC

Because of those thermoelectric effects which are subjected to the thermoelectric material, it is necessary to carefully analyse the performance of the thermoelectric device when subjected to different temperatures. This can be done by proper experimental setups or through the use of mathematical models. With the advancement in computer technology, several thermoelectric mathematical models have been incorporated into design software to analyse the performance of different prototypes before the actual implementation. With thermoelectric device analysis, there are basically two major categories of thermoelectric models: the simplified and the complex models.

2.5.1. The simplified thermoelectric models

The simplified thermoelectric models are derived based on the global balance of thermoelectric effects and heat transfer (macro approach) i.e. some of the thermoelectric effects are kept constant while others are neglected. For example in one instance the Seebeck effect is kept constant, rendering the Thomson effect to be zero or negligible (Fraisse et al. 2013). The simplified models include the standard simplified and improved simplified models.

2.5.1.1. Standard simplified thermoelectric models

Assuming the distribution of Joule effect between the hot and cold side to be symmetrical, the total energy balance is setup to formulate this model. It is mainly due to this popularly used assumption that the thermoelectric element is described in the thermoelectric heater (TEH) and TEC modelling. The heat flux convention in the thermoelectric leg used in the setup of the simplified model is shown in Figure 2.6.

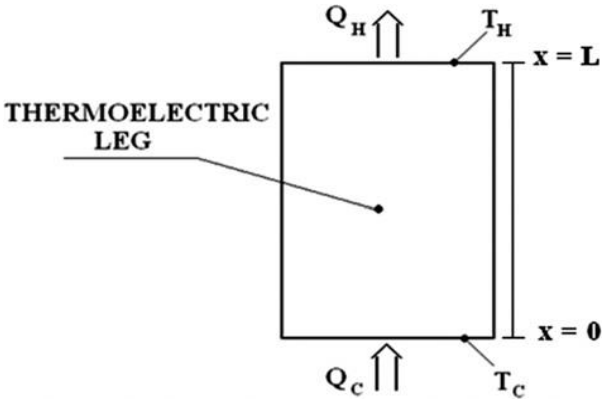


Figure 2.6. Heat flux convention in a thermoelectric leg

The electrical conductivity σ, thermal conductivity k, and the Seebeck coefficient α of thermoelectric element are held constant and calculated from the average temperature $\bar{T}$ of the cold and hot side temperatures T_C and T_H respectively, given as;

$$\bar{T} = \frac{T_H + T_c}{2} \quad (2.20)$$

This assumption is reliably applied in steady state as long as the Joule effect is kept to a minimum value. The variation of temperature in this case is a posteriori known, i.e. the variations have to be justified through experimental observations. The global energy balance therefore results into several equations for the heat fluxes for the thermoelectric element on the cold and hot side. In this study, the simulations are carried out based on the modified version of the standard simplified model as described in chapter 4.

2.5.1.2. Improved simplified thermoelectric models

In this improved version of thermoelectric model, the Thomson effect is considered (is never zero) and it's uniform distribution is ensured on the two sides of the semiconductor device. The model is found to have a notable improvement in terms of accuracy in prediction of various performance parameters in the TEC mode [4].

2.5.2. Complex thermoelectric models

Contrary to the simplified models, the complex models are those models in which the thermoelectric element behaviour is described more precisely with the use of local energy balance equations. This is because all thermoelectric effects are generated due to the bond between heat and charge transports. These transports are quantified based on the entropy, energy and mass equations which form the complex thermodynamic frameworks (Chakraborty et al. 2006).

The energy balance is expressed as;

$$\rho C_p . \frac{\partial T}{\partial t} = \nabla . (\lambda \nabla T) + \frac{(J)^2}{\sigma} - \tau J \nabla T \quad (2.21)$$

This equation is applied in a situation where heat and electric current flow parallel to each other from n- to p-leg or vice versa in the presence of an electric field. Lord Kelvin proposed a quasi-thermodynamic technique for thermoelectric effect to validate that $-\tau = \frac{\pi}{T} - \frac{d\pi}{dT}$ and $\tau = \alpha T$, where π is representing the Peltier heat.

Improved models have been applied in a number of research works in different thermoelectric applications. Three-dimensional transient modelling of TECs is done in which the model involves the analysis of the Thomson, Joule Fourier and Peltier thermoelectric effects (Meng et al. 2013). The results reveal that this model is able to predict the negative effect of the some of these thermoelectric effects. It is indicated that at a specific large current value, the heat transferred from hot to cold junction due to Fourier effect is observed to exceed the heat absorbed at the cold junction due to Peltier effect. This results into a high rise of temperature at both junctions, rendering the TEC to fail to reach the steady state. Through the use of exergy analysis, another improved standard model has been used to study the TEC (Kaushik & Manikandan 2015). The irreversible and exoreversible thermoelectric models are applied with consideration of Peltier, Thomson, Fourier and Joule effects at the junctions. The results demonstrate that the Thomson effect leads to the increase of the cooling power and efficiency of the TEC system for example the cooling power and energy efficiency increased to 16.36 W from 14.87 W and to 0.4998 from 0.4079 respectively for a temperature difference of 40 K after considering the Thomson effect in the exoreversible condition. It can be observed that the improved models are able to capture the effect of the other thermoelectric effect such as Thomson effect which are not catered for in the ordinary simplified model.

2.5.2.1. Analytical thermoelectric models

In this model type, an assumption is that the leg section and thermoelectric coefficients are constant along the length of the thermoelectric leg during the steady state condition and the Thomson effect is included.

2.5.2.2. Electrical analogy thermoelectric models

This model is also derived from the energy balance equation and assists in simplifying the modelling of complex problems for example the thermoelectric coefficients, non-constant leg section of the thermoelectric element and the transient regime (Fraisse et al. 2002) (Fraisse et al. 2010).

2.5.2.3. Numerical thermoelectric models

This model is implemented in software based on the energy balance where the numerical expressions of the thermoelectric effects are integrated. The steady state analyses in the thermal and electric fields are achieved using ANSYS software with the Newton–Raphson method. The advantage of this model is that it is appropriate for transient regime and for 3D geometries.

A reasonable number of research works have been carried out by using numerical thermoelectric models. In the aspect of thermal management, the study on improvement of thermal environment with TEC and numerical optimization of thermal performance is conducted (N. Wang et al. 2015). The Analysis shows that the maximum COP and minimum power consumed by TEC can be obtained with different optimum number of p-n couples, which is independent of electrical current across the TEC. Numerical simulations are also performed to analyze the temperature gradient and thermal stress of a TEG device (Wu et al. 2014). It is found that under a high heat flux imposed upon the hot end, the thermal stress is so strong that it has a decisive effect on the life expectancy of the device. Similarly, a numerical transient simulation tool

based on Transient System Simulation (TRNSYS) is used to assess and optimize a TEG system in real applications (Massaguer et al. 2014). This tool takes into account the whole energy system, and the designed TEG component is able to cope with both electrical and thermal dynamics. A mathematical model for simulating the electrical and thermal behaviours of a longitudinal thermoelectric energy harvester was additionally developed (Massaguer et al. 2015). A new TRNSYS component has been developed in order to implement the theoretical analysis and can be used as a design tool. In another work, a FORmula TRANslation (FORTRAN) computation program is used for numerical calculation in which a mathematical model of multi-element thermoelectric components connected in series is developed (He et al. 2015). The model considers internal and external irreversibilities as well as the temperature gradients along the flow direction. A 3-D numerical simulation and experimental analysis on turbulent flow of venting flue gas using TEG modules is also done (Jang et al. 2013). The numerical results for the power versus current are found to be in good agreement with the experimental data within an error of 9%.

2.6. Different structures of TEG units/Modules

In this section, we look at the TEG structure itself and how different modifications have been made in order to improve the TEG performance. The modifications are done by altering different TEG components, for example by stacking materials of different properties to form a segmented TEG device. First, the basic structure of TEG is highlighted followed by a detailed discussion of the progress on structural improvements.

2.6.1. The basic structure of TEG module

A TEG unit is primarily composed of an n-type and a p-type semiconductor. A number of TEG units are normally stacked to form a TEG module so as to produce the required power as illustrated in Figure 2.7. The n-type and a p-

type semiconductor TEG units are thermally connected in parallel and elecrically in series.

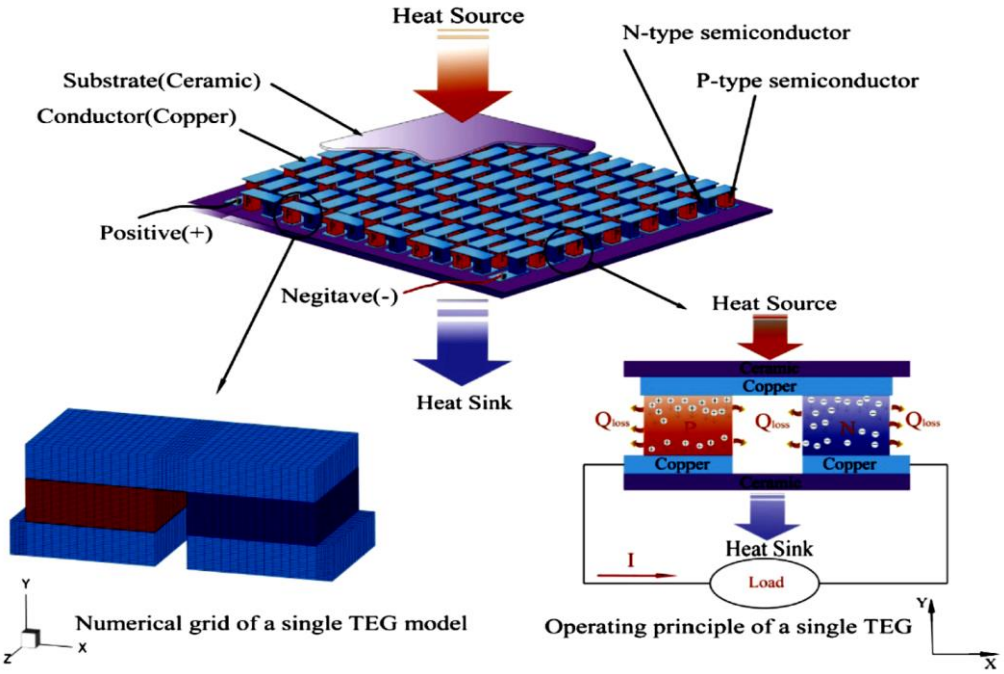


Figure 2.7. TEG setting for Power generation (Niu et al. 2015)

2.6.2. The modified structures of TEG module

With increased interest in TEG systems for different applications, research has been intensified, leading to the introduction of several advanced models into the TEG scenery. This has been done through various modifications of the basic TEG module in several ways such as hybridizing of the materials used to form TEG, geometrical modifications, etc. This has led to more improvements in the power output and efficiency.

2.6.3. Progress on TEG module structural improvement

Various TEG modules made up of different materials, design methodologies and thermal conditions have been reported in literatures. First to mention, a TEG is designed through numerical modelling and gradient-based optimization

with advanced multi-parameter. The TEG is made up of three segments each with a different material where a high power density material is used in the heat exchanger to enable thermal isolation in the direction of heat flow as shown in Figure 2.8 and Figure 2.9 (Crane & Bell 2006).

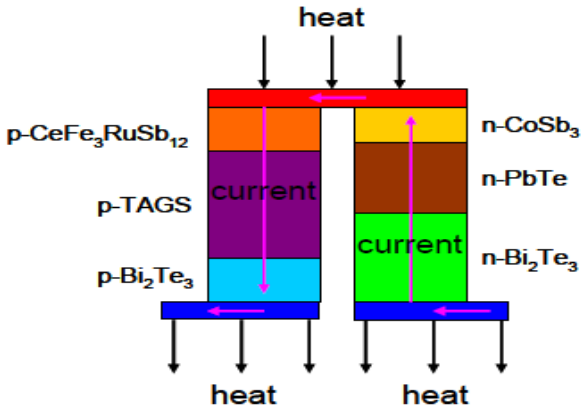


Figure 2.8. Traditional thermoelectric couple configuration with segmented elements

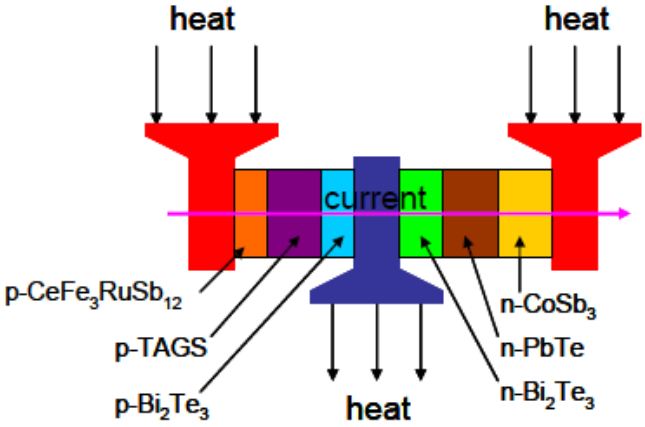


Figure 2.9. Alternative thermoelectric couple configuration with segmented elements of different total element thickness

Likewise a model is presented to determine the theoretical limit of electrical power generation that provides optimal electrical loading conditions for a given

exhaust stream and system configuration (Stevens et al. 2014). According to this study, ZT is not a sufficient parameter to describe system performance. Based on the predicted results, it was established that there is an optimum number of thermoelectric leg pairs that maximize the power extracted for any system and that adding more leg pairs beyond this optimum can reduce system performance.

In another study, an integrated thermoelectric device (iTED) is designed and tested, which consists of plates of p- and n-type semiconductor bonded on a highly electrical and thermal conducting inter-connector material with a hole through which a flow channel is drilled (Reddy et al. 2014). The iTED comprised of several elements connected thermally in parallel and electrically in series, where the top and bottom surfaces of the device are exposed to cold temperature whereas the flow channel walls contained a hot fluid.

In a different development, TEM architecture is designed with Bi_2Te_3 cells. The segmented TEGs are designed and manufactured with a counter-current arrangement of the hot and cold gaseous streams as well as a catalytic combustion chamber that ignites an air/fuel mixture (Bensaid et al. 2012). The designed TEG is able to accommodate a flexible electrical load and exhibits enhanced conversion efficiency due to improved thermal management.

Because of the fluctuations of the heat sources in industry, TEG system may experience these fluctuations, leading to poor power output and low efficiency. Therefore these fluctuations can be catered for to ensure a stable power output from the TEG system. Therefore, a novel TEG system with thermal switch is designed to address problem of instability of TEG power output (Gou et al. 2014). Results indicate that the thermal switch can efficiently decrease the temperature fluctuation and improve the output power and efficiency of the TEG system. (Gou et al. 2014).

The concept of thermoelectric self-cooling is introduced whereby a thermoelectric device can be cooled and the temperature controlled without consuming electricity (Martínez et al. 2011). The TEG is designed with an internal heat source and a usual cooling system is attached to the device to analyse its thermal performance. According to the results, thermal resistance between the heat source and the environment is reduced by 25 to 30% when the self-cooling concept is implemented. Robel et al. have studied the relationship between coolant flow rate and heat flux at heat source device to study the viability of self-cooling concept (Kiflemariam & Lin 2015). They found out that at an optimum flow rate of cooling fluid, the required temperature of the heat source is possible to be kept while at the same time providing power.

Thermoelectric power enhancement which is brought about by flow impeding panel “inserts” in a TEG's flow channels under the fixed thermal input conditions is investigated (Amaral et al. 2014b). This work is based on the advancements in TEG inner pipe flow optimization mainly to improve the conversion efficiency. The research tried to ensure TEG system’s ability to maintain an asymmetric thermal field across its component modules since this mechanism somehow determines the efficiency of the TEG device.

In another study, the columnar Cu film is found to be similar to parallel microchannel which can create some sort of channels for easy transportation of electrons and phonons in the thermoelectric device (Tan et al. 2014). The p-$Bi_{0.5}Sb_{1.5}Te_3$, n-$Bi_2Se_{0.3}Te_{2.7}$ and Cu films are fabricated by a magnetron sputtering method but the films are integrated into low-dimension cross-plane devices using mask-assisted deposition technology. The micro-device with densely columnar Cu film electrode is superior to those devices with ordinary structure electrode. For instance a typical device with 98 pairs of p-n couples, the output voltage and maximum power are up to 120.5 mV and 145.2 mW, respectively, for a temperature difference of 4 K.

The integrated thermoelectric devices (TEDs) which refers to the thermoelectric elements made of semiconductor plates laminated with a highly thermally and electrically conducting inter-connector are well investigated using fluid-thermo-electric coupled field numerical methods (Reddy et al. 2012). These are mainly made up of bulk crystalline n-type and p-type (Bi_2Te_3-Selenium) semiconducting materials with copper as a conducting material. At higher inlet fluid temperatures the increment in load resistance showed a significant change in the heat input value. The flow rate has been noted to cause a prominent effect on TED performance. It is recommended that the optimization of TED with flow channels can be done using fluid-thermo-electrical coupling field simulation. Alternatively, a composite thermoelectric device (CTED) that comprises of thermoelectric elements made of thermoelectric semiconductor materials bonded to highly electrically and thermally conductive material in a segmented fashion is investigated (Reddy et al. 2013). Compared to conventional TED with equivalent geometry, the CTED shows the ability of extracting more energy with heat recovery system.

2.6.4. Progress of TEG system improvement

Various studies have been carried out on the performance optimization of TEG as well as improvement of heat recovery efficiency. The optimizations of the configuration and layout of TEGs heated by exhaust gas are carried out (In et al. 2015). Figure 2.10 shows the layout of TEG module in a generator. As there is always a temperature difference between the rear and front ends of the generator, TEGs with different performance capabilities are installed in different positions where they would perform better. In the rear side where there is low temperature, HZ-14 modules are installed because they have lower operating range and therefore cannot produce good results if they are installed at the front side where the temperature is too high. Conversely, HZ-20 modules with higher operating range are installed at the front side where the temperature is high.

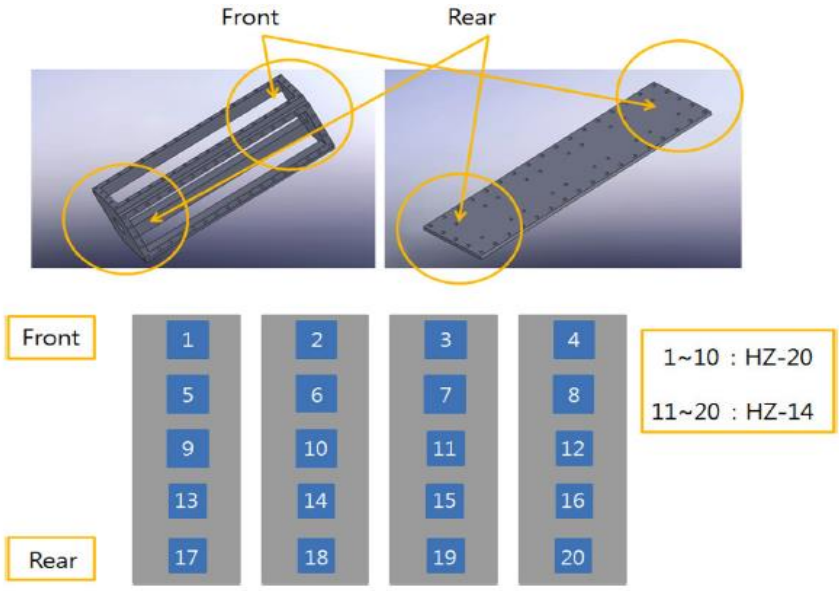


Figure 2.10. Schematic diagram of each module installation on TEGs (In et al. 2015)

Similarly, the performances of TEMs at various flow patterns, heating temperatures, flow rates of water and numbers of modules in series are studied (Chen et al. 2012). It is found that the effects of flow pattern of heat sink and water flow rate on the performance are insignificant, but the heat source or heating temperature plays an important role. Consequently, a lower water flow rate is suggested to minimize power consumption, while a higher hot side temperature leading to a larger temperature difference is suggested to improve TEMs performance.

The effect of temperature uniformity of the heat spreader on the TEG performance is studied (Admasu et al. 2013). The power output of the TEG with uniform temperature distribution is compared with that with non-uniform temperature distribution. The results demonstrate that the uniform temperature distribution over the heat spreader gives better results than the non-uniform temperature distribution.

Though most of the researchers concentrate on static placement of the TEG to improve the system performance, a novel rotating thermoelectric device is studied analytically while operating in periodic steady state in order to improve the energy conversion performance (Snarskii & Bezsudnov 2015). The rotating TEC device consists of a single thermoelectric conductor and operates in both the switching periodical mode (P-mode) in which the hot and cold ends of the thermoelectric conductor are periodically suddenly reversed, and the continuous sinusoidal mode (S-mode) in which the temperature of thermoelectric conductor edges varies continuously according to a sine wave. In addition to ZT, it is found that the cooling temperature and efficiency also depend on additional dimensionless parameters comprising of the rotation period, the size and the thermal diffusivity of the thermoelectric conductor.

A new TEG system based on liquid metal, used for harvesting waste heat is also designed and tested through a prototype which is a combination of commercially available TEMs with the electromagnetic pump (Dai et al. 2011). The maximum open circuit voltage of 34.7 V is attainable when the temperature of the waste heat source is 195.9 ^{o}C and the temperature gap between liquid metal heating plate and cooling water plate is about 100^{o}C while the efficiency of the TEG system is 2%. A two-stage TEG prototype for recovering waste heat from the vehicle exhaust gas is also investigated (Changxin Liu, Pan, et al. 2015). The two-stage TEG is found to generate a maximum output power of around 250 W at 473K hot side temperature whereas the thermal efficiency achieved is 5.35%, increased by 32% compared to 4.04% of single stage TEG in the same operating condition. Amaral et al. introduced mechanical methods to increase the thermal tension, driving the EMF responsible for thermoelectric power production (Amaral et al. 2014a). In this method, the flow impeding geometries are inserted into the flow channels of a liquid-to-liquid TEG which results into enhanced heat transfer near its embedded TEMs. In the end, the

thermal dipole across the modules is increased which consequently improves the overall power output.

Table 2.3 expresses the comparison of some of different TEG systems discussed above in terms of performance, outlining the TEG output voltage, maximum power and efficiency of each system.

Table 2.3. Comparison of different TEGs systems in terms of performance

TEG	Heat transport medium	Voltage (V)	Hot side Temperature (^{0}C)	Cold side temperature (^{0}C)	Temperature difference (^{0}C)	Maximum power output (W)	TEG efficiency (%)
Liquid metal based(Dai et al. 2011)	Liquid metal	34.7	195.9		100		2
GM200-71-14-16 type (Kossyvakis et al. 2015b)		2.74	200	30	170		5
Two-stage TEG (Changxin Liu, Pan, et al. 2015)	Vehicle exhaust gas	292 up from 200 for single stage TEG	199.85	29.94	170.25	248.49	5.35 up from 4.04 for single stage
HZQW and HZ20M (Karri et al. 2011)	Exhaust gas		562.8	76.61		453 and 140	8.53 and 2.25
Four-TEGs system (X Liu et al. 2015)		201.7	312	69		944	1.85

2.7. Methods of efficiency improvement of thermoelectric devices

The efficiency of thermoelectric device can be improved through various methods including proper matching of internal resistance of the thermoelectric device with external load, adjusting the boundary temperature and the number of TEG units, use of dc to dc converters etc. The performance and efficiency of thermoelectric conversion system can also be improved by minimizing the heat

losses to the ambient medium. A three-dimensional numerical model of TECs with consideration of coupling of temperature field and electric potential field is developed (Wang et al. 2012). The model is used to determine the performance of TEC with the temperature dependent thermal conductivity, Seebeck coefficient, and electric conductivity of semiconductor materials. The results indicate that the variable properties and the heat losses to the ambient gas have significant effects on the cooling capacity and the COP of the TEC.

2.7.1. Impedance matching

The usefulness of matching the TEG power output with the electrical load is demonstrated in the simulation and experimental work (Lesage et al. 2013). It is indicated that the internal resistance of the TEG module and the electrical resistance of the load have to be known to ensure load matching. For proper impedance matching, the optimal electrical load should be equal to the internal resistance of the TEG module in order to ensure that maximum power is transferred to the load. The normalized thermopower $P^* = P/P_{max}$ is defined as (Lesage et al. 2013);

$$P^* = \frac{4R_L^*}{(1+R_L^*)^2} \qquad (2.22)$$

Where $R_L^* = R_L/R_i$ stands for the normalized electrical load, R_L and R_i are the load and TEG module resistance respectively. A normalized power output curve is used to determine the optimal electrical load for peak power output under several working conditions. The curve is shown in Figure 2.11.

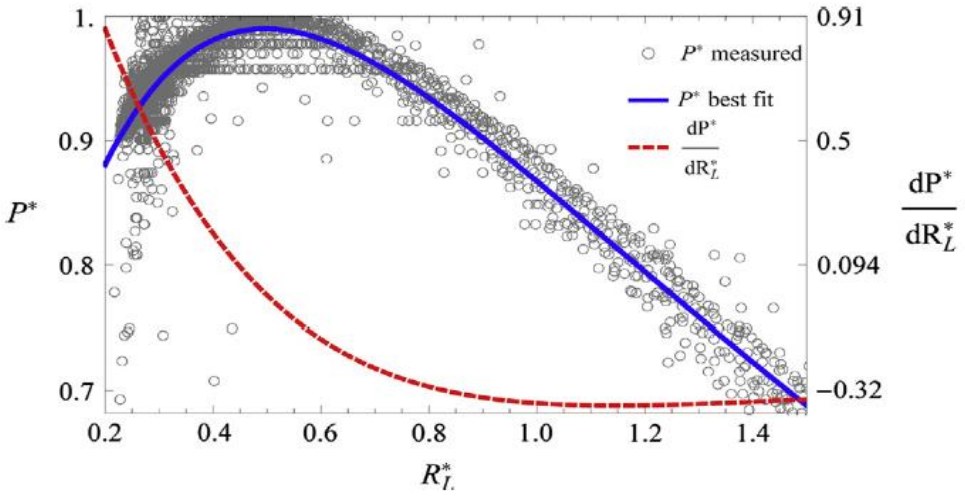


Figure 2.11. Normalized thermopower from all thermal conditions tested and its rate of change relative to the electrical load

The relatively large values of dP/dR_L^* are obtained prior to P = 1. This means that thermopower output is sensitive to small changes in load resistance in this region. After attaining a value of zero (0) near the maximum point, the dP/dR_L^* tends to a constant value. This implies that the thermoelectric power output is less sensitive to changes in electrical load when they are greater than optimal value. This method has some limitations which calls for the use of another method to improve the performance of TEG. By connecting the load directly to the output terminal of TEG, it is difficult get a stable output voltage without proper voltage regulation mechanism. It is also unlikely that the maximum power output can be extracted from the system as it is difficult to balance the internal resistance of TEG and the load resistance to ensure impedance matching.

2.7.2. Adjusting the boundary temperature and the TEG units

Several ways are suggested to improve TEG power output. One of them is to raise the hot side temperature and/or lowering the cold side temperature [66]. The aim of this is to widen the temperature difference on which the output from

TEG depends. An independent cooling system can be used to lower the temperature of the cold side as much as possible. However, for every type of TEG, there is limitation to the lowest and the highest junction temperature. Another method involves adjusting the number of TEG modules. Increasing the number of TEG units results into increase in TEG power output and vice versa. Similarly, there are limitations associated with this method. First, space where TEGs can be mounted in the heat pipe may be unavailable. Moreover, adding more TEG modules increases the cost of the system.

Because of the limitations associated with the above discussed methods, other alternative methods that involve proper use of the generated power from TEG can be applied to improve the performance of TEG. In order to further utilize the recovered heat, a method (Remeli et al. 2015) is introduced to recover heat not only for heating purposes but also for power generation using TEG. The results indicate that the proposed method can recover 1.345 kW of waste heat and generate 10.39 W of electrical power with 8 TEGs.

2.7.3. TEG power conditioning using DC-DC converters

To mitigate the problems associated with the above discussed methods, dc-dc converters are used. The dc-dc converters are capable of giving regulated dc voltage, step up or down the dc voltage and the maximum power can easily be extracted from TEG if the MPPT algorithm is used in conjunction with the converter. The dc-dc converter is an electronic circuit capable of converting from one source of dc voltage to another dc voltage. They are important in situations where a higher voltage is needed from a lower voltage level (boosting) or a low voltage is needed from a higher voltage (bucking). They are also applied to regulate the voltage from unregulated sources such as TEG devices, solar cells etc. Therefore, several configurations of dc-dc converters are available to suit different applications. Many of the readily available converters are designed to work under a (nearly) constant voltage source and

therefore their performance may not be as expected when connected to a variable current source like a TEG or PV system (Abusorrah et al. 2013). Therefore, the choice of a right converter affects the optimum performance of the whole system and therefore a proper criterion has to be followed to choose the best converter.

To give a big picture on the available converter architectures, Table 2.4 presents the the qualities and the implications of applying different dc-dc converters on TEGs.

Table 2.4. The qualities and implications of applying different dc-dc converters on TEGs

Converter	Features	Application	Advantage	Limitation
Boost	• Converts from a low voltage to higher voltage • Pulse width modulated (PWM) controlled • Load current smaller than the input current • Most commonly used • Middle and low level in the conversion network	• Suitable for TEG with unstable internal resistance and output voltage	• Precise and flexible conversion factor	• Requires a large Inductance to get high efficiency
Buck	• converts from a higher voltage to a lower voltage • PWM controlled			
Push-pull	• High level conversion of high power • Step up and step down tasks • Multiple outputs due to transformer isolation	• High power Application (range of kWs) • Fairly good efficiency	• Less likely to cause saturation than in the fly-back converter, • Hence smaller size.	• More complex • MOSFETs must be able to handle twice the input voltage

				• Used for low voltage applications
CUK	• Middle level conversion • Continuous output current • Can boost or buck the voltage	• suitable for sensitive environments	• Stable input and output terminal currents • Easy to cancel ripples • Emit less radio frequency (RF) noise	
Buck-	• Increase and decrease the output voltage • Load voltage is inverted			
Fly-back	• Increase or decrease the output voltage • Transformer is used • Multiple output can be obtained • Output energy is stored as magnetic energy and released to the load later.	• Where multiple outputs are required		

2.7.3.1. Use of dc-dc converter with MPPT

In an ordinary dc-dc converter, the switch is triggered by the use PWM signal. The duty cycle is normally adjusted to tune the required output voltage from the converter. However, with the change in the input to the converter, it is difficult to keep in touch with these changes to obtain the maximum power from the converter. With the use of MPPT algorithm, the maximum power can easily be tracked as the MPPT tracker is technically configured to respond to the changes in the input. The use of MPPT algorithm along with the dc-dc converter makes it possible to extract maximum power from TEG. The description of how the MPPT works can be accessed in (Ishaque et al. 2014a). The MPPT techniques may be grouped into two based on the parameter being monitored to achieve the tracking purpose: the first is based on voltage feedback and the

second is based on regulating the generated power. The method based on voltage feedback works in such a way that a predetermined reference voltage is compared with the voltage of TEG module in a feedback loop (Roshan & Moallem 2013). The second method is based on regulating the generated power by sensing the TEG voltage and current to track the maximum power point (MPP). Perturb and observe (P&O) and incremental conductance (IC) are the examples of this method. The MPPT functionality is normally integrated into the dc-dc converter to achieve higher power-extracting efficiency. The non-isolated dc-dc buck, boost, buck-boost, Cu´ k and Single-Ended Primary-Inductor Converter (SEPIC) converters have been assessed to find a converter that best suits an application with MPPT (Taghvaee et al. 2013).

A boost converter cascaded with a buck converter in a continuous MPPT mode is developed for conditioning the power generated from a TEG (Kim et al. 2008). Figure 2.12 shows the proposed system. The system is able to maximize the power while at the same time charging the battery. The MPPT employed in a boost converter makes use of P&O technique to ensure that maximum power is continuously extracted from TEG.

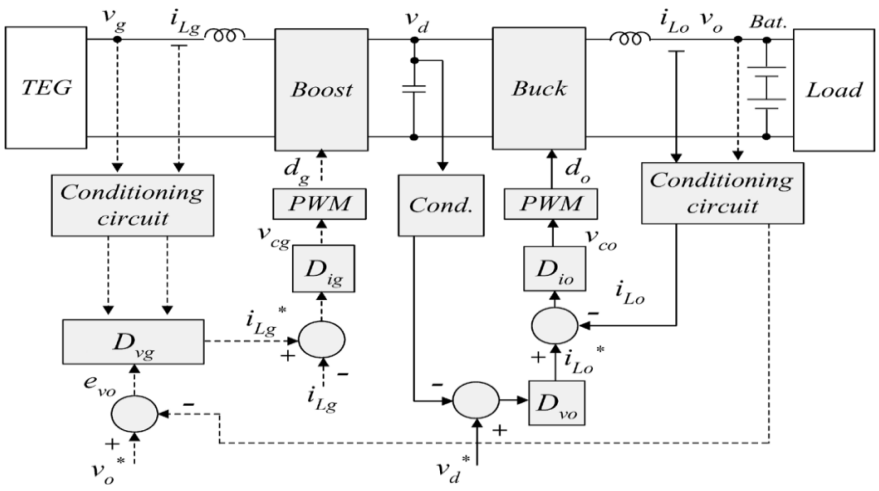


Figure 2.12. TEG power conditioning system MPPT controller (Kim et al. 2008)

The theoretical maximum power MPP is calculated to be 264.3 W at 35.5 A. When the load is reduced, the output voltage V_o reaches its level. The input current is reduced gradually, and the operating mode is changed to the power matching mode. The results reveal the stability of the proposed MPPT controller and output voltage regulation under load steps, source impedance variation and different dc link voltage commands. Alternatively, an MPPT for TEG to support a vehicle power supply is reported (Carstens & Gühmann 2015). This digital cascade controller for a boost-buck converter is used to charge a vehicle battery and supply the load. The tracking of the MPP is realized with a gradient algorithm and an input current control.

2.7.3.2. TEG output power regulation with dc-dc C´uk converter

Since its discovery, the C´uk converter has received much attention in power electronics research and industry. The main features that make it work well with TEG system is that the ripple amplitude can easily be reduced to a zero value by properly winding both the input and output inductor coils on the same core. This prevents the pulsating input from interfering with the voltage output of the converter, hence ensuring proper power conditioning of TEG power output. A basic C'uk converter is shown in Figure 2.13. The functioning of a C'uk is clearly reported in (Yu & Chau 2009).

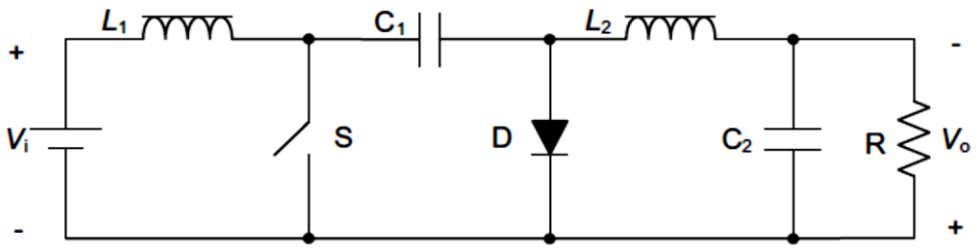


Figure 2.13. Basic C´uk converter

With TEG system, a dc-dc C´uk converter with MPPT is utilized to charge a battery. More stable output voltage is achieved with the use of this converter configuration.

2.7.3.3. MPPT control with C´uk dc-dc converter

MPPT control has been widely implemented in PV power systems, and its effectiveness in ensuring maximum extraction of power has been reported by various researchers. In addition to the classical P&O and IC MPPT methods, there are several MPPT algorithms including constant voltage and parasitic-capacitance techniques to mention but a few. As the TEG power system' voltage-current (V–I) characteristics is similar to that of a PV power system, P&O MPPT techniques used in PV power system can still be used for TEG system. So, this MPPT technique is proposed for use in the waste heat energy recovery system as shown in Figure 2.14.

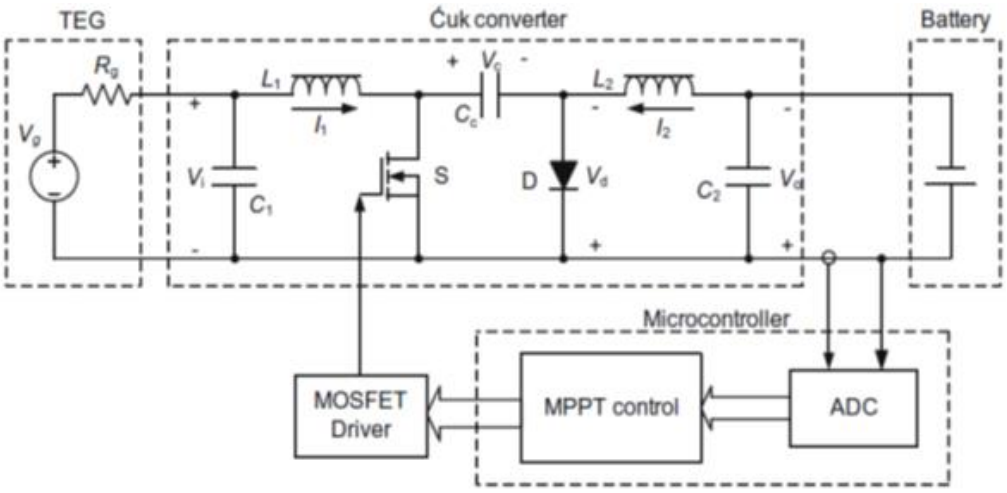


Figure 2.14. Power conditioning system based on C´uk converter with MPPT

The MPPT is implemented digitally with a microcontroller which is configured to detect and capture the feedback signals and a direct PWM signal is used to drive the power MOSFET. The MPPT is observed with good TEG performance

improvement because the power output is recorded to be increased to 22.6% with MPPT up from 14.5% without MPPT.

2.7.3.4. Distributed multi-section multilevel dc-dc conversion networks

Li et al proposed a network of dc-dc converters to be used in the regulation of power generated from TEG devices (Li et al. 2011). The thermoelectric-generator-based dc-dc conversion network is a distributed multi-section multi-stage network which is aimed to solve the problems facing the traditional single stage system for TEG application in EVs (Li 2011). The parameters of the network can be adjusted based on the needs of the intended application. Such parameters include the number of conversion levels, conversion locations, the number of TEG modules at each location and so on. The proposed network topology is shown in Figure 2.15.

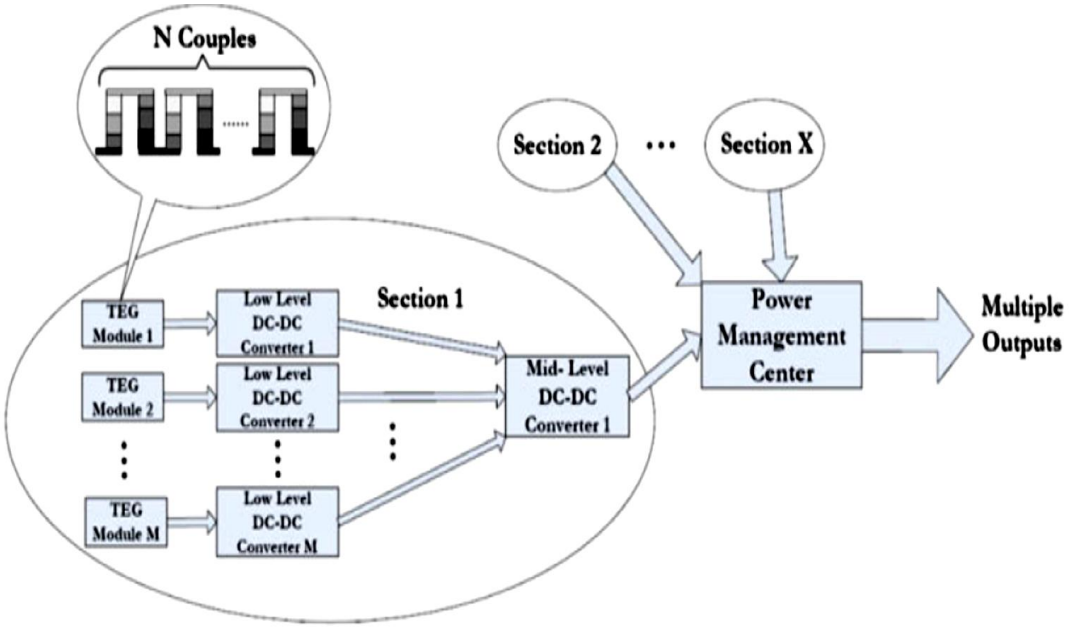


Figure 2.15. General topology of TEG based dc-dc conversion network (Li et al. 2011)

A relatively small voltage with a large current is obtainable from TEGs. However, many applications require high and more stable voltage supplies than the output level of TEGs. For an initial boost, the output of each TEG module is forwarded to a low level dc-dc converter. The outputs of all low level dc-dc converters in the same conversion location are then forwarded to a mid-level dc-dc converter for further voltage boost. There is a power management center with multiple outputs, which mainly consists of a high level dc-dc converter and it is responsible for the collection of the intermediate output voltage from mid-level converters. It is from this center that all the electronic systems (loads) on the vehicle are supplied with a stabilised power output. The advantages with this networked converter topology is that a high amount of heat is recovered due to multiple distribution of various TEGs within the system. It is also easy to designate a suitable TEG for a given location to ensure maximum efficiency and the system is less prone to faults, increasing its reliability. Interesting to note, the network topology increases the conversion efficiency up to about 400% as well as the matching efficiency of 99% with 200°C ~300°C temperature range at hot side.

2.7.4. Power conditioning using temperature sensor based MPPT

Another MPPT technique applied on TEG system is a temperature sensor based method with a tracking error of 1.15%. Significant amount of time is required for TEG systems to reach the steady state by the conventional MPPT methods. Unlike in conventional MPPT methods where complex microcontrollers are employed, in this case, the MPP tracking is based on the use of temperature sensors with inexpensive, stable and simple circuitry without measuring the instantaneous power implying that there is no TEG disconnection. The open circuit voltage characteristic of the TEG is used with respect to temperature gradient to produce a proper reference voltage signal which is maintained by the power converter at a given level such that the

maximum power can be harvested for a particular temperature (Park et al. 2014).

2.7.5. Other methods for TEDs performance improvement

In other efforts to improve the performance of TEG, the dollar/watt ($/W) value is used to indicate the device's practical use. Kim et al. presented a method of lowering a $/W value while keeping a reasonable power output by modifying the TEG device architecture (Kim & Kim 2015). The $/W means adjusting or reducing thermoelectric material consumption instead of increasing ZT to achieve higher efficiency. The power per volume of material however is proportional to the $/W, achieved by introducing the volumetric material cost. Only the cost of the thermoelectric material is considered and the results show that the $/W value can be reduced to about 10% while maintaining about 65–70% of the maximum possible power output with a constant ZT. A heat exchanger is used to recover heat from vehicle exhaust gas. A study (Lu et al. 2013) is completed by combining exhaust heat exchanger with muffler in the forms of 1-inlet 2-outlet, 2-inlet 2-outlet and the baseline empty cavity. The results indicate that the pressure drops of 1-inlet 2-outlet and 2-inlet 2-outlet are 165% and 318% more than that of an empty cavity for inlet temperature of 100 ^{o}C and mass flow rate of 131 kg/h. However, the pressure drops are 319% and 523% more than that of empty cavity for inlet temperature of 400 ^{o}C and mass flow rate of 156 kg/h, respectively for 1-inlet 2-outlet and 2-inlet 2-outlet.

Heat removal on the cold side of the generator, in order to achieve the required temperature difference, represents a serious challenge to the operation of thermoelectric devices. It is therefore suggested that enhancing heat dissipation on cold side is vital to improve power output. To address this challenge, a thermoelectric generation process coupled with methanol steam reforming for hydrogen production is proposed, a methanol steam reforming micro-reactor is heated with waste heat and coupled with TEG (F. Wang et al.

2015). Results show that the cold spot effect exists in the catalyst bed under all conditions and that in the micro-reactor, the temperature difference between the reforming and heating channel outlets decreases rapidly with an increase in the conductivity coefficient of thermoelectric material. Similarly, a dynamic model for waste heat recovery using TEG is developed to assess the influences of heat reservoir and heat sink (Gou et al. 2013). The dynamic response characteristics, such as maximum output power, system efficiency and cold and hot semiconductor surface temperatures, are studied. It is proven that enhancing heat dissipation on cold side is vital to improve power output whereas the fluctuation of hot reservoir results into rapid change of TEG output power, something undesirable.

2.8. Observations and recommendations for further research on TEDs

In this section some observations are highlighted from the literature review with regard to the current status of various aspects of thermoelectric technology including improvements and challenges.

On the thermoelectric materials, a tremendous improvement on ZT has been registered in recent years with ZT of more than seven reported. This is justified by the increased application of thermoelectric devices for heating and cooling which requires high ZT. Although several research works have been carried out to raise ZT in order to improve thermoelectric efficiency, a challenge of developing advanced thermoelectric materials with optimization of the conflicting properties for example increasing both ZT and power factor at the same time remains. This is because both ZT and power factor have to be increased to achieve a higher performance of TEG. Hence additional research is also necessary in this regard.

Furthermore, the miniaturization of thermoelectric devices has been made possible with increased thermoelectric material research. This has resulted into

the manufacture of micro thermoelectric devices which are used for different applications such as cooling of microprocessors, watches, micro medical equipment etc.

Thermoelectric technology has seen increasing applications in recent years due to increase in research. Although TEG devices were primarily being used for waste heat recovery, based on the discussion, it has been observed that they are now applied for harvesting of biomass, geothermal, solar and others. However, the main challenge is due to the low efficiency of thermoelectric devices, making them less competitive for use in specific applications. Therefore, more research is necessary to improve the efficiency of these devices in order to further boost and diversify their application.

Several modelling techniques are being used to analyse thermoelectric effects in order to come up with more efficient thermoelectric devices. It can be noted from the discussions that numerical methods are the most popular methods used in the design and analysis of thermoelectric effects. On the other hand, although the simplified methods are easy to implement, they are criticised for less representing some of the thermoelectric effects like Thomson effect. This makes the designed thermoelectric devices to perform less than predicted and therefore affect the overall efficiency of thermoelectric based products. With the increase in computer technology, more research is necessary to further implement the thermoelectric models in computer programs thereby improving the accuracy of predictions for thermoelectric device performance.

Thermoelectric device leg geometries such as leg length, shape and area are stated to be one the physical parameters (geometric features) that affect the performance of the TEG. In this review, we have presented several works in which it is generally concluded that the varying leg geometries significantly affect the TEG power output and result into different sizes and distribution of thermal stresses in the leg. Additionally, the geometric features have some

effects on thermoelectric properties of some thermoelectric elements like silicon nanowires where it is reported that the decrease in size and change in the shape of the silicon nanowire results into a significant increase in ZT, hence improving the performance of the thermoelectric device. Therefore, more research is necessary to ascertain the geometrical requirement of the thermoelectric element based on the type of material used.

The Joule effect, carrier density and Seebeck coefficient (that determines the Thomson effect) are some of the nonphysical performance parameters of the TEG. However, in some thermoelectric device analysis, these parameters are neglected resulting into under/overestimation of the TEG power output. To mitigate this problem, several complex thermoelectric models have been suggested by researchers such as transient thermoelectric model, numerical models and electrical analogy model that put into consideration of these effects. Unfortunately, some of these models like electrical analogy according to this study, have not been widely utilized. Therefore, the application of these models can improve the performance prediction of thermoelectric devices.

In recent years, the efficiency of thermoelectric devices has improved greatly due to thermoelectric material and device geometrical improvements. However, TEG/TEC efficiency is low, being a subject of further research for more improvement. In particular, to improve the performance of the overall TEG system, several power conditioning methods have been proposed and analysed. It can be observed that dc-dc converters are able to provide a more stable power output and improve the efficiency of TEG system. However, to facilitate better performance improvement, several MPPT methods can be applied to extract the maximum power from TEG system. Therefore, more research is necessary to test the performance several converter topologies with the available MPPT techniques on TEG system, especially those which are already tested on PV systems.

To further improve the performance of TEG/TEC, different structures of thermoelectric devices have been reported. Thermoelectric performance improvements have been demonstrated mainly by; the segmentation of different thermoelectric materials to form TEMs, the design of an integrated thermoelectric device (iTED) with respective alternating thermal and electrical connections in parallel and series as well as the introduction of a thermal switch to decrease the temperature fluctuation. Therefore, more TEG/TEC structural improvements should be a subject of research to advance the improvement of the overall performance and efficiency.

2.9. Summary

In this Chapter, a comprehensive literature review of thermoelectric technology encompassing the materials, applications, modelling techniques and performance improvements has been carried out. The literature review has covered a wide range of topics related to thermoelectric technology including the output power conditioning techniques especially dc-dc converters. It has been demonstrated that the increasing research into thermoelectric technology has led to an outstanding increase in the value of ZT, making the use thermoelectric devices in diversified application possible. The design of integrated thermoelectric devices and the increased thermoelectric material research as well as device geometrical adjustment have greatly contributed to thermoelectric device performance improvement. The use of advanced thermoelectric mathematical models which have facilitated appropriate segmentation TEMs using different materials, notwithstanding the use of several power conditioning methods more especially dc-dc converters have also played a significant role in improving the overall performance of TEG in terms of power output, stability of voltage and improved TEG systems efficiency. Thermoelectric devices have registered increased usage in many applications such as; in cooling, heating, power generation and hybrid applications. Notable applications of TEG/TEC devices to recover heat energy

from geothermal, biomass, infra-red radiation, have been observed in addition to the primary use of thermoelectric devices for waste heat recovery. Nevertheless, the main challenge remains in designing and optimizing advanced thermoelectric materials with appropriate values of ZT and power factor, calling for more research work into thermoelectric technology. Nonetheless, several power conditioning methods have been proposed and analysed to improve the performance of TEG system. It has been observed that dc-dc converters are able to provide a more stable power output and improve the efficiency of TEG system. However, to facilitate better performance improvement, several MPPT methods can be applied to extract the maximum power from TEG systems.

Chapter 3. Research Objectives and Methodology

This chapter presents the problem statement, research objectives, scope and the methodology for executing the research on TEG/converter systems during the period of study.

3.1. Problem statement

There are several challenges surrounding TEG systems which call for more research to address them. The figure of merit and the efficiency of TEG are particularly low, and consequently these devices have been applied only in niche applications. In recent years, the efficiency of thermoelectric devices has improved greatly due to thermoelectric material and device geometrical improvements. However, more efforts are necessary to improve TEG devices' efficiency and the overall performance of TEG system. In particular, to improve the performance of the overall TEG system, several power conditioning methods can be applied to contribute to this effort. The dc-dc converters have the abaility to stabilize the power output and improve the performance of TEG system. However, to facilitate better performance improvements, several MPPT approaches can be applied to extract the maximum power from TEG system. Therefore, more research is necessary to test the performance of several converter topologies together with the available MPPT techniques on TEG system, especially those which are already tested on PV systems.

3.2. Aims and objectives of the research

The main objective of the research carried out in this thesis is to analyse the performance of dc-dc converters with or without Maximum power point trackers (MPPT) in conditioning the power generated from TEG devices. This leads to the following specific objectives;

1. To analyse the performance of TEG/dc-dc boost converter system by applying the simplified TEG model to demonstrate the converters' ability to stabilize the power from TEG.
2. To propose, study and compare the performance of different MPPT algorithms in harvesting the maximum power from TEG system.
3. To analyse the parameters that affect the performance of TEG/dc-dc converter system with respect to different converter operating modes and different loads.
4. To propose and examine a power conditioning concept that can help to reduce the power quality challenges in the TEG system.

In power system, power quality is concerned with voltage quality and current quality. Voltage quality is refers to the deviation of the voltage from the ideal. The ideal voltage is a single signal of constant amplitude and frequency. On the other hand, Current quality is the complementary term to voltage quality: it is concerned with the deviation of the current from the ideal. The ideal current is again a single-frequency signal of constant amplitude and frequency, with the additional requirement that the current sine wave is in phase with the voltage sine wave (Bollen 2003). Power quality disturbances in power systems can be grouped into: Voltage Imbalance, transients, Long-Duration Voltage Variations, Short-Duration Voltage Variations, Waveform Distortion, Voltage Fluctuation and Power Frequency Variations (Huang & Jiang 2017).

3.3. Scope

Although, thermoelectric devices are faced with a multitude of challenges, research shows that thermoelectric technology has received much attention and that several methods have been employed to address these challenges. The ways of combating these challenges can generally be grouped into two categories. The first category comprises of those techniques that pertain the adjustment of the device structures and the associated device parameters,

which are called *Device-level TEG improvement methods*. The second category involves proper harvesting and utilization of the power generated by applying TEG devices, which is referred to as *External TEG improvement techniques*. Device level TEG improvement methods involve modification of the structure of TEG module for example by geometrical modifications, TEG material improvements such as hybridizing of TEG materials where some TEGs are made of three segments, each with different material type etc. External TEG improvement methods include TEG system improvement by; impedance matching, adjusting the boundary temperature conditions, variation of the number of TEG units and the use of output power conditioning methods, particularly the application of dc-dc converters. The research work conducted in this thesis mainly concentrates on external improvement techniques to examine how TEG system performance can be improved.

3.4. Modelling of TEG/converter system

To study how the external methods can be utilized to improve the performance of TEG devices, it is necessary to have a model representing the functionality of the real TEG device with input and output parameters. Therefore, MATLAB/Simulink has been used as a software tool to build the TEG model to analyse its performance analytically.

The model utilized in this research is a simplified model modified from previous research work. The previous model had some redundant parameters that affect the speed of model computation while running the simulations. In the current research, th model has been modified to improve its performance. A simple TEG model is used mainly because the research study is only limited to external TEG improvement methods and the performance comparison among them. Therefore, there is no need of using a complicated model with a great deal of parameters at the TEG device level, since various researches and textbooks have already covered these study areas.

3.5. Experimental work methodology

Selected dc-dc converters together with associated components were identified and procured from the market. The rig was setup in the laboratory for testing using laboratory measuring instruments as described in Chapter 8. Experimental tests were performed in the laboratory at the Univeristy of Nottingham, UK to assess the practical performance of TEG system and proposed converter design.

Chapter 4. Conditioning of TEG power using dc-dc converters

One of the challenges behind TEGs is that they have low efficiency due to low figure of merit. Moreover, the power generated is unstable and therefore needs proper power conditioning mechanism before it is connected to the load. The objective of this work is to analyse the performance of a TEG/dc-dc boost converter system. The simplified model has been used as the basis of TEG design. Results indicate that the converter is able to stabilise and boost the voltage and higher efficiencies are achieved at different hot side temperatures.

4.1. Introduction

To improve the performance of the overall TEG system, several power conditioning methods have been proposed and analysed (Abusorrah et al. 2013) (Li et al. 2011) (Park et al. 2014). It is observed that dc-dc converters are able to provide a more stable power output and improve the efficiency of TEG system. The purpose of this work is to analyse the performance of a TEG/dc-dc boost converter system.

4.2. Power conditioning and efficiency improvement of TEG

The voltage-current characteristics as well as power of TEG devices are nonlinear and therefore it is quite necessary to recondition their power output before it is supplied to the load. Additionally, in view of the application of TEG devices to serve specific loads, the generated voltage and power are unstable because the heat source from which the temperature difference is acquired to activate the Seebeck effect is itself unstable and nonlinear. Therefore, a power conditioning mechanism is necessary to stabilise the output power and boost the voltage to the desired level before the intended load is supplied. The use of dc-dc converters serves this purpose. The boost converter is typically used to boost or step up voltage to reuired level.

Several methods are reported which can be applied to stabilise the voltage and current generated from TEG, thereby enhancing the efficiency of the whole TEG system. These include; impedance matching technique. The usefulness of matching the TEG power output with the electrical load is demonstrated in the simulation and experimental work (Lesage et al. 2013). The second method involves the adjustment of the boundary temperature of TEG units. In this method the TEG power output can be improved by raising the hot side temperature or lowering the cold side temperature. An independent cooling system can be used to lower the temperature of the cold side. Alternatively, the hot side temperature can also be increased but this is limited to a certain level. The third technique involves increasing the quantity of TEG modules although the number of TEG modules is also limited by several factors. All these other methods that involve adjusting the heat source and TEG device parameters can help in controlling the quantity of TEG output power but cannot be used to stablise the output power as desired by the connected load since the heat sources from which waste heat is recovered such as for vehicles is naturally non-linear. Hence, dc-dc converters are still necessary to stabilize the generated power from TEG.The dc-dc converters are electronic circuits capable of converting from one source of direct current (DC) to another DC voltage. They are important in situations where a higher voltage is needed from a lower voltage level (boosting) or a low voltage is needed from a higher voltage (bucking). They are also applied to regulate the voltage from unregulated sources such as TEG devices, solar cells etc. Therefore, several configurations of dc-dc converters are available to suit different applications. Many of the readily available dc-dc converters are designed to work under a (nearly) constant voltage source and therefore their performance may not be as expected when connected to a variable current source like a TEG or PV system (Abusorrah et al. 2013). Therefore, the choice of a right converter affects the optimum performance of the whole system and therefore a proper criterion has to be followed to choose the best converter.

4.3. DC/DC converters performance features

The performance features of the dc-dc converters are described as follow:

a). Source impedance and converter impedance: The physical arrangement of the TEG module (whether in series, parallel or both), determines its source resistance. To ensure maximum transfer of power generated from the TEG, it is necessary to ensure that the source resistance is clearly matched with the converter impedance such that high converter efficiency is achieved (Shawwaf 2010).

The input impedance of the converter is dependent on the source resistance which and on the output impedance.

b). Input impedance of the converter: The converter' input impedance Zc is defined as;

$$Z_c = \frac{V_{in}}{I_{in}} \qquad (4.1)$$

Where V_{in} is the input voltage to the converter and I_{in} is the input current.

So the voltage at the converter terminal will be lower than the voltage at the source (TEG) due to the voltage drop caused by the source resistance. Hence the source resistance should be kept as low as possible. Figure 4.1 illustrates the relationship between the TEG, converter and load parameters.

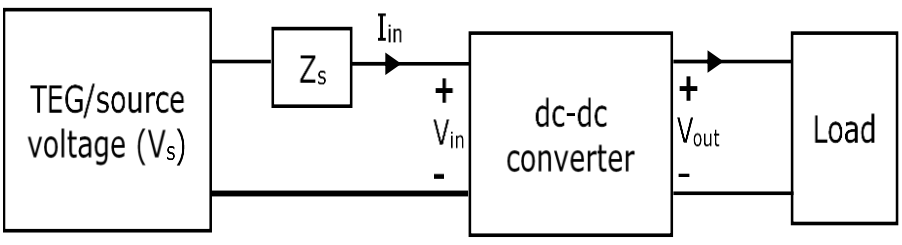


Figure 4.1. The relationship between the TEG, converter and load parameters

c). Source efficiency: The efficiency of the source will be;

$Eff_S = \frac{V_{in}*I_{in}}{V_s*I_{in}}$, Implying that;

$$Eff_S = \frac{V_{in}}{V_s} \quad (4.2)$$

The converter efficiency is defined as;

$$Eff_{Conv} = \frac{V_{out}*I_{out}}{V_{in}*I_{in}} \quad (4.3)$$

In other cases, if losses are included, the converter efficiency is expressed as (Kavitha & Jeyakumar 2012);

$$Eff_{Conv} = \frac{P_{out}}{P_{out}+Converter\ losses} * 100 \quad (4.4)$$

Where $P_{out} = V_{out} * I_{out}$ is the output power of the converter. The converter losses can be minimized depending the design and mainly due to the main MOSFET switching time. The current I_{in} is;

$$I_{in} = \frac{V_s - V_{in}}{R_s} \quad (4.5)$$

The efficiency is within the range of 75% to 95%. Combining (4.3) and (4.4);

$I_{in} = \frac{V_{out}*I_{out}}{V_{in}*Eff_{Conv}}$, from which;

$$V_{in} = \frac{V_s}{2} \pm \sqrt{\frac{V_s^2}{4} - \frac{V_{out}*I_{out}*R_s}{Eff_{Conv}}} \quad (4.6)$$

Hence, from equation (4.2), the source efficiency is finally expressed as;

$$Eff_s = \frac{1}{2} \pm \sqrt{\frac{1}{4} - \frac{V_{out}*I_{out}*R_s}{Eff_{Conv}*V_s^2}} \quad (4.7)$$

d). The Bistability condition: The bistability of the converter means that the converter's efficiency is very low due to two working points. This may occur when the source resistance is high. Bistability resistance is defined as;

$$R_{BIS} = \frac{Eff_{Conv} * V_{min} * (V_s - V_{min})}{P_{out}} \quad (4.8)$$

The bistability condition sets the lowest value of the voltage V_{min} for the working range of the TEG. With improvement in the quality of the TEG material, the bistability reduces, otherwise the resistance R_{bis} has to be computed in each case. However, this problem can be minimized by setting a minimum number of TEG units in parallel.

4.4. The proposed TEG power conditioning system

The proposed TEG power conditioning circuit consists of three main components; the TEG, the dc-dc converter and the PWM signal generator. Figure 4.2 shows a block diagram of the proposed circuit.

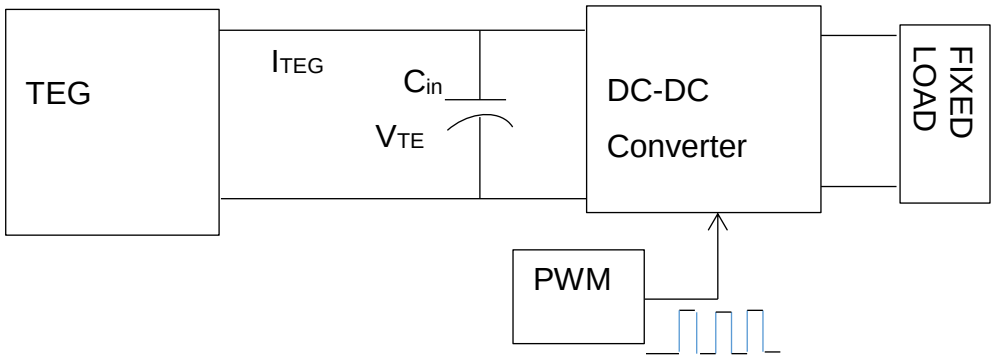


Figure 4.2. Block diagram of the proposed TEG Power conditioning system

4.4.1. TEG modelling

Because of the existence of such thermoelectric effects in a sole thermoelectric element that affect its performance, it is necessary to consider these effects in the modelling process to achieve a more accurate prediction of performance of

thermoelectric devices. In this regard, several models have been proposed including the standard simplified models in which the Seebeck coefficient is held constant and hence the Thomson effect is zero (Fraisse et al. 2013). The simplified TEG model can generate the voltage and internal resistance parameters as the output. This is very important especially when modelling thermoelectric device in conjunction with dc-dc converters which require voltage and current as input parameters to analyse the converter performance. Therefore, the simplified model is used as the basis for designing the TEG model. The complex TEG models can also be used in the modeling especially if the device level TEG improvements methods are being considered such as the adjustment of device geomery. However, this research work concentrate more on external improvement methods to stablize and improve the untilization of energy generated from TEG. Hence, for simplicity, the simplified model is used rather than the complex models since the output voltage and power of simplified models have similar trends as those of the complex models; the main difference in the magnitude of the output parameters as it is demonstarated in chapter 7 during model verification. In this study, the version of TEG device used in the simution is a TEG1-12611-6.0 TEG module. The module specifications are shown in Table 4.1.

Table 4.1. Specifications of the TEG module

Hot side temperature (^oC)	300
Cold side temperature (^oC)	30
Matched load output voltage (V)	4.2
Matched load output current (A)	3.4
Matched load resistance (Ohms)	1.2
Matched load output (W)	14.6
Open circuit voltage (V)	8.4
Heat flow across the module (W)	Approximately 365
Heat flow density (Wcm^{-2})	Approximately 11.6
Alternative Current (AC) Resistance measured at 27^oC at 1000 Hz (Ω)	0.5 – 0.7

The TEG is modelled based on the concept of simplified model in which some thermoelectric effects are ignored (Twaha et al. 2016). This is done for simplicity although there is reduced accuracy. The following equations are used to design the model;

$$Seebeck\ coefficient\ (S) = \frac{2V_{match}}{\Delta T_{sp}} \quad (4.9)$$

$$temperrature\ difference\ (\Delta T) = T_h - T_c \quad (4.10)$$

For TEG made of two semiconductor components, the output voltage of TEG is expressed as (Lv et al. 2016);

$$V_{oc} = (\alpha_p - \propto_n)(\Delta T)(N_{TEG-s}) \quad (4.11)$$

For TEG made of a single semiconductor type, V_{oc} is given as;

$$V_{oc} = (N_{TEG-s})(\Delta T)(S) \quad (4.12)$$

$$R_{int} = m\left[\frac{T_h+T_c}{2}\right] + n \quad (4.13)$$

Where α_p and $\propto_n$ are the Seebeck coefficients of the p- and n-type materials of TEG respectively; S is the Seebeck coefficients of a single material for TEG; V_{match} is the matched load voltage, ΔT_{sp} is the temperature difference of the measurement stated in TEG datasheet, T_h and T_c are the hot and cold side temperatures of TEG respectively; N_{TEG-s} is the number of TEG modules, R_{int} is the TEG internal resistance, *m* is the TEG internal resistance vs TEG temperature (R_{int}-T) curve slope and *n* is the R_{int}-T curve intercept;

The TEG model internal resistance R_{int} and the open circuit voltage V_{oc} vary in real time with temperature. The real time values of V_{oc} and R_{int} are mapped to the controlled voltage source and variable resistance respectively in the

converter to generate its input voltage and current (Li 2011). The model is designed with time-varying hot side temperature and a constant cold side temperature. It is masked to input other parameters included in the datasheets of practical TEG module from different manufacturer including V_{match}, $N_{TEG\text{-}s}$, ΔTsp, *m* and *n*. So the results of the model can be compared with the practical results of manufactured TEGs if experiments are carried out. Figure 4.3 shows the simplified model from the previous study (Li 2011).

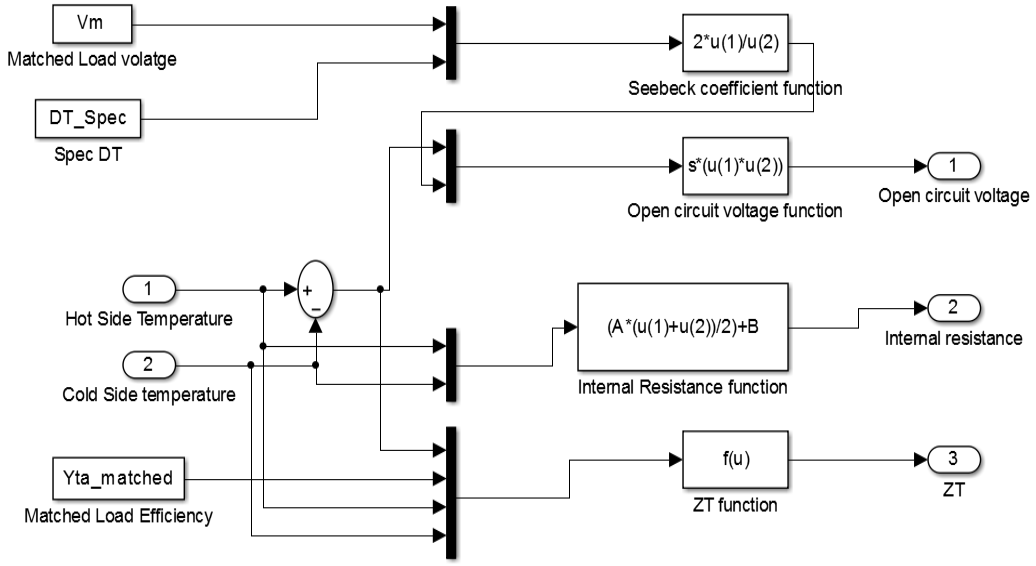


Figure 4.3. The simplified TEG model from the previous study (Li 2011)

In the research carried out in this thesis, the above TEG model has been modified by removing the matched load efficiency and the ZT function since these parameters are not considered. Hence the modified simplified TEG model is shown in Figure 4.4.

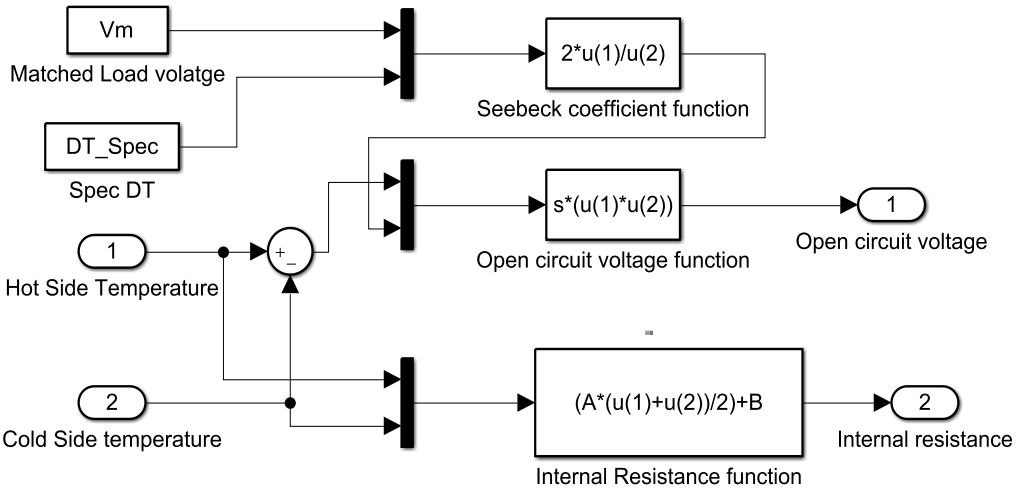


Figure 4.4.The modified simplified TEG model

4.4.2. Principle of operation of a dc-dc converter

A classical boost converter can take a low voltage for example 10 V, as input and step it up or boost it to high voltage say, to 15 V. Figure 4.5 shows a classical boost converter with a 10 V source as its input voltage.

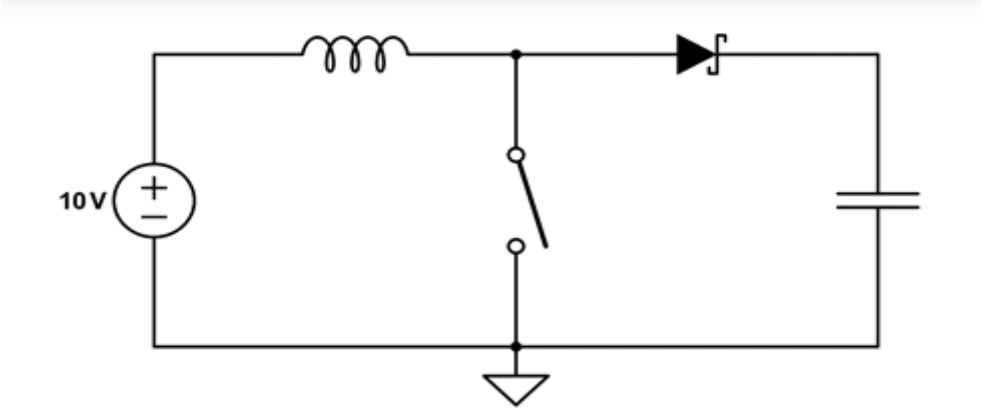


Figure 4.5. A classical boost converter equivalent circuit

Figure 4.6 shows how the boost converter operates to boost the voltage.

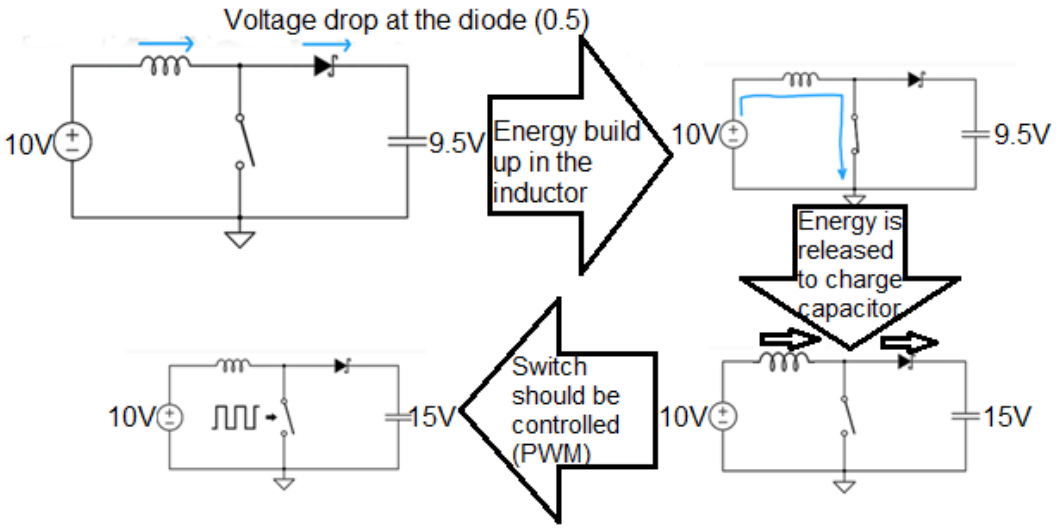


Figure 4.6. The working principle of a boost converter

When the switch is open, the output capacitor get charged to 9.5 V. So far, the voltage has dropped due to the voltage drop across the diode since it has some internal resistance. When the switch is closed, the diode prevents the capacitor from discharging, so the output stays at 9.5 V. But now we have a current path, from the source, through inductor and the switch to the ground. The switch is closed for a fraction of a second just long enough to allow some current flowing throw the inductor. This leads to the energy to be stored in the inductor in form of magnetic field. When the switch is opened and since the current in the inductor does not change instantly, current has to flow through the inductor and the diode into the output capacitor. Hence, the energy gets transferred from the inductor through the diode to the output capacitor and the voltage increases. The boost converter has now boosted or stepped up the voltage. Since the switch is not supposed to be closed for very long, it should be controlled with a high frequency pulse modulated wave (PMW). The boost converter circuit implemented with direct PWM signal is shown in Figure 4.7.

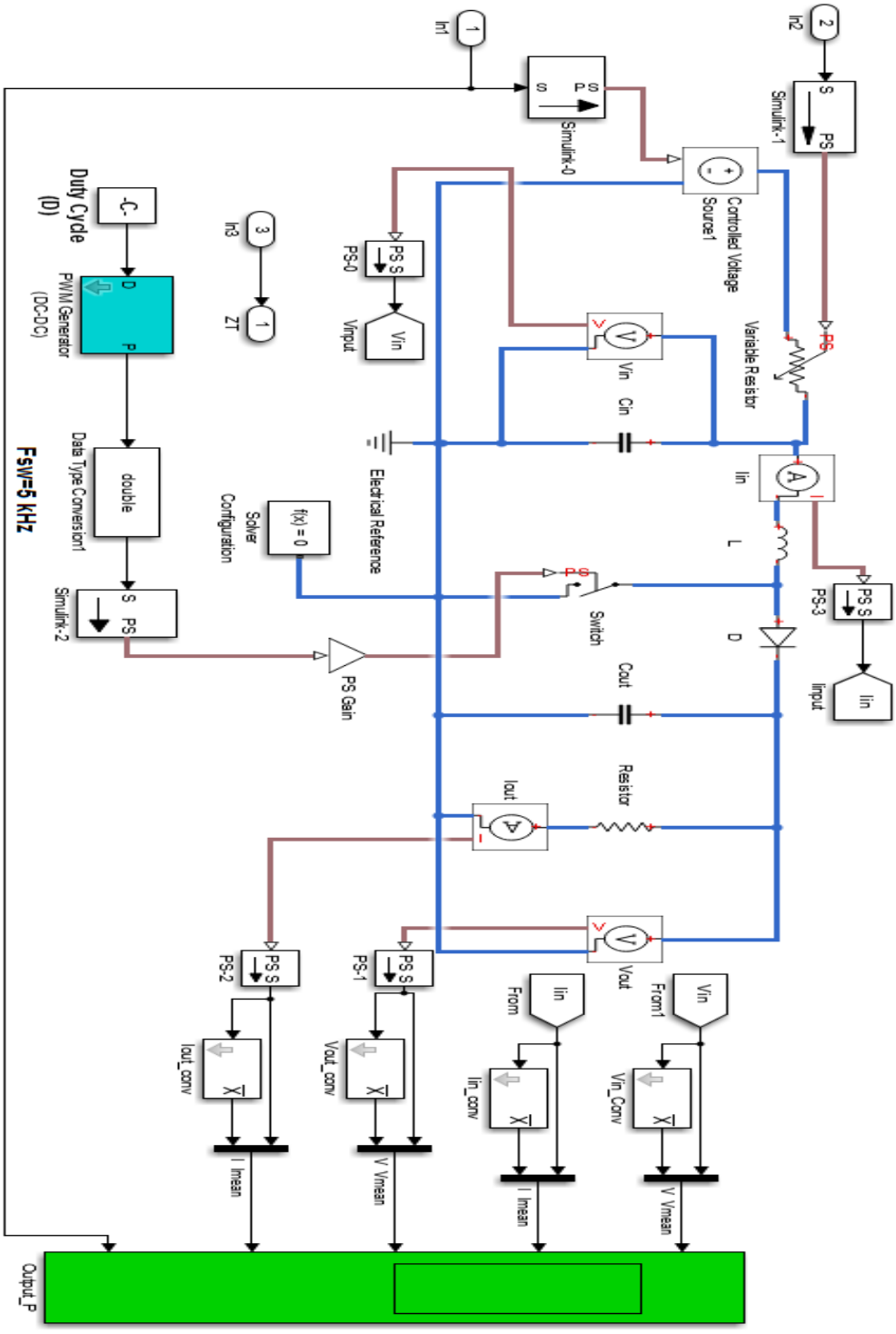


Figure 4.7. Boost converter circuit implemented in Simulink: with direct PWM signal

4.5. Results and discussion

As indicated earlier, the modelling is performed in Simulink. So, Figure 4.8 shows the modelled circuit in Simulink from which the results are obtained for analysis.

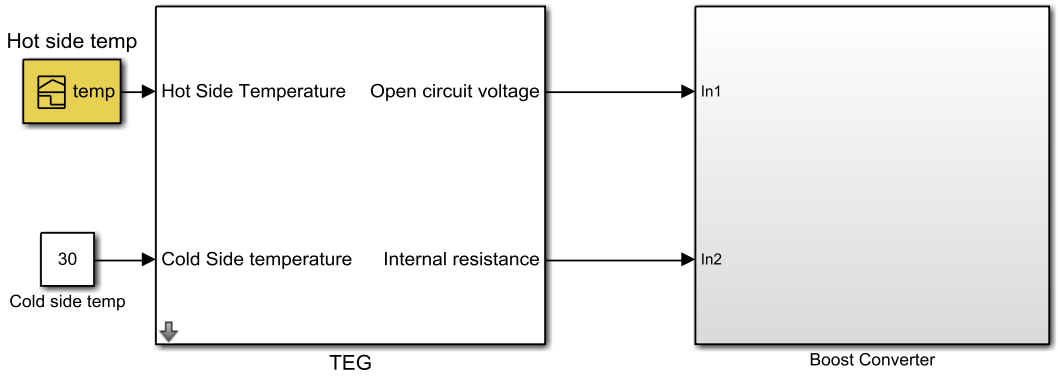


Figure 4.8. The proposed TEG Power conditioning system

The cold side temperature is set as 30 °C whereas hot side temperatures is set at 200 °C, 225 °C, 250 °C, 275 °C and 300 °C in order to test the performance of the converter system at those temperatures. The hot side temperature input to the TEG system is shown in Figure 4.9 in a ramp function. The results are discussed with different number of TEG modules in series. The results are presented with instantaneous and steady state values of voltage, current and power.

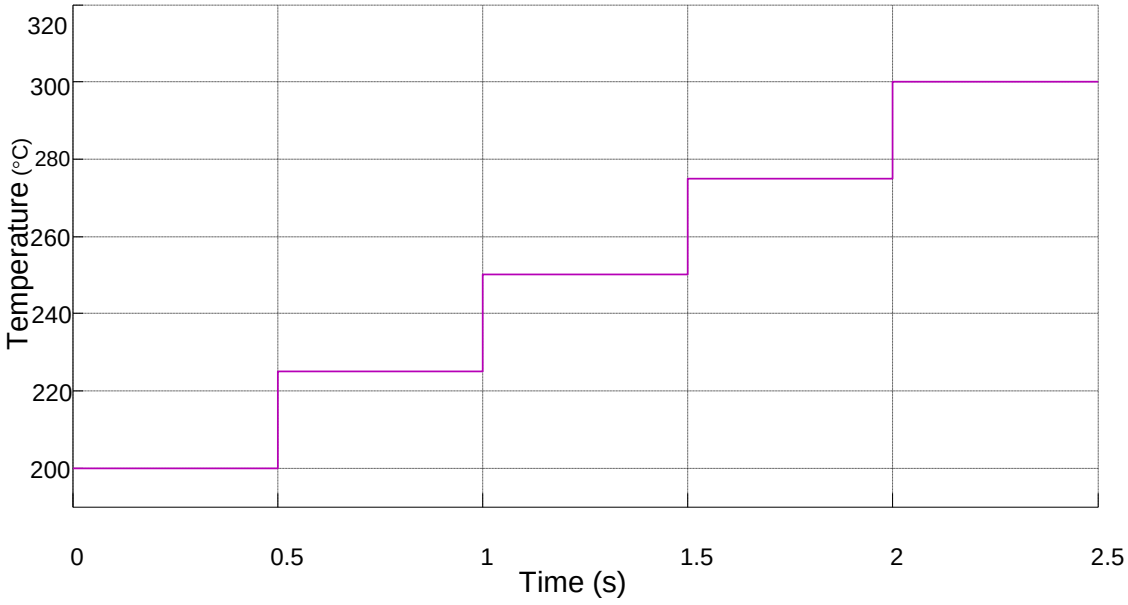


Figure 4.9. Hot side temperature input of the TEG module

4.5.1. Steady state model performance

At steady state, the values of voltages, currents and power as well as resistance of the systems are recorded by computing the average values at each hot temperature level. Figure 4.10 and Figure 4.11 shows the average input and output voltage of the converter at different temperature for a single and ten (10) modules respectively. It can be observed that as the number of TEG module are multiplied, the input and output voltage of the TEG and the converter is also multiplied. For example from Figure 4.10, the input voltage of the converter is 4.08V at a temperature of 200^{o}C for a single TEG module while in Figure 4.11 the input voltage is 41V at the same temperature for 10 TEG modules. It is noted that the voltage increases with the hot side temperature at a constant cold side temperature.

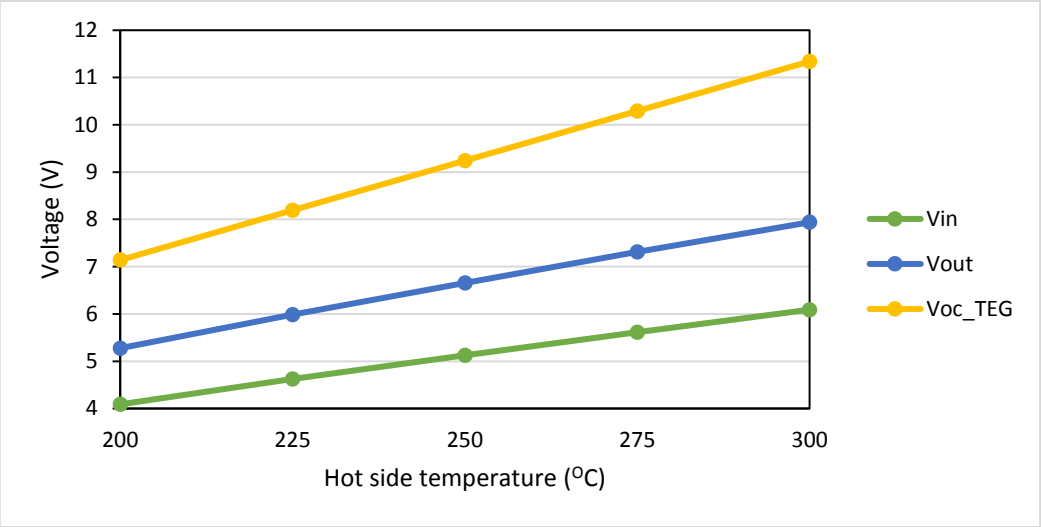


Figure 4.10. Average input, output voltage of the converter and open circuit voltage of TEG for a single TEG modules

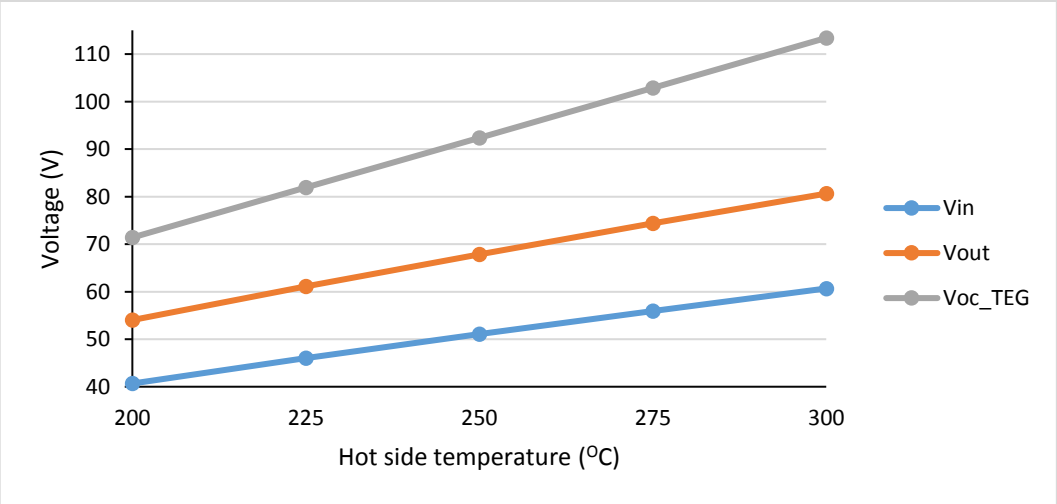


Figure 4.11. Average input and output voltage of the converter at different temperature for ten TEG modules

Figure 4.12 shows the input and output power of the converter which were recorded from the simulation results. The output also increases with temperature. It can also be observed that the output power is lower than the input power of the converter. This is due to the mismatch between the internal

resistance of the TEG, R_{int} and the overall converter resistance. However, if both are matched the input power can be balanced with the output though the matching point is difficult to achieve due to the varying nature of the loads that exists in practice. Also the output power is lower than the input power to the converter due to converter losses due to switching, presence of equvalent serries resistance of the input and output capacitors, etc.

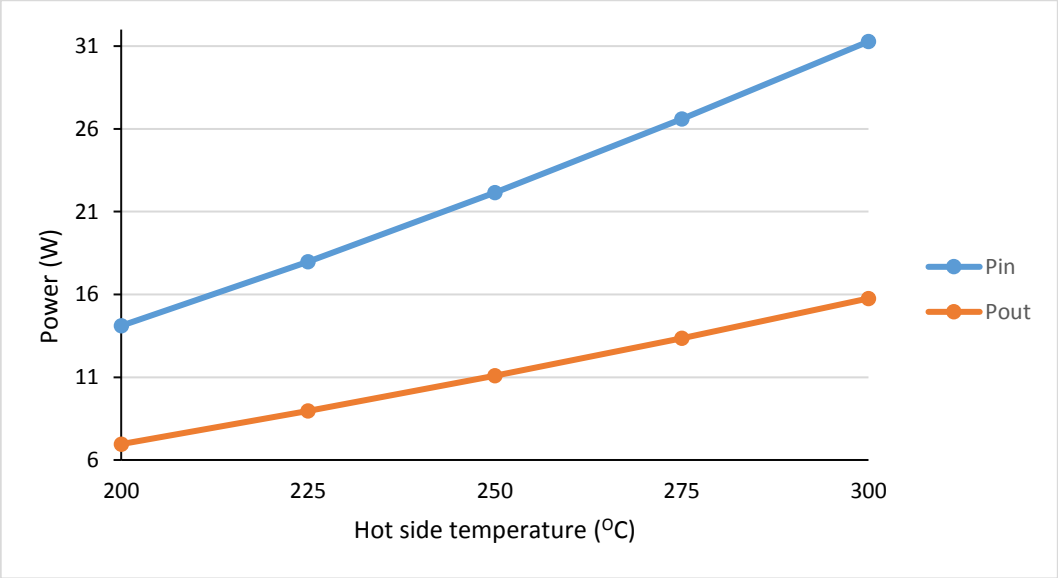


Figure 4.12. Average input and output power of the converter for a single TEG module

4.5.2. Verification of simulation results

The results of this study are compared with the results presented in the previous work done by (Li 2011). In (Li 2011), the author studied a similar TEG/boost converter model with the same TEG specifications as in the present study. It can be observed from Figure 4.13 that the matched power output from the converter at a temperature of 200°C is 14.1W for a single TEG module in previous work whereas it is 13.9W at the same temperature in this study. which is approximately the same value. The relationship between the hot side

temperature and the matched power is the same in both cases whereby the matched power output increases as the hot side temperature increases.

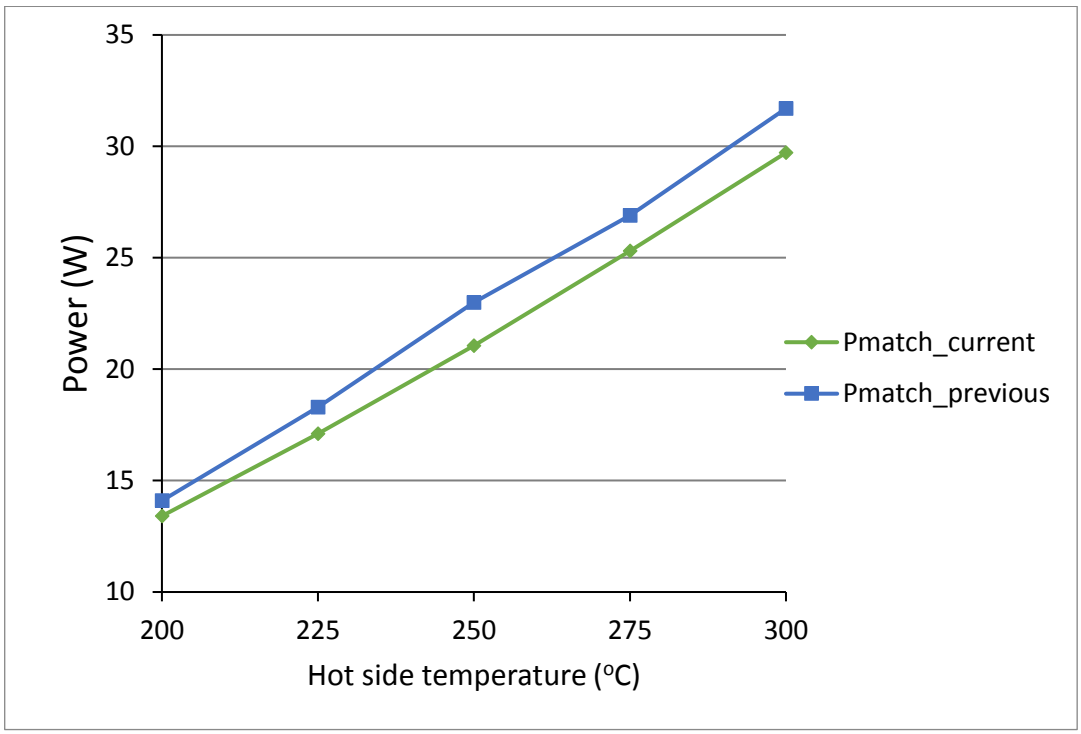


Figure 4.13. Input power to the converter under the matching conditions

From Figure 4.14, the highest conversion efficiency achieved in the previous work is about 81 % at a temperature of 300°C. However, a higher conversion efficiency of 88.7% is recorded in the current study which confirms the proper tuning of the converter circuit. In both cases the efficiency increases as the temperature increases which is expected since the matched power output has a similar trend.

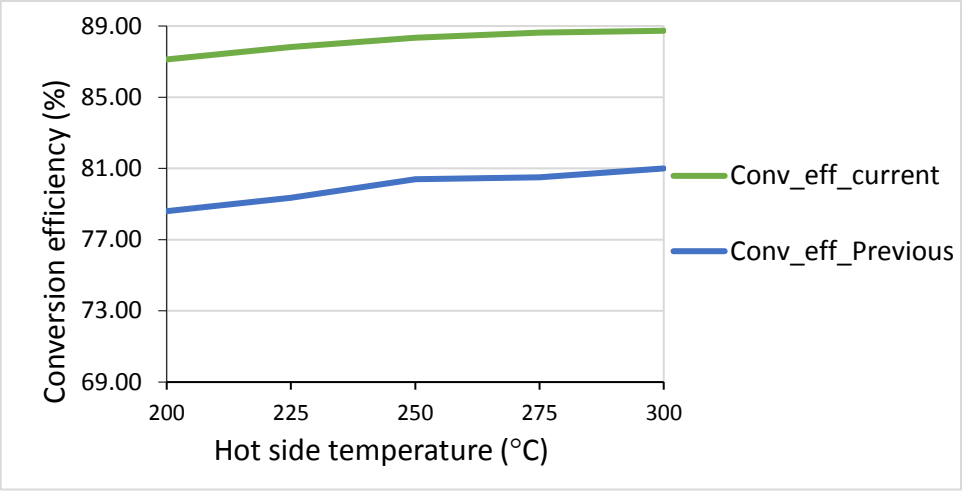


Figure 4.14. Conversion efficiency of the converters at different hot side temperatures

4.6. Summary

Thermoelectric technology is responsible for innovating thermoelectric devices such as TEGs which are used to generate electrical energy from heat in an environmentally friendly manner. In this chapter the dc-dc boost converter performance with TEG system has been analysed based on simplified model. The application of boost converter to TEG system is observed to have better steady state performance, hence improving the TEG performance and the overall system performance. The use of dc-dc converter with MPPT algorithms will be considered in subsquent chapters.

Chapter 5. Modelling of TEG/dc-dc converter system with IC MPPT

In this chapter, analysis of the performance of the dc-dc TEG/converter system with MPPT enabled by IC method is done. The results indicate that the IC based MPPT approach is able to track the maximum power point but with a relatively lower efficiency than the P&O based MPPT method. The matching efficiencies for the 200 – 300^{o}C temperature range are 99.92 – 99.95% and 99.46- 99.97% for P&O and IC methods respectively. However, IC based MPPT method has higher voltage gain and converter efficiencies than the P&O based MPPT method. Therefore, the dc – dc converters are able to improve the steady state performance of the TEG system as well as extacting maximum power with IC based MPPT, hence improving the overall performance of the TEG system

5.1. Research background

On the basis of the level of complexity of calculating/estimating these thermoelectric effects, several mathematical models such as simplified models (Fraisse et al. 2013), analytical models, electrical analogy models (Fraisse et al. 2002), etc. have been developed and used in the design and analysis of thermoelectric devices. These models have led to the development of several advanced thermoelectric devices with improved device efficiency. In recent years, there has been remarkable advancement of the thermoelectric devices and their efficiencies have been increased greatly due to thermoelectric material and device geometrical improvements (Weishu Liu, Jie, et al. 2015).

With the increase in computer technology, more research is possible to further implement the thermoelectric models in computer programs thereby improving the thermoelectric device performance. MPPT methods for a long time have been applied to improve the performance of PV system in both normal and partial shading conditions (Ramli et al. 2016). However, few MPPT applications

have been recorded on TEG systems yet TEG modules have similar characteristics to those of PV modules (Twaha et al. 2016). The purpose of this chapter is to analyse the performance of TEG/dc-dc converter system with IC based MPPT algorithm.

5.2. The proposed TEG power conditioning system

The proposed TEG power conditioning circuit consists of four main components: the TEG, the dc-dc converter, MPPT and the PWM signal generator. Figure 5.1 shows a block diagram of the proposed circuit.

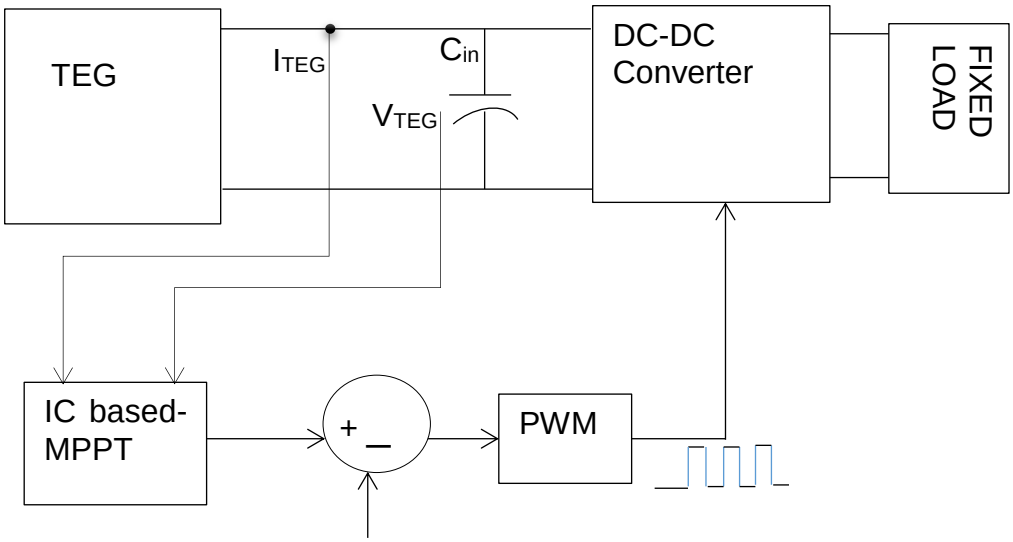


Figure 5.1. Block diagram of the proposed TEG power conditioning system

5.2.1. The structure and modelling of TEG device

In this chapter, the same simplified model discussed in chapter 4 is used. As well, TEG1-12611-6.0 TEG module parameters given in Table 4.1 have been utilized as the masked inputs to the TEG model.

5.2.2. The dc-dc converter with MPPT system

The same dc-dc converter circuit in chapter 4 has been utilized here except that the direct PWM circuit has been replaced with an MPPT circuit. The purpose of applying the MPPT is to ensure that at any temperature difference, maximum power is obtained from TEG. This is achieved by matching the TEG's MPP with the operating voltage and current of the MPPT controlled-converter. The dc-dc converters with MPPT have generally found applications in PV systems but can also be applied in TEG system. The MPPT methods can be divided into two main groups: the first is based on voltage feedback and the second based on regulating the generated power. The MPPT methods based on voltage feedback function in such a way that a predetermined reference voltage is compared with the voltage of TEG module in a feedback loop (Roshan & Moallem 2013). The second method is based on regulating the generated power by sensing the PV or TEG module voltage and current to track the MPP. P&O and IC MPPT algorithms are the examples of this category. The MPPT functionality is normally integrated into the dc-dc converter to achieve higher power-extracting efficiency (Taghvaee et al. 2013).

The MPPT works by sensing the current and voltage of the TEG. By using the current and voltage, the TEG power is calculated and compared with the present value of MPP. Accordingly, the duty cycle of the converter is adjusted to match the MPP, thereby forcing the converter to extract the maximum power. This is referred to as the direct duty cycle MPPT control. The duty cycle is computed directly in the MPPT algorithm. The direct control method is advantageous because it simplifies the tracking structure and reduces the computation time, and less tuning effort is needed for the gain. However, a proportional–integral (PI) or hysteresis controller can be used instead to adjust the duty cycle of the converter. This makes the MPPT control circuit complicated and much effort is needed to tune the PI gains while producing similar optimal results as the direct control method.

5.3. IC algorithm

The IC method operates by incrementally comparing the ratio of derivative of conductance with the instantaneous conductance. This is due to the fact that at MPP, the derivative of power with respect to voltage (dP/dV) is zero, i.e;

$$\frac{dP}{dV} = \frac{d(VI)}{dV} = I + V\frac{dI}{dV} = 0 \tag{5.1}$$

After re-arranging equation (5.1);

$$-\frac{I}{V} = \frac{dI}{dV} \cong \frac{\Delta I}{\Delta V} \tag{5.2}$$

Where I and V are the TEG output current and voltage; ΔI and ΔV are the increments of TEG output current and voltage, respectively. The basic rules for IC can be written as;

$$\begin{cases} {}^{dI}/_{dV} = -{}^{I}/_{V}, At\ MPP \\ {}^{dI}/_{dV} > -{}^{I}/_{V}, Left\ of\ MPP \\ {}^{dI}/_{dV} < -{}^{I}/_{V}, Right\ of\ MPP \end{cases} \tag{5.3}$$

It can be noticed that the MPP condition ($dI/dV + I/V = 0$) rarely exists in practical applications; hence another alternative yet effective way to utilize the IC was proposed by a number of researchers [17]. The idea is to generate a marginal error ε using the instantaneous conductance and the IC. Mathematically, it can be written as;

$${}^{dI}/_{dV} + {}^{I}/_{V} = \varepsilon \tag{5.4}$$

From equation (5.4) it can be seen that the value of ε is zero at MPP. Hence, based on the amount of ε and using the rules of (5.3) the basic flow chart for IC method is shown in Figure 5.2.

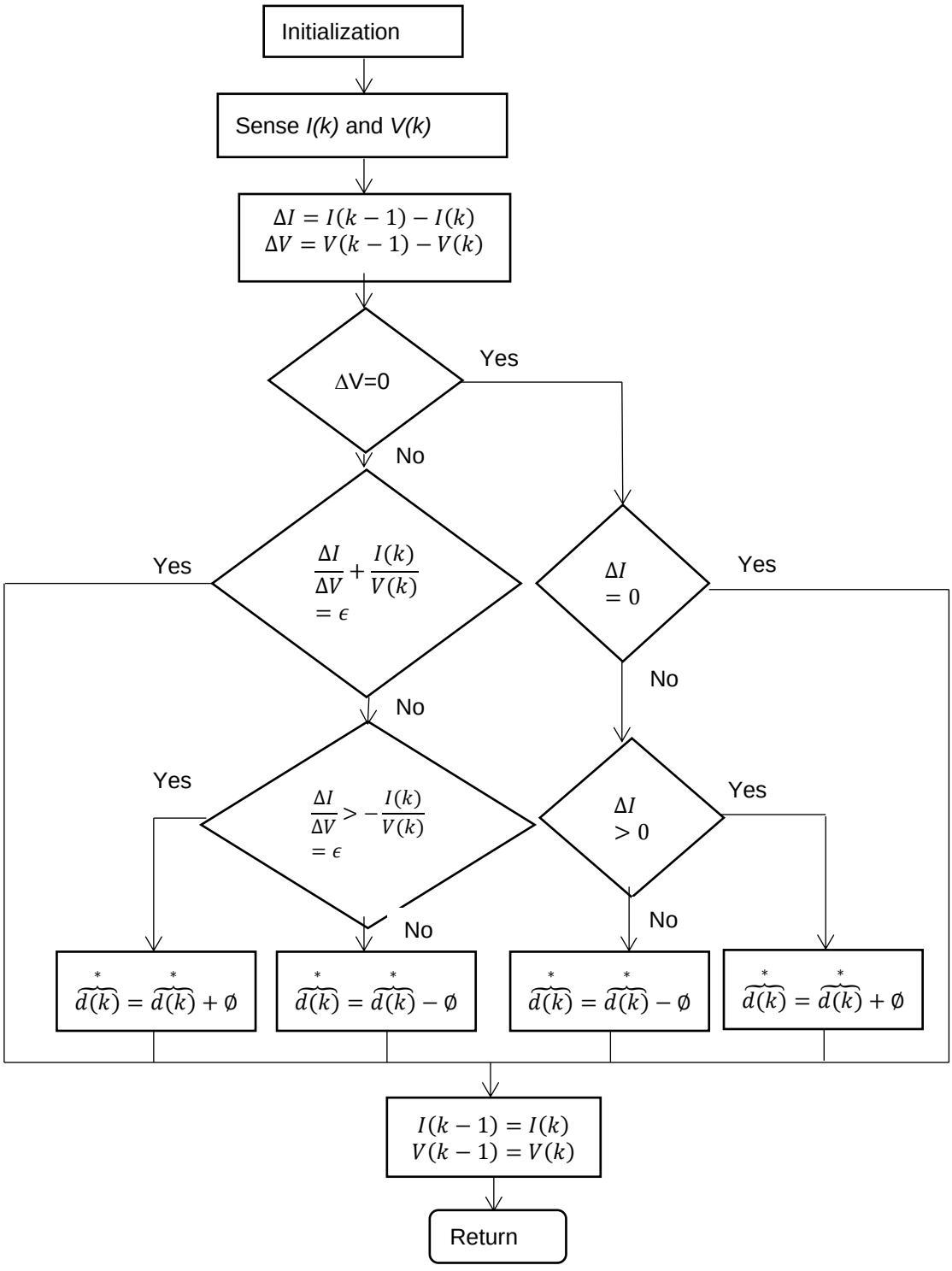


Figure 5.2. Basic flow chart of IC method (Ishaque et al. 2014b)

5.4. Results and discussion

As indicated earlier, the modelling is performed in Simulink. Accordingly, Figure 5.3 shows the modelled circuit from which the results are obtained for analysis.

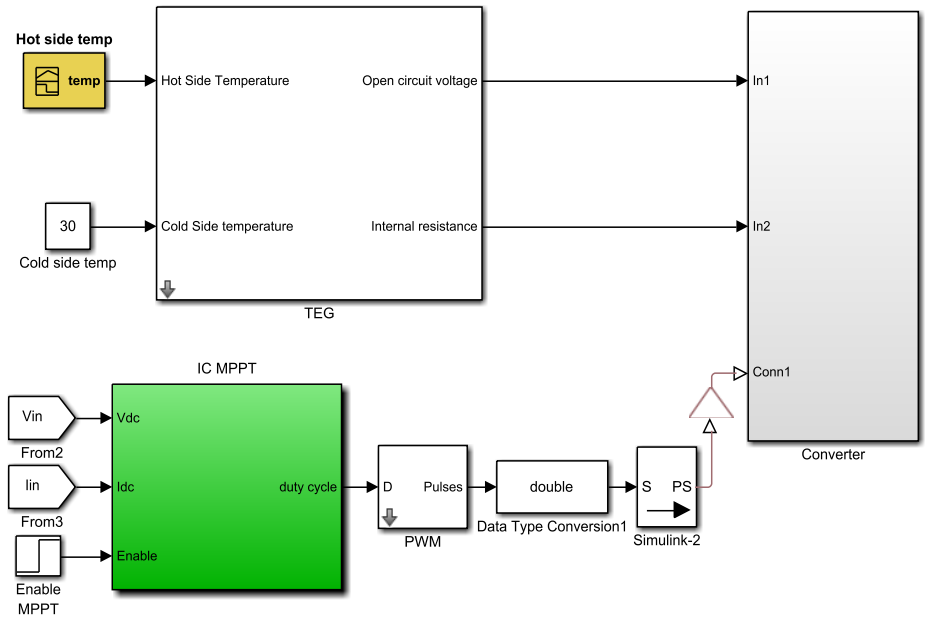


Figure 5.3. The proposed TEG Power conditioning system modelled in Simulink

The cold side temperature is set as 30°C whereas hot side temperatures are set at 200°C, 225°C, 250°C, 275°C and 300°C in order to test the performance of the converter system at 200°C – 300°C temperature range. The hot side temperature input to the TEG system is shown in Figure 5.4 in a ramp function. The TEG model is designed in such way that it is possible to change the number of TEG modules in series using a masked inputs as shown in Figure 5.5. Therefore, the results are shown with different number of TEG modules in series.

The results are presented with instantaneous and steady state values of voltage and power. In addition, the values of efficiencies of the MPPT and the converter are also reported and discussed.

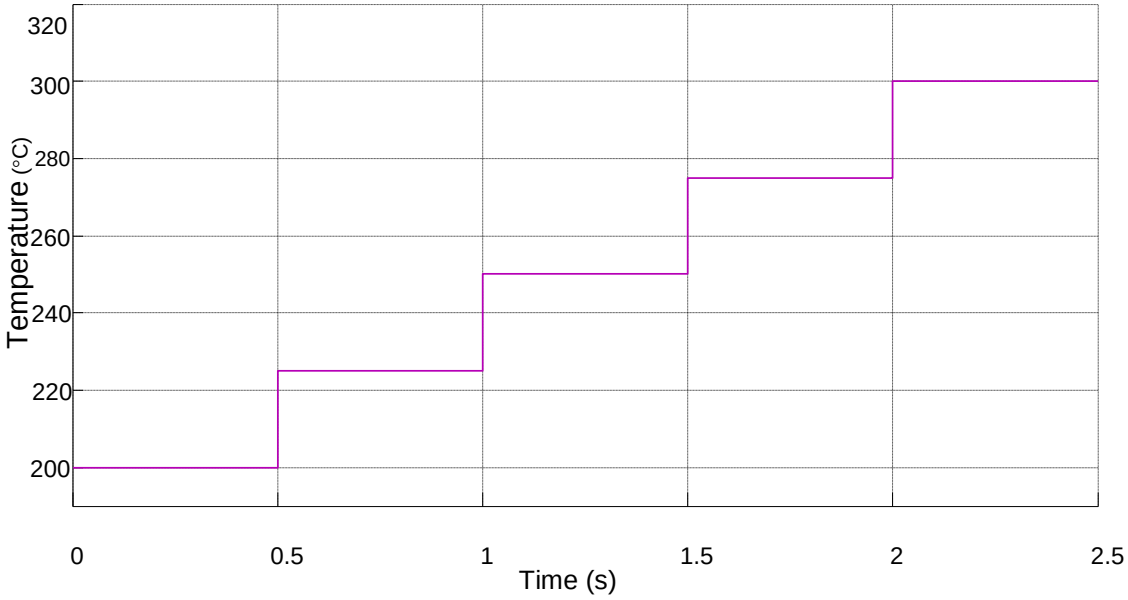


Figure 5.4. The hot side temperature input to the TEG system

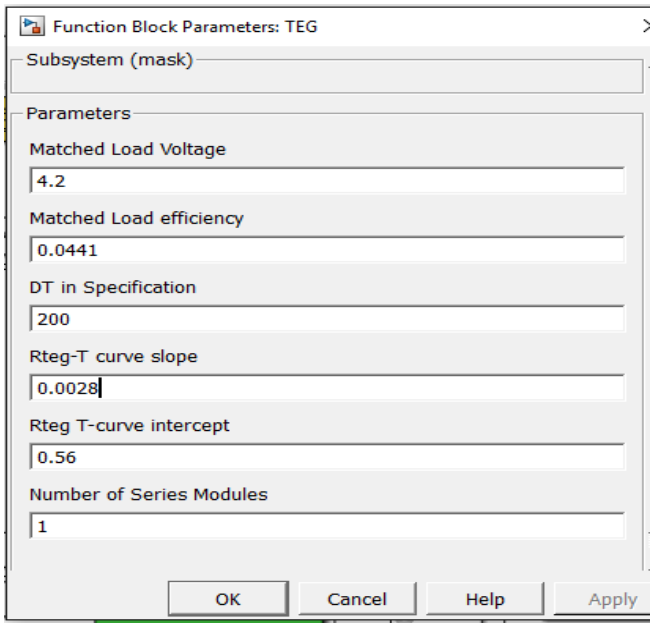


Figure 5.5. TEG block parameter adjustment in the simulation model

Figure 5.6 shows the instantaneous values of voltages for the systems. Obviously the open circuit voltage is higher than any other voltage values. The input voltage to the converter is the output of the MPPT algorithm. It can be clearly observed that the input voltage to the converter is unstable; the level of instability is demonstrated by the size of the output voltage trace. As observed from Figure 5.6, the output voltage from the converter is relatively stable and depending on the load requirement, the voltage can also be boosted to higher values. In this case, the input temperature is a ramp function for which is the temperature is uniform at each temperature level. However, with a non-uniform temperature input to the TEG system, the converter is equally capable of tracking the maximum power point. This is demonstrated by the replication of the trend of a ramp temperature input as seen from the output of the converter.

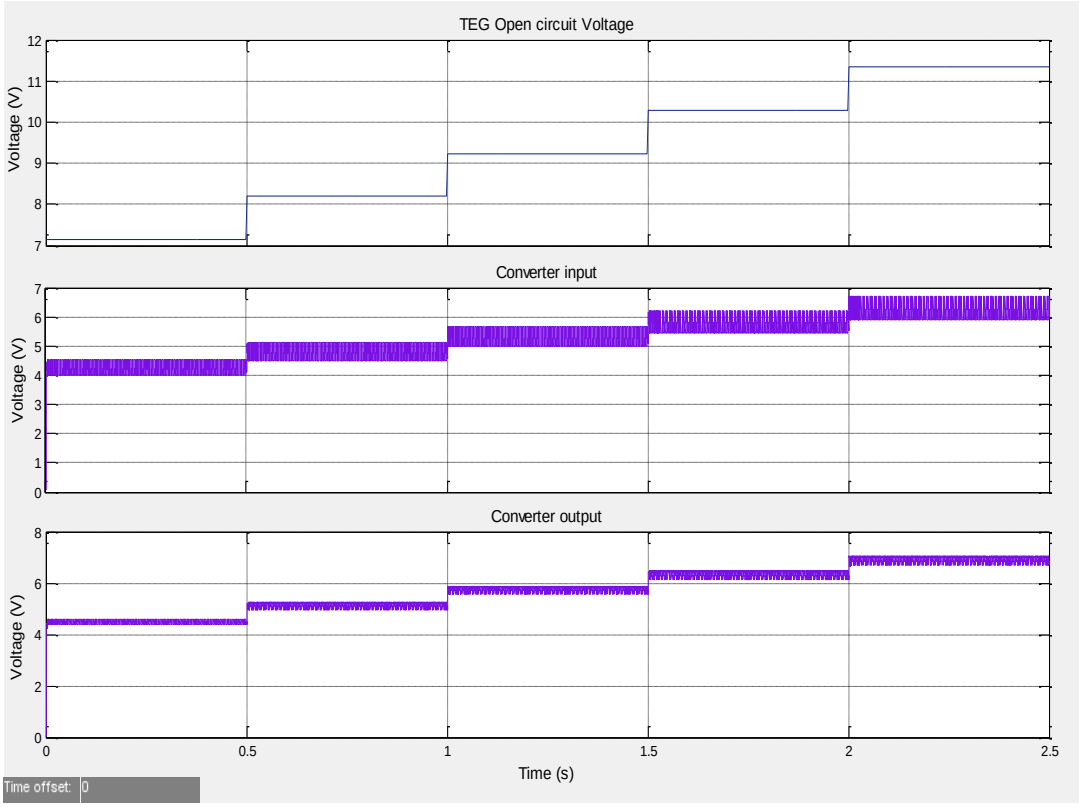


Figure 5.6. The instantaneous values of voltage for the systems

Figure 5.7 shows the values of TEG output power as well as the input and output power of the converter. The TEG output power is a product of the open circuit voltage seen in Figure 5.6 (above) and the highly unstable input current with a lot of harmonics. Similarly the converter input power is a product of its input voltage and the highly unstable input current. Therefore, the converter input power is unstable due to the relatively unstable voltage and highly unstable current with several harmonics. As observed from Figure 5.7, the output power is relatively stable with fewer harmonic. This is due to the filtering done by the converter because of the presence of the filter circuit in form of low pass filter. With proper tuning of the filter circuit, the stability of the output can be improved.

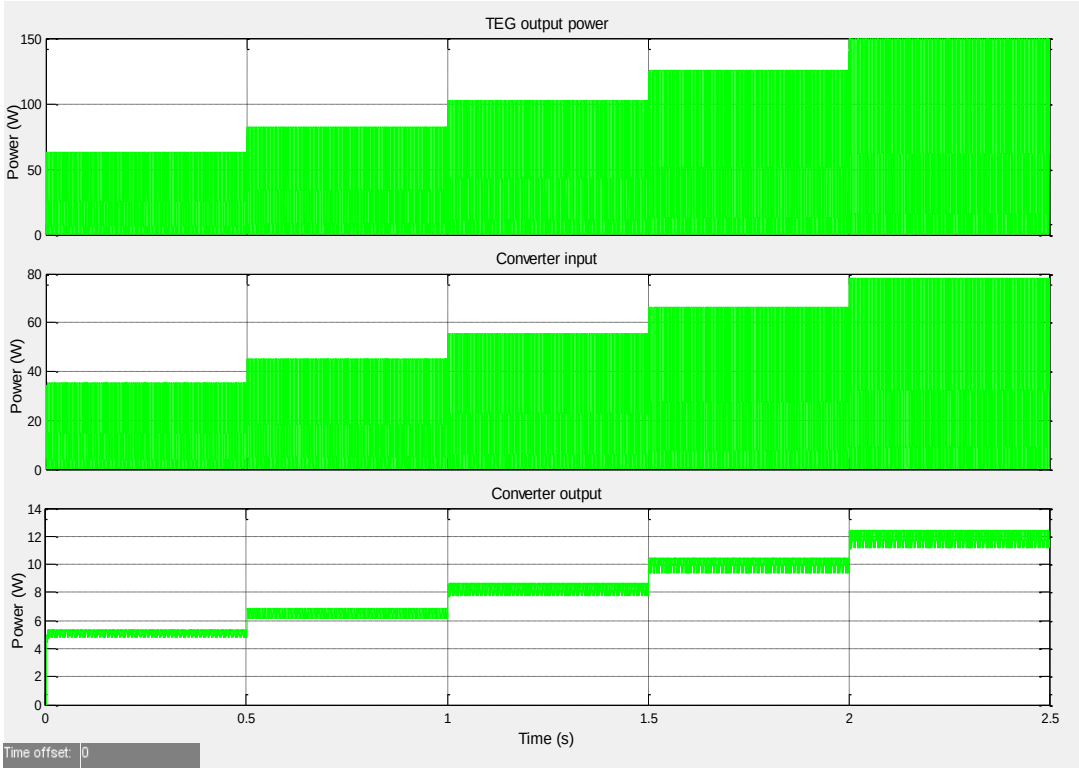


Figure 5.7. Values of power from TEG as well as to and from the converter

At steady state, the values of voltage and power of the systems are recorded by computing the average values at each hot temperature level. The step up of voltage is demonstrated in Figure 5.8 where the input and output voltages of the converter are shown for ten TEG modules in series. It is observed that at a temperature of 200^{o}C, the converter voltage input is about 41.18V which is boosted to 48.64V. Likewise, with a single TEG in series at the same temperature and an input voltage of 4.18V, the output voltage is stepped up to 4.5V as illustrated in Figure 5.9.

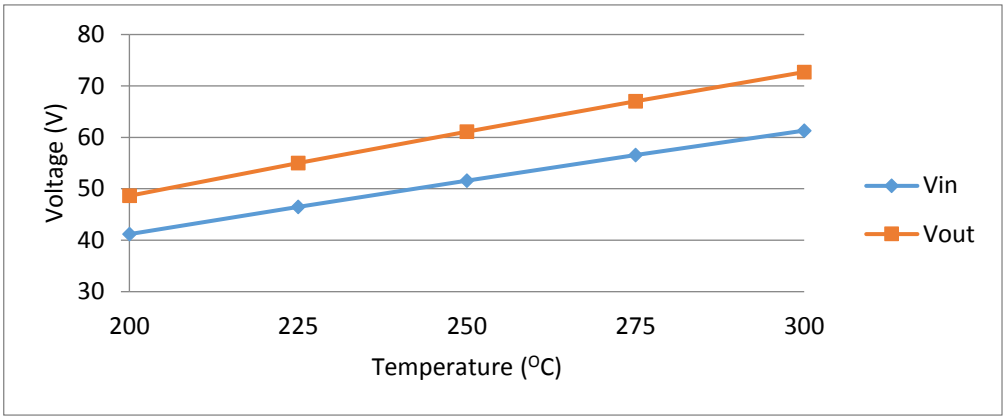


Figure 5.8. The average input and output voltages of the converter at different temperatures for ten TEG modules

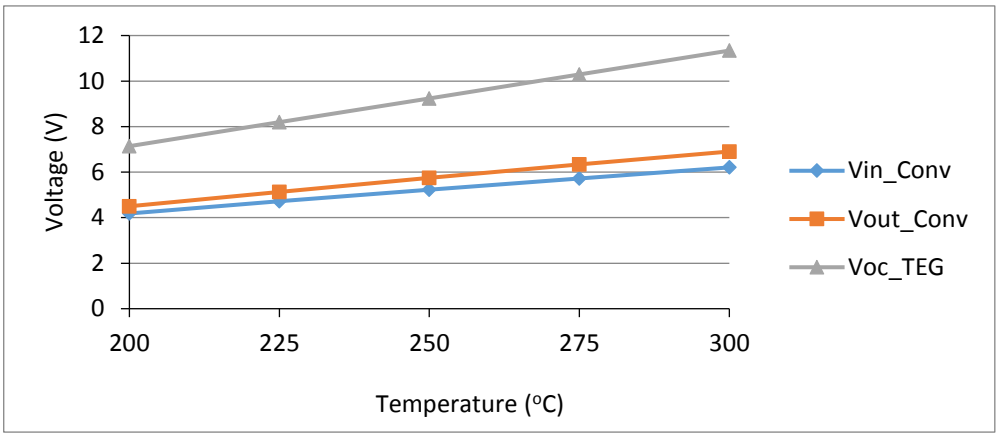


Figure 5.9. The average input, output voltages of the converter and open circuit voltages of the TEG at different temperatures and T_c=30°C for a single TEG module

Subsequently, the average power is shown in Figure 5.10 for a single TEG module. In all cases, the output power increases with the hot side temperature. This is attributed to the increase in the temperature difference (which is responsible for the Seebeck effect) as the hot side temperature increases since the cold side temperature Tc is kept constant at 30°C.

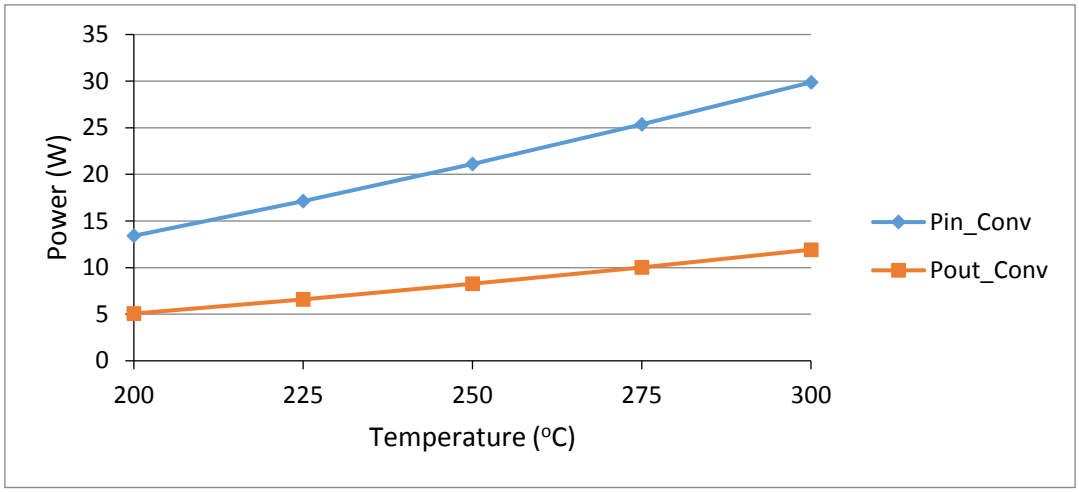


Figure 5.10. Average input and output powers of the converter and TEG output power at different hot side temperatures and T_c=30°C for a single TEG module

5.4.1. Verification of simulation results

The results in this chapter are compared with the those presented in literature (Li 2011). In the literature (Li 2011), the author studied a similar TEG/boost converter model with the same TEG specifications but with P&O MPPT method. Comparing with open circuit voltage of 7.2V at 200°C for the current study in Figure 5.9 (above) with that (about 7.2V at the same temperature) of the previous study in Figure 5.11, the results of both cases agree. This means there was no source of error in the TEG circuit. The difference in the results arises in the input voltage to the converter which is dictated by the nature of MPPT controller. As observed in Figure 5.9 and Figure 5.11, the input voltage to the converter is 4.1V and 3.6V at 200°C for IC based MPPT P&O based MPPT methods respectively. Similarly, the converter input power is 13.4W and 13.1W at 200°C as indicated in Figure 5.10 (above) and Figure 5.12 for the IC and P&O based MPPT methods respectively. The errors arises due to several factors, including looping errors in the MPPT algorithm leading to the simulation errors; component tolerances in the MPPT circuit, all of which reduce the

efficiency of the MPPT controller. Another cause of the difference in the results of both cases is the difference in the computing capability of the MPPT algorithms where it can be observed that when the voltage is compared alone, the IC based MPPT is more robust and less prone to errors than P&O method because it results into higher output voltage than the P&O based MPPT algorithm.

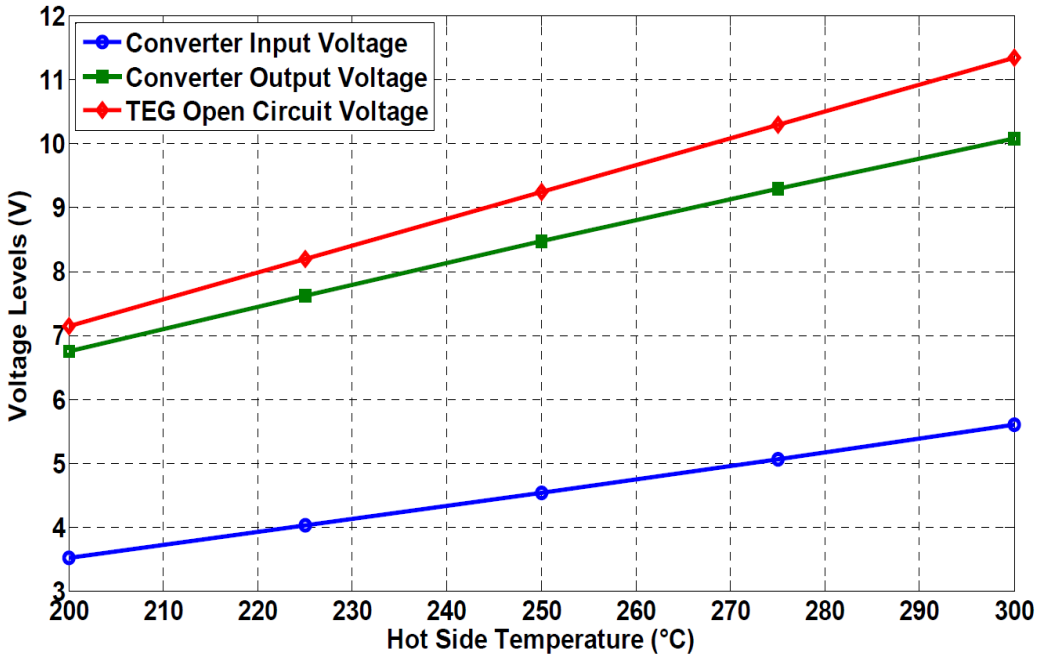


Figure 5.11. Converter input and output voltages and TEG open circuit voltages with P&O method at T_c=30°C (Li 2011)

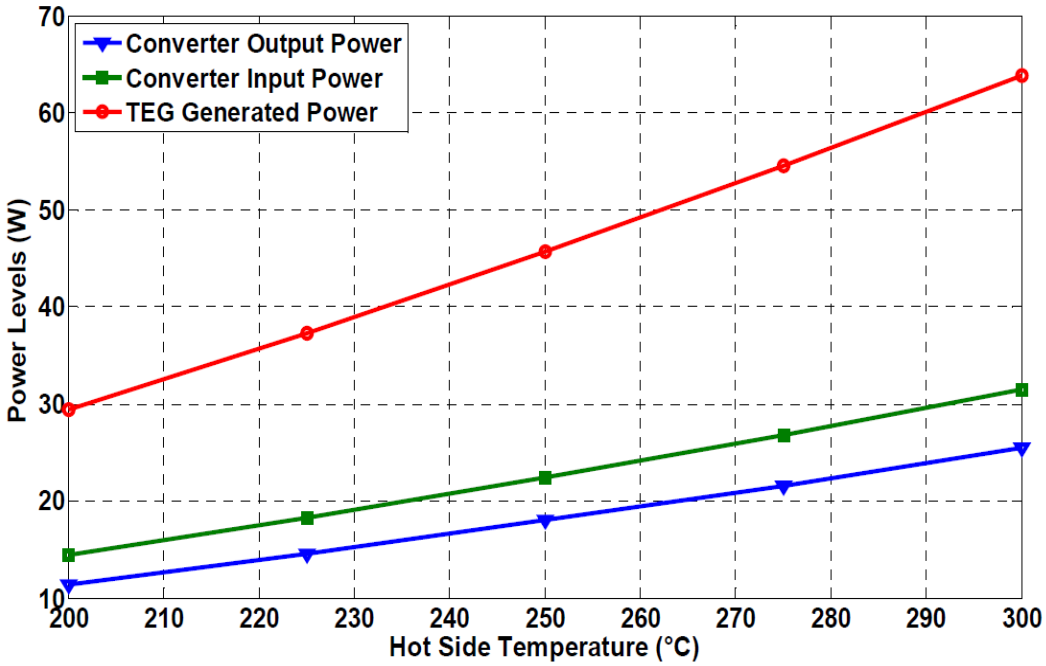


Figure 5.12. Input and output power of converter compared to the output power of TEG with P&O method at T_c=30°C (Li 2011)

5.4.2. Performance comparison of IC and P&O techniques

The matching efficiency for the 200 – 300°C temperature range is 99.92 – 99.95% and 99.46- 99.97% for P&O and IC methods as shown in Figure 5.13. Hence, the P&O algorithm is slightly more efficient than the IC based MPPT technique. However, the MPPT matching efficiency of IC degrades as the hot side temperature increases.

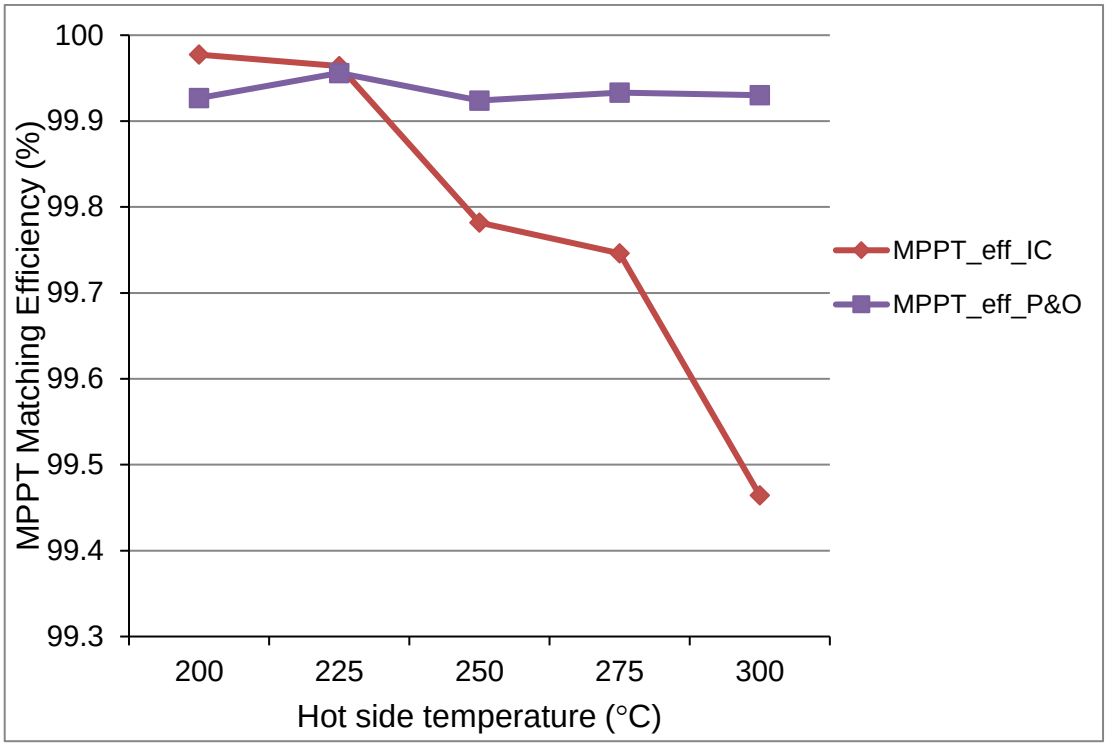


Figure 5.13. MPPT matching efficiency at different hot side temperatures and at T_c=30°C

5.4.3. Converter output without MPPT

In this case the switch is controlled with direct PWM signal. Theoretically the conversion ratio M (D) is defined as the ratio of the dc output voltage V to the dc input voltage V_g under steady state condition i.e;

$$M(D) = \frac{V}{V_g} = \frac{1}{1-D} \qquad (5.5)$$

Where D is the duty cycle.

Ideally the conversion ratio of a boost converter increases with the duty cycle, where the ideal converter efficiency of 100% is obtained with M (D) = 1 when D =0 as illustrated in Figure 5.14. However, as M (D) tends to infinity, D tends to one. At D =1, the output voltage of the converter is zero or minimum while

the current is maximum, i.e. the converter output terminals are short-circuited. Figure 5.15 shows the conversion ratio obtained from the simulation. In present work, M (D) =0.88 (point of maximum efficiency) when D =0 with an increasing trend of M (D) as D increases which is in line with the theoretical curve.

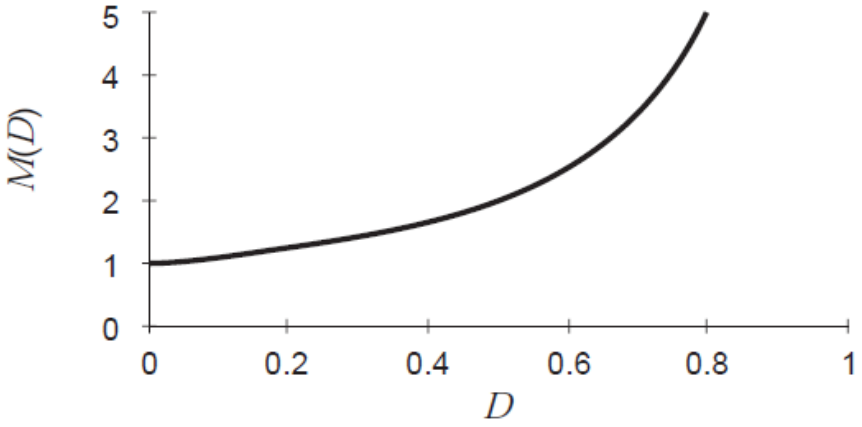


Figure 5.14. Theoretical conversion ratio of boost converter

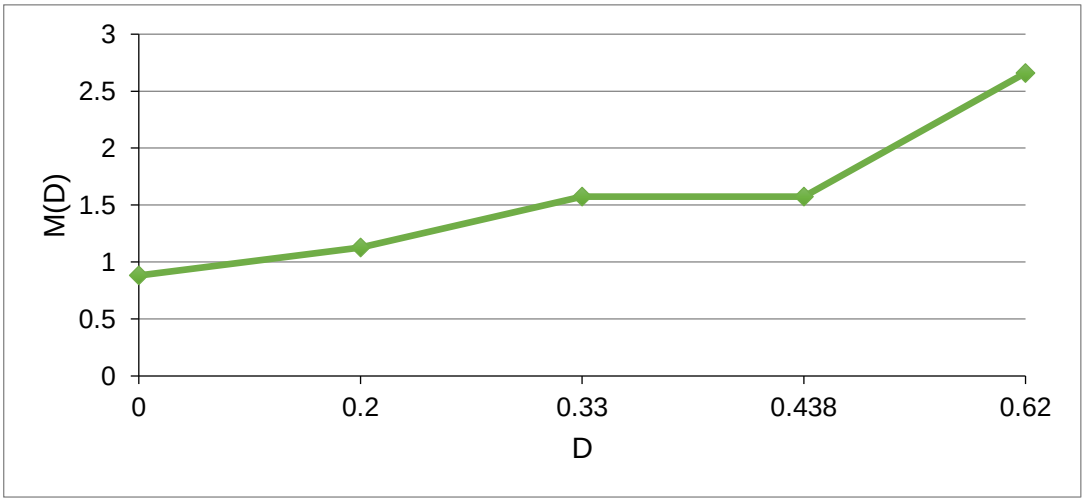


Figure 5.15. Conversion ratio of a boost converter obtained from the simulation

Figure 5.16 shows the output voltages of the converter at different values of the duty cycle D. Different values of duty cycle were sample to investigate the their effect on the output voltage It can be observed that at D =0, the highest values of the output voltages are obtained and hence the converter efficiency is computed at these values. At this point, the converter passes all the voltage to the load. As the duty cycle is increased to 0.2, the voltage across the output terminal reduces for all the temperatures. However, within the range of duty cycle values of 0.33 and 0.438, the the voltage at each temperature remains the same because the operation of the converter switch is not detected by the change in the duty cycle, hence the output voltage of the converter is unchanged. Further increase in the duty cycle to 0.62 reduces the voltage more. The use of direct PWM signal can provide different voltage levels to the load at different duty cycles. This is useful when loads of different voltage levels are to be supplied one at a time. However, to obtain the maximum power, an MPPT controller is necessary because the maximum power is obtained directly without the need to manually adjust the duty cycle as it is the case with the use of PWM controlled converter.

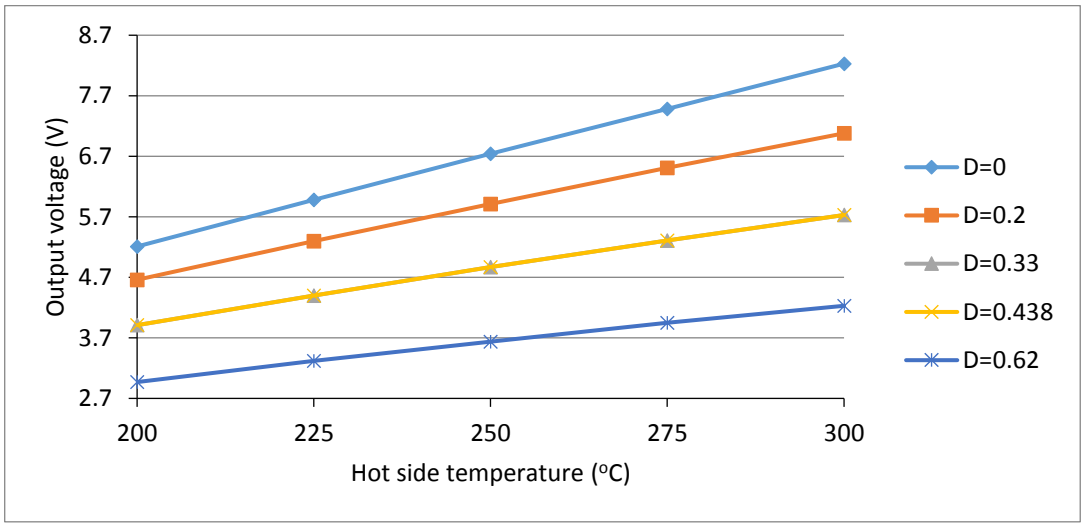


Figure 5.16. Output voltages of the converter at different values of D

5.4.4. Variation of voltage with TEG modules

A number of scenarios are considered with the number of TEG modules varied from 1, 5 and 10 in order to investigate how the voltages from TEG and converter respond to the increase in the number of TEG modules. It can be observed from Figure 5.17 that there is a linear relationship between the converter output voltage and the hot side temperature. Similarly, there is a direct relationship between converter output voltage and the number of TEG modules i.e. as the number of TEG modules (TEG-Mn) is increased, the voltage also increases.

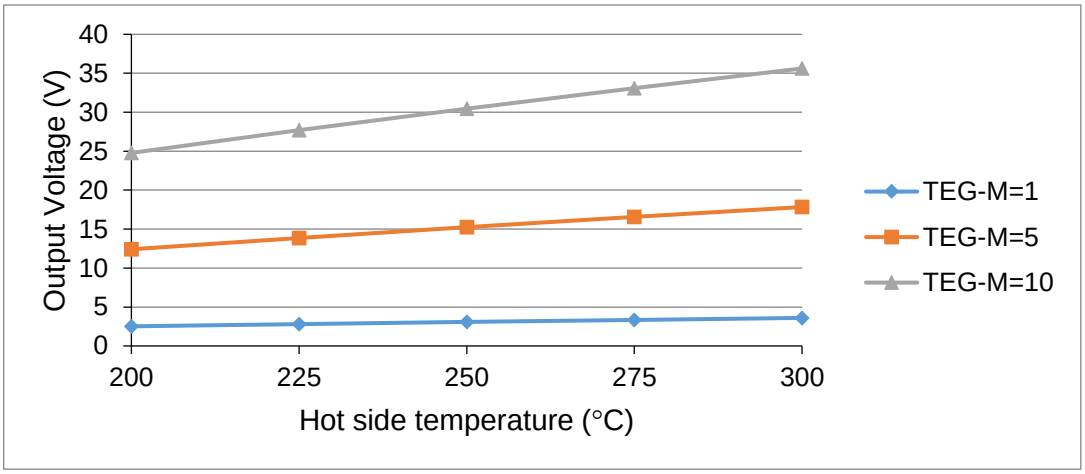


Figure 5.17. The relationship between the converter input voltage and the hot side temperature at different number of TEG modules

Introducing a new index called Module voltage multiplicity factor (MVMF), it is possible to clearly demonstrate the effect of increasing the number of TEG module on voltages and output powers of the TEG and converter. The MVMF is defined as;

$$\mathrm{MVMF}_{nb,na} = \frac{V_{na}}{V_{nb}} \qquad (5.6)$$

Where V_{na} is the TEG output voltage or converter *after* the number of modules are increased; V_{nb} is the voltage output of the TEG or converter *before* the number of TEG modules is increased.

The MVMF values are illustrated in Figure 5.18. It can be seen that at a given number of TEG modules, the temperature against the MVMF line is almost straight. This indicates that there is a linear and direct multiplier between the voltage and the number of modules. For example increasing the number of TEG modules from 1 to 5 at a temperature of 200^{o}C results into an MVMF of 4.92. Likewise increasing TEG modules from 1 to 10 at 275^{o}C results into MVMF of 9.88≅10. Therefore, assuming a uniform heat distribution, multiplying the number of TEG modules by n will result into the output voltage of TEG and hence the input voltage to the converter to be multiplied by n.

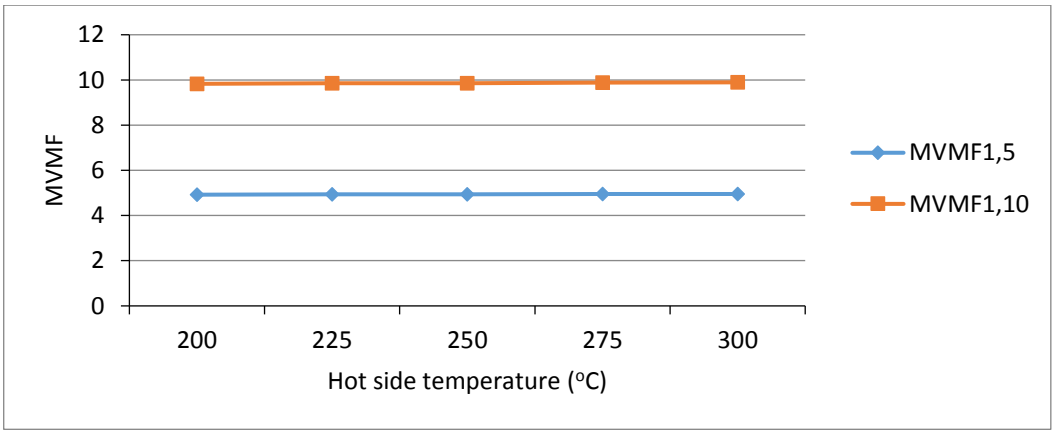


Figure 5.18. The MVMF at different temperature

5.5. Summary

A proper power conditioning circuitry is necessary to stabilise the power generated from TEG before it is connected to the load. In this chapter, the performance of the TEG/dc-dc converter system with MPPT enabled by IC method has been done. It has been noted that the output voltage and power from TEG can be increased by increasing the number of TEG modules and the

hot side temperature. It has also been observed that the IC based MPPT approach is able to track the maximum power point but with relatively lower efficiencies than the P&O based MPPT method. The matching efficiencies for the 200^{o}C – 300^{o}C temperature range are 99.92 – 99.95% and 99.46- 99.97% for P&O and IC methods respectively. It is noted that the IC based method has higher values of voltage gain and converter efficiencies than the P&O based MPPT method. Although the use of direct PWM signal to control the converter switching provides different voltage levels to the load at different duty cycles, the advantage of using MPPT outweighs its applicability to the TEG system because the MPPT automatically extracts the maximum power without the need to manualy adjust the duty cycle, in addition to the fast response to temperature changes. Therefore, the dc – dc converters are able to improve the steady state performance of the TEG system as well as extacting maximum power with IC based MPPT, hence improving the overall performance of the TEG system.

Chapter 6. Parameter Analysis of TEG/dc-dc converter system with MPPT and variable load

The power generated from TEG is relatively unstable due to varying nature of temperature applied to its hot and cold side terminals. The dc-dc converters can provide more stable power output thereby improving the overall efficiency of TEG system. However, to facilitate better performance improvement, MPPT algorithm can be applied to extract maximum power from TEG system. Therefore, this work has analysed the parameters for the performance of TEG/dc-dc converter system in different modes with a variable load. The system is tested in both MPPT and PWM modes. The TEG system is also subjected to different hot side temperatures, including increasing step, increasing random and constant cold side temperature to analyse the performance of the systems with these input signals. Results indicate that dc-dc converter with MPPT based model is able to extract maximum power from TEG better than the direct PWM based model. From the study, it is established that, for maximum power point to be achieved, the TEG/dc-dc converter system has to be operated at a certain optimum load which is determined at a point where the overall converter resistance is equivalent to the internal resistance of TEG modules. It has also been established that proper selection of the converter components is necessary to minimize the converter losses as well as interferences on the system load.

6.1. Background

The rapid development of power electronics technologies has enabled the realization of high energy-efficient systems such as hybrid EVs, pure EVs and plug-in hybrid electric vehicles(Q. Wang et al. 2016). Each of these energy saving strategies has its own advantages and challenges. However, if such energy systems are managed properly they can reduce fossil fuel consumption thereby contributing to positive climatic change.

Various research efforts are underway to improve the performance of thermoelectric conversion system. The integrated thermoelectric devices are also developed by restructuring them to allow more heat to enter the p–n junctions, thereby producing more power output (Barry et al. 2015). The accuracy of the mathematical models used in thermoelectric simulation is assessed with special reference to thermal influence of insulated air zone and radiation heat (Gao et al. 2015). Heat transfer analysis between the TEM cold and hot plates revealed that the developed model is of theoretical significance in guiding future design of TEMs for high power or large-temperature-difference thermoelectric conversion systems. Regarding the heat pipe for the TEG system, a study is conducted to enhance heat transfer in the radial direction of gas flow for thermoelectric power generation (X. Wang et al. 2016). It is noted that the installation of the TEG heat exchanger between muffler and catalytic converter guarantees a higher output power of 450W in the thermoelectric heat exchanger at an engine speed of 5000 rpm. Not forgetting to mention the concentric cylindrical design also applied to the TEG system with improved output power (Huang Kuo, Bo Li, Ssennoga Twaha 2016).

The objective of this work is to analyse the parameters of TEG/dc-dc converter system enabled by IC based MPPT and direct PWM signal. The converter parameters that determine its performance are analysed in detail. The TEG system has been subjected to different hot side temperature and constant cold side temperature. The converter performance is analysed with reference to the temperature variations at the hot side of TEG in addition to varying the external converter load.

6.2. The dc-dc converter model parameters

The developed model is shown in Figure 6.1 consisting of the TEG, MPPT and a dc-dc converter subjected to the variable resistive loads.

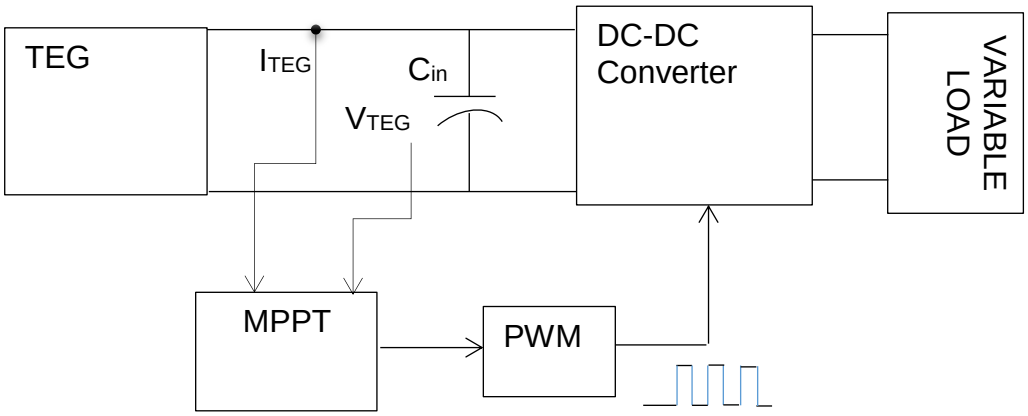


Figure 6.1. The TEG-converter simulation model

Unlike in Chapter 4, in this chapter, attempts have been made to give more detailed information about the design of dc-dc converters and the associated sources of errors in the circuit.

Here, the converter that operates in a continuous conduction mode is discussed with regard to the design specifications and components selection. The first step in designing a dc-dc boost converter is to find the appropriate value of the switching current which is the maximum current the switch or integrated circuit (IC), the inductor and the diode can withstand. But before that, the duty cycle D, and the ripple current have to be determined. The duty cycle of a practical dc-dc boost converter is expressed as;

$$D = \frac{V_{in\,(min)} * \eta_{conv}}{V_{out}} \qquad (6.1)$$

Where $V_{in\,(min)}$ is the minimum input voltage; η_{conv} the converter efficiency whereas V_{out} is the desired output voltage.

The efficiency is included in the duty cycle equation in order to compute a more realistic value of D in addition to catering for the dissipated energy since the converter has energy losses. Either an estimated efficiency value can be used e.g. 82% or a typical efficiency value can be selected from the converter

characteristics from the datasheet for use in equation (6.1). Before calculating the ripple current, it is necessary to first compute or determine the inductor value. Various ways are used to determine the inductor value; the recommended inductor value or the middle value in the inductor range given in the datasheet can be used if there is no recommended value given. Alternatively, the inductor value can be computed as;

$$L = \frac{V_{in} * \{V_{out} - V_{in}\}}{\Delta I_L * f_{sw} * V_{out}} \quad (6.2)$$

Where V_{in} is the typical input voltage; f_{sw} the minimum converter switching frequency while ΔI_L is the estimated inductor ripple current.

A suitable value of f_{sw} for the converter application without causing losses should be selected. The inductor ripple current is not calculated but estimated in the range of 20% - 40% of the output current as;

$$\Delta I_L = 0.2 * I_{out_max} * \frac{V_{in}}{V_{out}} \quad (6.3)$$

Where I_{out_max} is the maximum output current for designated converter load.

Therefore, the ripple current is expressed as;

$$\Delta I_L = \frac{V_{in_min} * D}{f_{sw} * L} \quad (6.4)$$

The ripple current should be reduced in the converter circuit because if it is left to penetrate the converter load such as the battery, it can reduce the battery life and degrade the operation of the load (Uddin et al. 2016). Switching ripple filters can be used to prevent the switching ripple current from reaching the load or grid (Büyük et al. 2016). The maximum output current delivered by the converter is calculated as;

$$I_{out_max} = \left[I_{IC_min} - \frac{\Delta I_L}{2}\right] * (1 - D) \quad (6.5)$$

Where I_{IC_min} is the minimum value of current for the IC given in datasheet.

Another IC of higher switching current has to be selected if I_{out_max} of the selected IC is below the targeted maximum current value of the intended application or the load. However, if I_{out_max} is slightly smaller than the required maximum load current, the inductor value can be increased as longer as the increased inductance remains within the recommended range in the datasheet. This is because increasing inductance reduces the ripple, thereby increasing the maximum output current to the desired value (according to equation (6.4) and (6.5). If the calculated I_{out_max} is above the required maximum output current, then the switching current I_{sw_max} is calculated as;

$$I_{sw_max} = \left[\frac{\Delta I_L}{2} + \frac{I_{out_max}}{1 - D}\right] \quad (6.6)$$

To select the diode, the average forward current rating required is equal to I_{out_max} i.e;

$$I_F = I_{out_max} \quad (6.7)$$

Where I_F is the diode's average forward current.

For reduced losses, Schottky diode types should be utilized. They also have higher peak current than their rating and the higher peak current is not a problem. The power dissipated by the diode is;

$$P_F = I_F * V_F \quad (6.8)$$

Where V_F is diode's Forward voltage.

The practical diodes have different threshold forward voltages (barrier potential) V_0 beyond which the diode is able to conduct large amount of current to the output terminal of the converter. The value of V_0 is normally 0.2V, 0.3V and 0.7V for Shockley, germanium and silicon diodes respectively. A practical or real diode has a barrier potential V_o and a drop-in forward resistance R_F. Therefore, the required voltage V_F to operate the diode in forward biased mode becomes;

$$V_F = V_0 + R_F I_F \tag{6.9}$$

The next step is to select the capacitance. Due to the peak current requirement of the converter the input voltage has to be stabilised by a minimum value of input capacitor. The minimum value of the input capacitor C_{in} is always specified in the datasheet. Ceramic capacitors are recommended because they have low Equivalent Series Resistance (ESR). The capacitance C_{in} can be increased if the input voltage has higher noise so that higher harmonics are suppressed to reduce or avoid the noise interference. Class 2 ceramic capacitors with dielectric material X7R standard should be used for higher temperature applications because they operate in the temperature range of -55 °C to +150 °C with a capacitance change ΔC/C0 of utmost ±15%. The X5R capacitors show a capacitance drift that may not exceed 15% of the nominal capacitance value at 25 ^oC in a temperature range of −55 to 85 ^oC (Mikkenie et al. 2012). If lower temperature rated capacitors are used, the capacitor would lose much of its capacitance due to temperature or DC bias.

During the selection of output capacitor C_{out}, a low ESR value should be put into consideration to reduce the ripple on the output voltage. Capacitors with similar qualities as C_{in} can be used as C_{out}. The recommended L and C values in the datasheet should be used if internal compensation is used in the converter. If external compensation is used, the capacitance has to be adjusted as;

$$C_{out_min} = \frac{I_{out_max} * D}{f_{sw} * \Delta V_{out}} \quad (6.10)$$

Where C_{out_min} is the minimum value of output capacitance; ΔV_{out} is the desired output voltage ripple. The additional ripple caused by ESR of C_{out} is expressed as;

$$\Delta V_{out_ESR} = \left[\frac{\Delta I_L}{2} + \frac{I_{out_max}}{1 - D}\right] * ESR \quad (6.11)$$

6.3. Results and discussion

The TEG/dc-dc converter system is tested with the input temperature in the range of 150ºC to 250ºC. The input temperature test scenarios for the model are shown in Figure 6.2 and Figure 6.3 for an increasing step and random signals respectively at hot side temperature terminal.

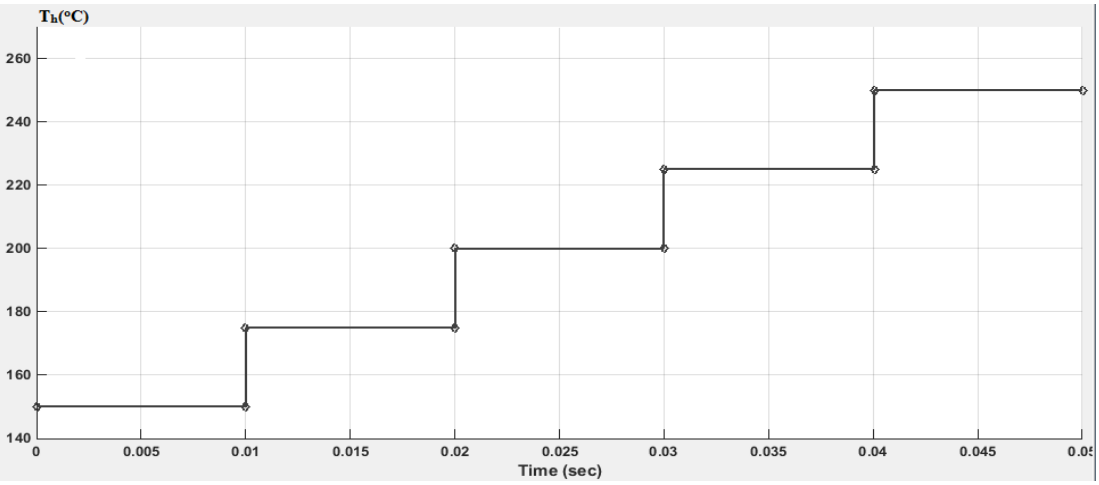


Figure 6.2. Increasing step hot side temperature

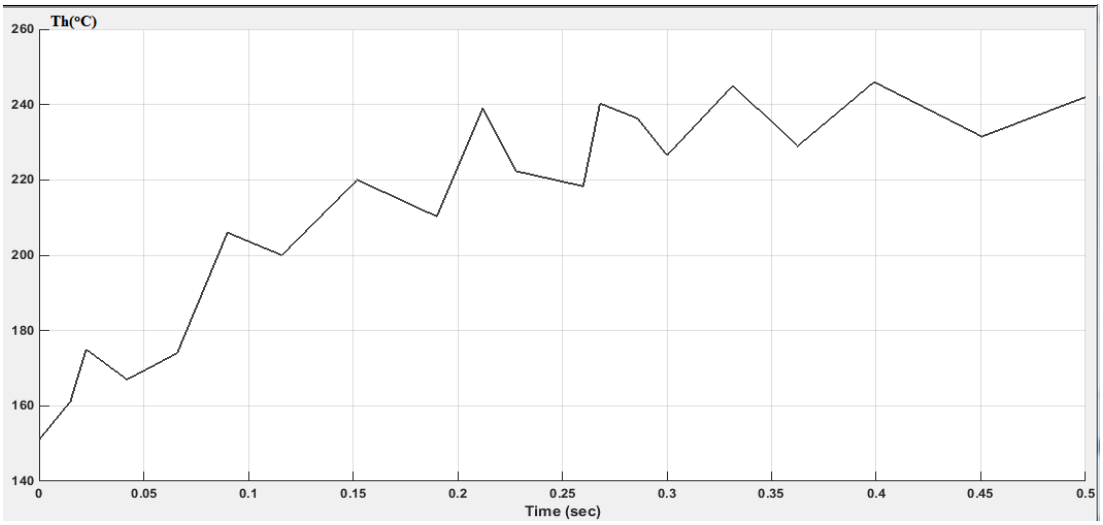


Figure 6.3. Increasing random hot side temperature

6.3.1. Results for the increasing step hot side temperature

The results in this section are based on the temperature input of an increasing step signal at the hot side temperature terminal of the model whereas at the cold side terminal, the temperature is maintained at a constant value of 30^{o}C. The model has been operated in both MPPT and direct PWM switching modes to compare the performances.

6.3.1.1 Converter parameters with the MPPT mode

During the MPPT mode, the model is subjected to varying loads in the range of 0-14 Ω to determine the effect of each load on the converter parameters including output voltage, current and power. Figure 6.4 and Figure 6.5 show the input and output voltages of the converter at different temperatures. It can be observed from both Figures that the input as well as the output voltages increase with the temperature as expected.

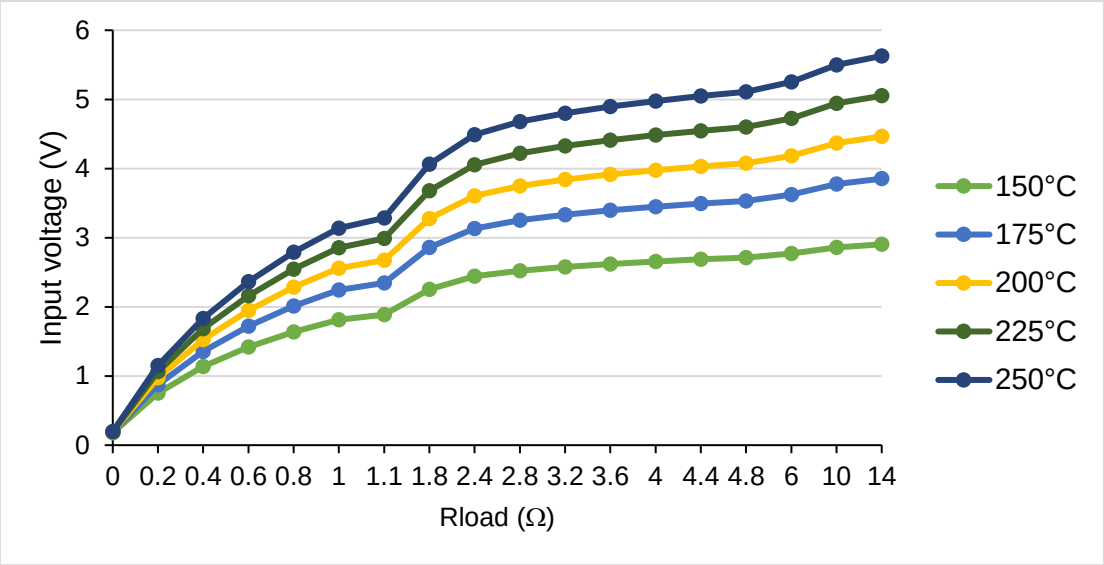


Figure 6.4. Variation of input voltage of the converter with resistance at different hot side temperatures

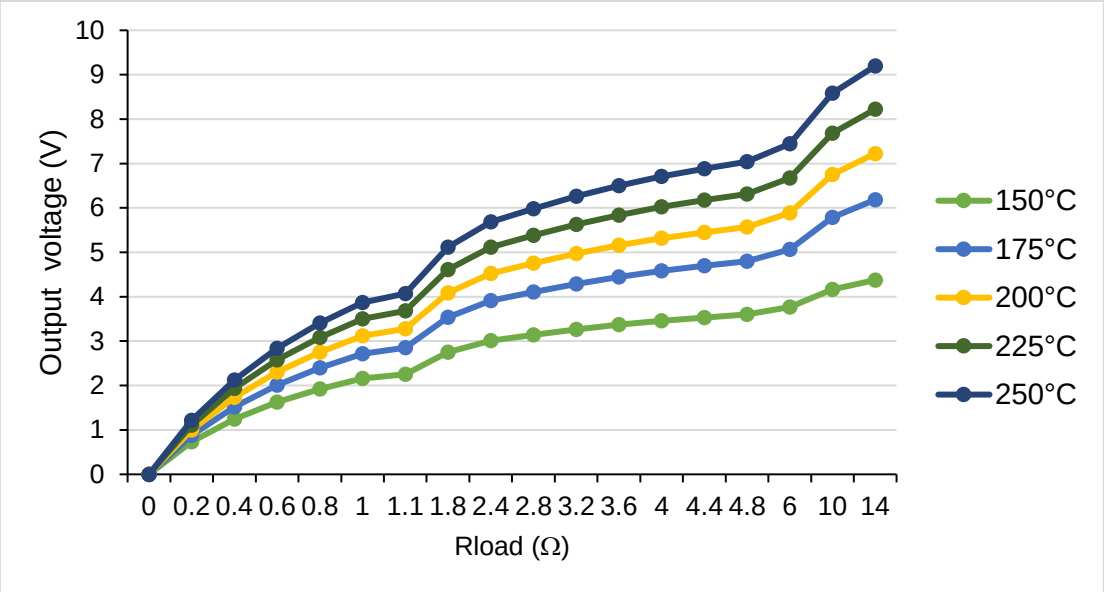


Figure 6.5. Variation of output voltage of the converter with resistance at different hot side temperatures

It is also clear that as the converter resistance increases, the input and output voltages also rise. However, a sharp increase in the voltage is observed from

zero resistance up to about 1.1Ω where the rate of rise changes after 1.1Ω load onwards up to the about 10Ω. The interpretation for this trend is best explained based on the power curve for the TEG shown in Figure 6.6. The graph of Rload against power output of the converter indicates that at a converter resistance of 1.1Ω, this is where the maximum power is obtained from the converter. This resistance is referred to as the optimal resistance at which the total resistance of the converter (including the ESR and other parasitic resistance of the components) is equal to the internal resistance of the TEG, R_{int}. At this point, the load is said to be matched and it is advisable to operate the converter at this load to harvest maximum power. The increase in T_h results in the corresponding increase in internal resistance of the TEG device, hence raising the optimum points because of the increase in the value of the matching load as seen in Figure 6.6. Also, the more the reistance is increased, the greater the output voltage increases as indicated at point where the output voltage increases further as the resistance is increased with a bigger value from 6Ω to 10Ω.

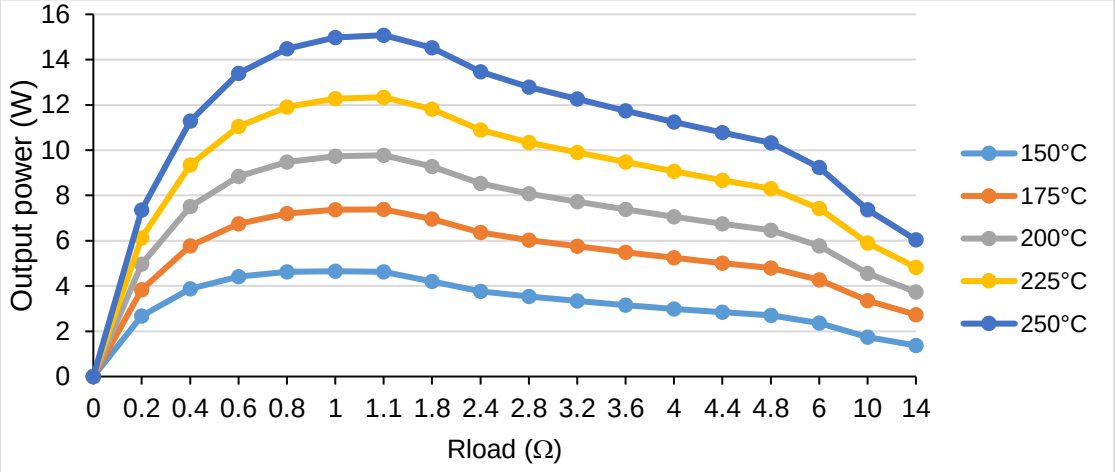


Figure 6.6. Variation of output power converter with resistance at different hot side temperature

Figure 6.7 shows the I-V characteristic of the converter plotted with output power. It is seen that as the converter resistance is increased, the output current reduces but the output voltage instead increases. The current and voltage curves meet almost at the maximum power point i.e. at the load matching point though the point of intersection is not the same for different hot side temperature. The output current is maximum at zero load. In ideal the circuit, the current is always zero at zero load but in this case the current is maximum since there is some ESR resistance in the output capacitor which is parallel to the output terminal. So, the current through the diode takes the easiest path to the ground.

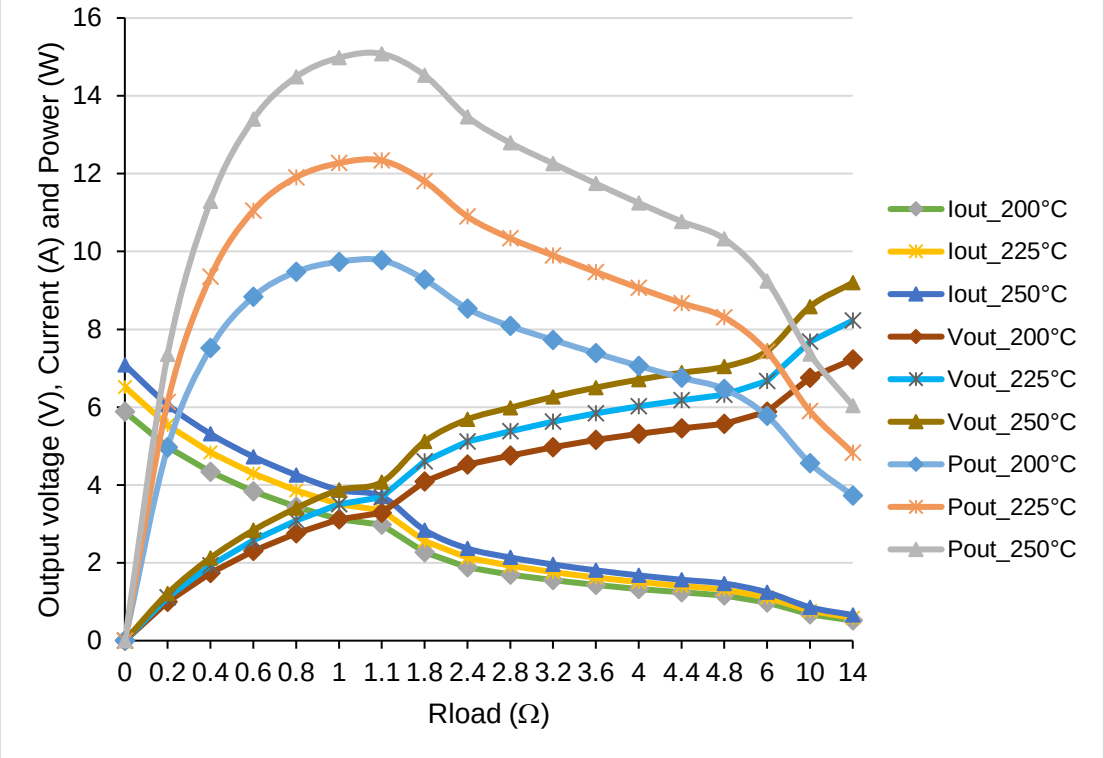


Figure 6.7. Variations of output power, voltage and current with load resistance at different hot side temperature

6.3.1.2. Converter parameters with direct PWM signal

During the direct PWM mode, the system is subjected to varying loads in the range of 0-40 Ω to determine the effect of each load on the converter parameters at different values of D. Figure 6.8 shows the output voltages of the converter at different temperatures and values of D. Higher output voltage is obtained at D = 10% and the least voltage is obtained at D = 80%. During simulation, it is noticed that different ranges of D give different output voltages as indicated in Figure 6.8. The maximum voltage is achieved at duty cycle range of 1 – 20%. Similarly the output power of the converter is shown in Figure 6.9. The only observable difference between the output voltage and output power is that the rate of increase of output power with T_h rises as D increases. Nevertheless in both cases the output voltage and power increase linearly with temperature. The slopes for the line graphs indicated in Figure 6.9 are different from each other whereby the highest slope is obtained at a duty cycle range of 1-20%. Since different duty cycle values respond differently to the cganges in temperature, a suitable value of D that suits the load must be determined for optimum performance of the system.

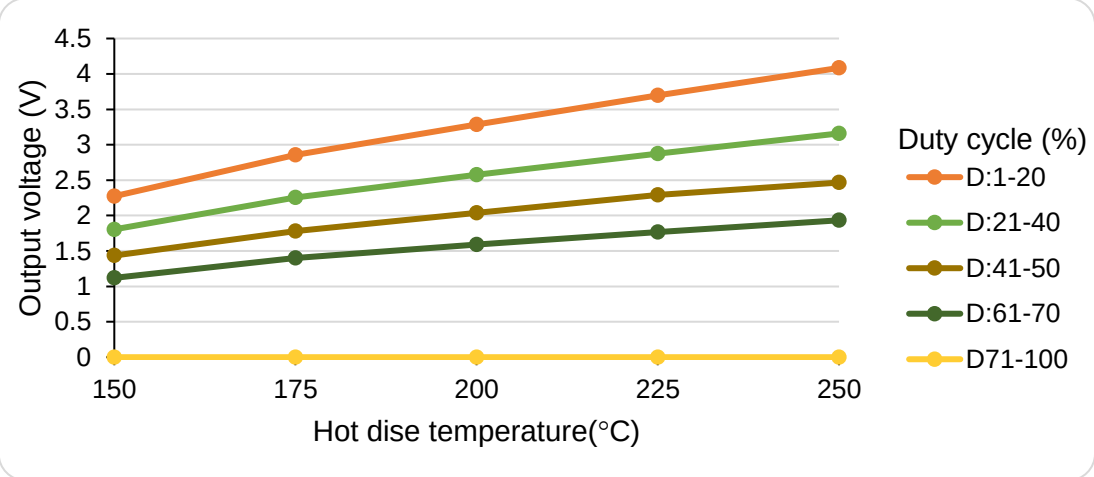


Figure 6.8. Variation of converter output voltage with hot side temperature and duty cycle at Rload = 1.1 Ω

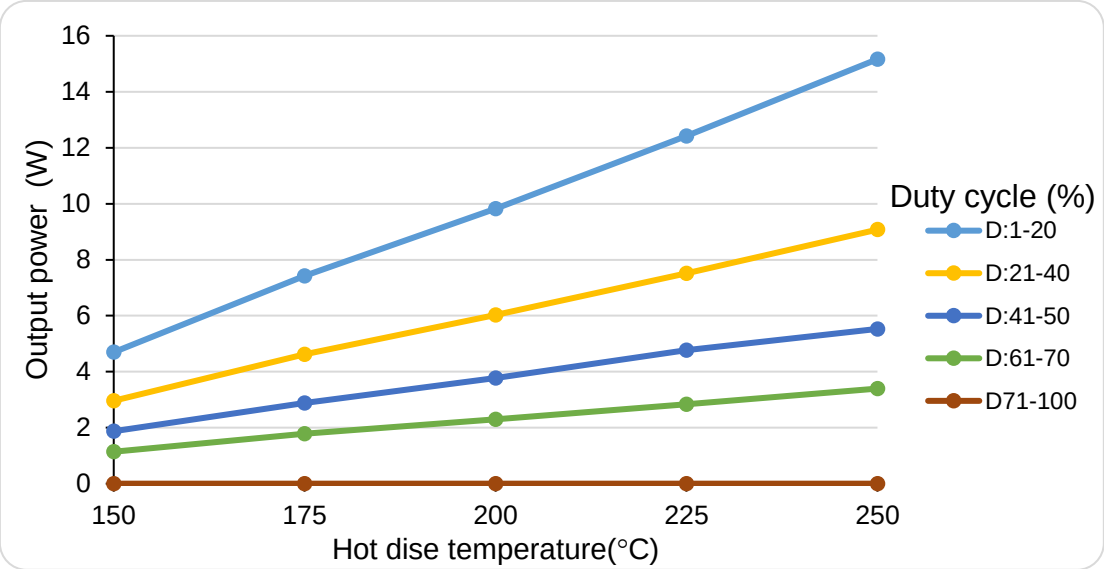


Figure 6.9. Variation of converter output power with hot side temperature and duty cycle at Rload = 1.1Ω

Figure 6.10 shows the output power at different values of D. For clarify, only three T_h and D values have been plotted. It is noted that for the same range of duty cycle, the matching load is the same even for different temperatures. For example in Figure 6.10 the matching load is 1.1Ω for T_h of 150^{o}C, 200^{o}C and 250^{o}C at a duty cycle of 10%. However, as soon as D is changed, the matching load also changes. For example the matching load is 1.1Ω, 1.8Ω and 2.4Ω for the D values of 10%, 30% and 50% respectively at the same T_h of 250^{o}C. Therefore, it can be concluded that in cases where a fixed load is connected to the converter, it is not suitable to change the duty cycle even at different values of T_h.

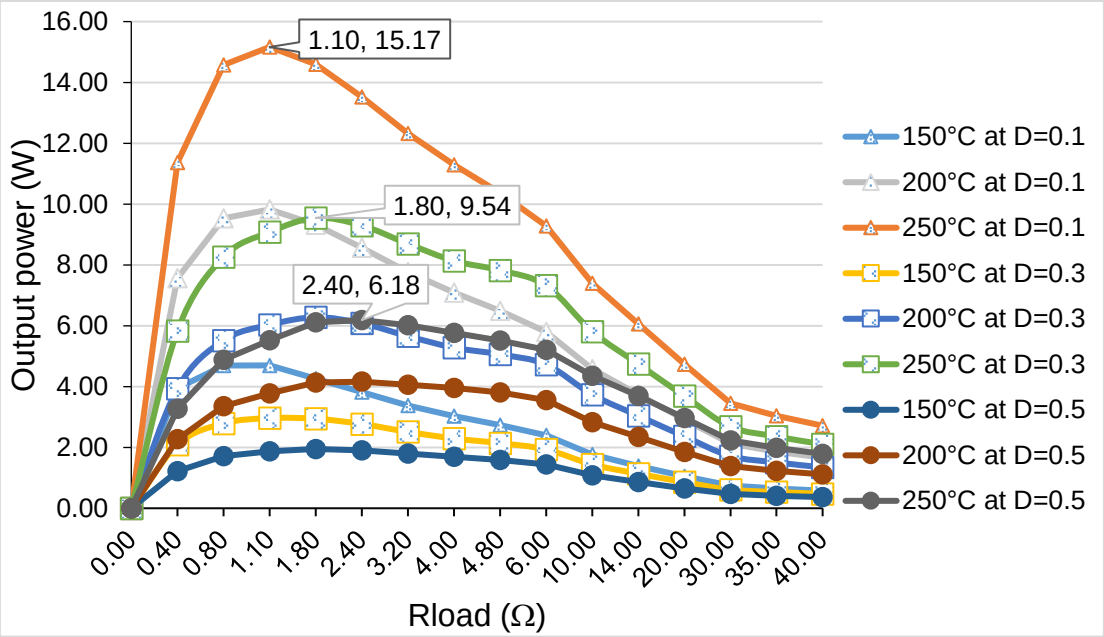


Figure 6.10. Comparison of output power at different values of D and hot side temperature

Figure 6.11 shows the MPPT and direct PWM model output powers. The maximum power from the converter is obtained at the duty cycle of 10%. The output power from MPPT based converter model is equal to the output power from the direct PWM mode at D =10% (as well as D in the range 1-20%). However, at higher values of D, the output power reduces. Therefore, the MPPT can automatically extract maximum power from the system without having to adjust any component from the MPPT algorithm as it is the case with direct PWM mode.

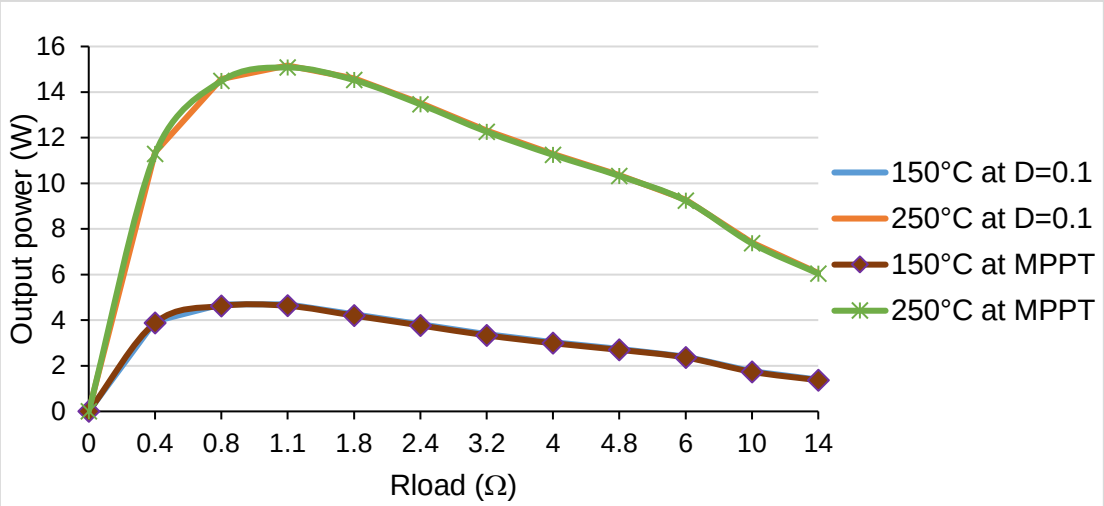


Figure 6.11. Comparison of MPPT and direct PWM mode output power

The voltage conversion ratios (VCR) at D =0.1 for different converter loads are shown in Figure 6.12. It is clearly observed that as the temperature increases, VCR reduces. However, VCR reduces with the converter load. Therefore in this TEG/dc-dc converter system, if a higher voltage is required, it is necessary to operate the TEG system at slightly lower or moderate hot side temperature so that the lower TEG output voltage can be boosted to the desired voltage level suitable for the application.

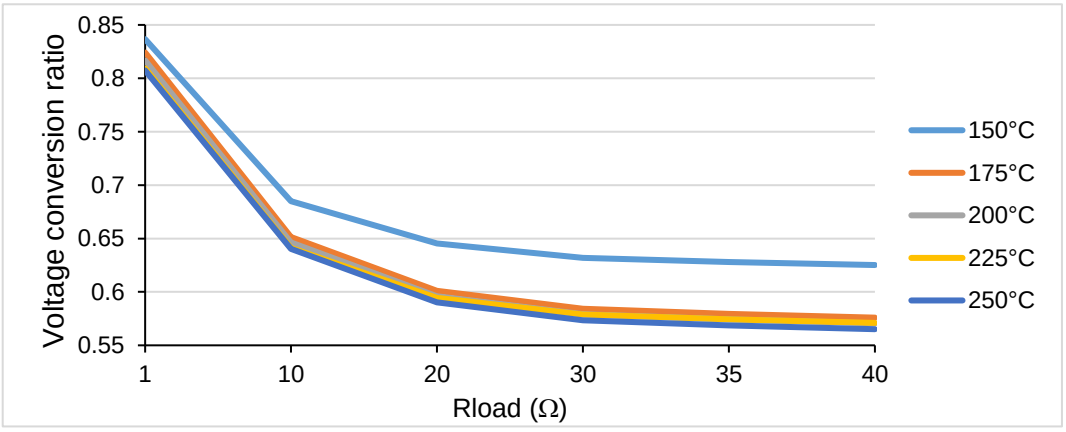


Figure 6.12. Voltage conversion ratio at D=0.1 for different converter loads at different hot side temperatures

6.3.2. Results for the increasing random hot side temperature

To further study the capability of the dc-dc converter to stabilise the power output from TEG, an increasing random hot side temperature in Figure 6.3 is applied to the MPPT and direct PWM based modes so that the behaviour of the output parameters can be analysed. Note that the cold side temperature is still maintained at 30^{o}C. Figure 6.13 shows the voltages and output current for MPPT based mode with a converter load Rload =1.1Ω. From this figure that although the input temperature is random in nature, the output voltage resulting from the converter is almost constant. Unlike the input random hot side temperature at the hot side terminal, the output voltages and currents have no several optimum points. Similar to the output voltage, the input voltage to the converter is almost constant because it is filtered by the input capacitor. Likewise, Figure 6.14 shows the voltages and output current for MPPT based model at Rload =4Ω. The noticeable difference is that the voltage is increased to 4.6V peak for Rload =4Ω load as compared to 2.9V peak for Rload =1.1Ω. Additionally, the output current is reduced to 1.2A peak down from 2.6A peak.

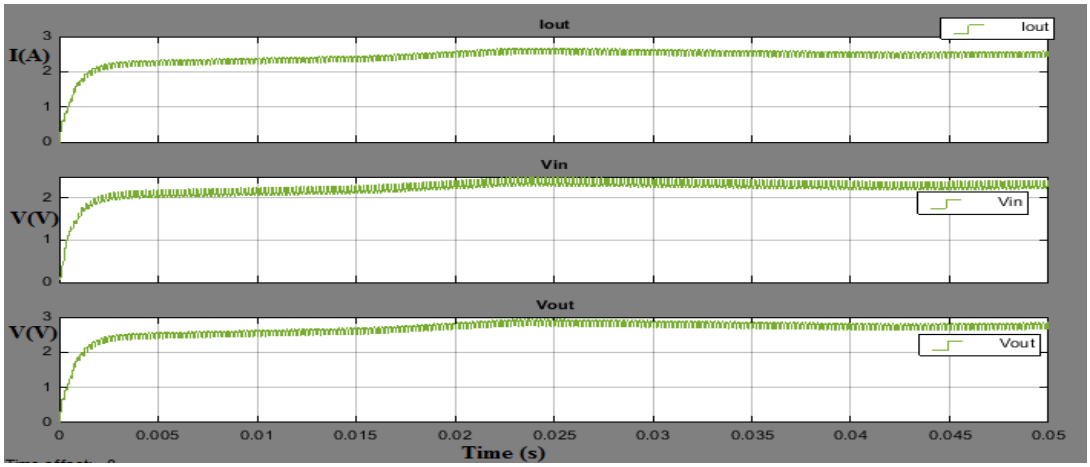


Figure 6.13. Voltages and output current for MPPT based model with Random increasing hot side temperature at Rload =1.1Ω

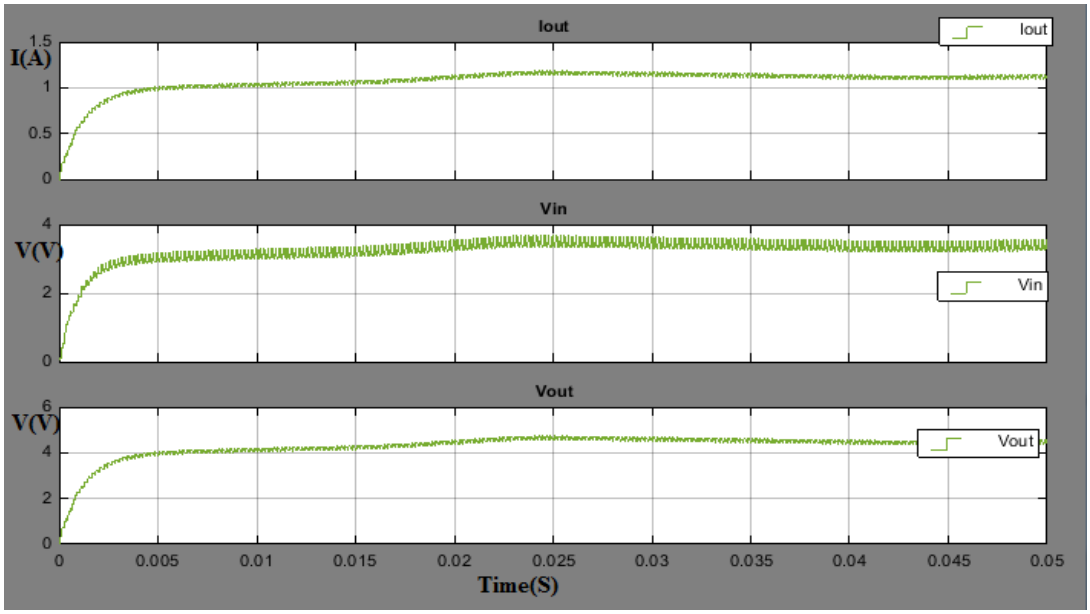


Figure 6.14. Voltages and output current for MPPT based model with Random increasing hot side temperature at Rload =4Ω

Figure 6.15 shows the voltages and output current for the direct PWM based model with random increasing hot side temperature at Rload =1.1Ω and D =10%. As already noted, the output voltage and current are more or less the same for direct PWM mode at D =0.1 and the MPPT mode. The difference cannot be clearly observed on the graph but rather by calculations. Therefore, similar results are indicated in Figure 6.15 and Figure 6.14 since the converter load is the same. However, at a higher value D i.e. D = 0.5, the converter fails to weed out some of the peaks from the input voltage. Hence the input voltage as well as the output voltage and current are observed with the over shooting behaviour in Figure 6.16, which may result into more converter losses. It is therefore recommended to use a converter at a lower duty cycle to get a highly stabilised output power. However, the best option is to make use of MPPT algorithm since it automatically choose the MPP without the need to adjust the duty cycle.

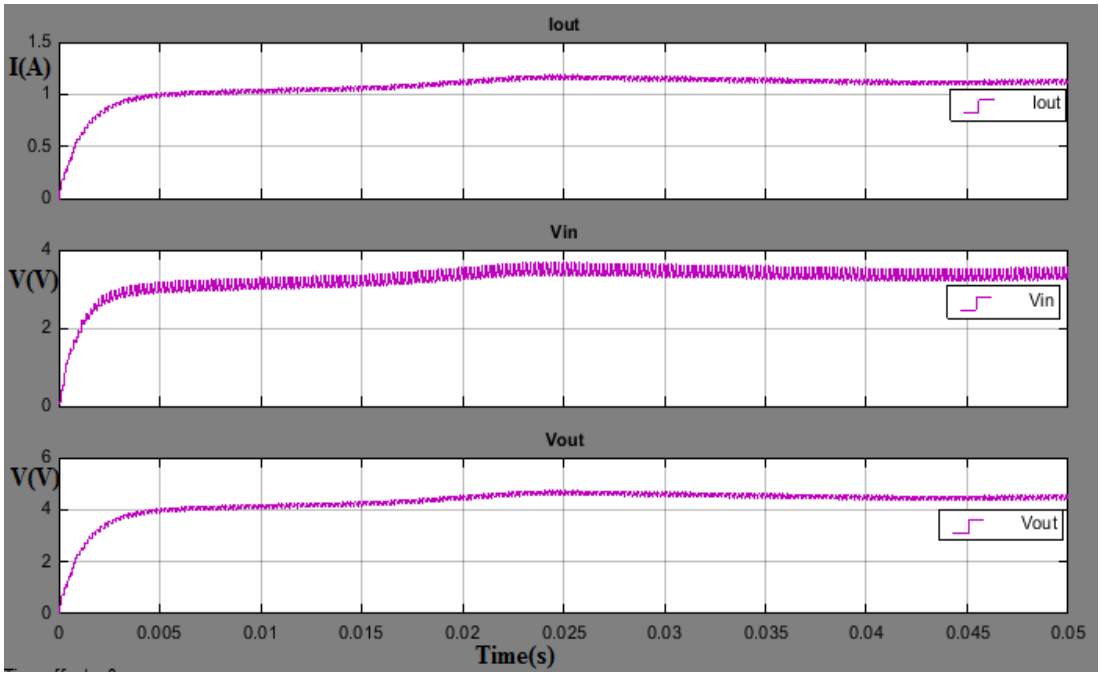


Figure 6.15. Voltages and output current for direct PWM based model with Random increasing hot side temperature at D =0.1 and Rload =4Ω

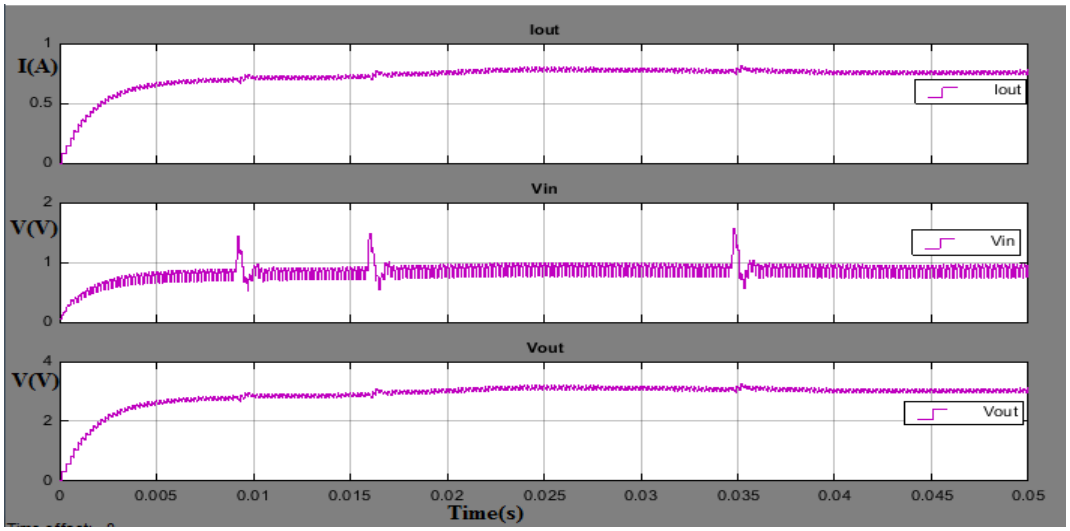


Figure 6.16. Voltage and output current for direct PWM based model with Random increasing hot side temperature at D =0.5 and Rload =4Ω

6.3.3. Effect of converter components on the accuracy of results

In this section, the causes of inaccuracies in the converter output parameters are discussed. As discussed earlier, the converter losses are mainly caused by the parasitic resistance of the converter components such as the ESR of the input and output capacitors, resistance of the inductor, sometimes the resistance of the switch and others. Figure 6.17 and Figure 6.18 indicate the residual voltage that remains when the converter is not loaded i.e. at Rload =0Ω. This represents the ripple voltage caused by the ESR of the output capacitor since the output capacitor is in parallel with Rload. In Figure 6.17, the ESR is kept at $1x10^{-9}\Omega$ while in Figure 6.18 it is $1x10^{-6}\Omega$. The voltage spikes on the ripple can be observed to increase when the ESR is increased from $1x10^{-9}\Omega$ to $1x10^{-6}\Omega$ in Figure 6.18.

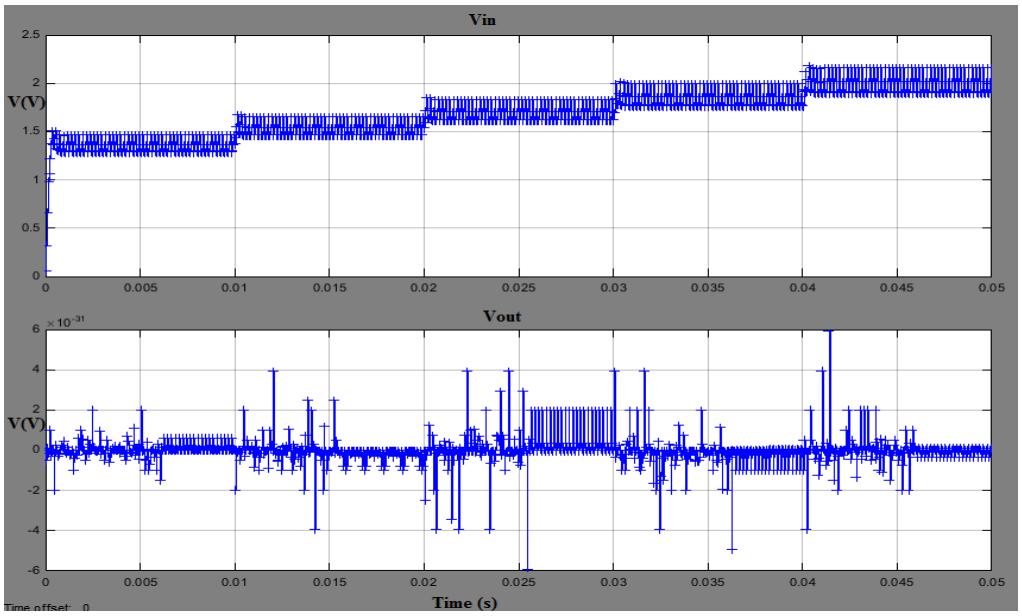


Figure 6.17. Ripple voltage at ESR = $1x10^{-9}\Omega$

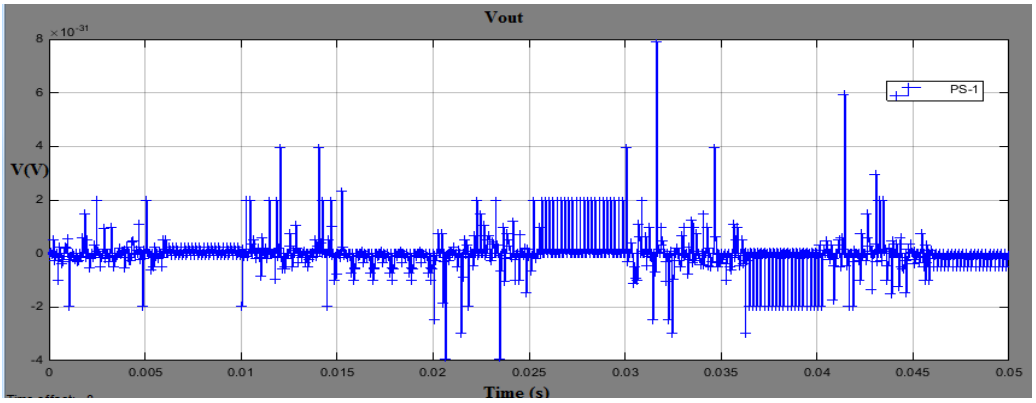


Figure 6.18. Ripple voltage at ESR = $1x10^{-6}\Omega$

The effect of the ripple voltage can clearly be noticed if the load is increased from 0 Ω to 1Ω. Figure 6.19 and Figure 6.20 show the ripple voltages for ESR of $1x10^{-6}\Omega$ and 1Ω respectively at Rload = 1Ω. In Figure 6.19, the spread of the ripple voltage on the output voltage is less than that of ESR of 1Ω. Since the ripples are higher frequency harmonics and are within the audible range, if the converter load is an audio equipment such as a radio receiver, the ripple will be audible within the output of the receiver and therefore causes noise interference. Hence, the ESR has to be kept as low as possible, else the ripple should be filtered to avoid such unnecessary occurrences within the TEG system.

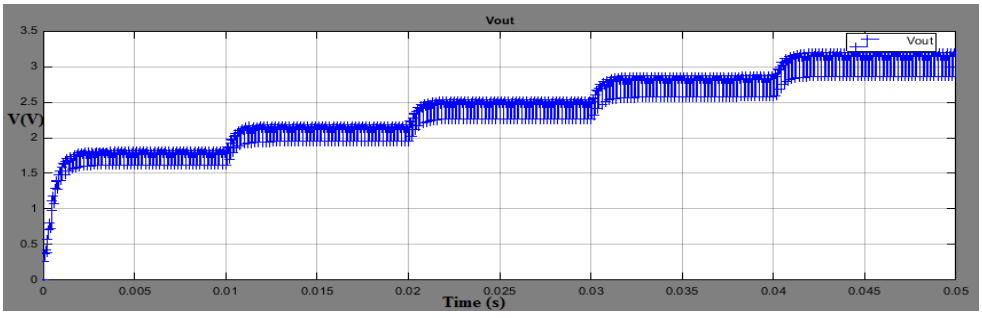


Figure 6.19. Ripple voltage at ESR = $1x10^{-6}\,\Omega$ when Rload = 1Ω

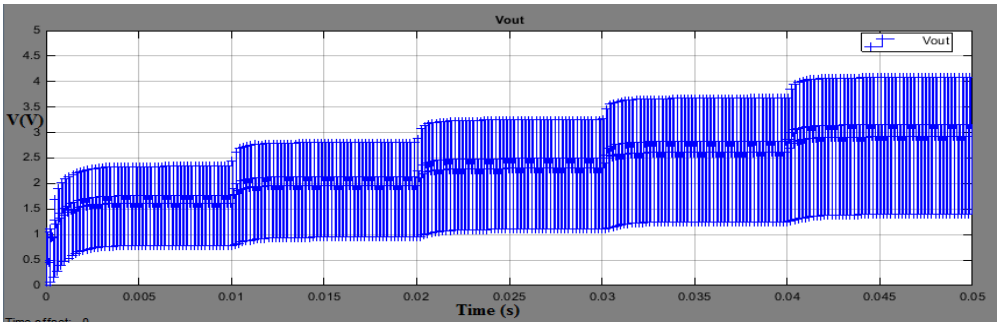


Figure 6.20. Ripple voltage at ESR = 1Ω when Rload = 1Ω

The switching frequency also needs proper tuning as it affects the output parameters. Figure 6.21 illustrates the effect of increasing the switching frequency from 5 kHz to 20 kHz on the input and output voltages where overshooting is observed. Although increasing F_{sw} reduces inductor ripple current and output ripple voltage, it has the disadvantage of increasing the switching losses, hence reducing converter efficiency. Therefore, care must be taken when choosing the value of the switching frequency to keep the value of the ripple current as low as possible.

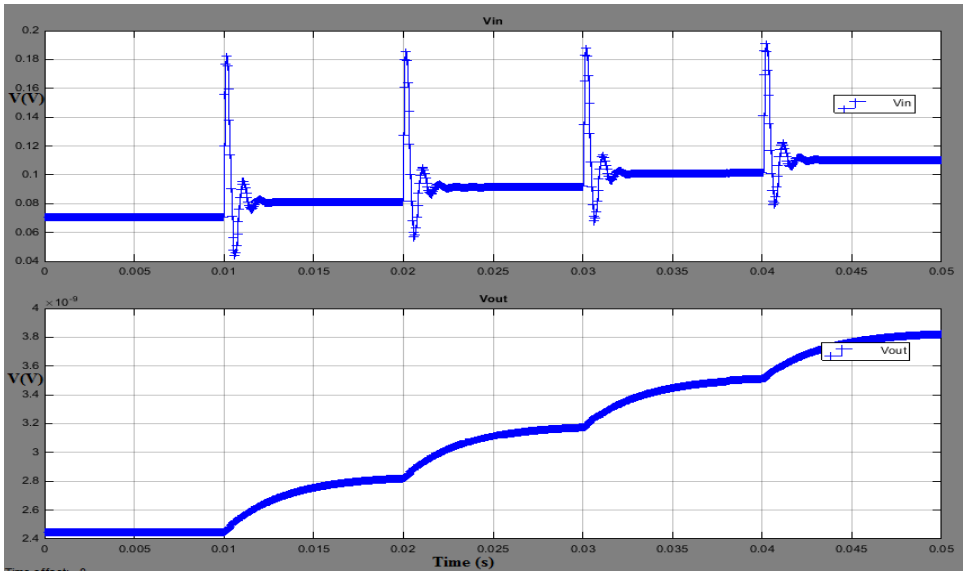


Figure 6.21. Effect of increasing the switching frequency from 5 kHz to 20 kHz on the input and output voltage

6.4. Summary

A dc-dc converter as a power conditioning device can provide a more stable power output and improve the efficiency of TEG system. But, to facilitate better performance improvement, MPPT algorithm can be applied to extract the maximum power from TEG system. Therefore, in this chapter the parameters that influence the performance of TEG with dc-dc converters in different modes have been analysed. A TEG/dc-dc boost converter system has been analysed in both MPPT and direct PWM modes. The converter performance has been analysed with reference to the temperature variations at the hot side of the TEG as well as the variation of the converter load. Results indicate that a dc-dc converter with MPPT based model is able to extract maximum power from TEG better than the direct PWM based model. From the study, it has been established that proper selection of converter components is necessary to avoid converter losses as well as noise interferences on the load connected to TEG-dc-dc converter system.

Chapter 7. Modelling of TEG/dc-dc converter system with ESC MPPT

This chapter presents the performance of extremum seeking control (ESC) MPPT algorithms applied to TEGs. The ESC technique is compared with both P&O and IC MPPT methods. The simplified TEG model is validated with results from multiphysics (COMSOL) modelling software. To assess the effect of temperature dependency of TEG parameters, two TEG materials have been chosen; Bi_2Te_3 with temperature dependent Seebeck effect (S), electrical conductivity (σ) and thermal conductivity (k), and PbTe with non-temperature dependent S, σ and k. Results indicate that ESC MPPT method extracts more power than P&O technique, where the output power of ESC MPPT is higher than that of P&O by 0.47 W, which is 6.1% higher at a temperature of 200°C. It is also noted that the ESC MPPT based model is almost fourfold faster than the P&O method in terms of computation speed. Hence, ESC MPPT method outperforms the P&O technique.

7.1. Background

There are several other MPPT methods that can be used to improve performance of TEG systems. In this chapter, the performance of ESC MPPT algorithms is conducted. ESC has been generally used for estimating the optimum operating point of nonlinear systems (Lei et al. 2011). The main advantage of ESC compared to many other optimization techniques is that no plant model, or just a relatively simple plant model, is used, making it suitable to optimize the performance of complex systems (Van De Wouw et al. 2012). Although the simplified TEG model implemented in the current study was first introduced in previous research, no attempt has been made to validate the TEG model to date. Hence, another aim of this chapter is to verify the TEG model as well as suggesting ways for its improvement. Therefore, the results of

Simulink TEG model are validated by comparing with those obtained from the COMSOL Multiphysics modelling software.

7.2. TEGs with different materials

A typical TEG device is shown in Figure 7.1(a). A TEG module consists of arrays of N and P-type semiconductors as shown in Figure 7.1(b), in which, by applying a heat source on the hot side and a cold heat sink to the other side, electric power is produced. In a thermoelectric material, there are free electrons or holes which carry both charges (negative and positive) and heat. If the free charges are positive (p-type material), positive charge will build up on the cold end which will have a positive potential (Shi et al. 2015). Similarly, negative free charges (n-type material) will produce a negative potential at the cold end (Bell 2008) as shown in Figure 7.1(c).

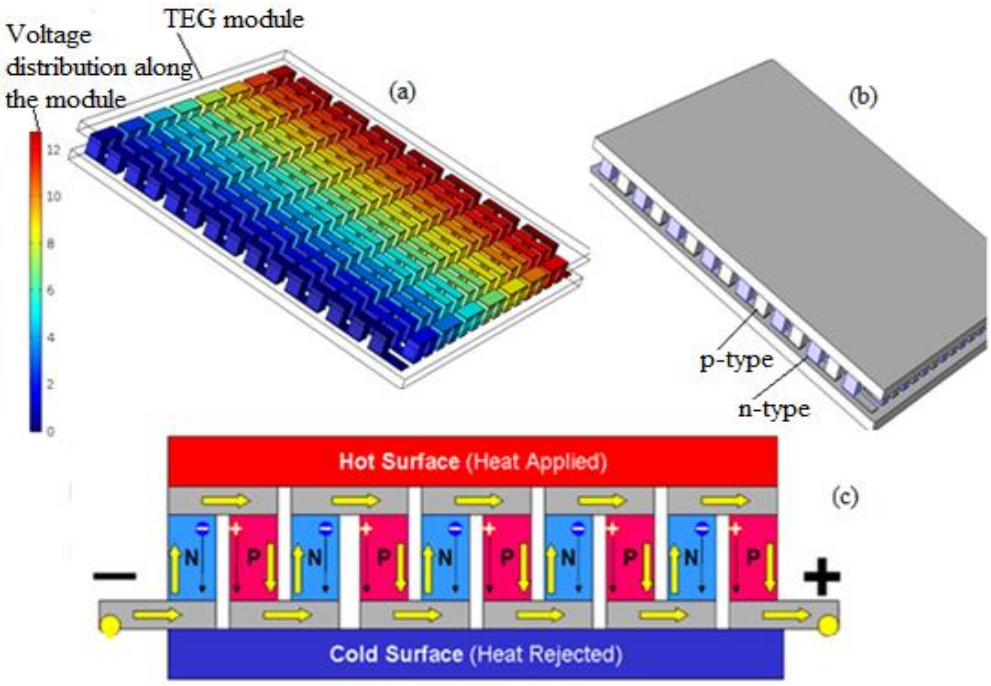


Figure 7.1. Principle of operation of a TEGs: part (C) is modified from (Electropaedia n.d.)

The most widely used TEG materials are Bismuth Tellurides (Bi_2Te_3) because their cost is low compared to other TEG materials. Figure 7.2 shows the temperature dependent Seebeck coefficient of Bi_2Te_3 material for N- and P-type semiconductors of a TEG device in Figure 7.1(a). Due to the nonlinear nature of the Seebeck effect, which is responsible for the generated electric potential, the output power of a TEG is also nonlinear. The maximum output power of the TEG can be calculated as (Shi et al. 2015);

$$P_{max} = \frac{(nS\Delta T)^2}{4R_{int}} \tag{7.1}$$

Where P_{max} is maximum output power of TEG; n is the number of thermoelectric pairs and R_{int} is the internal resistance of the TEG.

TEG devices must be operated at maximum efficiency to obtain maximum power. In waste heat recovery applications, the cost per watt can be minimized by operating the TEG device at maximum power with the efficiency expressed as (Kempf & Zhang 2016);

$$\eta_{TEG} = \frac{\Delta T}{T_h}\frac{ZT_h}{ZT_m + ZT_h + 4} \tag{7.2}$$

Where ZT_h is the ZT at T_h, and ZT_m is the mean ZT between T_h and T_c.

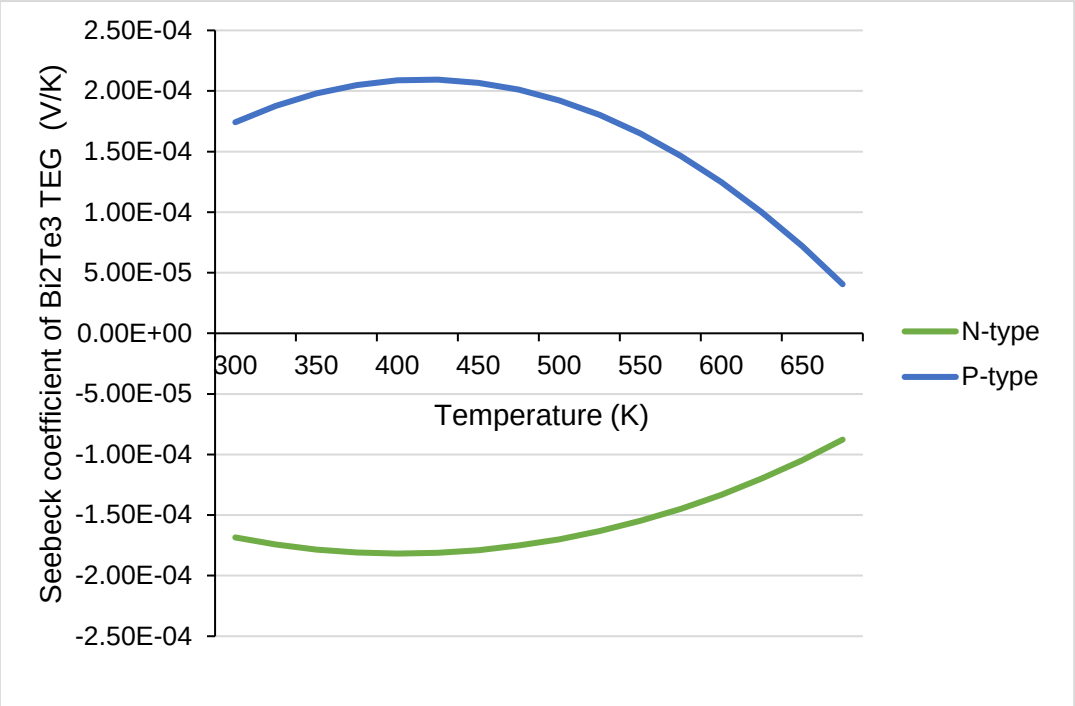


Figure 7.2. Seebeck coefficient of Bi_2Te_3 TEG

Other materials and techniques are being applied to enhance power generation and the efficiency of TEGs. The most prominent materials to be used for TEGs in the exhaust heat recovery systems would be the materials rated for high temperature such as PbTe and calcium manganese ($CaMn_4$) (Orr et al. 2016). Table 7.1 shows the properties of the PbTe TEG material. It should be clearly noted that the Seebeck coefficient is non-temperature dependent i.e. S is independent of temperature variation.

Table 7.1. Material properties for lead Telluride – PbTe

	Seebeck coefficient (V/K)	electrical conductivity (S/m)	Thermal conductivity (W/(m*K))
n-type	-187×10^{-6}	6.0976×10^{4}	1.46
p-type	187×10^{-6}	6.0976×10^{4}	1.46

During modelling, the TEG structure is simplified to a solid structure so as to make heat transfer analysis easy, keeping its thermal behaviour being equivalent to the TEG based on a 1D heat conduction theory (Li et al. 2016). In the simplified TEG models, some assumptions include: (1) homogeneity of TEG component materials as well as constant heat specific capacity, density thermal resistance i.e. they are independent of temperature; (2) negligible thermal contact effect inside the TEG and on the interfaces between the heat exchanger, the heater and the TEG; (3) the effects of the air inside, free heat convection and equivalent density of the TEG are not accounted for. In the three-dimensional Multiphysics model, energy equations of the metal connector, p-type semiconductor, n-type semiconductor, and ceramic plate are given as (Meng et al. 2016);

$$k_{j,p,n,ce}\nabla^2 T + \frac{J^2}{\sigma_{j,p,n,ce}} - \beta_{j,p,n,ce}\vec{J} * \Delta T = 0 \qquad (7.3)$$

Where; k is the thermal conductivity, σ is the electric conductivity, and β is the Thomson coefficient. The subscript j is for the connector, p for the p-type semiconductor, n for the n-type semiconductor and *ce* for the ceramic plate. The first term on the left side in Eq. (7.3) is the Fourier heat conduction, the second is the internal heat sources due to the Joule heating. J(x, y, z) is the local current density, where J = 0 represents the ceramic plate. The third term is the Thomson coefficient expressed as;

$$\beta = T\left[\frac{dS}{dt}\right] \qquad (7.4)$$

where S is the Seebeck coefficient of semiconductor materials.

However, if the Thomson effect is assumed constant, the third term of equation. (7.3) becomes zero. Figure 7.3 shows the temperature dependent values of k for the Bi_2Te_3 material with N and P-type semiconductors of a TEG. Especially for the n-type element, as the temperature increases, the thermal conductivity

increases. In some situations, the thermal conductivity can be maintained at a constant value as the temperature varies, such as for the PbTe material indicated in Table 7.1. In such a case, the output power of TEG is independent of the value of k.

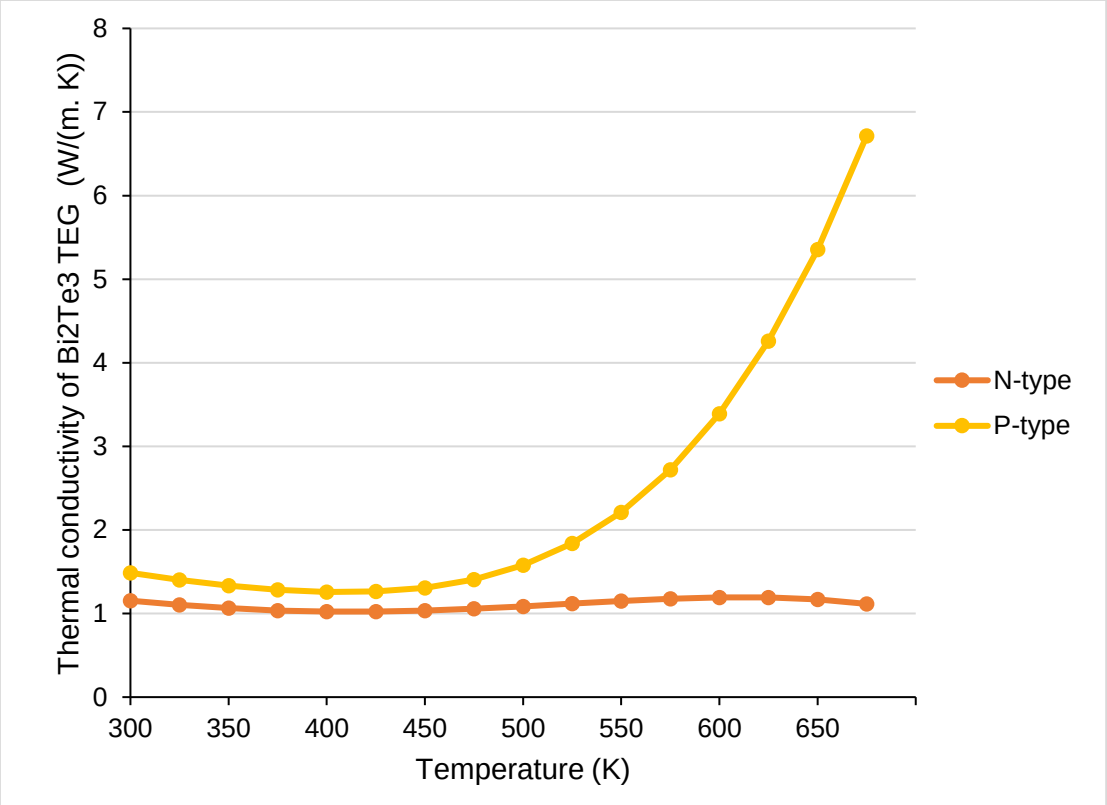


Figure 7.3. Variation of thermal conductivity with temperature for the Bi_2Te_3 material of TEG

Alternatively, the electrical conductivity (σ) can also sometimes be temperature dependent as illustrated in Figure 7.4 for the Bi_2Te_3 TEG material, where the values are the same for n- and p-type semiconductors. The electrical conductivity can also be considered as a constant value in some models for simplicity.

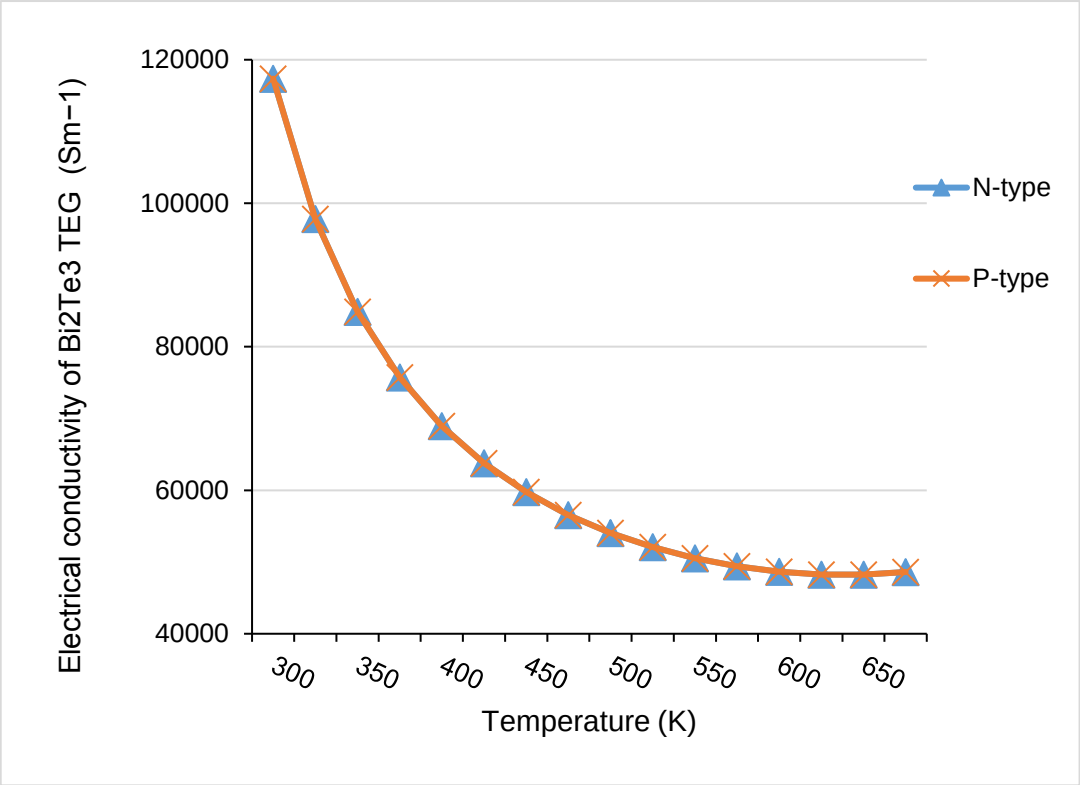


Figure 7.4. Variation of electrical conductivity with temperature for the Bi_2Te_3 material of TEG

As noted earlier, the TEG model implemented in the current study was first introduced by Molani (Li 2011) to simulate the TEG with real time temperature inputs. Although, it has been applied to the previous work (Ssennoga Twaha et al. 2017), no attempt has been made to validate the model. Hence, the simplified TEG model is verified here by using the results obtained for the Bi_2Te_3 and PbTe based TEG devices from COMSOL.

7.3. Principle of operation MPPT techniques

7.3.1. ESC MPPT technique

The ESC deals with the online optimization problem of finding and optimizing an input $U_{\text{opt}}(t)$ for mainly an unknown and/or time-varying cost function $l(t,u)$, where u(t) is the input parameter vector (Lei et al. 2011), i.e;

$$U_{\text{opt}}(t) = arg \min_{u \in R^m} l(u,t) \tag{7.5}$$

The block diagram of a classic ESC method is shown in Figure 7.5. In this method, it is assumed that the characteristics curve of the system under consideration is concave. Therefore, this method can find application in tracking the MPP in TEG systems where the P-V characteristic curves are nonlinear.

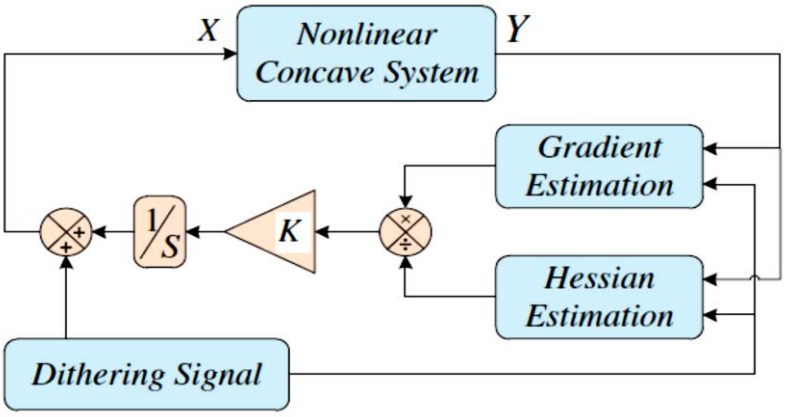


Figure 7.5. Classical ESC scheme (Heydari-doostabad et al. 2013)

A classic ESC algorithm should have a gradient estimator to fulfil the MPPT functionality. For MPPT, a nonlinear characteristic power curve for the TEG is expressed as;

$$P_{out_teg} = \varphi(x) \tag{7.6}$$

Where p is the output power of the TEG and x is the input of the TEG device which is a function of the signal u, and $u_0 \sin(\omega_0 t)$ is the dithering signal. Consequently, the output power is as follows;

$$P_{out_teg} = \varphi(u + u_0 \sin(\omega_0 t)) \tag{7.7}$$

The dithering signal aids in reducing the electromagnetic interference in the system, hence improving the performance of the MPPT algorithm (Biagi et al. 2012). However, there are some extremum seeking controllers without dither in the extremum seeking loop but instead depend on the past data of the performance map to estimate the gradient of the performance map by means of a 1st-order least squares fit (Hunnekens et al. 2014). The dither-less ESC controllers allow for an asymptotic stability result, as opposed to practical stability in dither-based schemes and, therefore enables convergence to the optimal performance of the parameters. Now, equation (7.7) can be approximated by Taylor's series around u;

$$P_{out_teg} \approx \varphi(u) + \frac{d\varphi(u)}{d\mathrm{u}} u_0 \sin(\omega_0 t) + \frac{1}{4}\frac{d^2\varphi(u)}{du^2} u_0^2 - \frac{1}{4}\frac{d^2\varphi(u)}{du^2} u_0^2 \cos(2\,\omega_0 t) \tag{7.8}$$

It could be seen that the TEG output power now has a low frequency with harmonics having frequencies of ω_0 and $2\omega_0$. Applying a high pass filter, the output becomes;

$$P_{out_f} \approx \frac{d\varphi(u)}{du^2} u_0 \sin(\omega_0 t) - \frac{1}{4}\frac{d^2\varphi(u)}{du^2} u_0^2 \cos(2\,\omega_0 t) \tag{7.9}$$

When P_{out_teg} has gone through a low pass filter, the output of ESC system is expressed as;

$$P_{est.} \approx -\frac{1}{6}\frac{d^2\varphi(u)}{du^2} u_0^4 \tag{7.10}$$

The block diagram of ESC system estimator is shown in Figure 7.6.

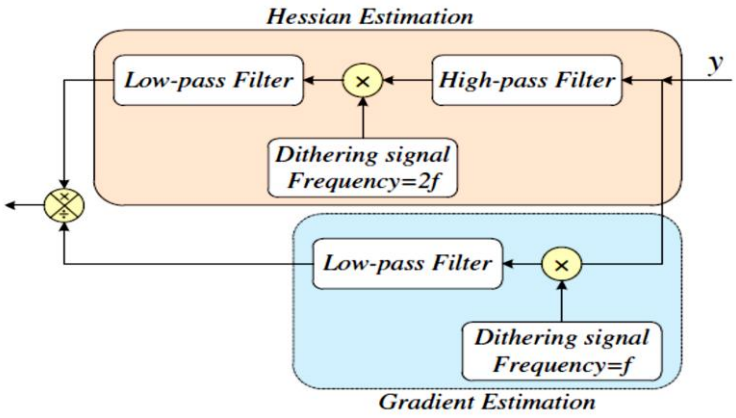


Figure 7.6. Classical ESC estimator (Heydari-doostabad et al. 2013)

The ESC algorithm applied in this study is modified from the ESC technique proposed and applied to PV systems by Malek (Malek 2016). The ESC MPPT is a fractional order extremum seeking algorithm that utilizes output measurements of the plant, with superior performance in various aspects such as robustness and convergence speed (Malek et al. 2016). The block diagram of the applied ESC circuit is shown in Figure 7.7. The constant k_1 and k_2 represent the frequencies of the low and high pass filters of the estimator, respectively. G1 is a proportional gain of the controller which is used to adjust the value from the integrator. The dithering sinusoidal signal is also passed through a gain G_2. The integrator 1/s is applied to the output of the low pass filter to eliminate the steady state offset of the controller. The gains G_1 and G_2 are tuned until a suitable output power is achieved from the converter.

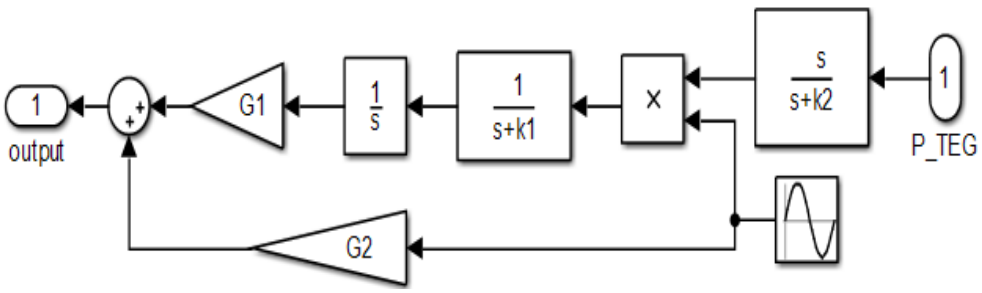


Figure 7.7. The block diagram of the applied ESC circuit

Figure 7.8 shows the block diagram of the implemented TEG/dc-dc converter system with ESC MPPT. The cold side temperature is maintained at 30ºC while the hot side temperature is varied, initially set at 200°C and incremented by 25°C up to the highest temperature of 400°C.

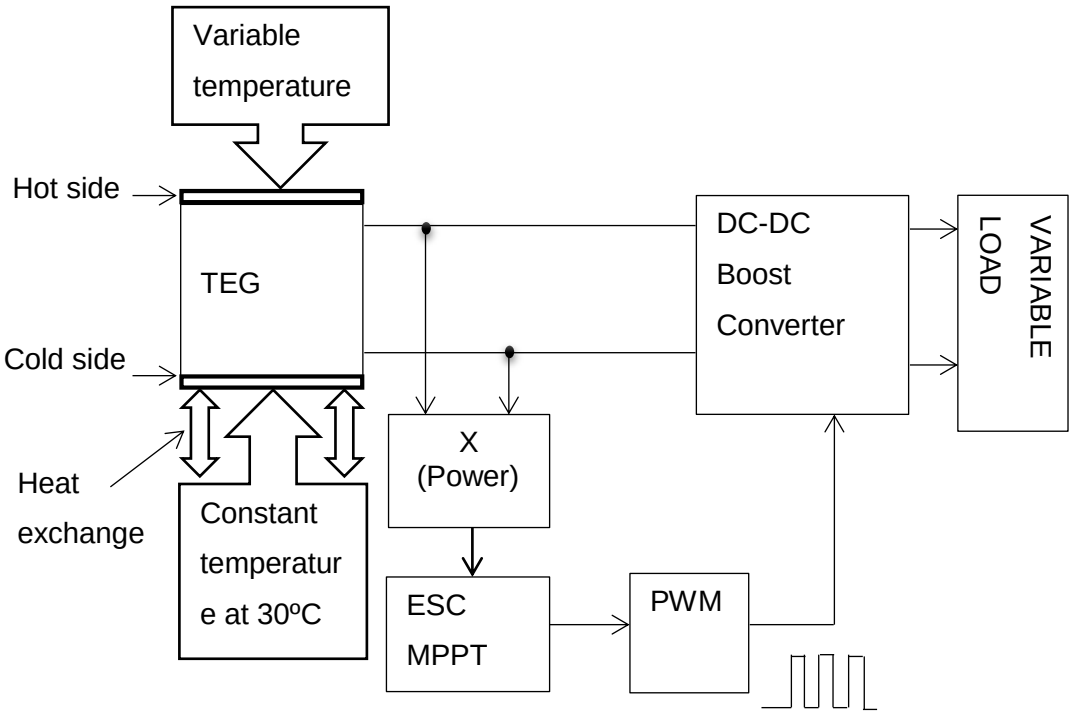


Figure 7.8. Block diagram of TEG/dc-dc converter system with ESC MPPT

7.3.2. P&O MPPT technique

Since P&O method is also compared with ESC, on top of IC method, its principle of operation is discussed here.The P&O algorithm whose working principle is demonstrated in Figure 7.9 introduces a perturbation ΔV in the operating voltage and current of TEG. As a result, the change in the operating power is observed. The relative increase in the operating power indicates that the converter is approaching the MPP. Similarly, during the succeeding sampling cycle, the slope (direction) of perturbation is maintained whereas the reference current and voltage are further increased by ΔV value. Once the

vicinity of MPP is reached, for each new perturbation (with alternating sign polarity), the algorithm will go back and forth around the MPP. Consequently, it does not reach exactly the MPP but it oscillates around that point indefinitely (Ishaque & Salam 2013). The P&O MPPT algorithm provides a change ΔV in V, due to the variation in P according to the following rule;

$$V(k) = \begin{cases} V(k-1) + \Delta V * slope; \ if \ P(k) > P(k-1) \\ V(k-1) - \Delta V * slope; \ if \ P(k) < P(k-1) \end{cases} \quad (7.11)$$

The slope in eqaution (7.11) indicates the perturbation direction, i.e. to the right (climbing) or left (descending). Obviously, the size of the perturbation, ΔV is crucial; the larger the value of ΔV, the faster the convergence, although this results in large fluctuation in P, and vice versa. In a conventional P&O technique, the oscillation is highly undesirable as it leads to a significant energy loss. Therefore, adaptive P&O is used to solve this problem (Ahmed & Salam 2015).

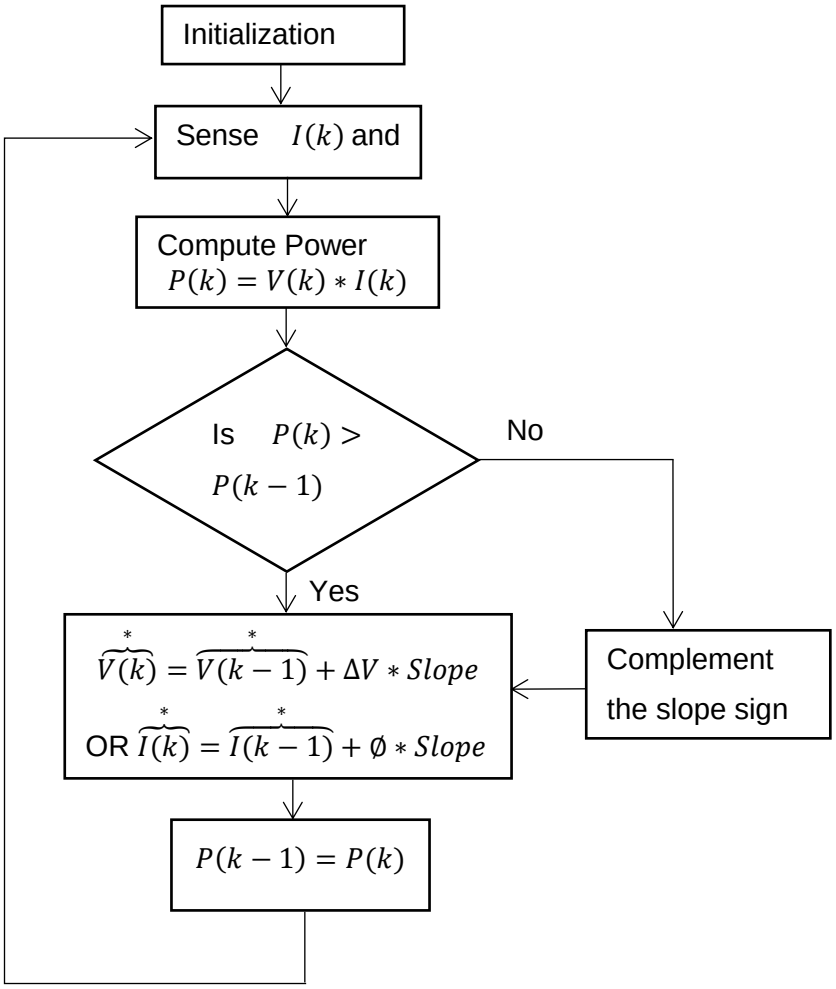


Figure 7.9. Flow chart of conventional P&O method (Ishaque & Salam 2013)

Figure 7.10 shows the block diagram of the implemented TEG/dc-dc converter system with P&O MPPT, with the same input temperature and load as in the ESC model described above.

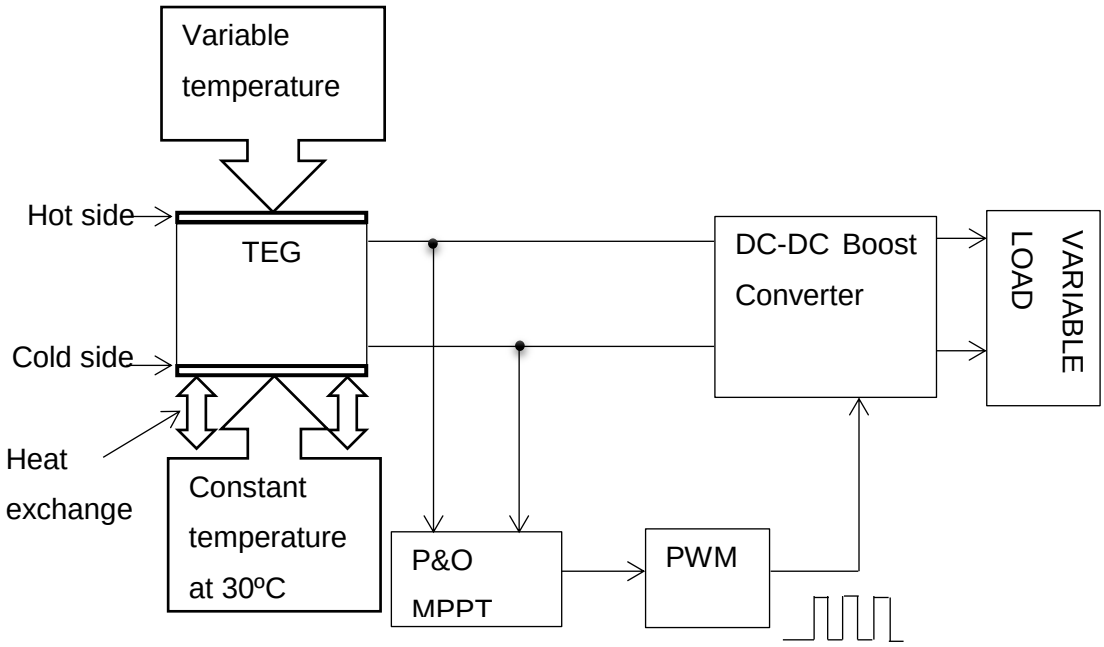


Figure 7.10. Block diagram of TEG/dc-dc converter system with P&O MPPT

Figure 7.11 shows the Simulink model of TEG/dc-dc boost converter system. The Simulink for TEG model is well explained in chapter 6. The same Simulink TEG model was used for P&O simulation except that the ESC block was replaced P&O block indicated in Figure 7.12. The P&O circuit was designed based on the flowchart in Figure 7.9.

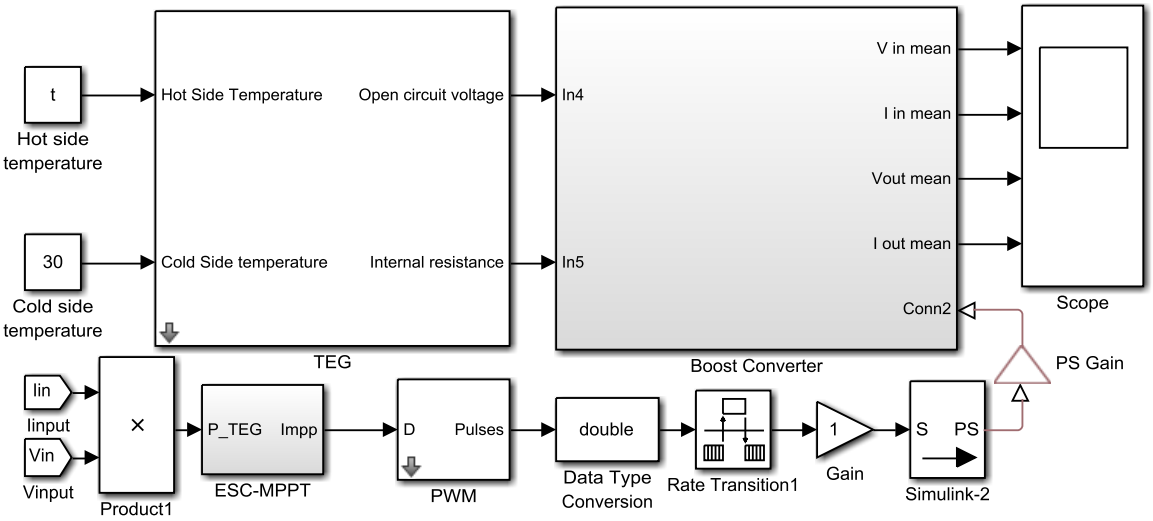


Figure 7.11. The Simulink model of TEG/dc-dc boost converter system

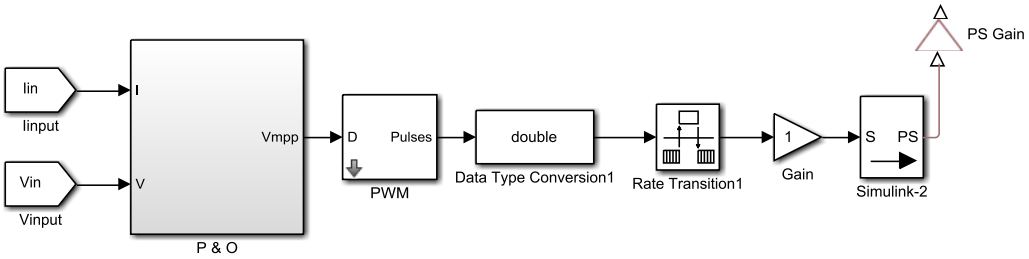


Figure 7.12. The simulink P&O block

The hot side temperature “t” was varied in step according to;

t = 200, 225, 250, 275, 300, 325, 350, 375 and 400 °C.

For each value of hot side temperature (t) and the cold side temperature (30°C), the TEG/dc-dc converter model was simulated to find the output voltage and current. The dc-dc converter was designed based on known the procedure in literature. The electronic components selection criteria for the boost converter are well described in our previous work (S. Twaha et al. 2017). Figure 7.13 shows the simulated boost converter circuit whereas Table 7.2 displays a list of electronic components and their values, used in the boost converter design.

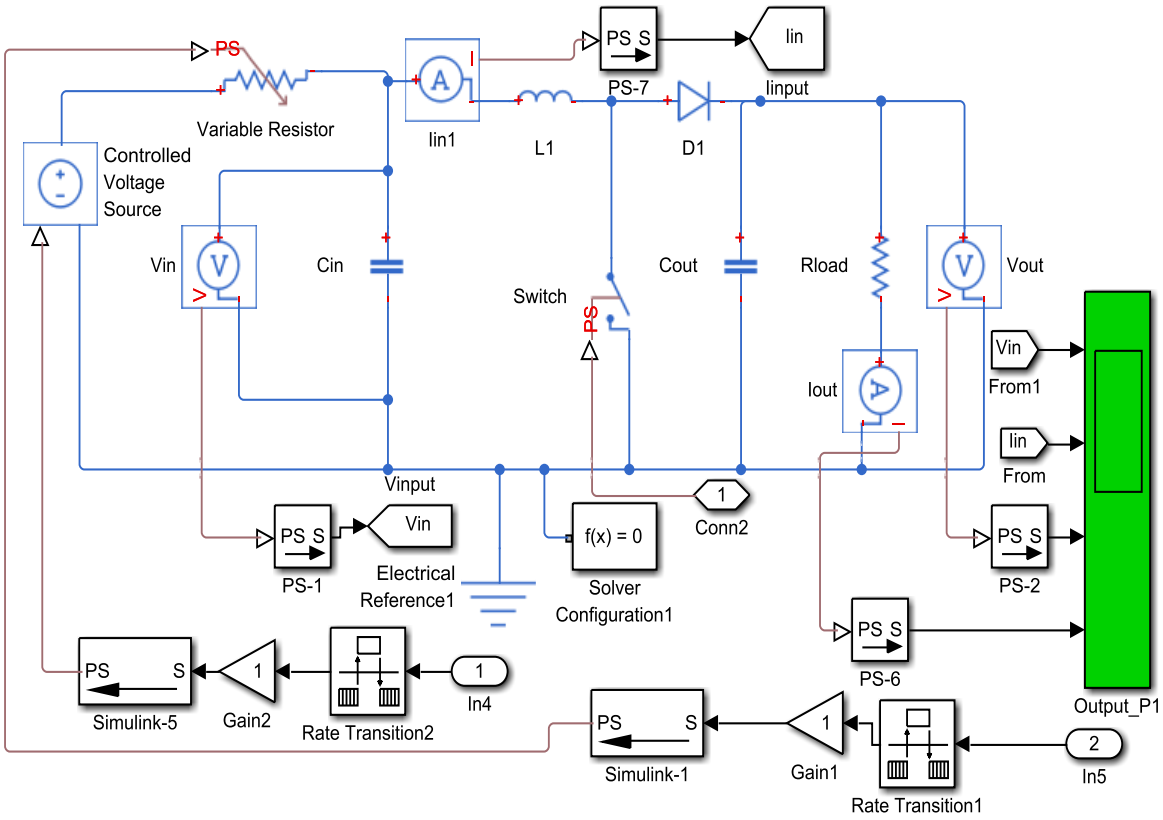


Figure 7.13. The simulated boost converter circuit

Table 7.2. List of electronic components for the boost converter design

Converter component	Symbol	Value-Unit
Inductor	L1	30 μH
Diode Forward voltage On resistance	D1	 0.38 V 0.2 Ω
Input capacitor	Cin	800 μF
Series resistance	ESR	0.05 Ω
Output capacitor	Cout	800 μF
SwitchClosed resistance Open conductance	R_closed G_open	0.0026 Ω 10 nS

The load resistance Rload was varied in steps based on;

Rload = 0,0.2,0.4,0.6, 0.8,1,1.1,1.8, 2.4,2.8,3.2,3.6,4,4.4,4.8,6,10 and 14Ω.

The range of load resistance is based on the internal resistance of the TEG of 1.1Ω, so that lower and upper values are tested to find the optimum point from the TEG simulation model. From Figure 7.13, the connection Conn2 represents a control signal from the MPPT circuit as indicated on the boots converter block in Figure 7.12.

7.4. Results and discussion

The results are discussed based on the steady state parameters from the TEG/dc-dc converter models. The parameters considered include the output voltage, output power and the simulation speed.

7.4.1. Results of ESC MPPT method

Figure 7.14 shows the output voltages of the converter against the load resistances, for all the hot side temperatures simulated for a single TEG module. It is observed that at a zero load i.e. when the output terminals of the converter are short circuited, the output voltages for all the temperature conditions also have zero value. It is clearly seen that the output voltages increase with the load resistance and temperature. However, the increase in output voltages is faster at smaller resistances than at larger ones, which is a moderately correct trend expected from such TEG/converter models.

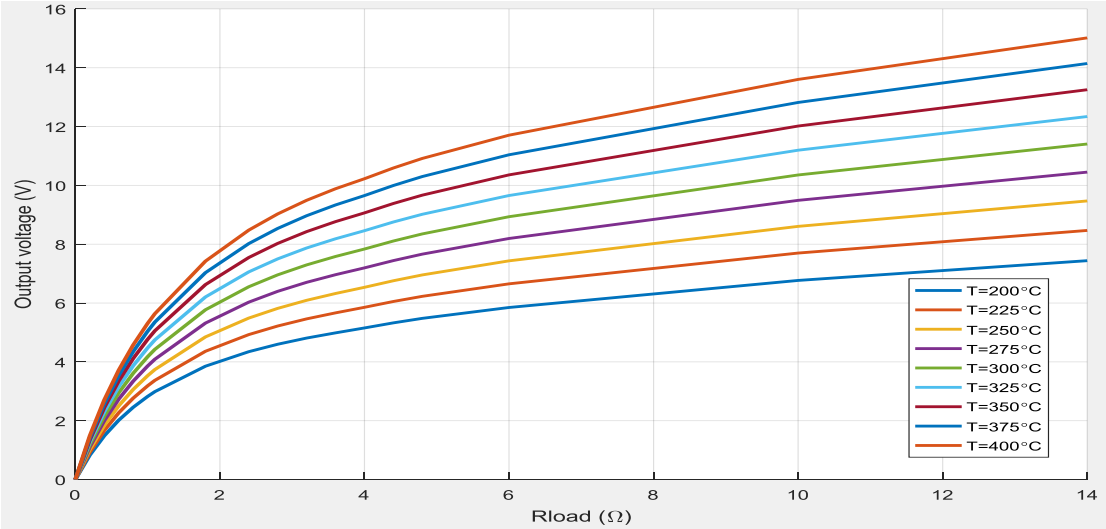


Figure 7.14. The output voltages of the ESC MPPT model for a single TEG

The output power of the ESC based model is illustrated in Figure 7.15. As clearly observed, the output power increases with the hot side temperature since the cold side temperature is fixed (30°C). Similarly, the output power increases faster with the load resistance at the left side of the optimum point whereas it decreases slowly with increase in the resistance on the right side of the optimum point, which is the normal trend for TEG, just like in PV systems.

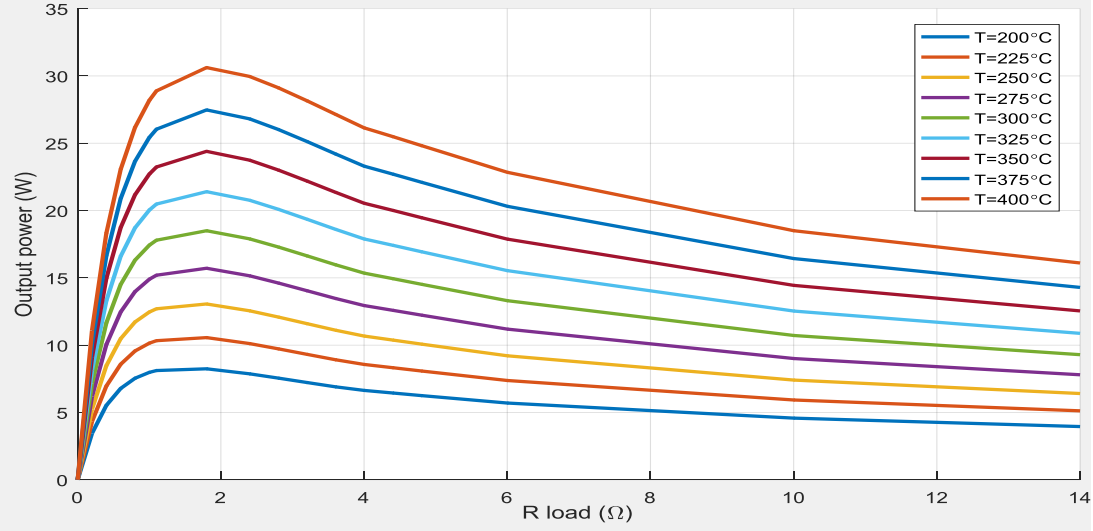


Figure 7.15. The output power of the ESC based model for a single TEG

Figure 7.16 displays a plot of output voltages, currents and the output power of ESC MPPT model. The trend of the output current is opposite to that of the output voltage i.e. as the output voltages increase, the output currents decrease with increase in hot side temperature and vice versa. However, the output voltages and currents for each temperature meet at the left of the optimum power points at about 1.1Ω resistance, which is almost the internal resistance (1.2Ω) of the TEG considered in the simulation. This is in conformity with the theoretical and practical nature of TEG.

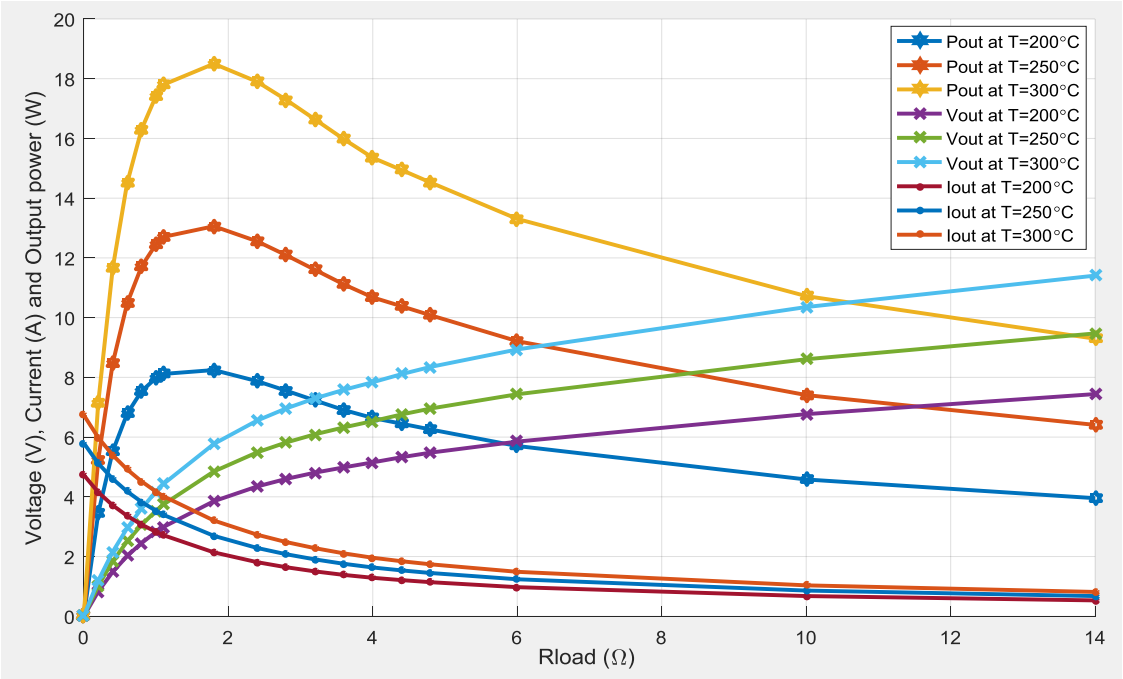


Figure 7.16. The voltage, current and output power of ESC MPPT model for a single TEG

7.4.2. Results of P&O MPPT method

Figure 7.17 demonstrates the output voltages against the resistances of the P&O MPPT based model for a single TEG module. Like the ESC MPPT based model, at zero load, the output voltages for all temperature conditions is zero while the output voltages increase with the resistance and the hot side temperature.

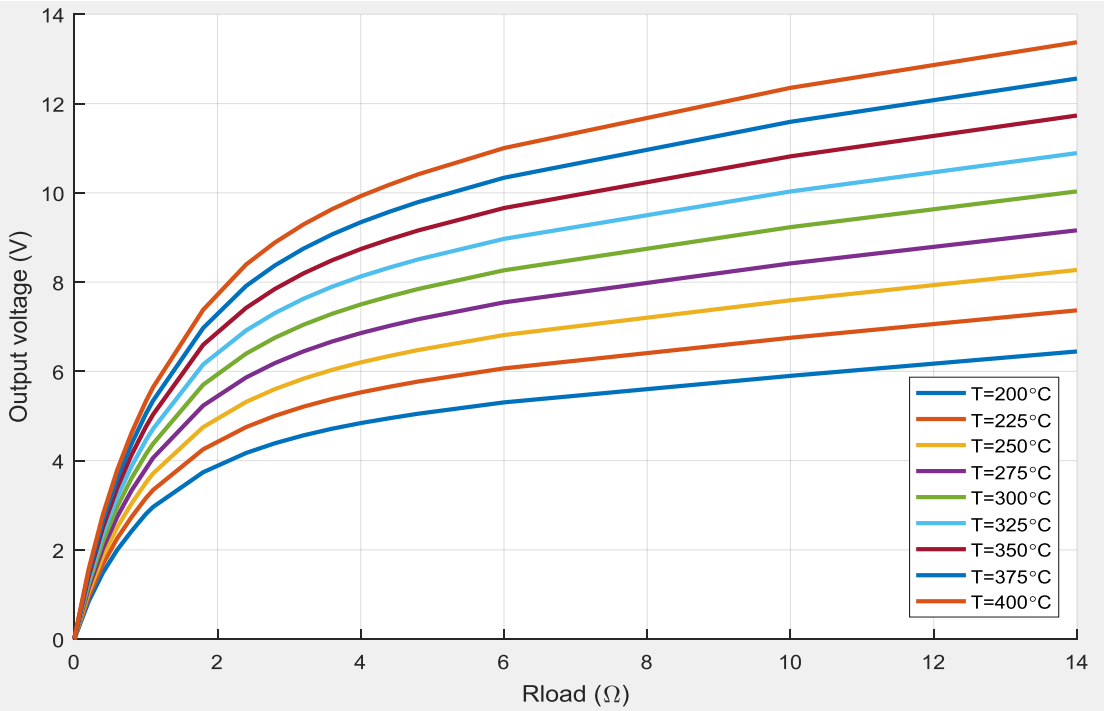


Figure 7.17. The output voltages of the P&O MPPT model for a single TEG

The output power is shown in Figure 7.18 with similar curves as those of the ESC method discussed above, but the difference will be discussed in the next section. Similarly, the output voltage, current and output power of the P&O MPPT model for a single TEG is indicated in Figure 7.19. The optimum or matching point is obtained at nearly 1.8 Ω with the output power of 30.6 W at a temperature of 400ºC.

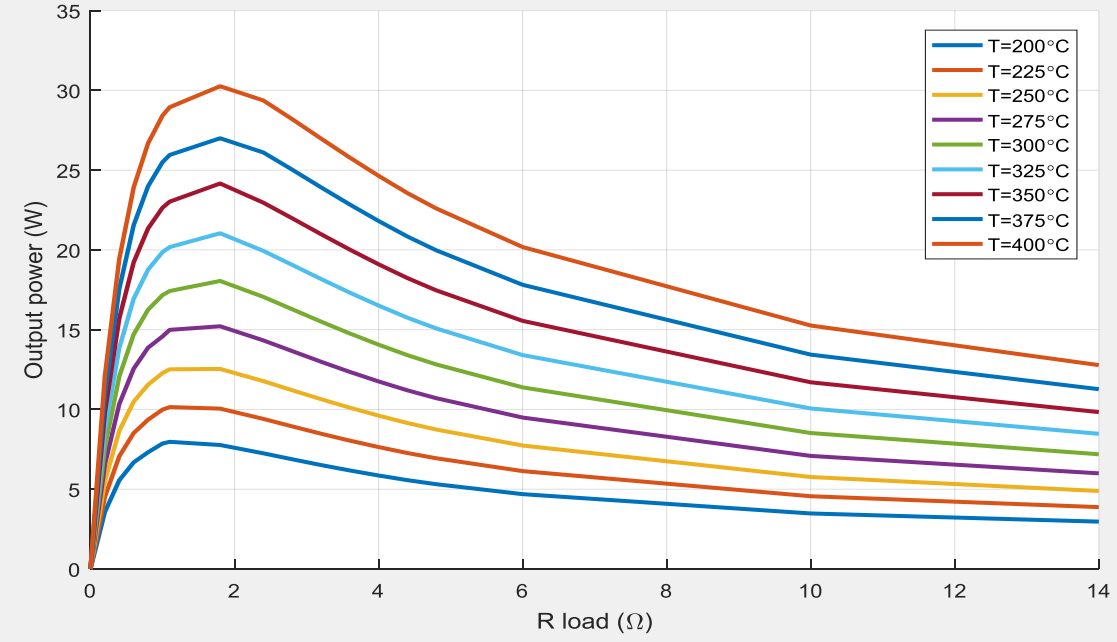


Figure 7.18. The output power of the P&O based model for a single TEG

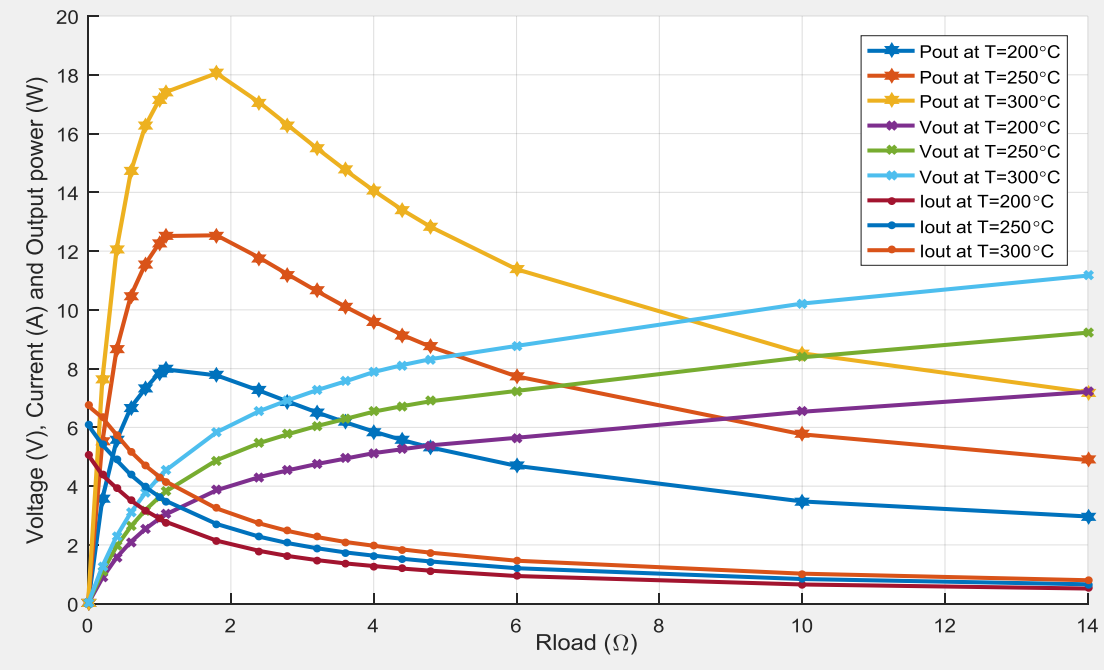


Figure 7.19. The output voltage, current and output power of P&O MPPT model for a single TEG

7.4.3. Comparison of ESC and P&O MPPT techniques

Figure 7.20 shows the comparison between the output voltages of ESC and P&O MPPT based models at hot side temperatures of 200°C, 300°C and 400°C. It is indicated that at the load resistances below 2Ω, there is a small difference between the output voltages of ESC and P&O based models. Beyond that point, the difference increases with increase in the load. The comparison of the output power is shown in Figure 7.21, where it is demonstrated that the output power of ESC MPPT model is generally higher than that of P&O based model. At the optimum load of 1.8Ω, the maximum power of ESC is 30.6 W whereas for P&O method, it is 30.2 W.

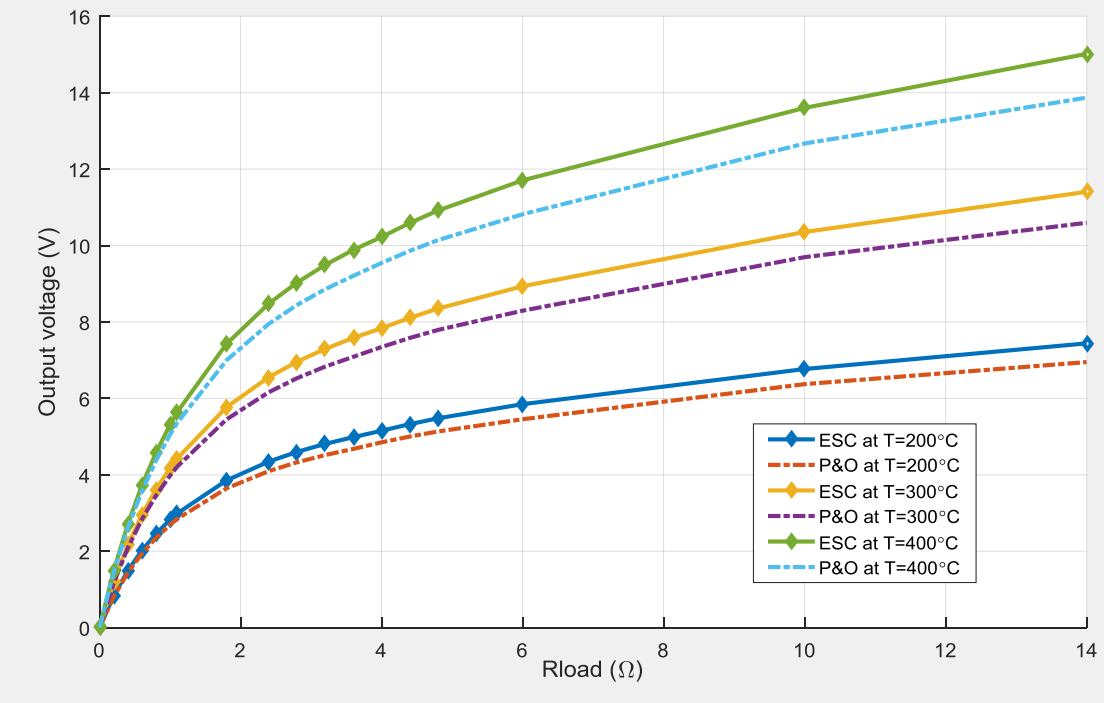


Figure 7.20. The comparison between the output voltages of ESC and P&O based models

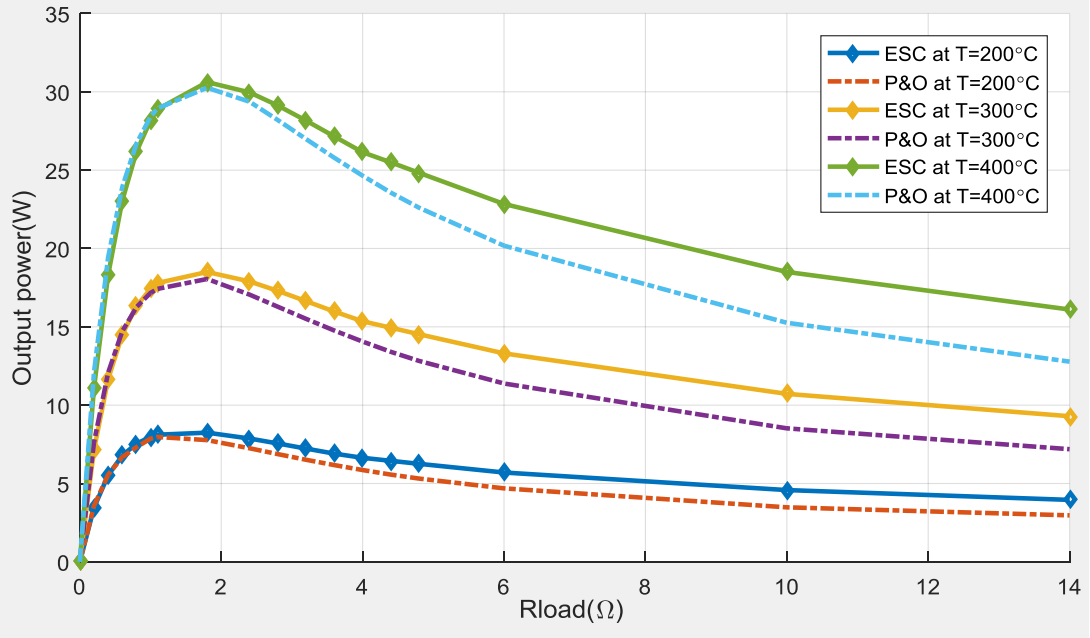


Figure 7.21. The comparison of output power of ESC and P&O based models

The difference in the performance of these methods in terms of harvesting maximum power is clearly illustrated in Figure 7.22. The output power of the P&O technique is deducted from that of the ESC method to get the difference which is plotted in Figure 7.22. It is observed that at load resistances below 1.2Ω, the output power difference is generally negative, indicating that the output power of P&O is more than that of ESC method. This implies that P&O technique has better performance in terms of the amount of harvested output power in that range. Particularly, at lower hot side temperatures in the same load range, for example at 200°C, the output power difference is negative for only a short range of the load resistances (0 - 0.5Ω), though the performance improves towards higher temperatures with the maximum difference of 1.13 W recorded at a load resistance of 0.4Ω for a hot side temperature of 400°C.

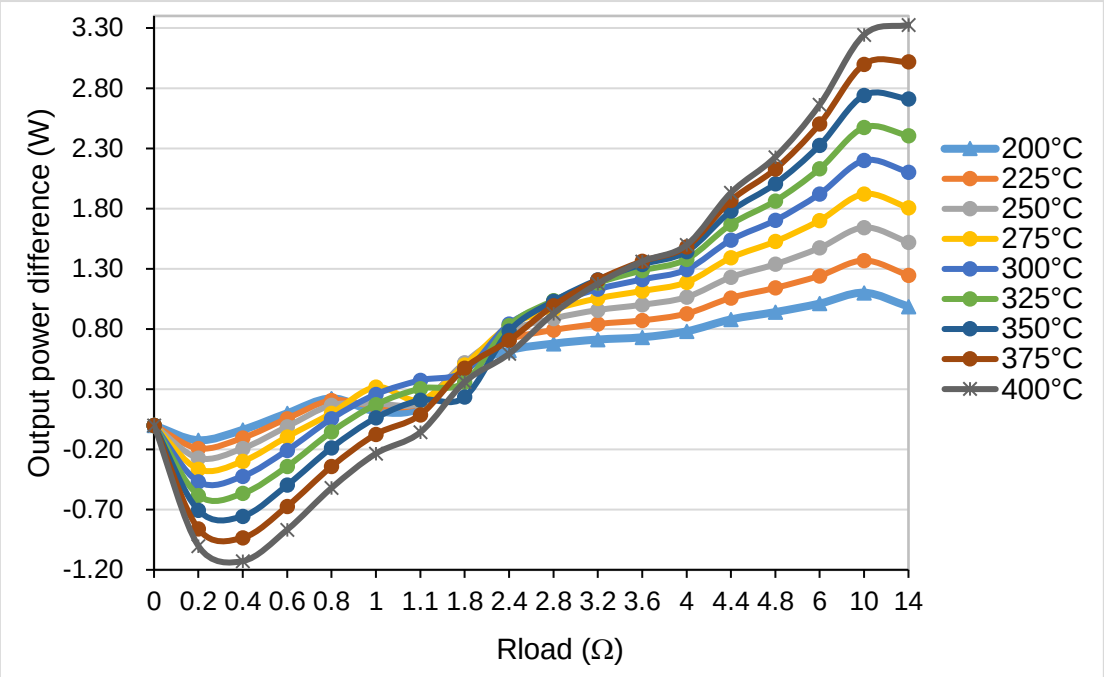


Figure 7.22. The output power difference between ESC and P&O based models

For a load range of 1.2Ω-14Ω, the output power difference is positive throughout, indicating that ESC method is better than P&O method in terms of output power performance in this region. Faster increase in the output power difference is manifested after the optimum point (1.8Ω). However, the difference generally degrades at 10Ω load resistance. It is clearly observed from Figure 7.23 that the performance of ESC MPPT algorithm is better than that of P&O at the optimum point throughout the range of temperature.

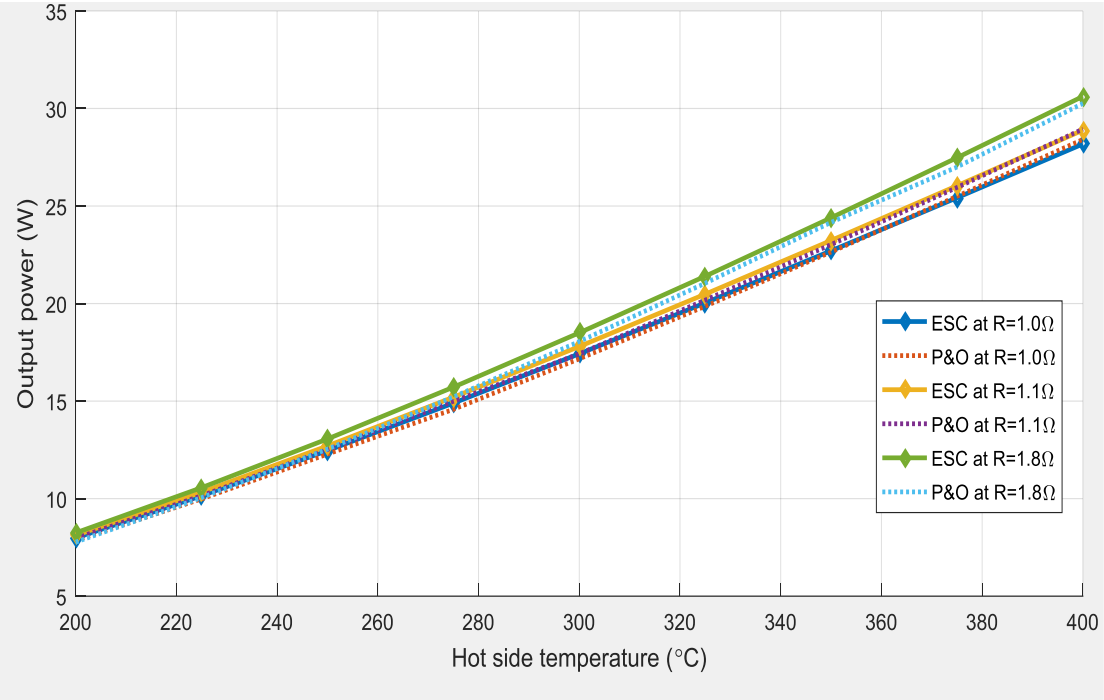


Figure 7.23. Output of ESC and P&O near the optimum point

Figure 7.24 shows the percentage increase in the output power of the converter due to the application of ESC MPPT method. The percentage is computed by taking the output power of the P&O method as the base case i.e. the output power of P&O (Pout) minus that of ESC divide by Pout times 100. It is indicated that the minimum and maximum percentage increase in Pout is 1.0% and 6.1% achieved at hot side temperatures of 200°C and 350°C respectively. It is therefore of no doubt that the ESC MPPT algorithm is better than P&O in extracting maximum power from TEG.

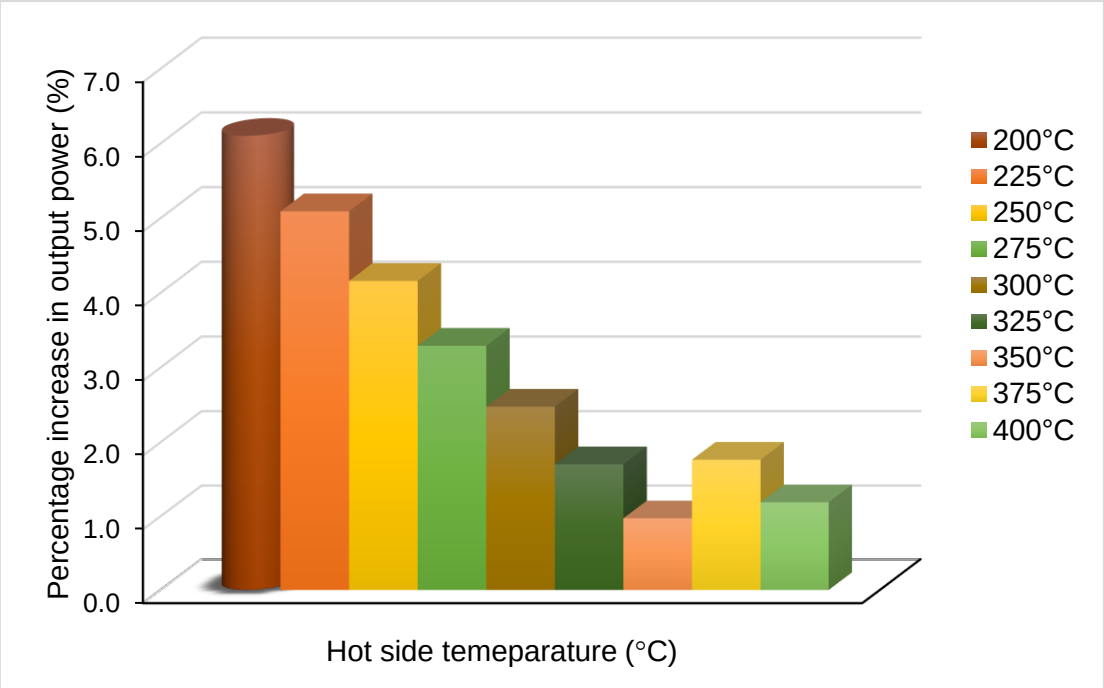


Figure 7.24. Percentage increase of the output of the converter due to the application of ESC MPPT method

Another aspect of MPPT performance is the speed of computation of both methods. It is noted from the simulation that the ESC MPPT model takes 159.9 seconds to complete all the loops for the ranges of the simulated hot side temperatures and load resistances of 200°C -400°C and 0 - 14Ω, respectively. However, for the same simulation settings, the simulation of the P&O MPPT model is completed within a simulation time of 602.6 seconds, which is almost four times the time taken by the ESC MPPT algorithm. This implies that P&O algorithm is slower than the ESC technique. Based on the computation time, the ESC MPPT technique can be a better choice for fast speed applications than P&O method.

7.4.4. Validation: Comparison of Simulink and COMSOL TEG models

In this section, the simplified model used to study the TEG model is verified by using the results obtained from COMSOL software. For purposes of verification, the TEG model has been simulated without connecting the dc-dc converter as well as obviously without the MPPT circuit. The model has been loaded with similar range of resistive loads as those connected to the TEG/dc-dc converter model with MPPT, that is, between 0Ω and 14Ω range, with the same input temperatures at the cold and hot sides of the TEG. Correspondingly, the TEG indicated in Figure 7.1 has been simulated in COMSOL with the same temperature inputs and resistive loads as for the Simulink model. In search of the best way to improve the model, two TEG materials have been chosen; Bi_2Te_3 material with temperature dependent S, σ and k, and the PbTe TEG material with non-temperature dependent S, σ and k as demonstrated in section 7.2.

Figure 7.25 shows the output voltages of the Bi_2Te_3 based TEG, for all the simulated temperatures. Despite the slight point of reflection at a load of about 6.5Ω on the voltage curves, the output voltages of Bi_2Te_3 TEG have a similar trend as those of the Simulink models in Figure 7.14 and Figure 7.17 for the output voltages of the ESC and P&O based TEG models respectively, i.e. in all the cases, the output voltages of individual temperatures increase with the load as expected.

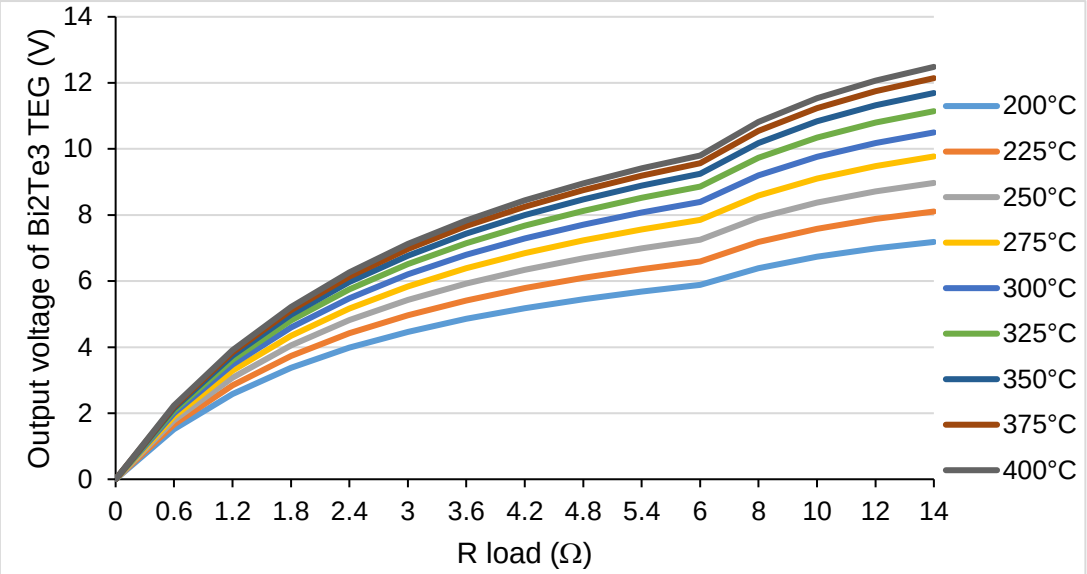


Figure 7.25. Output voltage of Bi_2Te_3 TEG

Similarly, the output power of the Bi_2Te_3 based TEG is indicated in Figure 7.26 for all the simulated temperatures. Likewise, the trend of the output power curves is comparable to the those for Simulink TEG models illustrated in Figure 7.15 and Figure 7.18. The major observable difference is the rate of rise of the output power as the load increases, whereby the COMSOL models have lower rate than the Simulink models. This results into another difference; the optimal value of the matching load is not the same for all the models. However, the optimum points also vary with the temperature for the COMSOL based model, with the matching load of 3Ω established for the 200°C and 300°C whereas 3.6Ω is the optimal load for the temperature of 400°C.

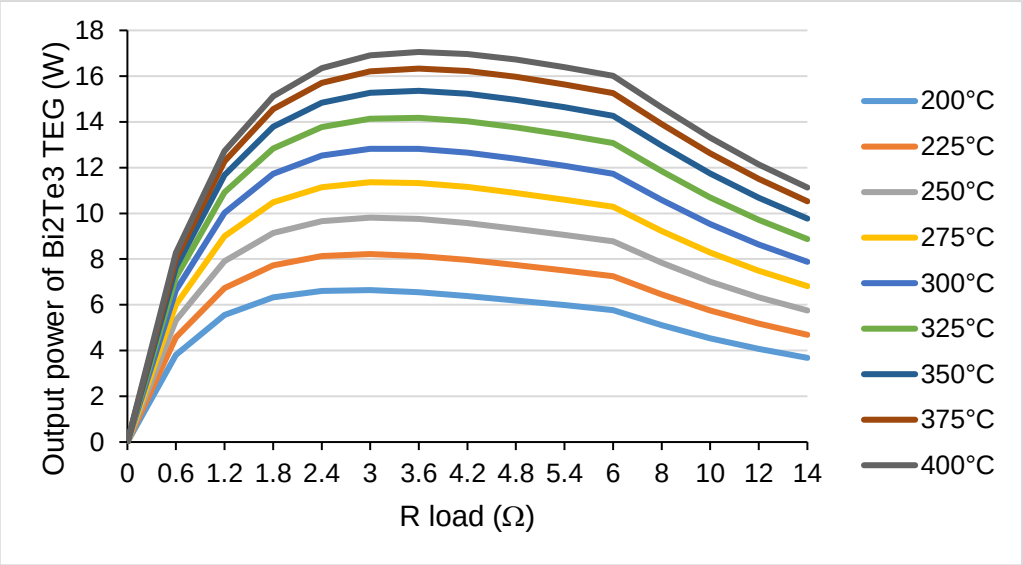


Figure 7.26. Output power of Bi_2Te_3 TEG (From simulink)

It is also very important to analyse the difference in the magnitudes of the corresponding curves of both models. For the meantime, it is necessary to compare the effect of temperature dependence of the TEG parameters in COMSOL models before analysing the magnitudes of the curves for the different models. From Figure 7.27 it can be observed that at a temperature of 200°C (473.15K), the output power of the Bi_2Te_3 based TEG is somewhat higher than that of the PbTe TEG, while at 300°C or 573.15K, the output power is almost the same. This is because there is a small change in S and σ of Bi_2Te_3 material according to Figure 7.2 and Figure 7.4 respectively. However, at a hot side temperature of 400°C (673.15K), thermal conductance k is high since k is temperature dependent, based on Figure 7.3. Hence, the combined effect of the variation of S, σ and k, due to the change in temperature at 400°C results into an increased value of the output power of the Bi_2Te_3 TEG unlike the PbTe TEG whose parameters are kept constant throughout the tested temperature range.

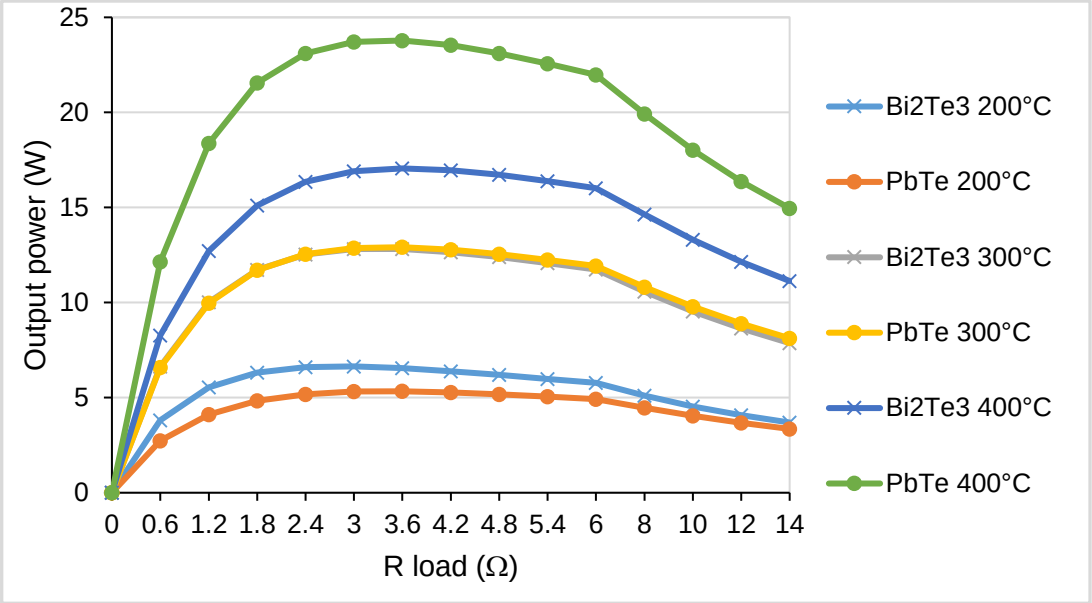


Figure 7.27. Comparison of output power of TEG for different materials

On the magnitudes of the output power for each modelling software tool, Figure 7.28 indicates the comparison between the output power of the Simulink and PbTe based COMSOL models, for the hot side temperature of 200°C, 300°C and 400°C. It can be observed that for all the temperatures, the output power of the Simulink based model is higher than that of the PbTe based COMSOL model, with the largest difference registered at the optimum points. At a resistive load of 3.6Ω, for the hot side temperatures of 200°C, 300°C and 400°C, the output power of PbTe based model is 5.3 W, 12.9 W and 23.7 W whereas for the Simulink model it is 7.8 W, 17.2 W and 28.4 W, accounting for the percentage increase in the output power of 46.8%, 33.5% and 19.7%, respectively, because of the implementation of Simulink model. The percentage increase in the output power is computed with the PbTe based COMSOL model values as the base values.

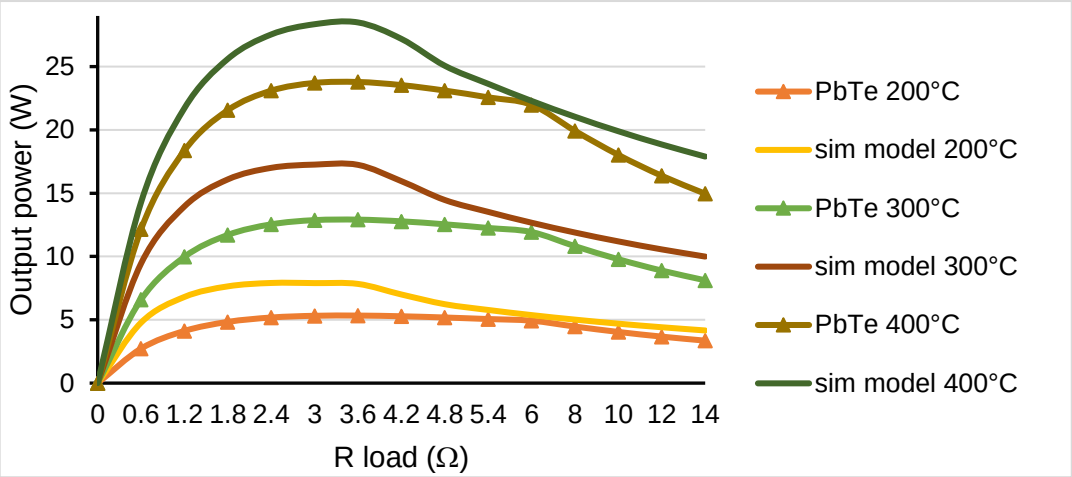


Figure 7.28. Comparison of output power of Simulink and PbTe based COMSOL models

Considering the temperature dependent Bi_2Te_3 based COMSOL TEG model, Figure 7.29 illustrates the comparison between the output power of Simulink and Bi_2Te_3 based model. The output power of the Bi_2Te_3 based model at 200°C, 300°C and 400°C is 6.5 W, 12.8 W and 17.1 W whereas for the Simulink model it is 7.8 W, 17.2 W and 28.4 W (the same as the those compared with PbTe base model), representing the percentage increase in the output power of 19.5%, 34.5% and 67%, respectively, with Bi_2Te_3 based COMSOL model as the base values. It is worth to note that at 400°C, a higher increase in the output power of 67% is obtained, compared to only 19.7% with PbTe model as the base. This is due to the combined effect of the temperature dependent parameters (S, σ, and k) of the Bi_2Te_3 based COMSOL model at this temperature.

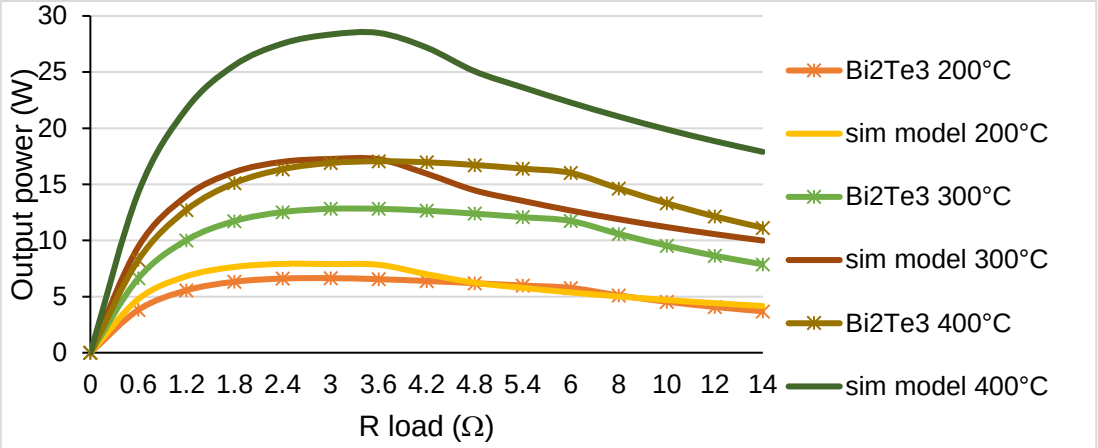


Figure 7.29. Comparison of output power of Simulink and Bi_2Te_3 based COMSOL models

The simulation time is another important factor worthy of analysis. Table 7.3 shows the simulation times for the COMSOL TEG models. For the Bi_2Te_3 based TEG model, the simulation time has been recorded for the temperate range of 200°C to 400°C with the increment of 25°C whereas for the PbTe based TEG model, simulation times of 200°C, 300°C and 400°C are only noted.

Table 7.3. Simulation time for the COMSOL TEG model

Temperature (°C)	Simulation time for Bi_2Te_3 based TEG model (min, s)	Simulation time for PbTe based TEG model (min, s)
200	37, 28	35, 55
225	40, 08	
250	41, 44	
275	46, 00	
300	41, 33	37, 38
325	52, 11	
350	54, 26	
375	51, 36	
400	51, 34	34, 28

Figure 7.30 indicates the plot of the simulation time for the COMSOL models in seconds at different temperatures. In general, the computation time for the non-temperature dependent PbTe model is very low compared to the time for the

temperature dependent Bi_2Te_3 model. Also, the simulation time increases with temperature for the Bi_2Te_3 model, with the highest time of 3066s observed at 350°C. On the other hand, the PbTe model exhibits a random simulation time which does not increase beyond 2258s (at 300°C) for the three temperature values considered. Specifically, to complete the simulation for the temperatures of 200°C, 300°C and 400°C, it takes a total simulation time of 8250s (about 2.29 hrs) for the Bi_2Te_3 model compared to 6481s (about 1.8 hrs) for the PbTe model.

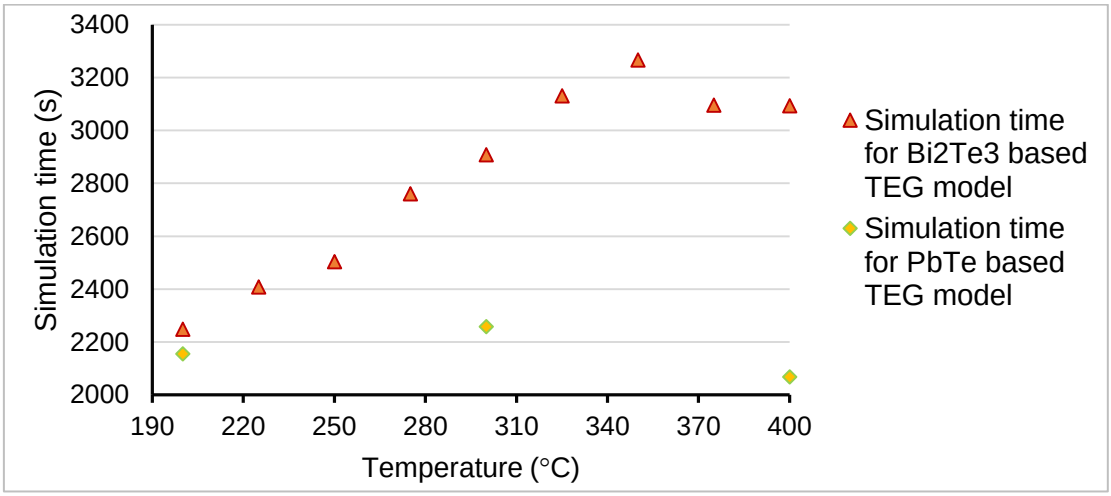


Figure 7.30. The plot of the simulation time for the COMSOL models at different temperature

On the modelling software point of view, it has already been noted that the ESC MPPT model takes 159.9s (2min, 40s) to complete the all the loops for simulated temperatures and the load resistances. In the same way, for the same simulation settings, the P&O MPPT model completes the simulation in 602.6s (10min, 3s). Comparably, both the ESC and P&O models take only about 763s (about 0.21hours) which far much less than the 25415s (about 7 hours or more than half a day), the time taken by only the Bi_2Te_3 model in COMSOL to complete the simulations with the same input and load conditions. Remarkably, the COMSOL models are simulated on a computer with more

memory and speed, through Intel core i3 4150 CPU with two processors each with a speed of 3.50GHz and 16 GB of RAM, unlike the Simulink model which is simulated on an Intel core i3 4150 CPU and two processors each having a speed of 3.40GHz with 8 GB of RAM.

7.5. Performance Comparison of ESC and IC methods

The purpose of this section is to compare the performance of ESC algorithm with a classical IC method.

7.5.1. Voltages, current and power curves of ESC and IC techniques

Figure 7.31 shows the output voltages, currents and power of the IC method at different temperature. It is observed that the maximum power occurs at a load of about 1.8Ω. Also, as expected, as the voltages increase, the currents reduce.

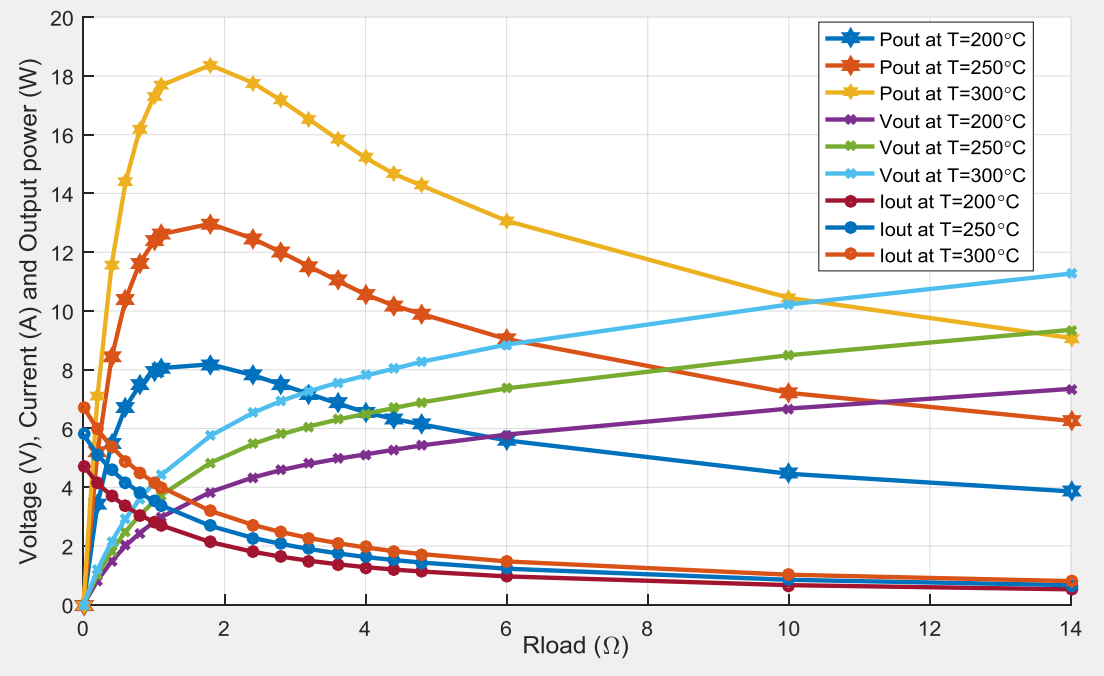


Figure 7.31. Output voltages, currents and power of IC method for different temperature

Similarly, Figure 7.32 shows the output voltages, currents and power of the ESC technique. The highest output power also occurs at about 1.8Ω loads. The difference between the results of IC and ESC methods are discussed in the following section.

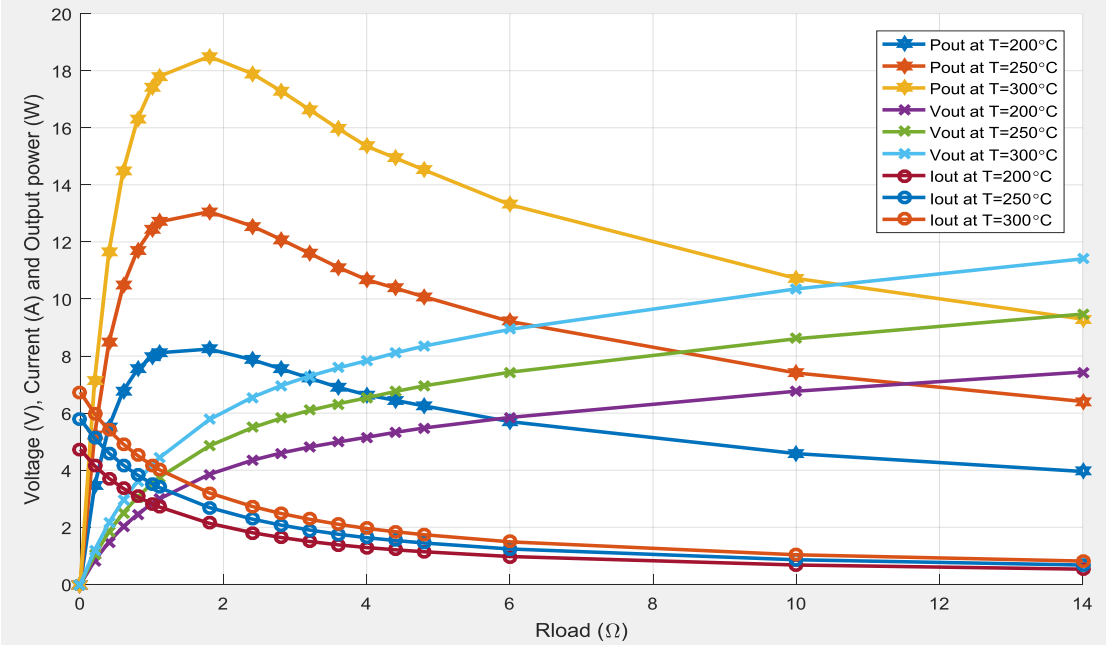


Figure 7.32. Output voltages, currents and power of ESC method for different temperature

7.5.2. Comparison of the ESC and IC methods

Figure 7.33 indicates the comparison of output voltages of both methods where it is seen that the output voltages of IC methods are slightly lower than those for ESC although both have the same trend. Likewise, the output power of ESC method is higher than that of IC technique but both methods have a similar shape of power curves as depicted in Figure 7.34. For example, for ESC at hot side temperature of 400°C, the output power is 31.7 W at the maximum load while for IC method it is 30.9 W at the same temperature and load.

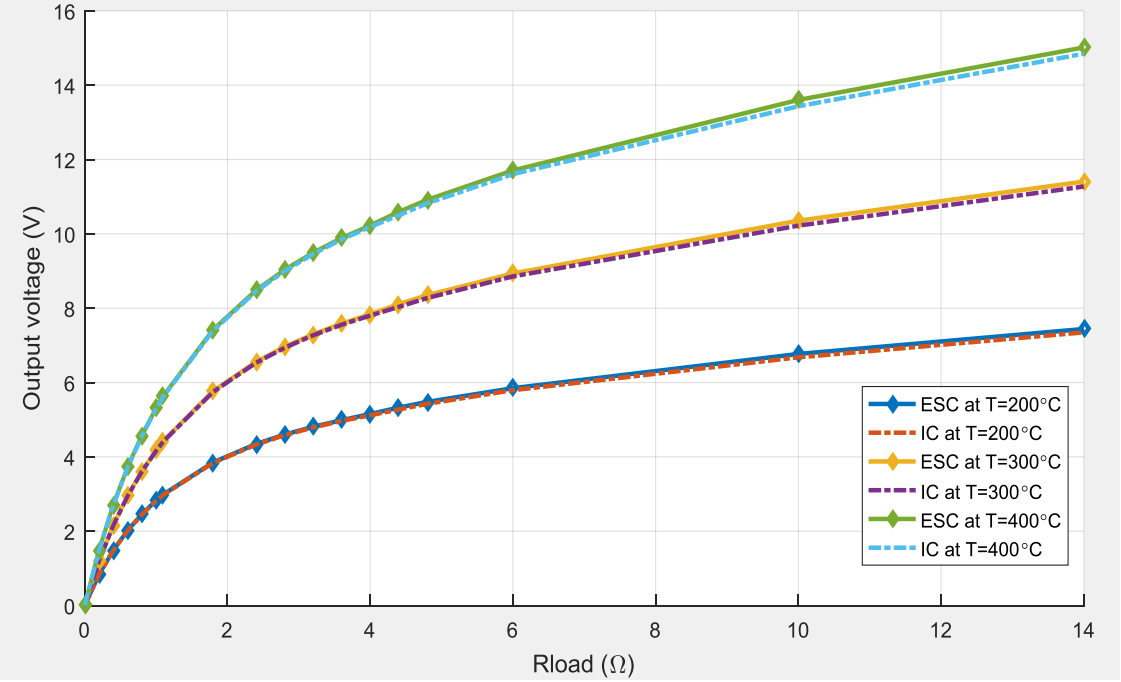


Figure 7.33. Comparison of output voltages of ESC and IC methods

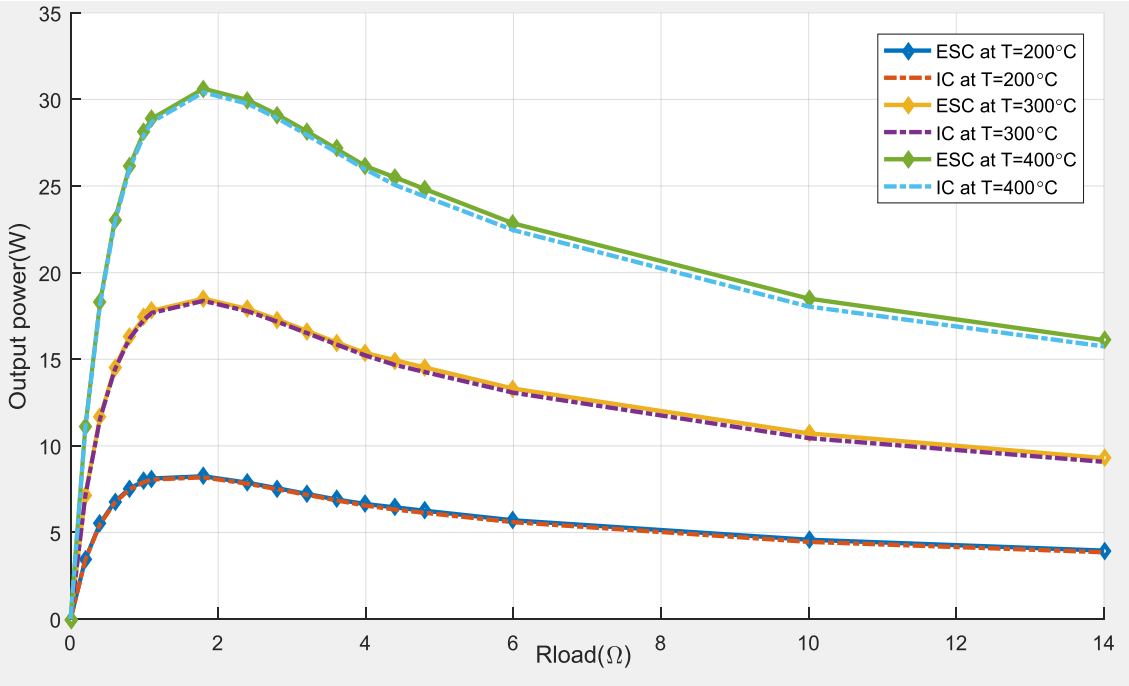


Figure 7.34. Comparison of output power of both methods

With a 24 GB RAM computer, the two methods are found with simulation times in Table 7.4. It is clearly observed that ESC method is faster than the IC method with simulation time of 102.1s and 781.8s respectively. In addition, ESC method is less complicated to implement than IC since it has less building blocks than its counterpart.

Table 7.4. The computation times for ESC and IC techniques

MPPT technique	Time (s)
Extremum seeking control	152.1
Incremental conductance	728.8

7.6. Summary

This chapter has compared the performance of ESC, P&O and IC MPPT algorithms applied on the TEG system. The TEG system has been analysed based on a simplified model while the boost dc-dc converter with MPPT has been applied to the TEG system to improve the stability of the generated power as well as harvesting maximum power from TEG. Three algorithms, ESC, P&O and IC based MPPT techniques have been applied to control the converter so that the results are compared in terms of output voltage, power and speed of computation of the model. The TEG model has been validated by comparing the results obtained from COMSOL Multiphysics modelling software.

The results indicate that the ESC MPPT method extracts more power than the P&O technique, whereby the output power of the converter controlled by ESC MPPT is higher than for P&O by 0.47W, which is equivalent to 6.1% higher at the optimum load. It has also been noted that the ESC MPPT algorithm is almost four-fold faster than the P&O method. This makes it a better choice for fast speed applications, than the P&O method.

It has also been noted that both the ESC and P&O Simulink models take only about 12min and 43s (approximately 0.21 hours) which is far much less than

the 25415s (about 7 hours or more than half a day), the time taken by only the Bi_2Te_3 model in COMSOL to complete the simulations, with the same input temperature and load conditions as the Simulink models. Surprisingly, the COMSOL models are simulated on a computer with more memory and higher speed, unlike the Simulink models which are simulated on computers with less speed and memory. Therefore, the Matlab/Simulink based simplified models are computed much faster than the COMSOL based complex models.

On the accuracy point of view, the COMSOL complex TEG models, much as they consume a lot of time during computation, they more accurately represent the functionality of TEG because the modelling accounts for the various thermoelectric parameters. Consequently, as a basis for future research, the Simulink TEG model should be improved to incorporate more thermoelectric parameters such as electrical conductivity, thermal conductivity, in addition to incorporating heat transfer analysis.

Results have also indicated that ESC outperforms the IC technique in terms of extracting maximum power and the speed of computation. ESC method is faster than the IC method with simulation time of 152.1s and 781.8s respectively. Moreover, ESC is less complex in terms of model implementation since it is made up of few circuit components than the IC method.

Chapter 8. Application of distributed dc-dc converter Architecture

In this chapter, application of the concept and the design of a distributed dc-dc converter architecture (DCA) on TEG system is discussed. The usefulness of the proposed design is demonstrated with the simulation and experimental works. Besides, during the experiment, some of the factors that affect the performance of TEG systems are correspondingly investigated and analysed.

8.1. The concept and the design of DCA for regulation of TEG output

In this section, the state of the art DCA is discussed first, followed by the new DCA design for power conditioning of TEG system.

8.1.1. The concept of distributed dc-dc converters

The distributed or cascaded converter architecture involves the use of non-isolated per-TEG dc-dc converter connected to the load. Alternatively, for some specific loads, especially in automotive applications, soft-switched, isolated bi-directional dc-dc converters can be used instead of non-isolated converters because these integrated converters enable bi-directional power flow control capability as well as galvanic isolation to eliminate stray currents between the low- and high voltage level to meet safety requirements (Su & Peng 2005). Soft switching especially through the use of insulated-gate bipolar transistors (IGBTs) is preferred over hard switching because of the reduced level of converter features, leads to higher efficiency, low switching losses, reduce torque ripples and improved speed as compared to hard switching (Rathi et al. 2011).

Generally, several dc-dc converter topologies including boost, buck, Ćuk and buck-boost converters are used as individual converters that can be cascaded. In case of PV systems, it is observed that this setting offers the advantage of a “converter-per-panel” approach without the cost or efficiency penalties of

individual dc–ac grid connected converters (Walker & Sernia 2004). The same concept can be adopted for TEG system since TEG devices have similar behaviour as PV system, because of several reasons. First, as discussed in chapter 2, different dc-dc converter topologies have different implications when applied to TEG devices for waste heat recovery. It is therefore necessary to utilize the combined advantages of most of these converter topologies to maximize the performance of TEG systems, given the fact that TEG devices still have low efficiencies. Secondly, TEG modules are prone to malfunctions during operation. In case several TEG devices are connected in series, if one of them fails, the operation of the whole dc-dc converter/TEG system will be affected. This might affect the connected load, resulting into power quality issues such as voltage drops and power losses, in addtion to jeopardizing the lifespan of the load, especially if the load has sensitive digital circuitry. In the worst case, the connected load may perhaps be damaged and causes financial and technical losses to the user.

The application of distributed dc-dc converters on TEG system is also based on multiple voltage level requirements in hybrid vehicles. The TEG/Converter models presented in the previous chapters are general models whose results are not targeting specific applications. In this chapter, the output power from TEG and dc-dc converters is demonstrated for automotive applications and other similar applications. In automotive applications, special types of dc-dc converters are used since different loads with different voltage levels and power requirements are distributed throughout the vehicle. Numerous loads within the vehicle are designed to operate at different voltage levels such as 5V, 6V, 12V, 24V and 48V. This requires the use of different converter topologies to achieve these voltage levels within the specified operation margins/tolerances and frequencies. Utility trucks, transit buses, safari trams, ambulances and long haul trucks are some of the specialty vehicles in which batteries with voltage levels of 12V, 24V or 48V are used (Shang et al. 2016). Batteries are used to

provide power to feed loads such as pumps, air conditioners, compressors, power tools, pipe fusion and fans, etc. All these loads typically have a 120V or 240V AC voltage interface and their power levels range from hundreds of watts to several kW, and in some cases may reach up to 20 kW.

In general, the proposed design of DCA can subsequently provide the vehicle loads with different output voltages at reduced risk of system interruption as well as improved system performance.

8.1.2. Distributed versus centralized dc-dc converters

A centralized controller is a multi-input dc-dc converter system that consists of two or more input ports suitable to draw power from two different dc sources while feeding a common dc bus (Veerachary et al. 2013). The input is any dc source such as TEG, PV, wind, fuel cell etc. This type of control strategy is mainly suitable for distributed generation systems. Apart from accommodating different energy sources and storages, a multi-port converter incorporates the bi-directional power flow capability for the ports connected to the storages to enable the battery to be charged and discharged (Zhao et al. 2008).

In power network topologies, especially in microgrids [1], multiple dc power sources connected in parallel, each interfaced with a dc-dc converter, provide power at their common output (dc link or bus) at a regulated voltage; this power can directly feed dc loads or be used by an inverter to interface with AC loads. Voltage controllers form an integral component of dc-dc converters in such systems (Baranwal et al. 2016). This setting is criticised to have lower reliability as well as lower output power. A paralleled architecture for multiple power sources is preferred since it enables higher output power, higher reliability and ease of use, where two major control architectures are suggested; the first one is *master-slave control*, where the voltage regulation error from the master converter is utilized to provide an error signal to all the parallel connected converters; while the second is the *decentralized or distributed control*, where

each converter utilizes an independent and variable voltage reference depending on the output of each unit. In the distributed control, the converters are designed such that the voltage at the output terminal is set at a prescribed set point e.g. 9V, 12V, 24V, etc.

For good system performance, the converter to be used for the integrated or distributed architecture should be assessed in terms of the following features (Li & Wolfs 2008);

1) Power density

The power density is a converter feature that indicates its compactness. As the power conversion system is becoming miniaturized, increasing the power density is one of the challenging issues for the power supply designers. One of the main orientations in power electronics in the last decade has been the development of switching-mode converters with higher power density and low electromagnetic interference (Veerachary et al. 2013).

2) Efficiency

The converter should have high efficiency, especially the module integrated converters, if compactness is to be achieved. According to Texas Instruments (Raj 2010), the efficiency of the converter is mainly affected by power dissipation due to MOSFET conduction losses (P_{FET}), MOSFET switching losses as well as inductor conduction losses (P_L). Therefore, the total power dissipated in the converter, P_D is given by;

$$P_D = P_L + P_{FET} + Other\ losses \qquad (8.1)$$

The other losses are due to quiescent current losses and MOSFET switching losses. So, the overall converter efficiency is expressed as;

$$\eta_{conv} = \frac{P_O}{P_O + P_D} \qquad (8.2)$$

Where P_O is the output power of the converter

3) Reliability

Since the converter operates hand in hand with the energy source, it is necessary to compare the converter life time with that of the energy source for which it is connected e.g. PV or TEG. The converter reliability is quantified in terms of the mean time between failure (MTBF) and mean time to first failure (MTFF). Generally, the overall system reliability is quantified using the mean time to failure (MTTF). This is because, since no repairs are included, the MTTF is more applicable as compared to the MTBF, which would typically find application in describing the reliability of repairable systems (Dhople et al. 2009). For an N-phase converter, the MTTF for a specified system is given as;

$$MTTF = \sum_{i=0}^{N-1} \sum_{j=0}^{N-1} P_{ij}\,(0) \qquad (8.3)$$

Where, $P_{ij}\,(0)$ is the Laplace transform of the transition probability from Chapman-Kolmogorov equations which are used to quantify the system reliability.

For two- and three- phase converters, the increase in switch resistance r_{SW} rises the MTTF because for a fixed impedance load, an increase in r_{SW} reduces the output voltage. This consequently reduces the stress on the output capacitor, rendering them more reliable. This in turn increases the MTTF as the capacitor dominates the converter reliability (Dhople et al. 2009).

4) Balance of system cost

This is defined as part of the system other than the PV or TEG device cost and will become increasingly important as the energy source system cost drops. The major component of balance of system cost in the module integrated systems is the cost of the inverters due to the absence of the storage batteries.

Therefore, the cost component must be well considered during converter design to minimize the overall cost of the system.

8.1.3. The design of distributed dc-dc converters for TEG system

Conventionally, the output from the TEG is mainly connected in series before it is subsequently linked to the sized converter or directly to the appropriate load. In other words, the integrated design converter architecture is applied which is associated with some challenges already mentioned above. In this section, the DCA that involves the use of non-isolated dc-dc converter per-TEG or group of TEGs, depending on the required voltage level, is designed.

The TEG devices in the DCA design can be connected in the same location (e.g. at the exhaust) under the same heating and cooling blocks or separated. Alternatively, the design allows for the flexibility of location, whereby the TEG devices can be physically located at different locations but electrically connected to the same group of converters which may be located at the same location or distributed in different locations depending on the load requirement, space availability and other technical issues. For example for application in pasenger vehicles, some TEGs may be placed at the exhaust while others at from the radiator. Figure 8.1, Figure 8.2, and Figure 8.3 show the design options for the DCA.

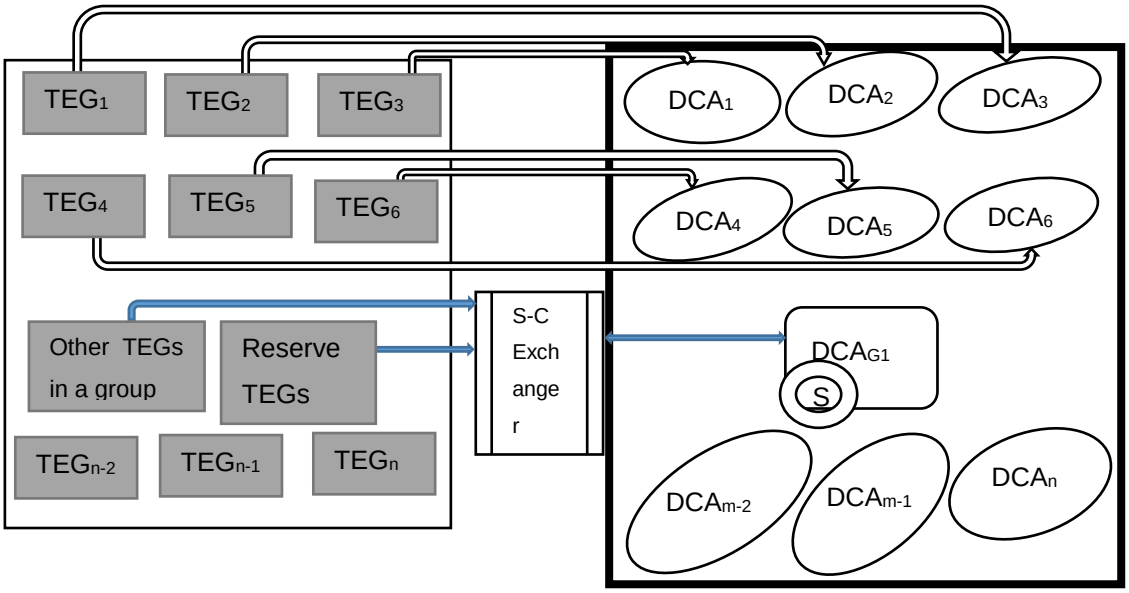


Figure 8.1. Design option 1: The DCA design when TEG devices are within the same location (the same heat and cooling blocks or otherwise) and the converters are confined in the same location

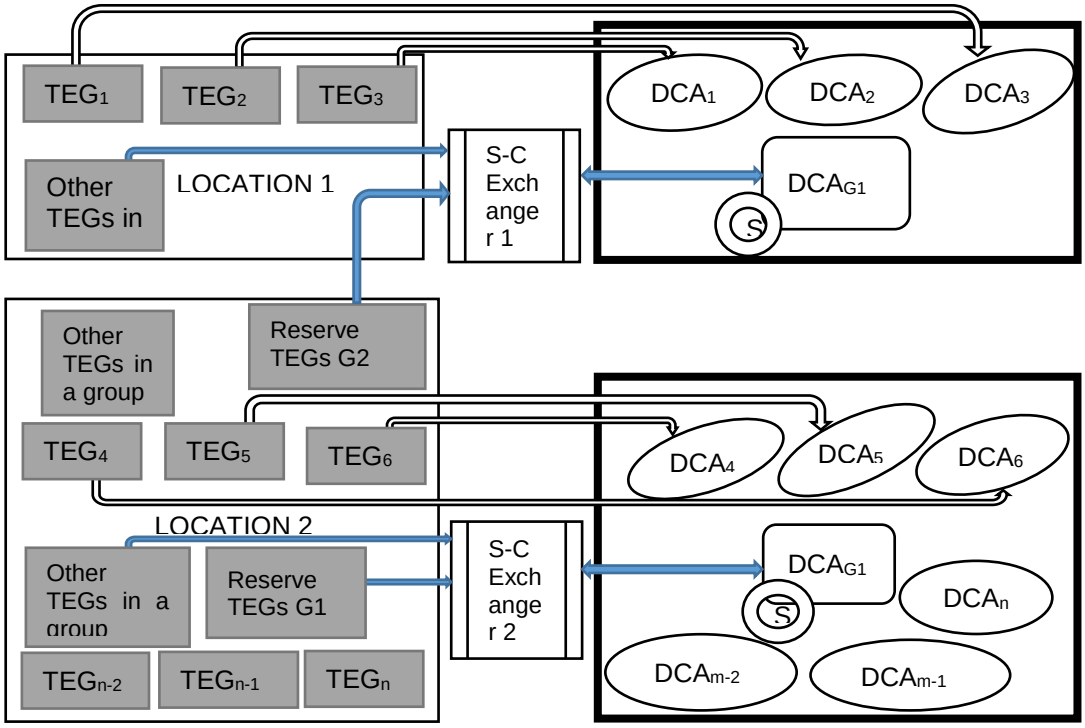


Figure 8.2. Design option 2: The DCA design when TEG devices are within two locations and the converters are kept in two different locations

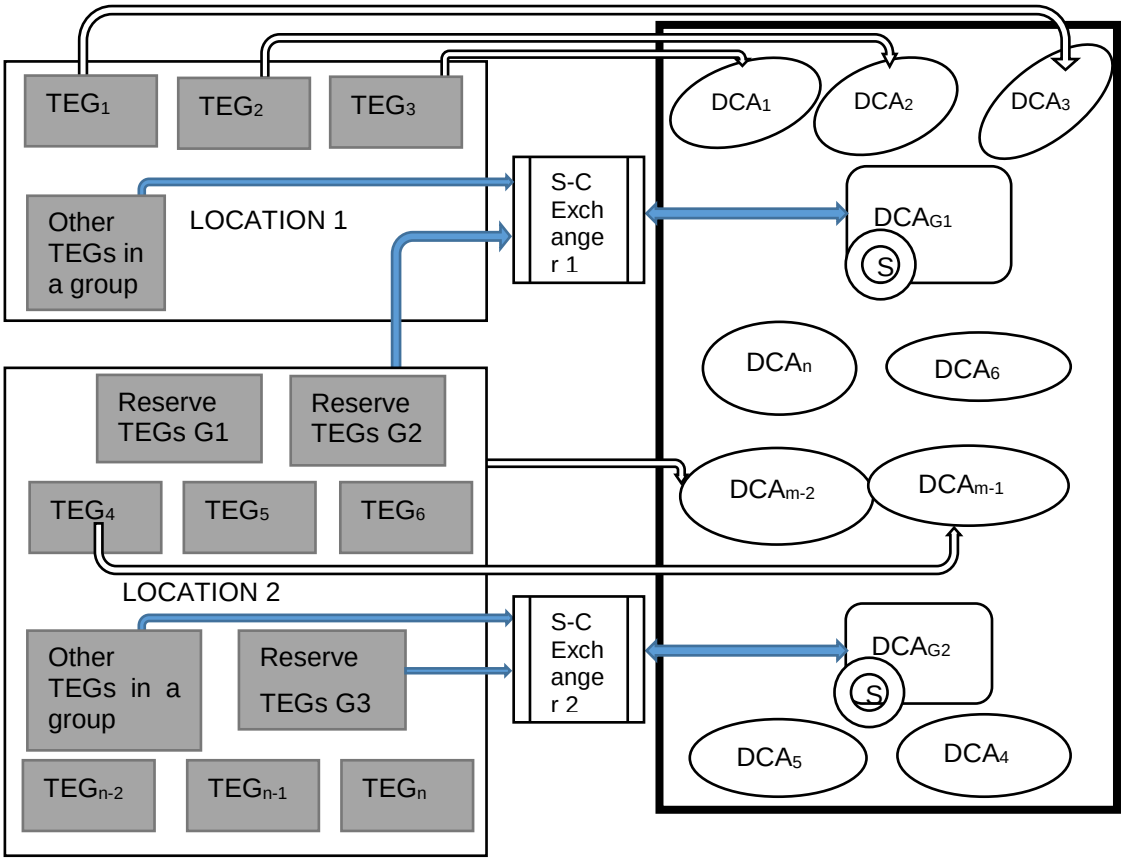


Figure 8.3. Design option 3: The DCA design when TEG devices are within two locations (the same heat and cooling blocks or otherwise) and the converters are confined in the same location

From Figure 8.1 to Figure 8.3, there are n-number of TEGs (from TEG1, TEG2 to…TEGn-1 and TEGn) whose output is controlled by m-number of DCAs (from DCA1, DCA2…DCAm-1 and DCAm). The value of n and m is not necessarily the same because some TEGs are connected electrically in series to form a group that is controlled by a specific DCA of higher power rating. Alternatively, a group of TEGs might be in a low temperature region, implying that their power output could be low, thus it becomes economical to control them with a single converter rather than connecting each of them individually to an independent converter.

Because the heat sources are not always constant, at some point when the heat source as well as the output power of the TEGs have declined drastically below a set or given threshold, the reserve TEGs (which must be of lower power rating than the main TEGs) should be utilized to compensate for the power loss or voltage drop at the load side. This is helpful to maintain the voltage and power quality requirement of the connected load. Some loads are designed to operate within specific range of voltages, outside which they might start malfunctioning when they experience the voltage surges or voltage dips. If such power quality issues occur frequently, the life of the load can deteriorate and eventually it could be damaged or completely fail. Therefore, a source-to-converter exchanger (S-C) is proposed to manage the connection btween the reserve TEGs and individual or group of TEGs through the converter for the voltage compensation of a given load.

An S-C exchanger should have a microcontroller connected to relays to be able to connect the TEG output to the required DCA converter based on the sensed signal (by a sensor, S) from the load connected to that specific converter. Voltage sensors are used to detect the dc voltage level at the load; the sensors function in such way that they are able to detect the voltage below or above a specified limit. For example, industrial voltage detectors are designed to detect the voltage above a certain limit such as 20V. When the voltage exceeds that limit, the LED is illuminated but it can only be extinguished if the voltage goes below 20V (Abb 2015). There are several types of voltage sensors which can be applied in the DCA design including closed and open loop half effect technology sensors and electronic sensors. However, electronic sensors are preferred because they are entirely made of electronic components without any magnetic circuits involved, making them immune from magnetic fields which might cause the electromagnetic interference.

8.1.4. Factor considered while selecting the converter topology

Before a converter topology is selected for application, the following are the selection criteria that should be considered during the design (Lenk 2005).

1. *Voltage step down or step-down requirement:* it shoud be known whether the input voltage is always higher or lower than the output. If the input is lower than the output, then the buck or non-isolated fly-back converter cannot be used because it is meant to step down the voltage.

2. *Converter Duty cycle*. Is the output voltage different by more than a factor of five from the input voltage? If so, you probably will need a transformer, calculate duty cycle to ensure that it doesn't have to get too small or too large.

3. *Number of output voltages:* If more than one output voltages levels are required, a transformer may be necessary, unless you can post-regulate. Large numbers of outputs suggest more than one converter may be a good choice. That's why the DCA design is considered in this case.

4*. Isolation requirement:* Isolation necessitates a transformer and it is important to know the output voltage requirement.

5. *Electromagnetic interference (EMI) requirements*: Tight requirements suggest staying away from topologies with discontinuous input current, such as a buck, and choosing continuous mode operation such as a CUK or buck-boost converter. The EMI can be conducted, which is caused by physical contact of conductors, or radiated EMI, which is as a result of induction without any physical contact, depending on the frequency of operation (Li 2009). For lower frequency, EMI is caused by conduction while for higher frequency, it is by radiation.

6. *The cost of the components*: Is cost so paramount that a bipolar junction transistor (BJT) might be a choice? Or if off-line, an IGBT? Otherwise, plan on MOSFETs.

7. *Necessity of synchronous rectification be afforded:* This makes the converter continuous regardless of the load.

8. *Load requirement***:** If the converter is supplying the load, then choose discontinuous mode--unless the converter has synchronous rectification, which makes it continuous.

9. *Level of output current:* if the output current is high, then it might be good to use voltage mode rather than current mode.

8.2. Demonstration of DCA design for TEG system

To prove the feasibility of the DCA design for the TEG system, two case studies have been developed. The first one involves the simulation of the DCA with TEG system to demonstrate the operation of different converter topologies and how they respond to the changes in the input voltages. The second case is the experimental study aimed at signifying how different converter topologies respond to temperature changes and the output of the TEG devices. The next two sub-sections are dedicated for the respective simulation and experimental case studies.

8.3. Simulation of DCA with TEG system

In this case study, five converter topologies, including boost, buck, buck-boost, SEPIC and C´uk topologies have been considered in the modelling and simulation to demonstrate the operation of different converter topologies and how they respond to changes in input voltages and the variation in the load. Figure 8.4 shows the model representation of the five converter topologies. For simplicity, the converter topologies are modified from (Ravi 2016), to

demonstrate the usefulness of the new design. In Figure 8.4, different dc-dc converter topologies are supplied by the same voltage source but have different output voltages because their functioning is not the same.

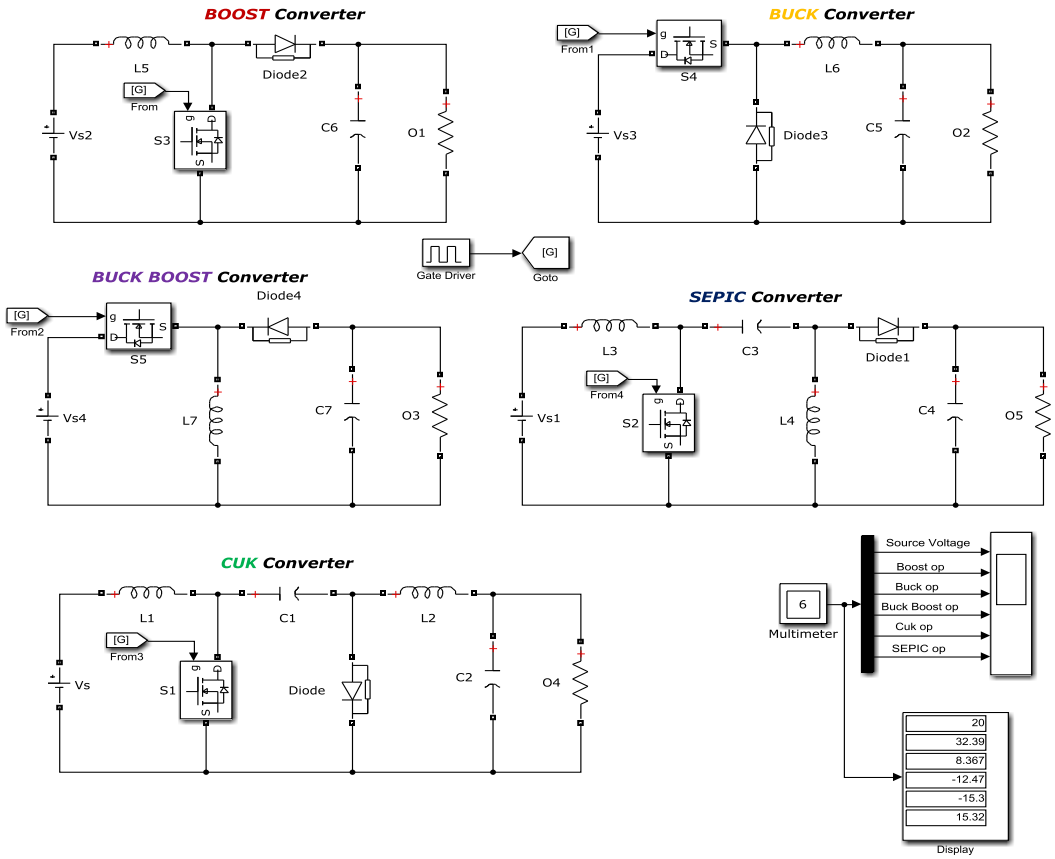


Figure 8.4. Simulation of different dc-dc converter topologies supplied by the same voltage source

Figure 8.5 shows the DCA applied to TEG system. The TEG device is electrically represented as a voltage source in series with a resistor that represents the TEG internal resistance. Five converter topologies are tested each connected to a single TEG. All the five TEGs are physically combined into a sub-system purposely to minimize the space occupied by the TEGs.

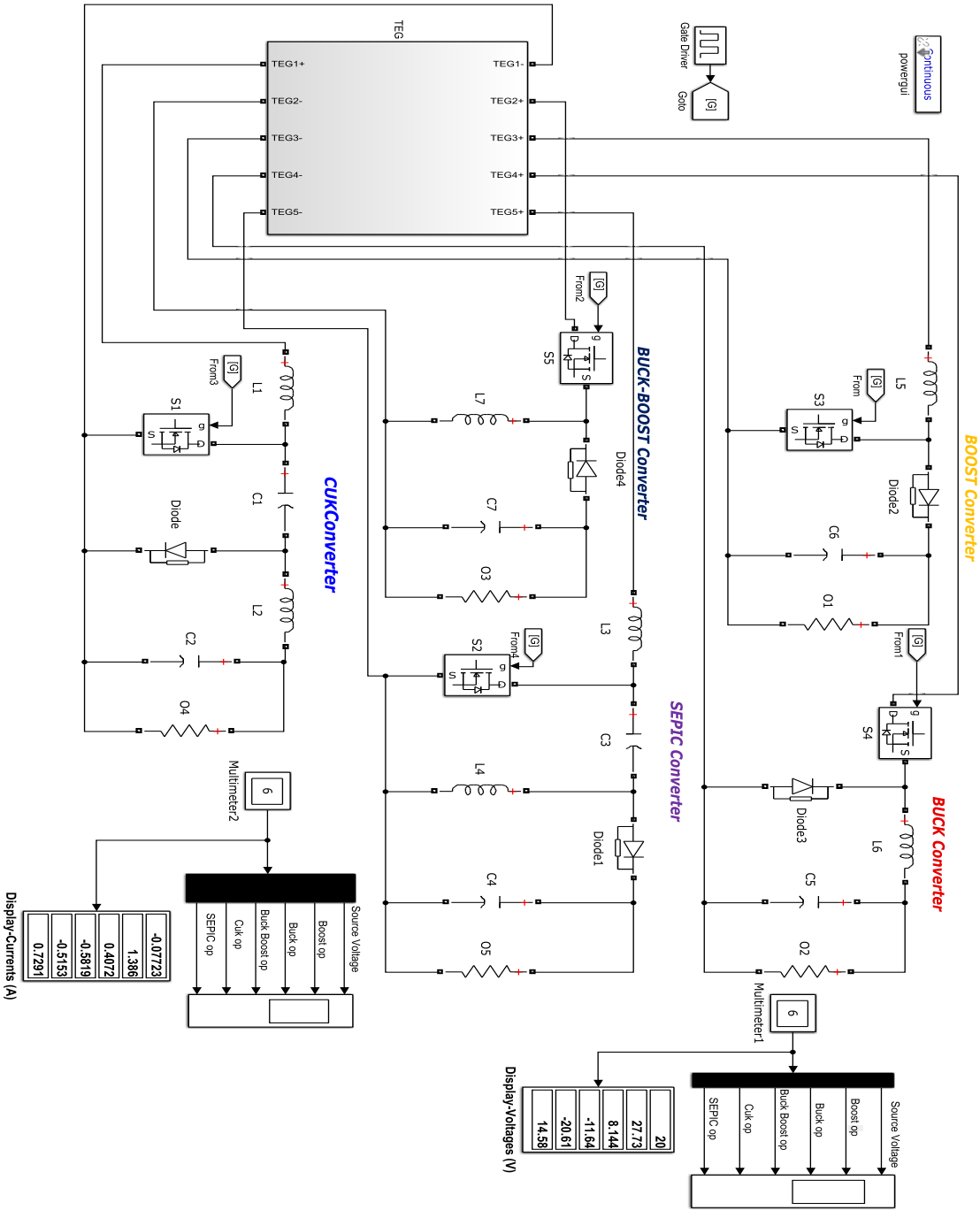


Figure 8.5. Simulation of DCA applied to TEG system

The SEPIC or its modification, is one of the converter topologies with continuous input current and it has been applied to many industrial applications including power factor correction, LED driving, and in situations where a symmetric voltage is needed. Its features include; (i) Positive output voltage, (ii) there is no dc-current from the input to the output when the converter is off, as the case with other topologies (Rosas-Caro et al. 2016). The SEPIC topology has already been applied with MPPT for improving energy harvesting from PV systems. The authors presented a new fuzzy logic controller as an MPP tracker with a SEPIC converter. The MPPT controller is found to improve the P&O search method with rules to fuzzy which eliminate its drawbacks (El Khateb et al. 2013). The output voltage of a SEPIC converter is given by;

$$\frac{V_{c4}}{V_{s4}} = \frac{D}{1-D} \qquad (8.4)$$

Where V_{c4} and V_{s4} are the output and input voltages of the SEPIC converter

The duty cycle is ideally between zero and 1 but due to the losses in different converter components, the maximum value can be up to 0.8. For purposes of increasing the switching frequency, D can be kept up to 0.5. The high switching frequency results into a reduced converter size, since small capacitors and inductors can be used with reduced voltage ripples.

The pricniples of operation of the C´UK and boost converter topologies are already described in the previous chapters but in this case, they both have inverted output voltages. The C´UK converter transforms the input dc voltage to the output terminals with reversed polarity. The output voltage can either be lower or greater than the input voltage. Unlike the boost, buck and buck-boost topologies, the C´UK converter has extra inductor and capacitor to store energy.

Figure 8.6 shows the plots of the output voltages from all the five converter topologies with a resistive load of 4Ω connected to each converter. The common voltage at the top left is the input voltage (20V) to all the converters. From these Figures, it can be seen that the output voltages for the converters are different with the boost topology having the highest steady state voltage of about 27.2V.

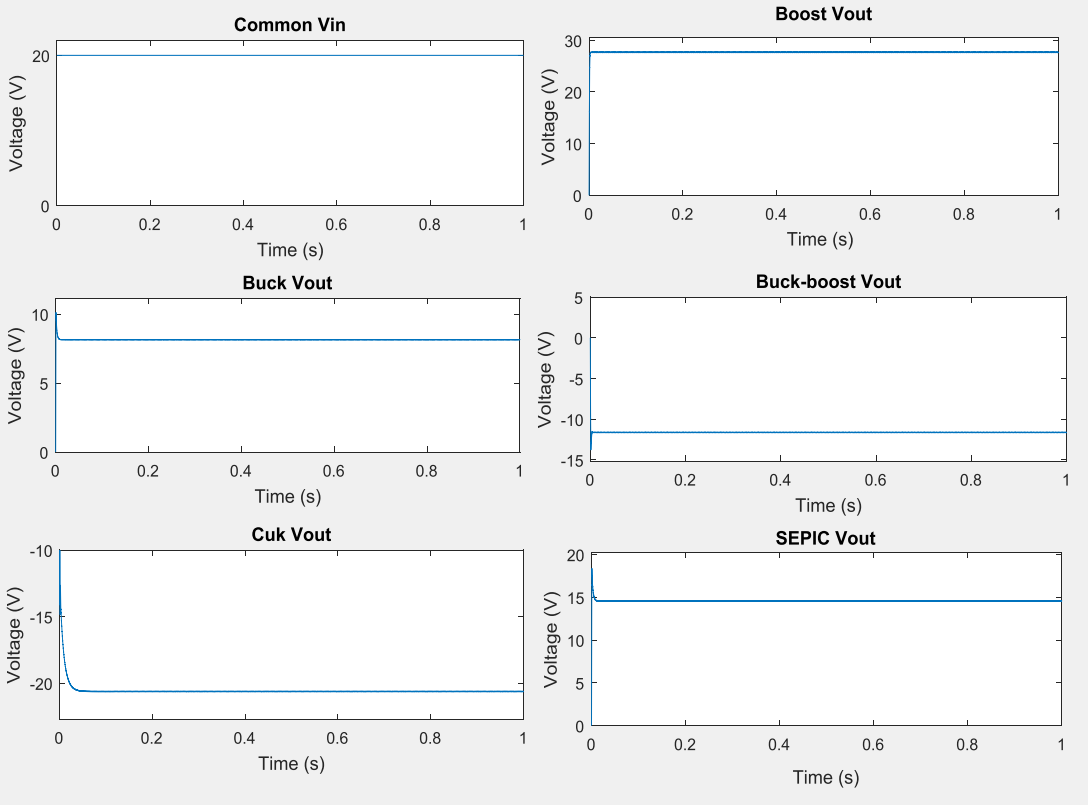


Figure 8.6. Voltages from DCA applied to TEG system at the same input voltages

Figure 8.7 shows the output currents of the distributed dc-dc converter topologies with the same common input voltage of 20V. Similarly, the boost converter has the highest output current of 1.4A whereas the C´UK and buck-boost topologies have inverted currents of -0.51A and -0.58A respectively as expected.

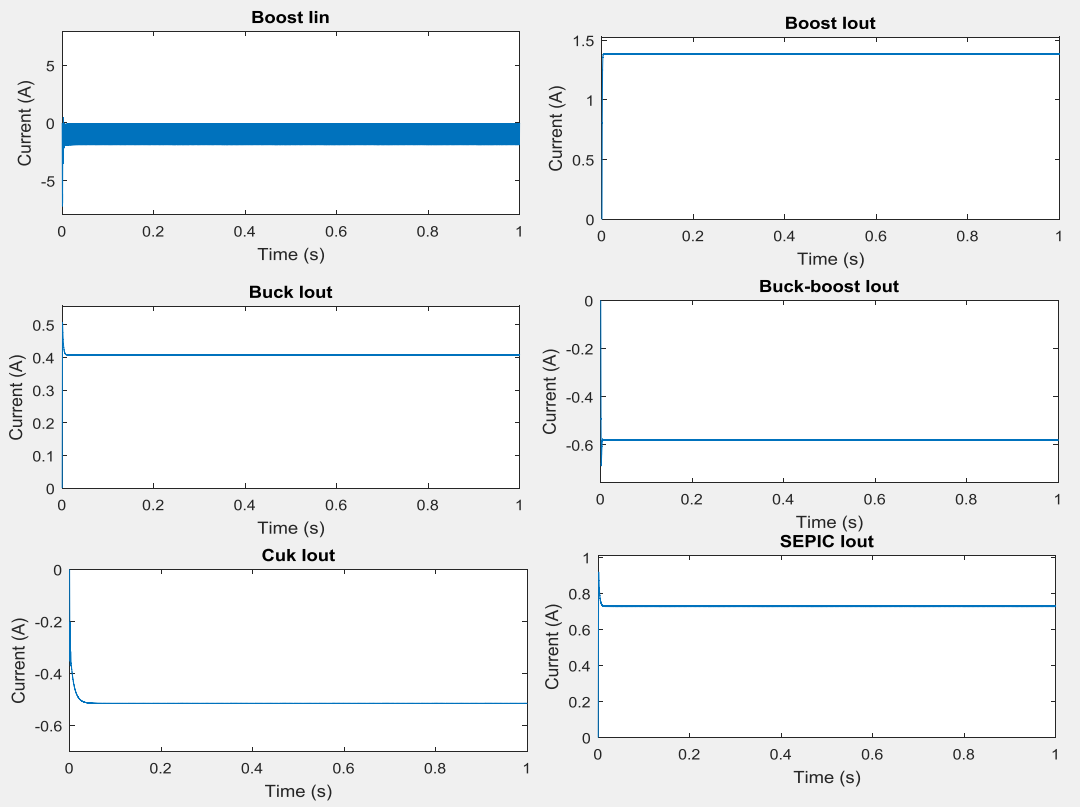


Figure 8.7. Currents from distributed dc-dc converter architecture applied to TEG system at the same input voltages

To further analyse the operation of these five converter topologies, their loads are varied from 0.2Ω to 40Ω and the input voltages are each kept at 7.4V. Figure 8.8 and Figure 8.9 show the input voltages and currents respectively. It is observed that the buck-boost converter has the highest input terminal voltage with a maximum value of 6.3V at a load of 0.2Ω, followed by a SEPIC converter with a maximum value of 3.7V at the same load. As for the C´UK converter, all the input voltages at any load are zero since all the input voltages are normally transformed into the output voltages. A similar trend applies to all the output currents of these converters as observed in Figure 8.9 where some currents overlap each other. The input currents of the C´UK and buck converters are

both zero, so their plots overlap each other. Similarly, the SEPIC and the boost converter input currents and voltages have the same values for all the loads.

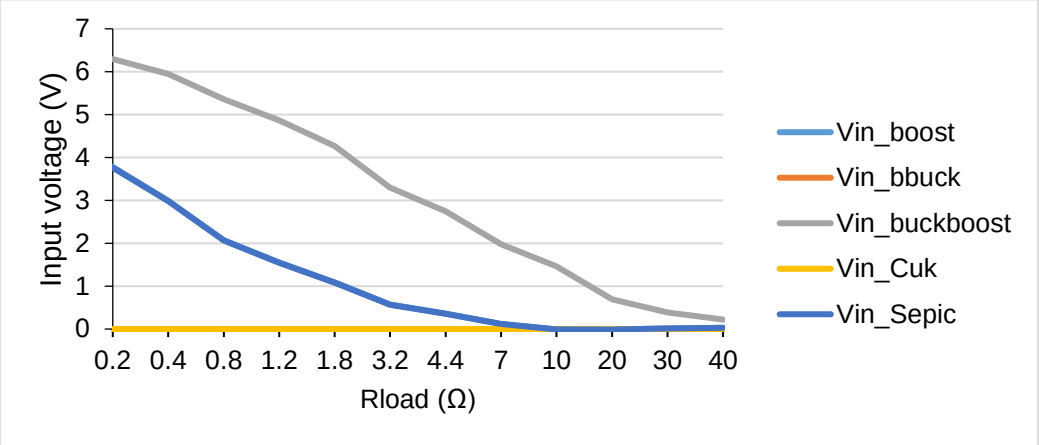


Figure 8.8. Converter input voltages at the same TEG voltage of 7.4V

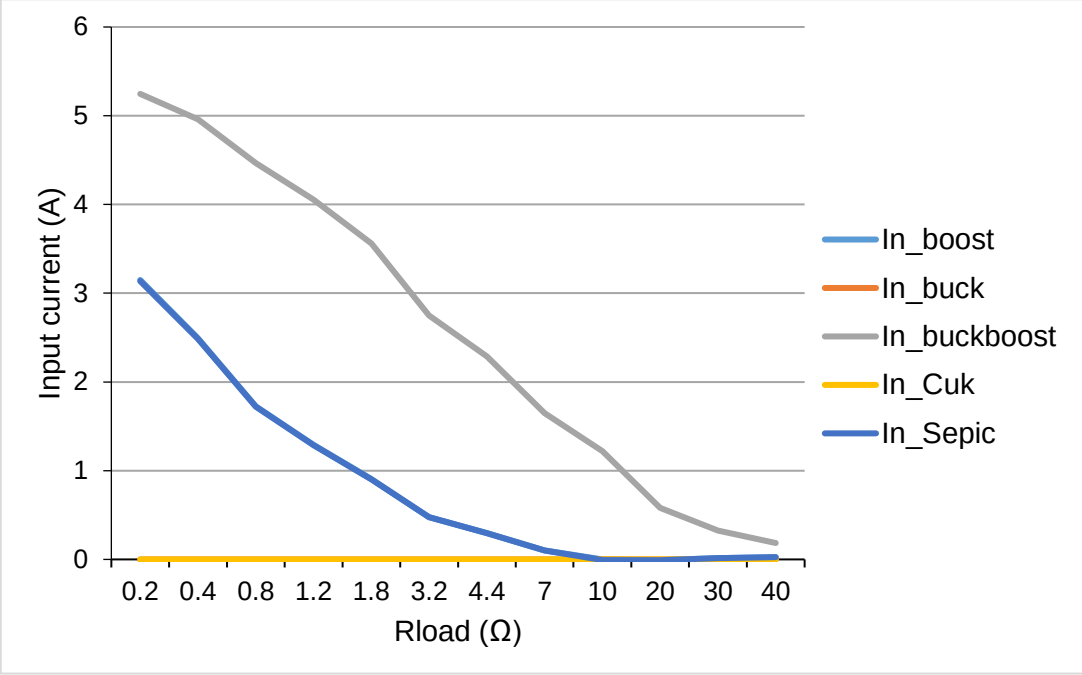


Figure 8.9. Converter input currents at the same TEG voltage of 7.4V

To show a clear distinction between the individual converter input powers, Figure 8.10 and Figure 8.11 show the detailed input power of all the topologies.

From Figure 8.10, the input power of the buck converter whose value is zero for all loads is like that of the C´uk converter in Figure 8.11. This is because the C´UK converter is operating in the step-down mode just like the buck converter with the same components though this does not necessarily mean that these topologies have the same operating principles.

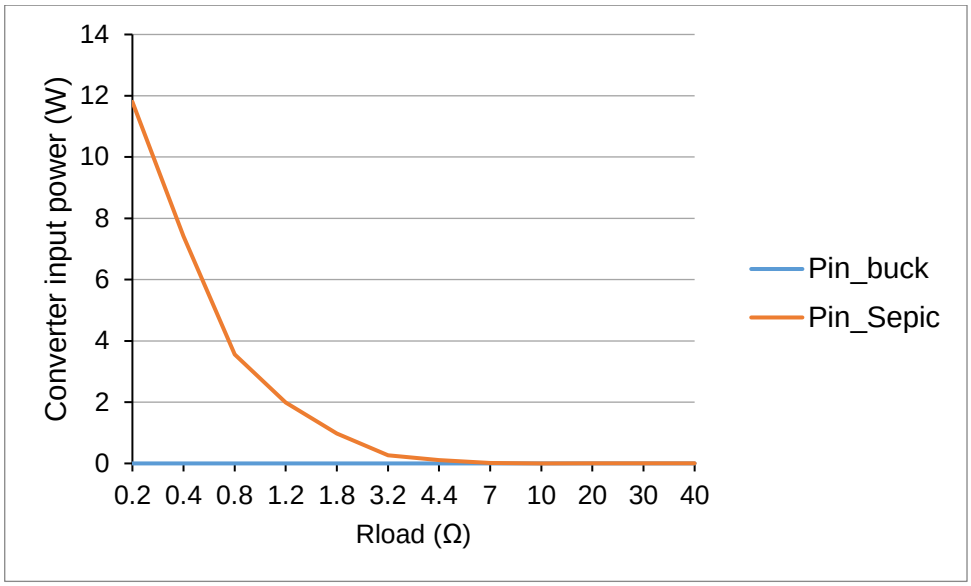


Figure 8.10. Converter input power at the same TEG voltage of 7.4V for Buck and SEPIC topologies

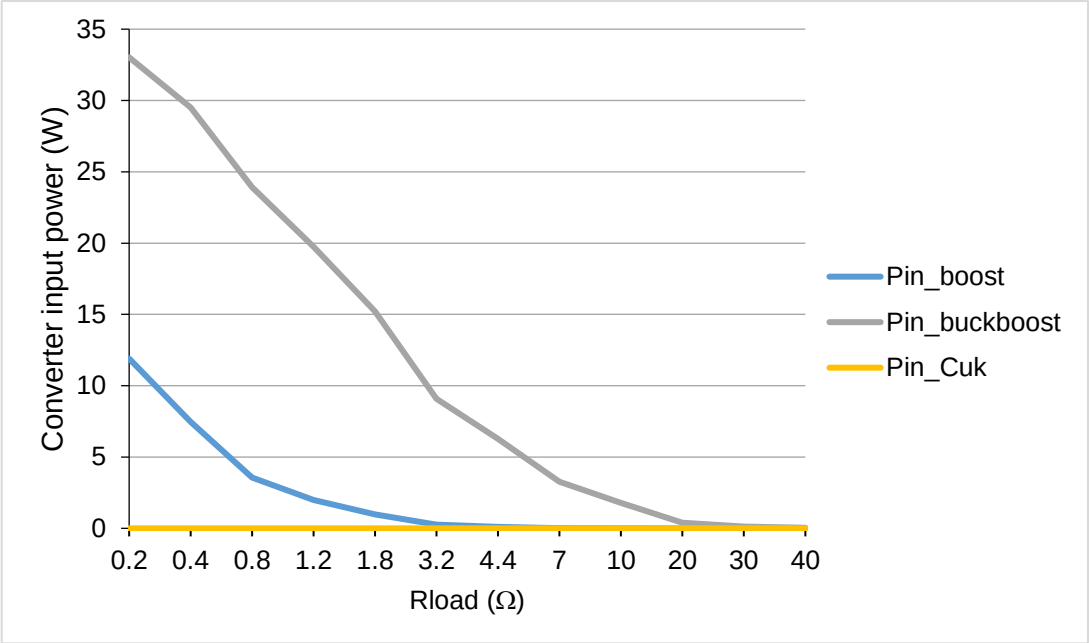


Figure 8.11. Converter input power at the same TEG voltage of 7.4V for Boost, Buck-boost and C´UK topologies

The output powers are depicted in Figure 8.12 where is it indicated that the boost converter has the highest output power. It can be observed that each of these topologies have their own maximum or matching output power. It is clear that the boost converter has the highest value of the matching power of 9.7W at a load of 3.2Ω. This explains why it is the most commonly used with MPPT circuit to harvest maximum power from PV or TEG systems. However, as observed above, because it has large value of input voltage, even its losses are high, making it unsuitable for specific applications.

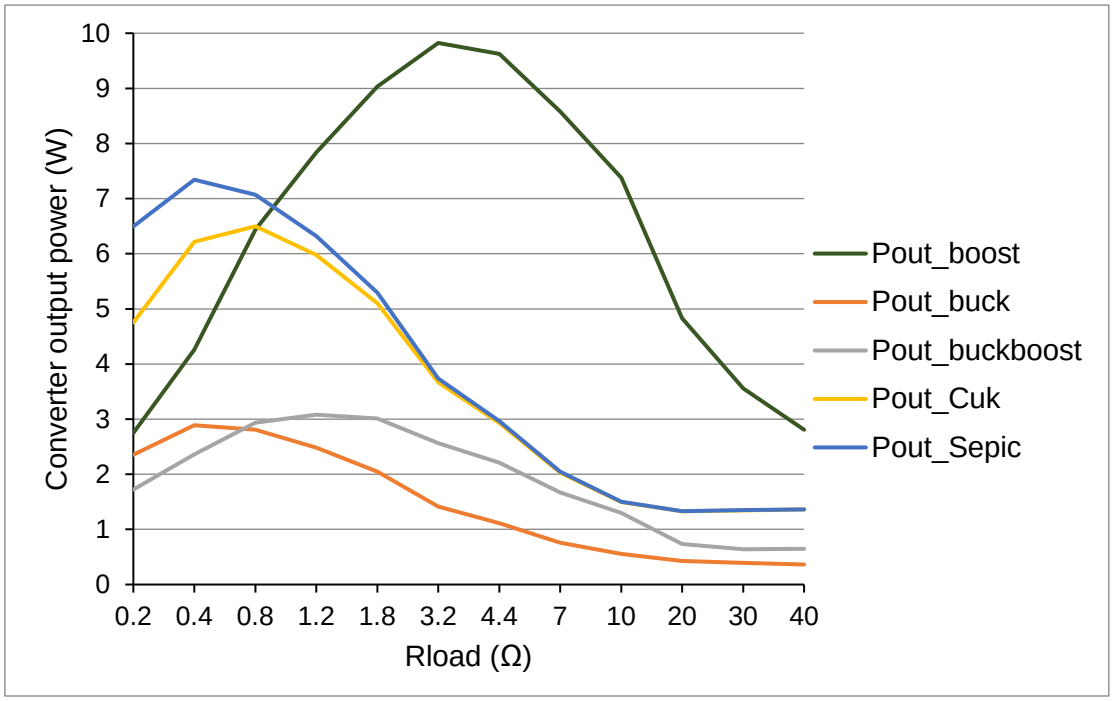


Figure 8.12. Converter output powers at the same TEG voltage of 7.4V

The I-V characteristics curves of the five converters are shown in Figure 8.13 and Figure 8.14. In all cases, it is clear that the optimum points differ depending on the type of converter topology applied. Much as the C'uk converter has zero input current, it is demonstrated that it has the highest output current. This implies that almost all its input power is transferred to the output since it has both zero input current and terminal input voltage and therefore its losses are minimal as compared to other topologies. Similarly, the SEPIC converter has a high output power which is almost the same as that of the C'uk, although the input current of the SEPIC converter is not zero and hence it transfers less power than the C'uK converter.

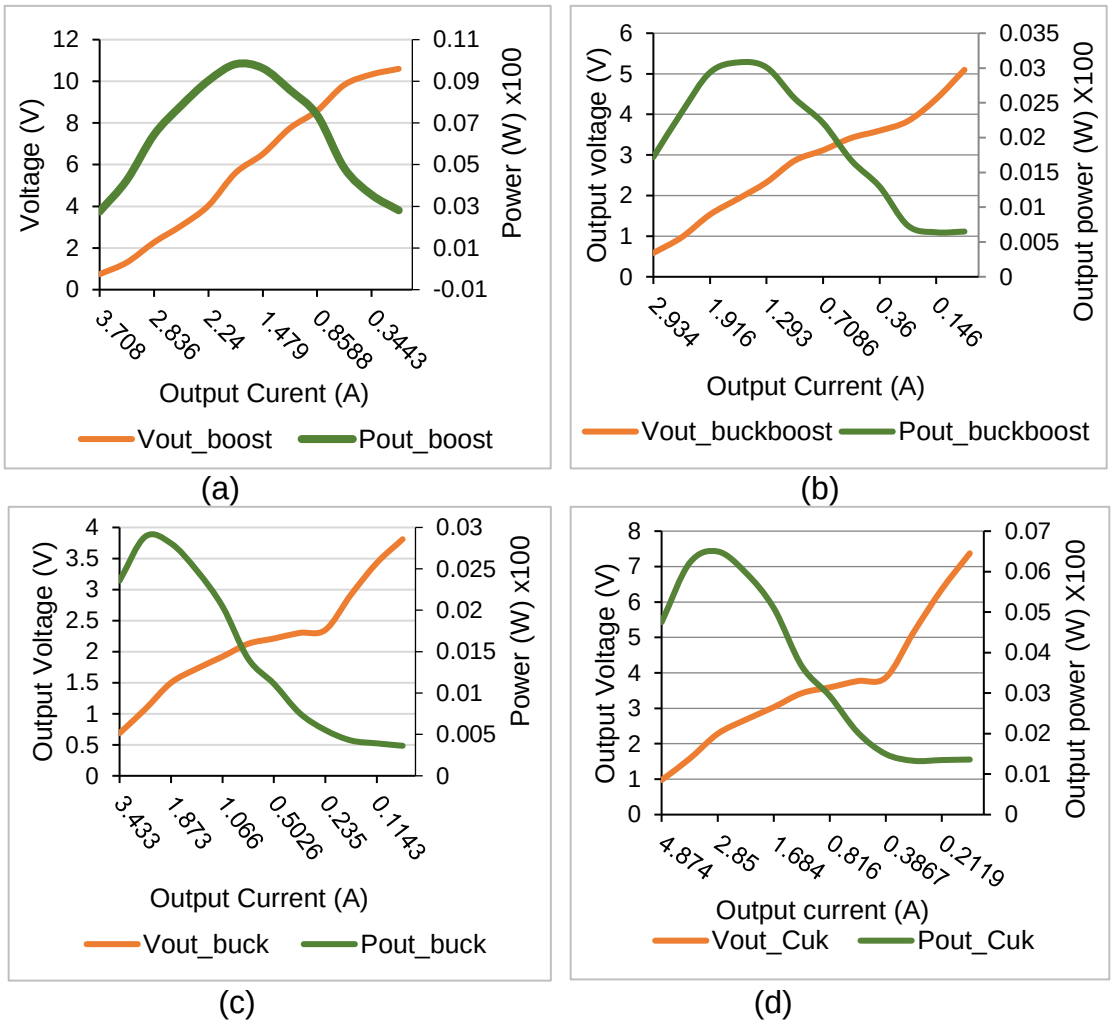


Figure 8.13. The I-V characteristics curves: (a) Boost; (b) Buck-boost; (c) Buck; (d) C´UK

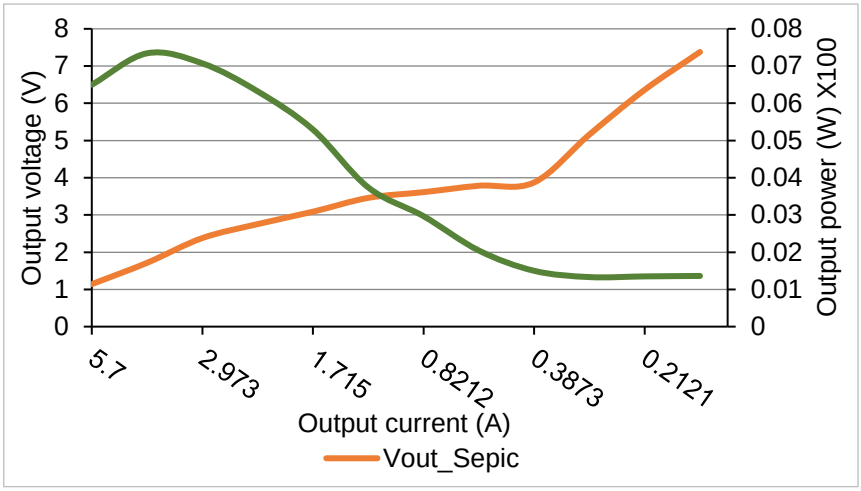


Figure 8.14. The I-V characteristics curve for the SEPIC converter topology

8.4. Experimental study on DCA with TEG system

The main objective of this experimental study is to verify the feasibility of applying the DCA for conditioning the power generated from TEG system. The other specific objectives include (1) to show capability of different dc-dc converter topologies in stabilising the nonlinear output voltage from TEG devices; (2) and to demonstrate the functionality of different converters and how they respond to changes in temperature and the corresponding output voltages of TEG devices.

As already noted, there are several dc-dc converter topologies with different functionalities. However, in this experimental work, two converter topologies are chosen; the boost converter and the buck-boost converter. These two topologies were chosen to demonstrate the design because their evaluation circuits are readily available in the market at lower cost for evaluation purposes.

The boost converter used is the microchip ADM00664 evaluation board which is an integrated switch PWM boost regulator manufactured by microchip technology (Microchip n.d.). The ADM00664 boost regulator is used to demonstrate the performance of MCP1663 boost switching regulator.

MCP1663 device is a compact, high efficiency, fixed frequency, non-synchronous step up dc-dc converter which integrates a NMOS (negative channel metal oxide semiconductor) switch. It provides a space-efficient high voltage step up power supply solution for applications powered by either two-cell or three-cell alkaline, Lithium, NiCd, NiMH, one-cell Li-Ion or Li-Polymer batteries (Microchip n.d.). However, from its manual, it is clearly specified that it can be used for TEG application, which is the reason why it was selected for this experimental study.

The ADM00664 board is made up of two distinct boost converter circuits. The first circuit is used to demonstrate the boost configuration which has a 2.4-5.5V input voltage range and a 9V or 12V interchangeable output voltages. The second one is made of a higher voltage input of 9-16V with the output voltage of 24V. However, with a slight change in the output resistance, the circuit can reach up to a maximum output voltage of 32V. Table 8.1 shows the specifications for the ADM00664 boost regulator whereas Figure 8.15 shows the ADM00664 integrated switch PWM Boost converter.

Table 8.1. Specifications for integrated switch PWM boost converter evaluation module

Parameter	**Value**
Converter topology	Boost regulator,
Switching frequency	500 kHz PWM Switching,
Input voltage	2.4-5.5V
Output	0.25A/9V/12V & 24V

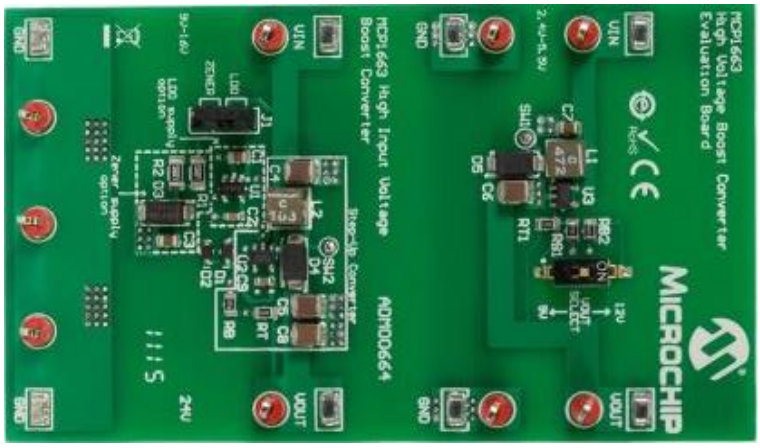


Figure 8.15. The ADM00664 integrated switch PWM Boost converter

The buck-boost converter topology is demonstrated with a TPS63060EVM-619 evaluation module (EVM) buck-boost converter from Texas Instruments as indicated in Figure 8.16. The EVM is designed to evaluate and test the operation and functionality of the TPS63060 boost converter chip manufactured by Texas Instruments (Texas Instruments n.d.). The TPS63060 is a highly efficient, single inductor, internally compensated, buck-boost converter. The evaluation module uses the TPS63060 adjustable output voltage version of the integrated circuit and is set to a 5V output. Table 8.2 sows the specifications of the EVM buck-boost converter.

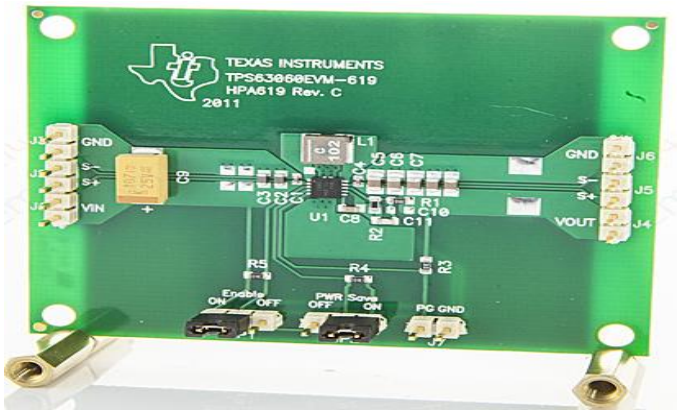


Figure 8.16. TPS63060EVM-619 evaluation Module for a Buck-Boost Converter

Table 8.2. Specifications for a TPS63060EVM-619 buck-boost converter evaluation module

Parameter	Value
Input voltage range	2.5V to 12V
Typical device quiescent current	less than 60µA
Efficiency	Up to 93%
Output current	2A/1A at 5V in step down mode 1.3A at 5V in boost mode (VIN>4V)
Transition between modes	Automatic transition between step down and boost mode
Output voltage	Fixed and adjustable output voltage options from 2.5V to 8V

The other main components for the experiment include;

- Digital dc dual power supply
- Digital multimeter
- Breadboard
- TEG modules (6 pieces)
- Aluminum cooling block
- Hot plate (heating block)
- Data loggers (3)
- Resistors (as loads)
- K-type thermocouples

8.5. Experimental test with the hotplate based TEG system

8.5.1. Experimental design of the TEG rig and dc-dc converters

The experiment involves testing the DCA design with TEG. The dc-dc converter circuit is tested with the boost and buck-boost converter topologies. The six TEG devices are connected between the heating and cooling blocks, where by the heating block is made of a hotplate controlled by a proportional-integral-derivative (PID) controller. The purpose of employing the PID controller is to

enable the generation of a nonlinear temperature profile from the hotplate. The nonlinear temperature, according to the Seebeck effect, results into the generated voltage from TEG to be nonlinear too, such that a nonlinear output voltage is supplied to the dc-dc converters as their inputs. The nonlinear input helps to test the capability of the converter in stabling the output voltage from TEG if relatively stable output voltages are obtained from the converters.

In this part of experiment, both boost and buck-boost converters are connected to one of the six TEG modules to regulate the power generated from these TEGs. Figure 8.17 shows the block diagram of the experimental setup. The TEG system basically consists of a cooling block with normal water used as the cooling fluid. The chiller is used to circulate the cooling water into the cooling block. The heating block is made of a cast iron hotplate which is used as the heat source. A pump is used to pump the heated water from the cooling block back to the chiller. Six TEG modules are placed between the cooling and the heating block.

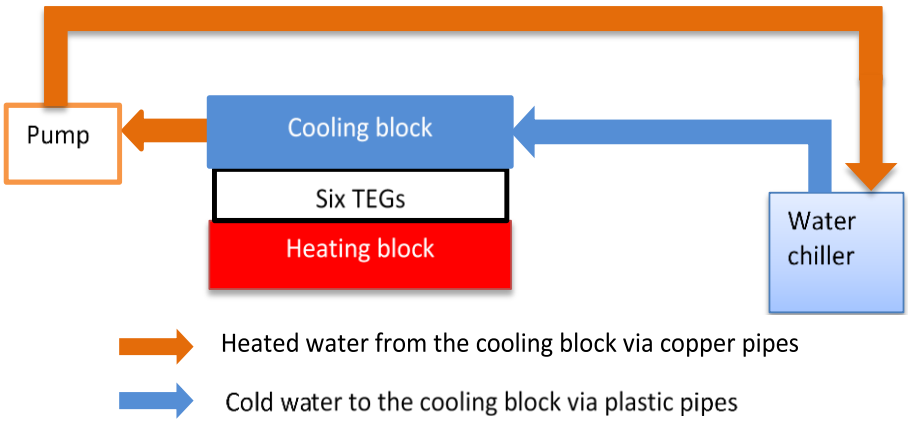


Figure 8.17. The Block diagram for the experimental setup of the TEG system

Figure 8.18 shows parts of the actual experimental rig in the laboratory. The experiment consists of the heat exchanger, cooling fluid or water supply part, data acquisition section and the load connection section as the main parts. The cold water is supplied to the cooling block through a plastic pipe from the chiller.

The vertical-type flow meter is connected between the plastic pipe and the chiller to measure the water flow rate. The chiller is a Grant type, which contains a refrigerator for cooling water to the desired temperature and is equipped with a controller which is used to set the require temperature. The hot water circulated through the aluminium cooling block is pumped back to the chiller by a Grundfos UPA 15-90N which is a small stainless-steel circulator pump. The hot water returns to the chiller through a copper pipe to easily radiate the heat to the ambient.

The hotplate is a robust one-piece cast iron construction, which is free standing on a bench or recessed into a fume cupboard with maximum temperature of approximately 410°C and a supply voltage of 230/240V AC single phase. Top plate dimensions are 457mm x 457mm with a rated load of 4KW. The hotplate is linked to the digital PID controller via 1.5m protected flexible cables and is powered by 16A 1-phase power socket connected through a PID controller which enables it to adjust the temperature of the heating block to the required value. The hotplate is placed on the table covered with a hard-paste porcelain tile which shield the metallic table from being heated by high temperature of the hotplate.

The data acquisition system is composed of three data takers, two of which are DT500 for logging both the temperature and currents while DT80 data taker type is employed to record the voltages. Each of these data takers is connected to a separate computer for monitoring and storing the logged data. All the TEGs are terminated to the breadboard where the connection of resistive loads and converters as well as the sensing of voltages and currents take place.

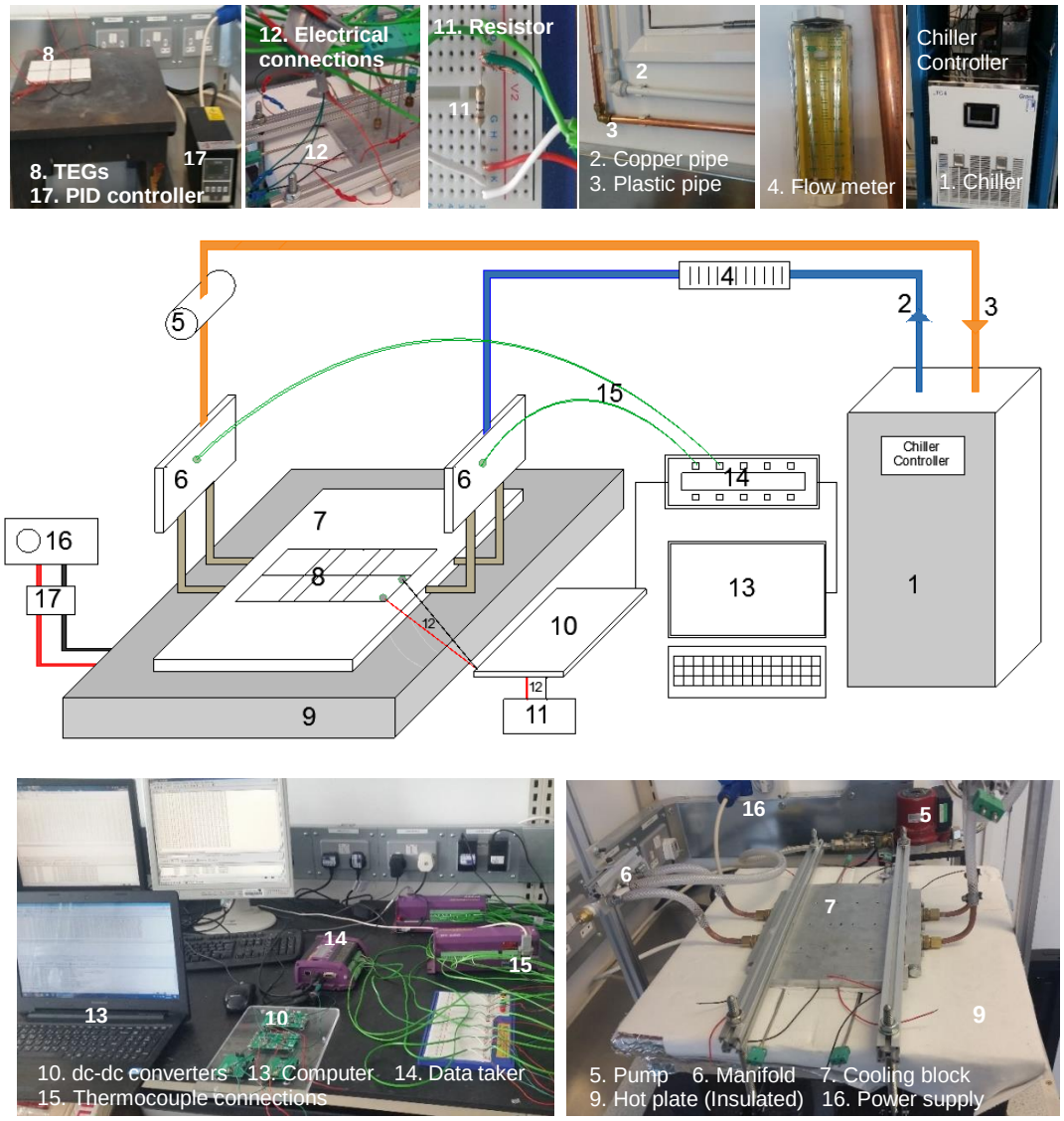


Figure 8.18. Parts of the actual experimental rig and the associated components in the laboratory

Figure 8.19 demonstrates in detail the heat exchanger system, thermocouple points, heat isolation and the electrical connections to the TEGs. The cooling block has two manifolds; cold and hot water manifolds connected to it. The cold-water manifold is connected to the cooling block through two pipes that distribute the cold water to the six holes within the cooling block to create the

temperature difference. The cold-water manifold is supplied by the cold-water inlet pipe which is connected to the plastic pipe that delivers cold water from the chiller. Likewise, the hot water manifold is connected in a similar way to the cooling block but it is also connected to the hot water copper pipe through the pump that forces water back to the chiller.

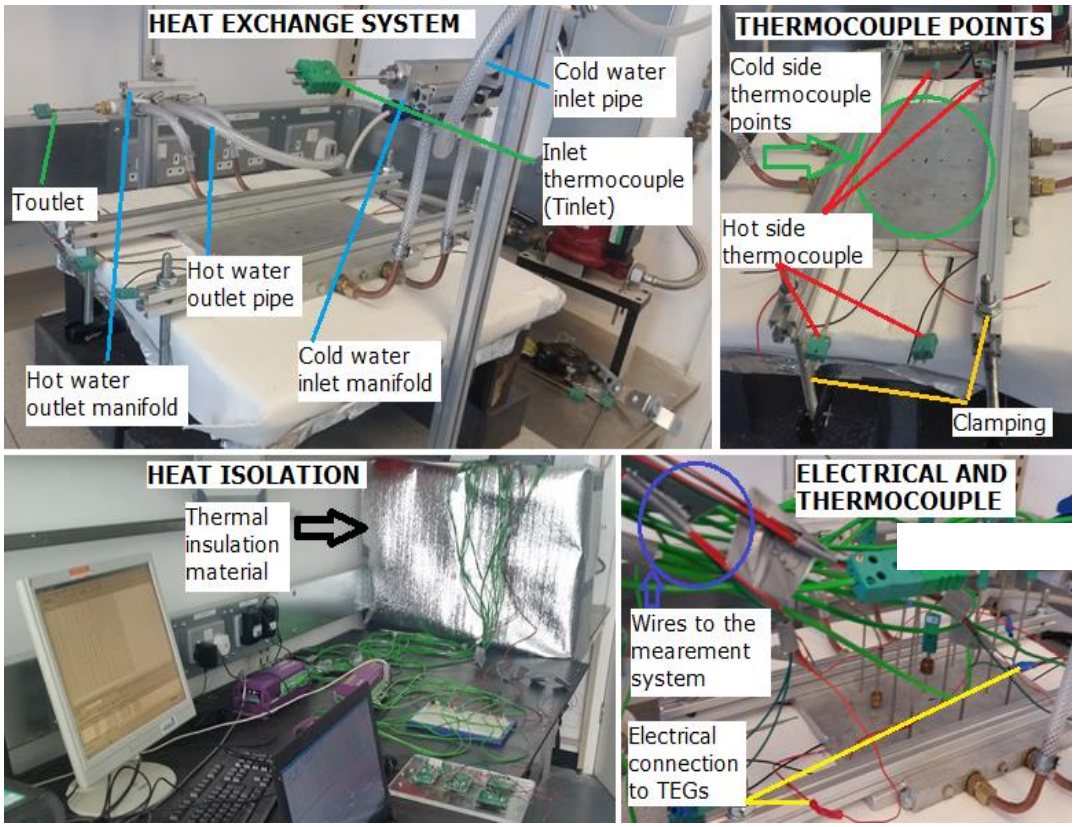


Figure 8.19. Demonstration of the Heat exchanger system, thermocouple points, heat isolation and the electrical connections

The layout of the cooling block and the TEGs on top of the hotplate surface is illustrated in Figure 8.20. The size of cooling block is 265mm in length and 189mm wide, which is enough to cover the total surfaces of the six TEGs whose dimensions are 62mm X62mm and are placed on top surface of the hotplate in 3 X2 TEGs format. Since the top surfsce of the hotplate is 457mm x 457mm, the remaining part after covering the cooling block together with TEGs, is

insulated with two layers of a high temperature thermal insulating sheet, rated 1200°C according to the datasheets indicated in Appendix 1, to prevent heat from radiating into the ambient which might interfere with the comfort of the working environment within the laboratory. Another thermal insulating material rated at 80°C is also used to isolate the heated areas from the electronic components such as dc-dc converters, breadboards, and the computers used for measuring and storing the experimental data.

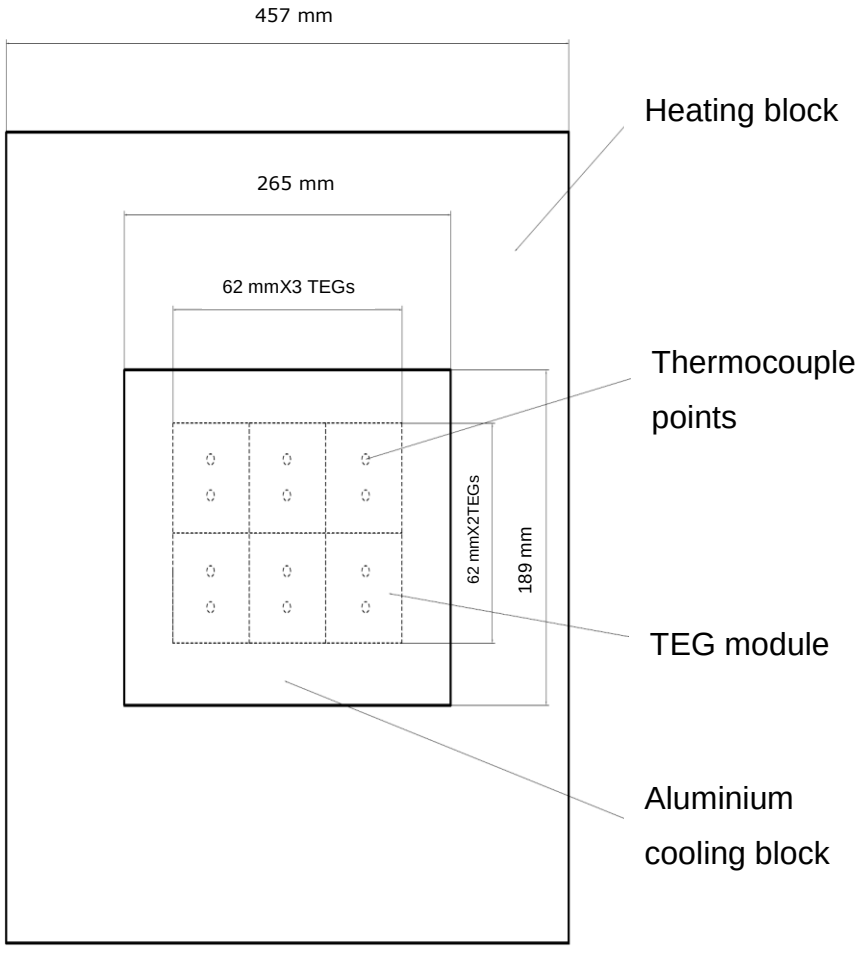


Figure 8.20. The dimensions of layout of the cooling block on top of the hotplate

8.5.2. Results: Analysis of parameters affecting TEG perormance

Several factors affecting the output parameters from TEG are analysed including; the effect of the time of switching on/off of different components, the effect of thermocouple malfunctioning, the impact of temperature variation of the hot and cold side etc. The results are plotted from the raw data that was recorded using K-type thermocouples.

8.5.2.1. Effect of switching time for different components

Figure 8.21 shows the thermocouple readings of the hot side, cold side, inlet and outlet temperature. It can be seen that all the thermocouple readings begin at about 20°C, which is the value of the room tempearture. Before switching it on, the water in the chiller is initially recorded at 18°C. the temperature of the chiller is set at 5°C using the chiller controller but the refrigerator of chiller takes some time to reduce the temperature of water to the set value. In this case, both the chiller and the hotplate are switched on at the same time and the period when both are ON is indicated before point “A” in the temperature plots. The temperature variations as indicated in the plots are almost saw-toothed or sisusoidal; this demonstrates the nature of the PID controller where the temperature rises and falls after a specific period of time. As observed, the the hot side temperatures T_{h1}, T_{h2}, T_{h3} and T_{h4} are the highest of all the temperatures, with T_{h1} and T_{h4} having higher and almost the same tempearture than T_{h2} and T_{h3}. The inlet temperature T_{in} has the lowest value which is constant at 8°C from the time of 14:44:46. Another lower point is the cold side temperature T_{c9} whose thermocouple point is very near to the inlet thermocouple point, hence the temperature readings at that point are almost the same as T_{in}. The value of the outlet temeparture T_{out} is comaparable in value to those temperature readings of the cold side thermocouples whose points are near to it.

At point “A”, both the chiller and the hotplate are turned off at the same time. As observed, the temperature of the hot side steadily resuces until almost constant values are attained. Alternatively, the inlet and some of the cold side temperatures rise at a faster rate for some time and fall steadily after some time and becomes almost same as the hot side temperatures. However, some two points takes the opposite path i.e their temepartaure reduces abruptly when both the chiller and the hotplate are off at the same time, but starts to increse steadily after a short time and finally aligns with the other temperatures at almost the room temperature.

This kind of temperature variation is not good for analysis of the performance of dc-dc conevretrs when both the chiller and hotplate are off at the same time, as the profile of TEGs output voltages would be difficult to analyse.

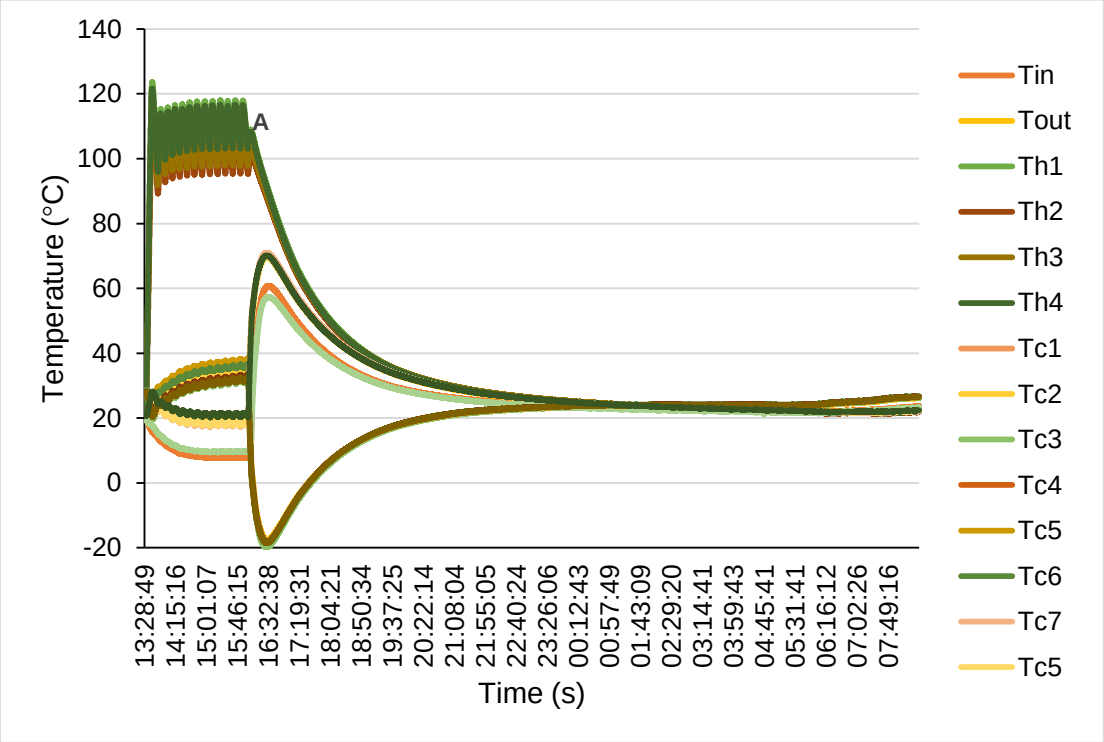


Figure 8.21. Temperature readings of the thermocouples, when both the hotplate and the chiller are switched off at the same time (at 15:58:16)

Figure 8.22 shows the temperature readings when the chiller and the hotplate are off at different times. In this case, the chiller temperature is set at 3°C. It can be observed that the cold side temperature profile take on different paths unlike those when both the chiller and the hotplate are switched on at the same time. The trend of the hot side temperature remains the same but the rate at which the temperature falls increases because the chiller is still operating. Since the heat supply from the hotplate is cut off, the temperature already supplied within the hot side becomes the source of heat which spreads to other parts of the hotplate and the cooling block in their proximity. Therefore, the temperatures of some areas within the cold side rise to some values to about 48°C and become almost constant at that value. Nevertheless, some points which are near the cooling pipes/holes within the cooling block supplied by the cold water from the inlet, have their temperature reduced, because the effect of cooling is stronger than the effect of heating. Similarly, after a short period, their temperature also attains almost constant values equivalent to the inlet temperature of about 5°C. When the chiller is finally switched off, the higher cold side temperatures reduce quickly to reach almost constant values which are slightly higher than the room temperature. Likewise, the lower cold side temperatures, the inlet and the hot side temperature also rises faster and stabilises at about the room temperature value. The corresponding output voltages of the TEGs are shown in Figure 8.23. The output voltages decline steadily when the hotplate is switched off and reduces to lower values where they become almost constant. When the chiller is turned off, the voltages gradually reduces to zero values. With this voltage profile, the analysis of the TEG performance is somehow simplified and in practice, the connected load can easily be compensated by the power conditioning system, in case some of the heat supply points are cut off due to some abnormalities in the system.

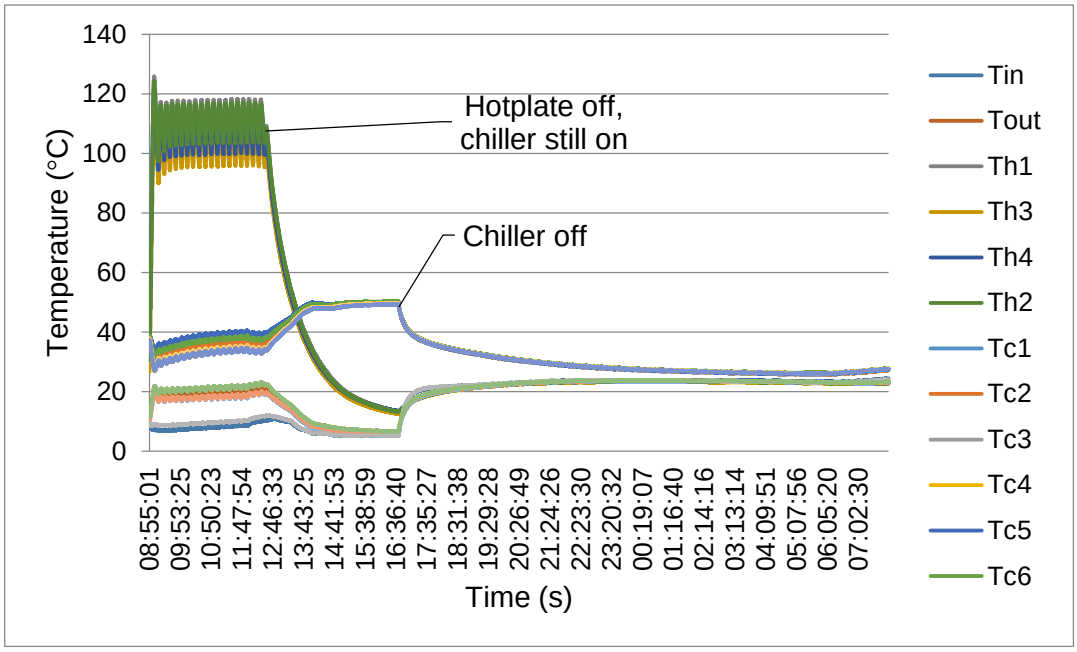


Figure 8.22. Temperature readings of the thermocouples, when the hotplate and the chiller are switched off at different times

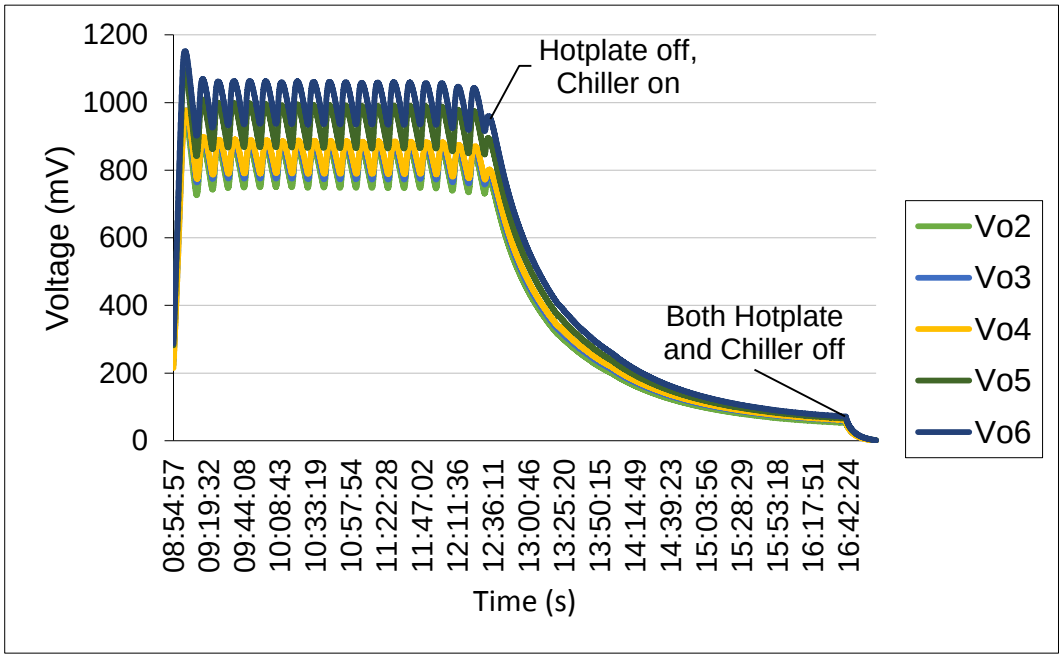


Figure 8.23. OCVs when hotplate is off while the chiller is left on until 16:59:21

8.5.2.2. Effect of the ambient temperature

To assess the effect of the ambient on the experiment, the rig is operated overnight until about 10am of the following day as indicated in Figure 8.24. It is clearly seen that since the time the hotplate is switched off, the temperatures of some cooling side thermocouples are reducing whereas the other cooling side plus all the hot side thermocouple temperatures rise steadily until they are about to meet the declining temperatures. From roughly 1:17pm to 5:43pm, all the temperatures are declining at a very slow pace. However, from that time, all the thermocouple temperatures start rising steadily until the experiment is turned off. This is due to the fact that during day time in summer on 25 May, the weather is hot as compared to the rig which is being cooled by the chiller at 3°C when the hotplate is off at night. Therefore, the ambient temperature is found to influence the rise of the experimental temperature to that level. Hence, it is concluded that the effect of the ambient slightly affects the output of the TEG as demonstrated by the output voltages of the TEGs in Figure 8.25.

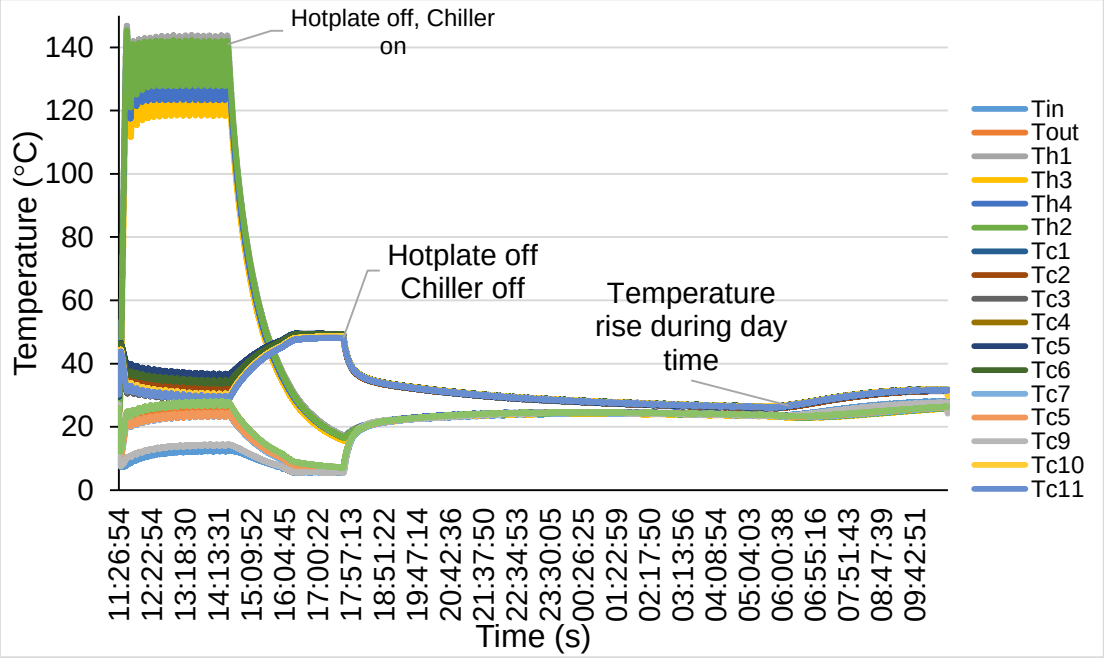


Figure 8.24. Effect of ambient temperature on thermocouple readings

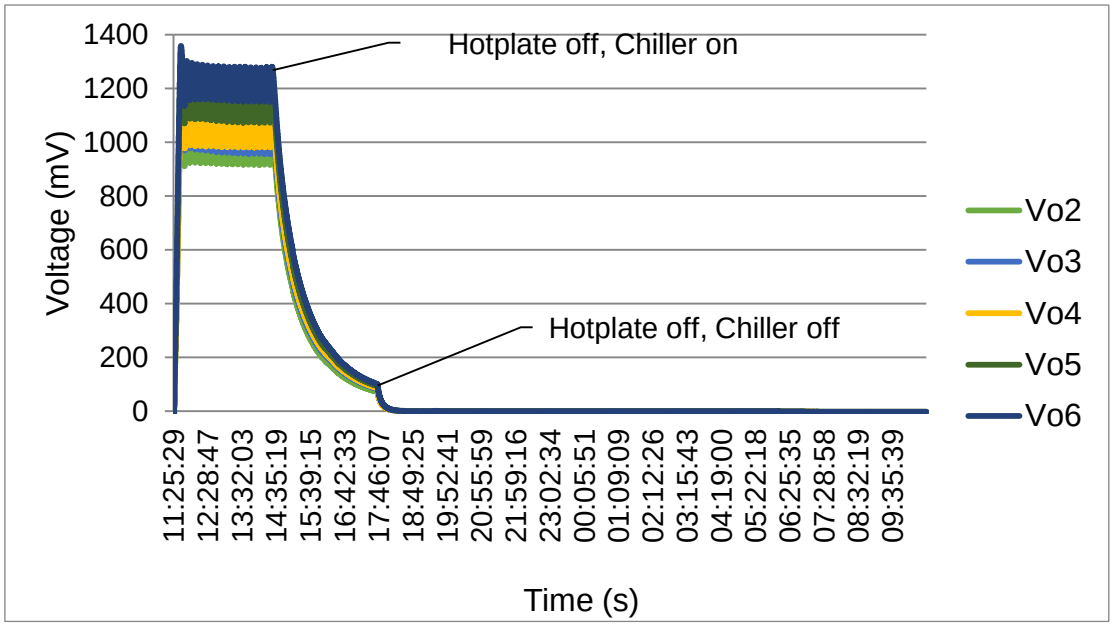


Figure 8.25. The OCVs for TEGs with the effect of external temperature

8.5.3. TEG and the converter output

In this experimet, only voltages and currents are analysed for the reasons which will be discussed later in the follwong sections. The OCVs of the six TEGs are displayed in Figure 8.26. As observed, the TEG output voltage follows a similar trend to that of the corresponding temperature, with the effect of the PID controller still observed when the hotplate is operating whereas the temperature steadily declines when the hotplate is off and the chiller is left on. Likewise, it is observed that the regions of the hotplate which have high temperatures, also produce higher output voltages from the TEGs, confirming the principle of the seebeck effect.

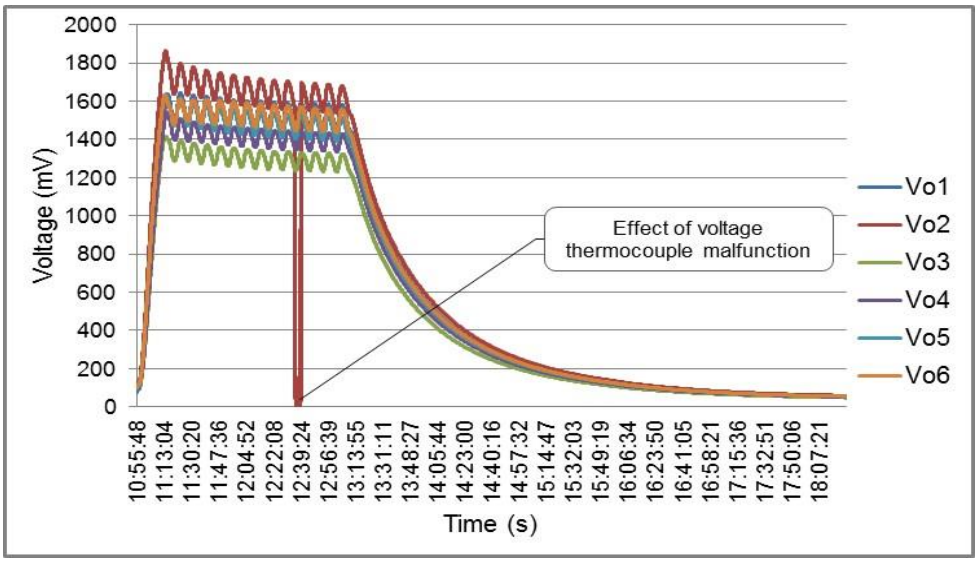


Figure 8.26. The OCVs for TEGs with the effect of thermocouple malfunctioning

Back to the purpose of the experiment, the purpose of the dc-dc converter is to stablise the output voltages from the TEGs to make them appropriately steady for proper operation of the load. Therefore, Figure 8.27 shows the output of the two boost converters alongside the OCVs from the other TEGs which are not connected with the converters. As seen, the input voltages of the boost converetrs 1 and 2 which are almost sinusoidal, are stablised with the converter ouputs Vout_boost_conv1 and Vout_conv2 with almost constant converter output voltages achieved. Moreover, at the time when the hotplate is switched off, the output from the TEG immediatelly starts declining, nevertheless the output voltages of the converters remain steady for some time before they commence to reduce steadily. This is necessary for the proposed DCA since at a time when a certain temperature region declines, it is easier to switch that converter to the reserved TEGs to continue appropriately supplying the load connected to it. In additon, the effect of mannual switch over of the TEGs in serries is illustated where it is obseved that the voltages almost double from 1500mV to about 3000mV after the combination of simimlar TEG output

voltages (V_{o4} +V_{o5}). However, as described ealrlier, an automatic miniature switch controlled by a microprocessor controlled relay is necessary to switch over the TEG outputs in addition to setting the correct voltage level for the given/required load because mannual switch over takes longer time of about more that 10 seconds, which could affect the real time operation of the load.

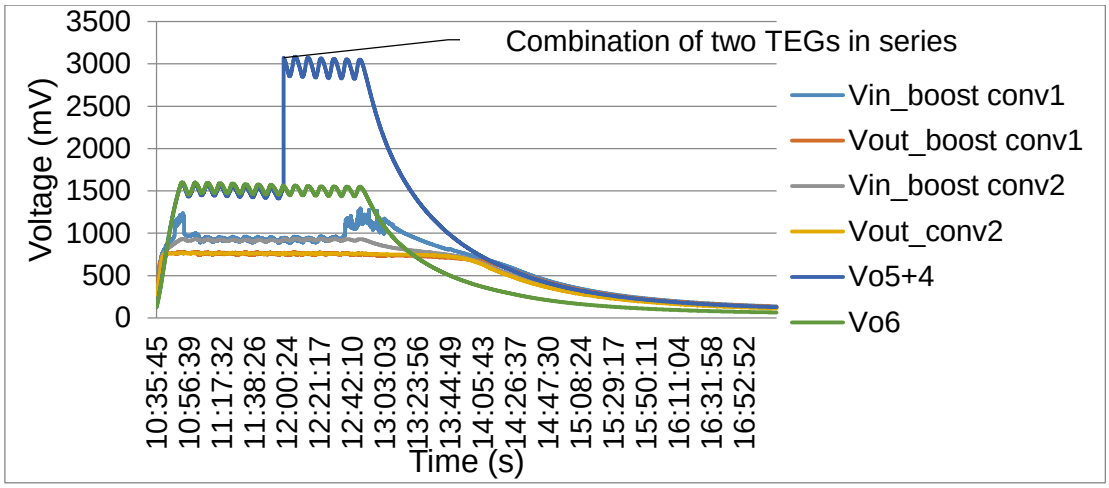


Figure 8.27. Illustration of the relationship between the OCVs and terminal voltages of TEGs and the effect of manual combination of TEGs in series

Figure 8.28 indicates the input and open circuit output voltages of the boost and buck-boost converters when the hotplate temperature is increased to 185°C. It is observed that the output voltages of both converter topologies is amost constant although the input is unstable. However, the output of the buck-boost converter is lower compared to the boost converter, notwithstanding its input voltage being the highest of all. This is because the buck-boost converter is operating in the step-down or buck mode. Normally, the output of the boost converter is expected to be higher than the input, however, as observed, the input voltage is higher than the output. This implies that the boosting has not taken place because of the non-linear nature of the input voltage and spiking current which are detected by the converter as an overload and therefore, the overload protection function is turned on which prevents the converter to

operate as expected. This is done at the expense of gauranteeing the safety of the converter. Another reason for the low output voltage values of the boost converter is because there is a high voltage drop caused by the overall impedance of the boost converter being much higher than the connected load, so that much of the input voltage is lost within the converter. This could be solved by connecting higher loads like in the case of the first experimental test performed with laboratory power supply in section 8.4.2. However, this is not done as it is out of study scope since the main aim is to demonstrate the difference in performance between the boost and buck-boost topologies, which fourtunately is already achieved.

The highly changing voltage Vin_boost conv1 is caused by the effect of thermocouple malfunctiong. Some thermocouples were not functioning properly, leading to false readings. However, the problem was solved by replacing them and finally clear results were obtained.

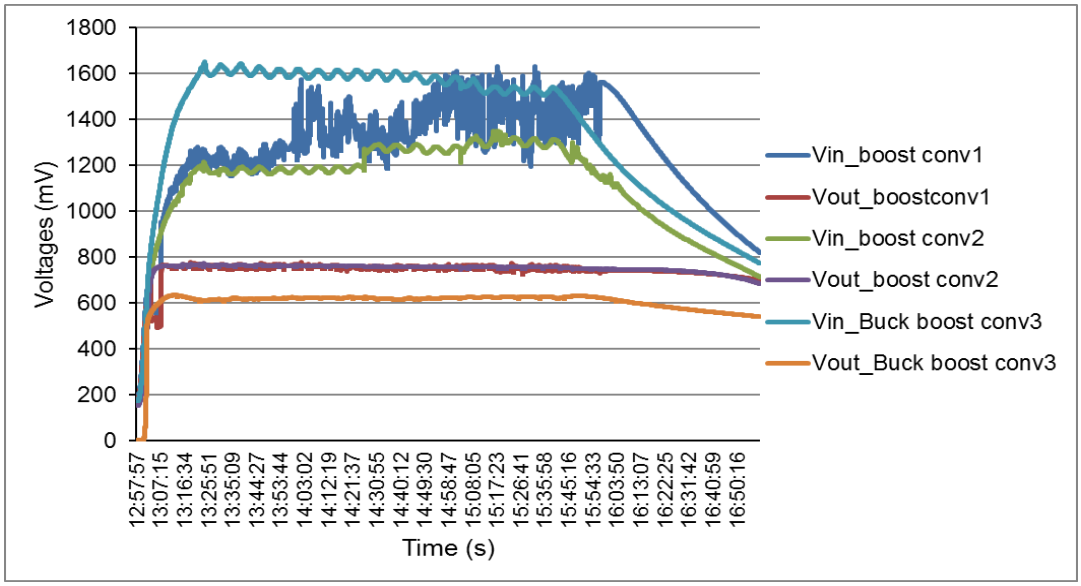
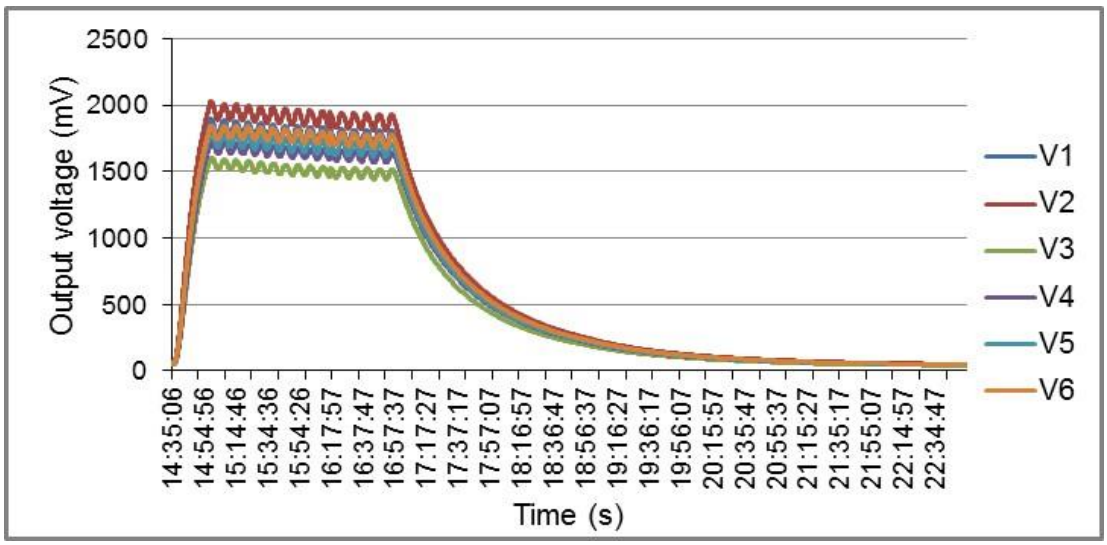


Figure 8.28. Input volatges and output OCVs of the boost and buck-boost converters when the hotplate temperature is increased to 185°C

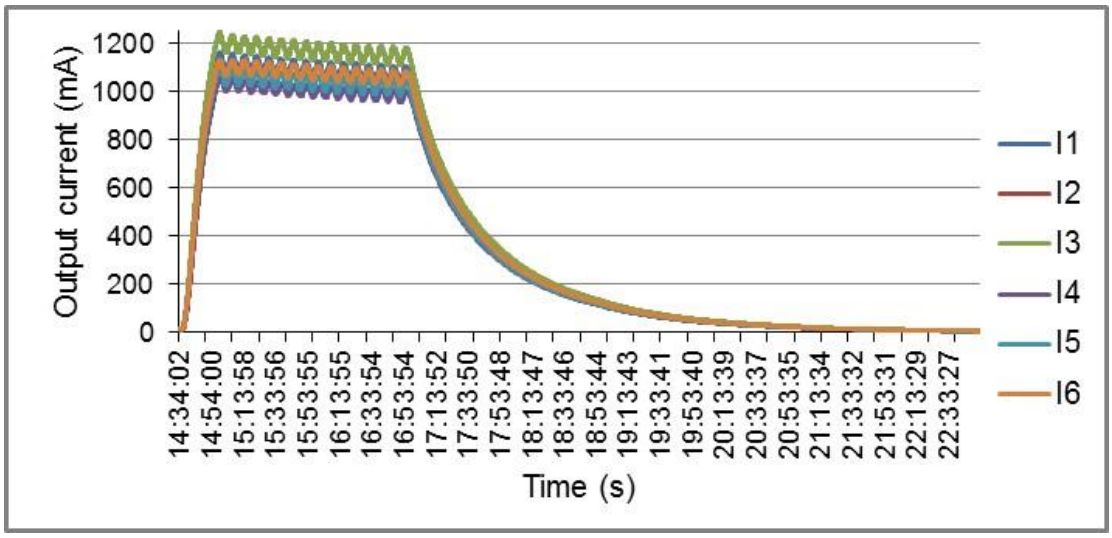
8.5.4. Output voltages and currents under loading conditions

8.5.4.1. Output with resistors connected to TEGs

In this case, the load resistance is connected to the TEGs to monitor the output voltages and currrents. Figure 8.29 (a) depicts the output voltages of the TEGs when 10Ω loads are connected on each TEG. It is demonstrated that when both the hotplate and the chiller are still operating, the output voltage gradually reduces. This is the same trend for the output current as indicated in Figure 8.29 (b). This is due to the effect of the ambient temperature because the experiment is operated during day time between about 2:00pm and 5:00pm when the ambient temperature is declining. The highest output voltage V_2 is obtained from TEG2, with a maximum of about 2.02V which is recorded from the hotplate location with the highest temperature. Although the lowest output voltage V_3 is obtained from TEG3, the highest current is recorded from the same TEG. This is true as demonstrated by the I-V curves for TEG, because ordinarily as the voltages increase, the current reduces.



(a)

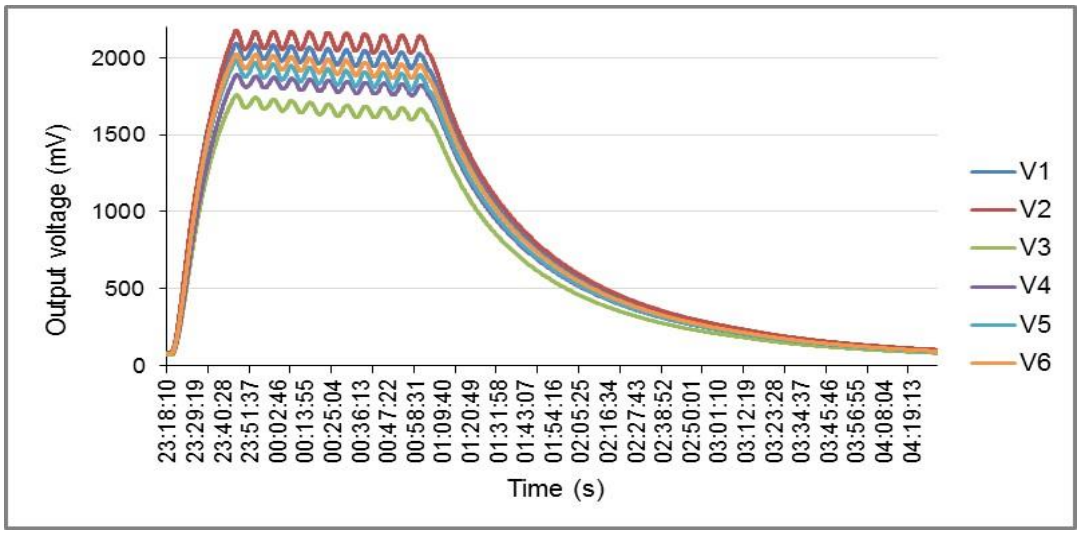


(b)

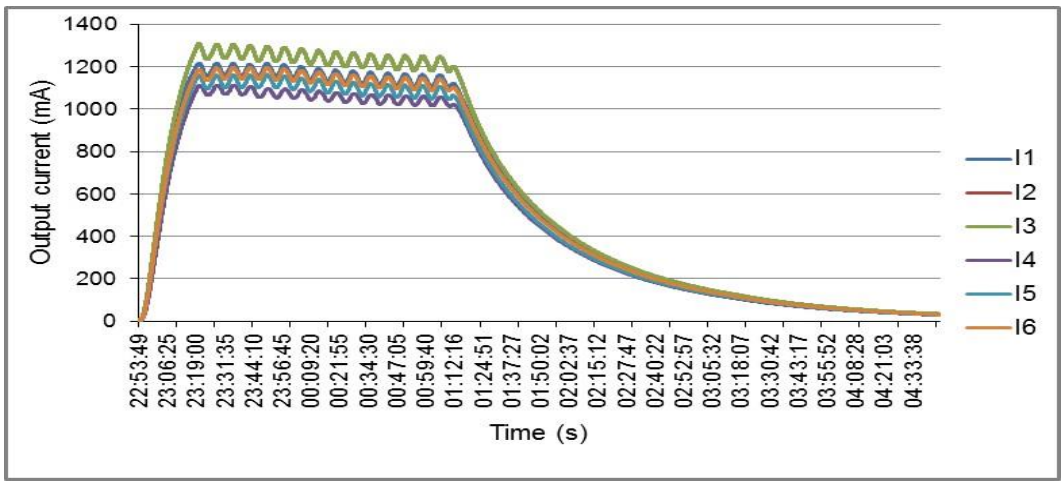
Figure 8.29. Output parameters of the TEGs for a 10Ω load connected on each TEG after the hotplate temperature is increased to 170°C: (a) Output voltage (b) Output current urrent

The output voltages of the TEGs when a 10Ω resistor is connected on each TEG, are indicated in Figure 8.30 (a). For this scenario, the hotplate

temperature is increased from 170°C (Figure 8.29) to 185°C. It is clear that when the temperature is increased, the maximum output voltage of V_2 increases from 2.02V (in Figure 8.29) to about 2.21V, confirming that the increase in hot side temperature while maintaining the cold side temperature constant results into the increase in temperature difference which subsquently increases the TEG output voltage. In this case, the experiment is conducted during night time when the ambient temperatures are alsmost constant, therefore there was no external interference from the ambient. Accordingly, it is noticed that the sinusoidal-like output voltages when both the hotplate and the chiller are operating, especially V_2 are almost steady without declining like in the previous case when the experiment was conducted during day time. However, the output current still declines at slightly lower rate as shown in Figure 8.30 (b), most probably due to other reasons.



(a)

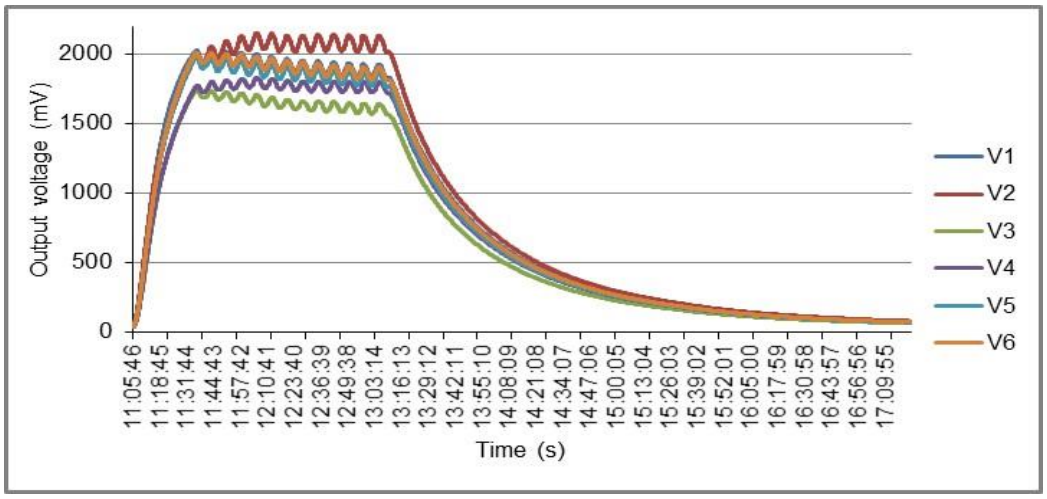


(b)

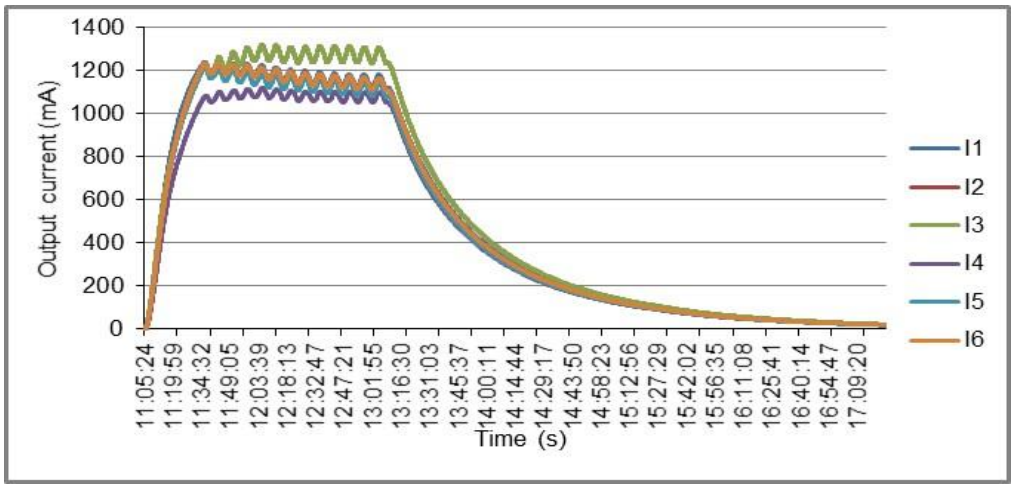
Figure 8.30. Output parameters of the TEGs for a 10Ω load connected on each TEG when the hotplate temperature is increased to 185°C: (a) Output voltage (b) Output current urrent

The load is increased from 10Ω to 15Ω to observe the impact of the load increase on the output voltages and currents. Figure 8.31 (a) shows the output voltages of the TEGs when the 15Ω loads are connected on each TEG for the

hotplate temperature of 185°C. The maximum output volatge of V_2 increases to 2.18V for the 15Ω load from 2.02V noted for the 10Ω resitance. On the other hand, the maximum current I_3 of TEG3 increases from 1.3A for 10Ω load to about 1.32A for the 15 Ω as shown in Figure 8.31 (b).



(a)



(b)

Figure 8.31. The output parameters of the TEGs for a 15Ω load connected on each TEG when the hotplate temperature is increased to 185°C: (a) Output voltage (b) Output current urrent

8.5.4.2. Output with resistors connected through dc-dc converters

The same resistors of 10Ω and 15Ω, in this case are connected to the TEGs through the converters. Figure 8.32 illustrates the output voltages with a 15Ω load connected to each of the six TEGs at 185°C hotplate temperature. The output voltages of the buck-boost converters are observed to be higher than those of the boost converters, yet in Figure 8.28 the boost converters have higher OCVs than the buck-boost at the same temperature as already observed above.

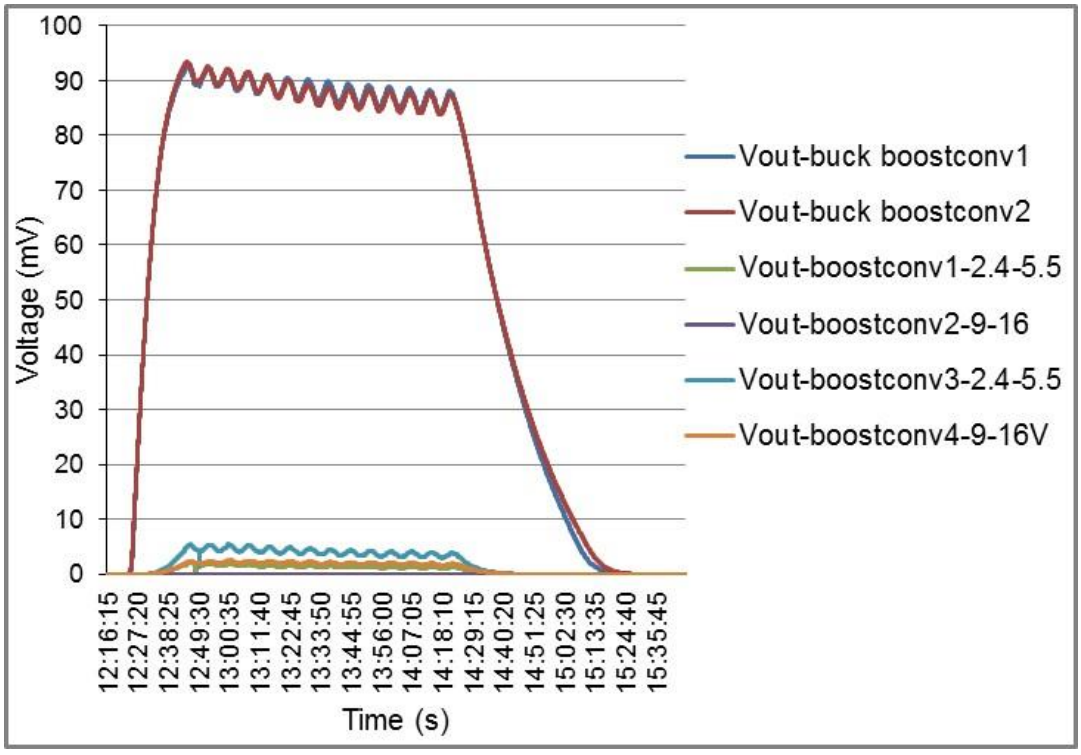


Figure 8.32. Voltages with a 15Ω load connected to each of the six TEG devices through a dc-dc converter at 185°C hotplate temperature

It is therefore proved that these two converter topologies have different responses, especially during loading condtions, confirming that the proposed DCA can be applied when different loads are to be served by the TEG system

to improve the power quality and the performance of the overall TEG system especialy in low carbon vehicles where heat recovery takes place.

8.5.5. Challenges and limitations of the experiment

There are some challenges and limitations faced during the expeimental perod.

- The thermocouples used to measure the hot side temperature could not be placed directly on the hot side of the TEGs because the hotplate used had no holes beneath it through which the thermocouples could be inserted directly on the hot side surface of the TEGs. This definitely affected the accuracy of the hot side temperature readings.
- All the presented results from TEG experiment were recorded for the water flow rate of 2.8 ltrs/min. This is because when the pump was turned on to pump the heated water back to the chiller, although the flow rate increased to 4.2 ltr/min, the cooling block was being drained or left with a small volume of water which could not be sufficient for cooling. This is because there was a mismatch in the water flow rate between the water supply and drain from the cooling block. The flow rate at the chiller side had no means of adjustment so that the respective rates of water supply and drain to and from the cooling block could be balanced.

8.6. Summary

In this chapter, a new design of the distributed converter architecture (DCA) has been presented. The background and design options of the DCA have been clearly elaborated. The DCA design involves using several enabling components such as different converter topologies, sensors, relays, microprocessors etc. A robust computer algorithm is also indispensable if the idea of voltage compensation to the loads with the reserve TEGs, through the source-converter (S-C) exchanger is to be successful. Due to numerous parts comprising the proposed design, it has not been possible to fully prove how the

dsign operates. However, simulations and experimatal studies have been carried out to atleast demonstrate and prove the necessity of the DCA concept for application on TEG systems. As well, during the experiment, some of the factors that affect the performance of TEG systems are correspondingly analysed. It has been revealed that the times of switching off of the chiller and the hotplate affect both the temperature and voltage profiles of the TEG system. If the chiller is turned of at the same time with the hotplate, the resulting TEG output voltage declines at high rate, making it unsuitable for voltage compesation application. However, if the chiller is switched off later than the hotplate, an improved voltage profile is achieved. With this improved voltage profile, the analysis of the TEG performance is somehow simplified and in practice, the connected load can easily be compensated by the power conditioning system, in case some of the heat supply points are cut off due to some abnormalities in the system. It has also been confirmed that some thermocouples are not functioning properly, leading to false readings from the experiment. Moreover, it has been established that the the ambient temperature slightly affects the output of the TEG.

Chapter 9. Conclusion and future work

In this chapter, conclusions and the future research work are deliberated..

9.1. Conclusion

In recent years, the efficiency of thermoelectric devices has been improved greatly due to thermoelectric material and device geometrical improvements. However, the efficiency of TEG is still low. Therefore, more research is necessary to test the performance of dc-dc converters with the available MPPT techniques on TEG system, especially those which are already tested on PV systems. Hence, this research has analysed the performance of dc-dc converters with or without MPPT in conditioning the power generated from TEG. Consequently, the following case studies have been carried out.

The initial study has analysed the performance of a TEG/dc-dc boost converter system. The simplified model has been used as the basis of TEG design. Results indicate that the converter is able to stabilise and boost the voltage and higher efficiencies are achieved at different hot side temperatures.

The next study has proposed the use of MPPT algorithm to harvest maximum power from TEG system. Hence, the analysis of the performance of the TEG/dc-dc converter system with MPPT enabled by Incremental conductance (IC) method has been performed. The results indicate that the IC based MPPT approach is able to track the maximum power point with relatively lower efficiencies than the P&O based MPPT method. The matching efficiencies for the 200°C – 300°C temperature range is 99.92 – 99.95% and 99.46- 99.97% for P&O and IC methods respectively. However, IC based method has higher values of voltage gain and converter efficiency than the P&O based MPPT method. Although the use of direct PWM signal to control the converter switching provides different voltage levels to the load at different duty cycles, the advantage of using MPPT outweighs its applicability to the TEG system

because the MPPT automatically extracts the maximum power without the need to manualy adjust the duty cycle, in addition to the fast response to temperature changes. Therefore, the dc – dc converters are able to improve the steady state performance of the TEG system as well as extacting maximum power with IC based MPPT, hence improving the overall performance of the TEG system.

Another study has analysed the parameters for the performance of TEG/dc-dc converter system in different modes with a variable load. The TEG system is subjected to different hot side temperatures, including increasing step, increasing random and constant cold side temperature profiles. Results indicate that a dc-dc converter with MPPT based model is able to extract maximum power from TEG better than the direct PWM based model. From the study, it has been established that proper selection of converter components such as capacitors, switching frequency etc, is necessary to avoid converter losses as well as noise interferences on the load connected to TEG-dc-dc converter system. This is very improtant to address the power quality issues in the TEg system.

Furthermore, another study has compared the performance of extremum seeking control (ESC) with P&O and IC MPPT algorithms applied to TEG system. The simplified TEG model has been validated with the results from multiphysics (COMSOL) modelling software. To assess the effect of temperature dependency of TEG parameters, two TEG materials have been chosen; Bi_2Te_3 material with temperature dependent Seebeck effect (S), electrical conductivity (σ) and thermal conductivity (k), and lead telluride (PbTe) with non-temperature dependent S, σ and k. Results indicate that ESC MPPT method extracts more power than P&O technique, where the output power of ESC MPPT is higher than that of P&O by 0.47 W, which is 6.1% higher at a temperature of 200°C. It is also noted that the ESC MPPT based model is

almost fourfold faster than the P&O method. Hence, ESC MPPT method outperforms the P&O technique. The comparison of the magnitudes of output power curves at different temperatures indicates that the combined effect of the variation of S, σ and k results in the increase in the value of the output power of the Bi_2Te_3 TEG especially at a high temperature of 400°C. The ESC algorithm has also been observed to outperform the IC technique in terms of extracting maximum power and the speed of computation. ESC method is faster than the IC method with simulation time of 152.1s and 781.8s respectively. Moreover, ESC is less complex in terms of model implementation since it is made up of few circuit components than the IC method.

In the final study, the application of the concept and the design of a distributed dc-dc converter architecture (DCA) on TEG system has been accomplished. The distributed converter architecture involves the use of isolated or non-isolated per-TEG dc-dc converter connected to the load. The DCA design involves using several enabling components such as different converter topologies, sensors, relays, microprocessors etc. A robust computer algorithm is also indispensable if the idea of voltage compensation to the loads with the reserve TEGs, through the source-converter (S-C) exchanger, is to be successful. Because DCA design is composed of various parts, it has not been possible to fully prove how the design operates due to time and resource constraints. However, the simulations and experimental studies have been carried out to at least demonstrate and prove the necessity of the DCA concept application on TEG systems. Besides, during the experiment, some of the factors that affect the performance of TEG systems are correspondingly analysed including the effect of the time of switching on/off of different components, the effect of thermocouple mulfunctioning as well as the impact of variation of the hot temperature. It has been revealed that the times of switching off of the chiller and the hotplate affect both the temperature and voltage profiles of the TEG system. If the chiller is turned of at the same time

with the hotplate, the resulting TEG output voltage declines at high rate, making it unsuitable for voltage compesation application. However, if the chiller is switched off later than the hotplate, an improved voltage profile is achieved. With this improved voltage profile, the analysis of the TEG performance is somehow simplified and in practice, the connected load can easily be compensated by the power conditioning system, in case some of the heat supply points are cut off due to some abnormalities in the system. It has also been confirmed that some thermocouples are not functioning properly, leading to false readings from the experiment. Moreover, it has been established that the the ambient temperature slightly affects the output of the TEG. Consequently, appropriate tuning of the TEG system parameters is necessary to improve the performance of the TEG system.

9.2. Future work

First of all, the future research will concentrate on improving the utilized TEG model to accommodate the other thermoelectric effects as per the recommendations of the TEG model verification carried out in Chapter 7. Moreover, a lot of work has to be done to streamline the designed DCA concept presented in chapter 8, by concenrtrating on the other design components which have not been tackled in this study such as the S-C exchanger, dsign of the individual dc-dc converters that make up the whole architecture and identification of the specific loads based on specific application (for example in passenger car) that have to be connected on these converters as well as specifying the practical working paramaters such as the rated voltages, currents, powers etc. based on the international standards.

References

Abb, 2015. *Technical catalog: Current sensors - Voltage sensors*,

Abusorrah, A. et al., 2013. Stability of a boost converter fed from photovoltaic source. *Solar Energy*, 98(PC), pp.458–471. Available at: http://dx.doi.org/10.1016/j.solener.2013.09.001.

Admasu, B.T., Luo, X. & Yao, J., 2013. Effects of temperature non-uniformity over the heat spreader on the outputs of thermoelectric power generation system. *Energy Conversion and Management*, 76(0), pp.533–540. Available at: http://www.sciencedirect.com/science/article/pii/S0196890413004573.

Ahmed, J. & Salam, Z., 2015. An improved perturb and observe (P&O) maximum power point tracking (MPPT) algorithm for higher efficiency. *Applied Energy*, 150, pp.97–108. Available at: http://dx.doi.org/10.1016/j.apenergy.2015.04.006.

Akhtar, F. & Husain, M., 2015. Energy replenishment using renewable and traditional energy resources for sustainable wireless sensor networks : A review. *Renewable and Sustainable Energy Reviews*, 45, pp.769–784. Available at: http://dx.doi.org/10.1016/j.rser.2015.02.021.

Al-Merbati, a. S., Yilbas, B.S. & Sahin, a. Z., 2013. Thermodynamics and thermal stress analysis of thermoelectric power generator: Influence of pin geometry on device performance. *Applied Thermal Engineering*, 50(1), pp.683–692. Available at: http://dx.doi.org/10.1016/j.applthermaleng.2012.07.021.

Alvarez-Quintana, J., 2015. Impact of the Substrate on the Efficiency of Thin Film Thermoelectric Technology. *Applied Thermal Engineering*, 84, pp.206–210. Available at: http://linkinghub.elsevier.com/retrieve/pii/S1359431115002860.

Amaral, C. et al., 2014a. Net thermoelectric generator power output using inner channel geometries with alternating flow impeding panels. *Applied Thermal Engineering*, 65(1–2), pp.91–101. Available at: http://dx.doi.org/10.1016/j.applthermaleng.2013.12.044.

Amaral, C. et al., 2014b. Thermoelectric power enhancement by way of flow impedance for fixed thermal input conditions. *Journal of Power Sources*, 272, pp.672–680. Available at: http://linkinghub.elsevier.com/retrieve/pii/S0378775314014098.

American Elements, Bismuth Antimonide (BiSb). Available at: http://www.americanelements.com/bisb.html [Accessed June 19, 2015].

Baranwal, M., Salapaka, S.M. & Salapaka, M. V, 2016. Robust Decentralized Voltage Control of DC-DC Converters with Applications to Power Sharing and Ripple Sharing. , (3), pp.7444–7449.

Barma, M.C. et al., 2015. Estimation of thermoelectric power generation by recovering waste heat from Biomass fired thermal oil heater. *Energy Conversion and Management*, 98, pp.303–313. Available at:

http://linkinghub.elsevier.com/retrieve/pii/S0196890415003295.
Barry, M.M., Agbim, K.A. & Chyu, M.K., 2015. Performance of a Thermoelectric Device with Integrated Heat Exchangers. *Journal of Electronic Materials*, 44(6), pp.1394–1401.
Bazmi, A.A. & Zahedi, G., 2011. Sustainable energy systems: Role of optimization modeling techniques in power generation and supply - A review. *Renewable and Sustainable Energy Reviews*, 15(8), pp.3480–3500. Available at: http://dx.doi.org/10.1016/j.rser.2011.05.003.
Bell, L.E., 2008. Cooling, heating, generating power, and recovering waste heat with thermoelectric systems. *Science (New York, N.Y.)*, 321(5895), pp.1457–1461.
Bennett, N.S. et al., 2015. Efficient thermoelectric performance in silicon nano-films by vacancy-engineering. *Nano Energy*, pp.350–356. Available at: http://linkinghub.elsevier.com/retrieve/pii/S2211285515003006.
Bensaid, S. et al., 2012. High efficiency Thermo-Electric power generator. *International Journal of Hydrogen Energy*, 37(2), pp.1385–1398. Available at: http://dx.doi.org/10.1016/j.ijhydene.2011.09.125.
Biagi, E. et al., 2012. A High Voltage High Power high frequency Boost/Flyback DC-DC converter for automotive applications. *International Symposium on Power Electronics Power Electronics, Electrical Drives, Automation and Motion*, pp.1166–1171. Available at: http://ieeexplore.ieee.org/lpdocs/epic03/wrapper.htm?arnumber=6264567.
Bianchini, A., Pellegrini, M. & Saccani, C., 2014. Thermoelectric cells cogeneration from biomass power plant. *Energy Procedia*, 45, pp.268–277. Available at: http://dx.doi.org/10.1016/j.egypro.2014.01.029.
Bitschi, A., 2009. Modelling of Thermoelectric Devices for Electric Power Generation. , (18441). Available at: http://e-collection.library.ethz.ch/view/eth:470.
Bollen, M.H.J., 2003. What is power quality? *Electric Power Systems Research*, 66(1), pp.5–14. Available at: http://linkinghub.elsevier.com/retrieve/pii/S0378779603000671.
Boukettaya, G. & Krichen, L., 2014. A dynamic power management strategy of a grid connected hybrid generation system using wind, photovoltaic and Flywheel Energy Storage System in residential applications. *Energy*, 71, pp.148–159.
Büyük, M. et al., 2016. Topologies, generalized designs, passive and active damping methods of switching ripple filters for voltage source inverter: A comprehensive review. *Renewable and Sustainable Energy Reviews*, 62, pp.46–69.
Carstens, J.H. & Gühmann, C., 2015. Maximum Power Point Controller for Thermoelectric Generators to Support a Vehicle Power Supply. *Materials Today: Proceedings*, 2(2), pp.790–803. Available at: http://linkinghub.elsevier.com/retrieve/pii/S2214785315001704.

Casano, G. & Piva, S., 2011. Experimental investigation of the performance of a thermoelectric generator based on Peltier cells. *Experimental Thermal and Fluid Science*, 35(4), pp.660–669. Available at: http://dx.doi.org/10.1016/j.expthermflusci.2010.12.016.

Chakraborty, a. et al., 2006. Thermodynamic modelling of a solid state thermoelectric cooling device: Temperature-entropy analysis. *International Journal of Heat and Mass Transfer*, 49(19–20), pp.3547–3554.

Chein, R. & Huang, G., 2004. Thermoelectric cooler application in electronic cooling. *Applied Thermal Engineering*, 24(14–15), pp.2207–2217.

Chen, J. & Wu, C., 2000. Analysis on the Performance of a Thermoelectric Generator. *Journal of Energy Resources Technology*, 122(2), p.61. Available at: http://dx.doi.org/10.1115/1.483163.

Chen, W.-H. et al., 2015. Evaluation of power generation from thermoelectric cooler at normal and low-temperature cooling conditions. *Energy for Sustainable Development*, 25, pp.8–16. Available at: http://linkinghub.elsevier.com/retrieve/pii/S0973082614001215.

Chen, W.-H., Wang, C.-C. & Hung, C.-I., 2014. Geometric effect on cooling power and performance of an integrated thermoelectric generation-cooling system. *Energy Conversion and Management*, 87, pp.566–575. Available at: http://linkinghub.elsevier.com/retrieve/pii/S0196890414006852.

Chen, W.H. et al., 2012. Experimental study on thermoelectric modules for power generation at various operating conditions. *Energy*, 45(1), pp.874–881. Available at: http://dx.doi.org/10.1016/j.energy.2012.06.076.

Crane, D.T. & Bell, L.E., 2006. Progress towards maximizing the performance of a thermoelectric power generator. *Proceedings of the International Conference on Thermoelectrics, ICT,*, pp.11–16.

Crane, D.T. & Jackson, G.S., 2004. Optimization of cross flow heat exchangers for thermoelectric waste heat recovery. *Energy Conversion and Management*, 45(9–10), pp.1565–1582.

Dai, D., Zhou, Y. & Liu, J., 2011. Liquid metal based thermoelectric generation system for waste heat recovery. *Renewable Energy*, 36(12), pp.3530–3536. Available at: http://dx.doi.org/10.1016/j.renene.2011.06.012.

Dhople, S. V. et al., 2009. Reliability assessment of fault-tolerant dc-dc converters for photovoltaic applications. *2009 IEEE Energy Conversion Congress and Exposition, ECCE 2009*, pp.2271–2276.

Eakburanawat, J. & Boonyaroonate, I., 2006. Development of a thermoelectric battery-charger with microcontroller-based maximum power point tracking technique. *Applied Energy*, 83(7), pp.687–704.

Ebrahimi, K., Jones, G.F. & Fleischer, A.S., 2014. A review of data center cooling technology, operating conditions and the corresponding low-grade waste heat recovery opportunities. *Renewable and Sustainable Energy Reviews*, 31, pp.622–638. Available at: http://dx.doi.org/10.1016/j.rser.2013.12.007.

Electropaedia, Battery and Energy Technologies. Available at:

http://www.mpoweruk.com/thermoelectricity.htm [Accessed March 13, 2017].
Erturun, U., Erermis, K. & Mossi, K., 2014. Effect of various leg geometries on thermo-mechanical and power generation performance of thermoelectric devices. *Applied Thermal Engineering*, 73(1), pp.126–139. Available at: http://linkinghub.elsevier.com/retrieve/pii/S1359431114005894.
Fairbanks, J., 2008. Thermoelectric applications in vehicles status 2008. *US Department of Energy*. Available at: http://ect2008.icmpe.cnrs.fr/Contributions/0-PL-00-Fairbanks.pdf.
Fateh, H. et al., 2014. High fidelity finite difference model for exploring multi-parameter thermoelectric generator design space. *Applied Energy*, 129, pp.373–383. Available at: http://dx.doi.org/10.1016/j.apenergy.2014.04.088.
Fraisse, G. et al., 2013. Comparison of different modeling approaches for thermoelectric elements. *Energy Conversion and Management*, 65, pp.351–356. Available at: http://dx.doi.org/10.1016/j.enconman.2012.08.022.
Fraisse, G. et al., 2002. Development of a simplified and accurate building model based on electrical analogy. *Energy and Buildings*, 34(10), pp.1017–1031.
Fraisse, G. et al., 2010. Study of a thermoelement's behaviour through a modelling based on electrical analogy. *International Journal of Heat and Mass Transfer*, 53(17–18), pp.3503–3512. Available at: http://dx.doi.org/10.1016/j.ijheatmasstransfer.2010.04.011.
Gao, J. et al., 2015. Assessing the accuracy of mathematical models used in thermoelectric simulation: Thermal influence of insulated air zone and radiation heat. *Applied Thermal Engineering*, 82, pp.162–169.
Ge, Z., Jin, L. & Yang, C., 2015. Microfluidic concentration of sample solutes using Joule heating effects under a combined AC and DC electric field. *International Journal of Heat and Mass Transfer*, 85, pp.158–165. Available at: http://linkinghub.elsevier.com/retrieve/pii/S0017931015000617.
Goldstein, R.J. et al., 2010. Heat transfer - A review of 2005 literature. *International Journal of Heat and Mass Transfer*, 53(21–22), pp.4397–4447. Available at: http://dx.doi.org/10.1016/j.ijheatmasstransfer.2010.05.005.
Gou, X. et al., 2013. A dynamic model for thermoelectric generator applied in waste heat recovery. *Energy*, 52, pp.201–209. Available at: http://dx.doi.org/10.1016/j.energy.2013.01.040.
Gou, X. et al., 2014. A novel thermoelectric generation system with thermal switch. *Applied Energy*. Available at: http://linkinghub.elsevier.com/retrieve/pii/S0306261914012185.
Haddad, C. et al., 2014. Some Efficient Solutions to Recover Low and Medium Waste Heat: Competitiveness of the Thermoacoustic Technology. *Energy*

Procedia, 50, pp.1056–1069. Available at: http://linkinghub.elsevier.com/retrieve/pii/S1876610214008613.

Hamid Elsheikh, M. et al., 2014. A review on thermoelectric renewable energy: Principle parameters that affect their performance. *Renewable and Sustainable Energy Reviews*, 30, pp.337–355. Available at: http://dx.doi.org/10.1016/j.rser.2013.10.027.

Hannan, M. a., Azidin, F. a. & Mohamed, a., 2014. Hybrid electric vehicles and their challenges: A review. *Renewable and Sustainable Energy Reviews*, 29, pp.135–150. Available at: http://dx.doi.org/10.1016/j.rser.2013.08.097.

He, W. et al., 2015. Influence of different cooling methods on thermoelectric performance of an engine exhaust gas waste heat recovery system. *Applied Energy*. Available at: http://linkinghub.elsevier.com/retrieve/pii/S0306261915003207.

Heydari-doostabad, H., Keypour, R. & Reza, M., 2013. A new approach in MPPT for photovoltaic array based on Extremum Seeking Control under uniform and non-uniform irradiances. *Solar Energy*, 94, pp.28–36. Available at: http://dx.doi.org/10.1016/j.solener.2013.04.025.

Huang, J. & Jiang, Z., 2017. Power Quality Assessment of Different Load Categories. *Energy Procedia*, 141, pp.345–351. Available at: http://linkinghub.elsevier.com/retrieve/pii/S1876610217354474.

Huang, W., Koong, C.S. & Liang, G., 2010. Theoretical Study on Thermoelectric Properties of Ge Nanowires Based on Electronic Band Structures. *Semiconductors and Semimetals*, 31(9), pp.1026–1028.

Huang Kuo, Bo Li, Ssennoga Twaha, Y.Y., 2016. Comprehensive Study on Novel Concentric Cylindrical Thermoelectric Power Generation System. *Applied Thermal Engineering*, 117, pp.501–510.

Hunnekens, B.G.B. et al., 2014. A dither-free extremum-seeking control approach using 1st-order least-squares fits for gradient estimation. *Proceedings of the IEEE Conference on Decision and Control*, 2015–Febru(February), pp.2679–2684.

Ibrahim, A. et al., 2014. Multi-objective thermal analysis of a thermoelectric device: Influence of geometric features on device characteristics. *Energy*, 77, pp.305–317. Available at: http://linkinghub.elsevier.com/retrieve/pii/S0360544214009773.

In, B.D. et al., 2015. The study of a thermoelectric generator with various thermal conditions of exhaust gas from a diesel engine. *International Journal of Heat and Mass Transfer*, 86, pp.667–680. Available at: http://linkinghub.elsevier.com/retrieve/pii/S0017931015003105.

Ishaque, K. & Salam, Z., 2013. A review of maximum power point tracking techniques of PV system for uniform insolation and partial shading condition. *Renewable and Sustainable Energy Reviews*, 19, pp.475–488. Available at: http://dx.doi.org/10.1016/j.rser.2012.11.032.

Ishaque, K., Salam, Z. & Lauss, G., 2014a. The performance of perturb and observe and incremental conductance maximum power point tracking

method under dynamic weather conditions. *Applied Energy*, 119, pp.228–236. Available at: http://dx.doi.org/10.1016/j.apenergy.2013.12.054.

Ishaque, K., Salam, Z. & Lauss, G., 2014b. The performance of perturb and observe and incremental conductance maximum power point tracking method under dynamic weather conditions. *Applied Energy*, 119, pp.228–236. Available at: http://dx.doi.org/10.1016/j.apenergy.2013.12.054.

Jang, J.-Y., Tsai, Y.-C. & Wu, C.-W., 2013. A study of 3-D numerical simulation and comparison with experimental results on turbulent flow of venting flue gas using thermoelectric generator modules and plate fin heat sink. *Energy*, 53(0), pp.270–281. Available at: http://www.sciencedirect.com/science/article/pii/S0360544213001862.

Jang, J.Y. & Tsai, Y.C., 2013. Optimization of thermoelectric generator module spacing and spreader thickness used in a waste heat recovery system. *Applied Thermal Engineering*, 51(1–2), pp.677–689. Available at: http://dx.doi.org/10.1016/j.applthermaleng.2012.10.024.

Karri, M. a., Thacher, E.F. & Helenbrook, B.T., 2011. Exhaust energy conversion by thermoelectric generator: Two case studies. *Energy Conversion and Management*, 52(3), pp.1596–1611. Available at: http://dx.doi.org/10.1016/j.enconman.2010.10.013.

Kaushik, S.C. & Manikandan, S., 2015. The influence of Thomson effect in the performance optimization of a two stage thermoelectric cooler. *Cryogenics*, 72, pp.57–64.

Kavitha, K. & Jeyakumar, E., 2012. A Synchronous Cuk Converter Based Photovoltaic Energy System Design and Simulation. *Ijsrp.Org*, 2(10), pp.1–8. Available at: http://www.ijsrp.org/research-paper-1012/ijsrp-p1060.pdf.

Kempf, N. & Zhang, Y., 2016. Design and optimization of automotive thermoelectric generators for maximum fuel efficiency improvement. *Energy Conversion and Management*, 121, pp.224–231. Available at: http://dx.doi.org/10.1016/j.enconman.2016.05.035.

El Khateb, A., Rahim, N. & Selvaraj, J., 2013. Fuzzy logic control approach of a maximum power point employing SEPIC converter for standalone photovoltaic system. *The 3rd International Conference on Sustainable Future for Human Security*, 17(1), pp.529–536. Available at: http://linkinghub.elsevier.com/retrieve/pii/S1878029613000704.

Kiflemariam, R. & Lin, C.-X., 2015. Numerical simulation of integrated liquid cooling and thermoelectric generation for self-cooling of electronic devices. *International Journal of Thermal Sciences*, 94, pp.193–203. Available at: http://linkinghub.elsevier.com/retrieve/pii/S1290072915000708.

Kim, H. & Kim, W., 2015. A way of achieving a low $/W and a decent power output from a thermoelectric device. *Applied Energy*, 139, pp.205–211. Available at: http://linkinghub.elsevier.com/retrieve/pii/S0306261914012021.

Kim, R. et al., 2008. A Seamless Mode Transfer Maximum Power Point Tracking Controller For Thermoelectric Generator Applications. *IEEE Transactions on Power Electronics*, 23(5), pp.2310–2318.

Kinsella, C.E. et al., 2014. Battery charging considerations in small scale electricity generation from a thermoelectric module. *Applied Energy*, 114, pp.80–90. Available at: http://dx.doi.org/10.1016/j.apenergy.2013.09.025.

Kossyvakis, D.N. et al., 2015a. Computational analysis and performance optimization of a solar thermoelectric generator. *Renewable Energy*, 81, pp.150–161. Available at: http://linkinghub.elsevier.com/retrieve/pii/S0960148115002086.

Kossyvakis, D.N. et al., 2015b. Computational and experimental analysis of a commercially available Seebeck module. *Renewable Energy*, 74, pp.1–10. Available at: http://www.sciencedirect.com/science/article/pii/S0960148114004108.

Leblanc, S., 2014. Sustainable Materials and Technologies Thermoelectric generators : Linking material properties and systems engineering for waste heat recovery applications. *Susmat*, 1–2, pp.26–35. Available at: http://dx.doi.org/10.1016/j.susmat.2014.11.002.

Lee, H., 2013. Optimal design of thermoelectric devices with dimensional analysis. *Applied Energy*, 106, pp.79–88. Available at: http://dx.doi.org/10.1016/j.apenergy.2013.01.052.

Lei, P., Li, Y. & Seem, J.E., 2011. Sequential ESC-Based Global MPPT Control for Photovoltaic Array With Variable Shading. *IEEE TRANSACTIONS ON SUSTAINABLE ENERGY*, 2(3), pp.348–358.

Lenk, R., 2005. Practical Selection of Topology. In *Practical Design of Power Supplies*. Wiley-IEEE Press, pp. 17–36. Available at: http://ieeexplore.ieee.org/xpl/articleDetails.jsp?arnumber=5264220.

Lertsatitthanakorn, C., Jamradloedluk, J. & Rungsiyopas, M., 2014. Electricity Generation from a Solar Parabolic Concentrator Coupled to a Thermoelectric Module. *Energy Procedia*, 52, pp.150–158. Available at: http://linkinghub.elsevier.com/retrieve/pii/S1876610214009278.

Lesage, F.J. et al., 2013. Optimal electrical load for peak power of a thermoelectric module with a solar electric application. *Energy Conversion and Management*, 74, pp.51–59.

Li, H., 2009. *Reducing Electromagnetic Interference in DC-DC Converters with Chaos control*. University of Hagen. Available at: http://www.fernuni-hagen.de/IT/EMVdurchChaos/Dissertation_Hong_Li.pdf.

Li, M., 2011. *Thermoelectric-Generator-Based DC-DC Conversion Network for Automotive Applications*. KTH Information and Communication Technology.

Li, M. et al., 2011. Thermoelectric-generator-based DC-DC conversion networks for automotive applications. *Journal of Electronic Materials*, 40(5), pp.1136–1143. Available at: http://dx.doi.org/10.1007/s11664-011-1557-5.

Li, Q. & Wolfs, P., 2008. A review of the single phase photovoltaic module integrated converter topologies with three different DC link configurations. *IEEE Transactions on Power Electronics*, 23(3), pp.1320–1333.

Li, W. et al., 2016. Thermal performance of two heat exchangers for thermoelectric generators. *Case Studies in Thermal Engineering*, 8, pp.164–175.

Liang, G. et al., 2010. Geometry effects on thermoelectric properties of silicon nanowires based on electronic band structures. *Journal of Applied Physics*, 107(1).

Liu, C., Pan, X., et al., 2015. An experimental study of a novel prototype for two-stage thermoelectric generator from vehicle exhaust. *Journal of the Energy Institute*, 86, pp.1–11. Available at: http://linkinghub.elsevier.com/retrieve/pii/S1743967115000069.

Liu, W., Jie, Q., et al., 2015. Current progress and future challenges in thermoelectric power generation: From materials to devices. *Acta Materialia*, 87(155), pp.357–376. Available at: http://linkinghub.elsevier.com/retrieve/pii/S1359645414009689.

Liu, X. et al., 2015. An energy-harvesting system using thermoelectric power generation for automotive application. *International Journal of Electrical Power & Energy Systems*, 67, pp.510–516. Available at: http://linkinghub.elsevier.com/retrieve/pii/S0142061514007728.

Liu, X. et al., 2015. Performance analysis of a waste heat recovery thermoelectric generation system for automotive application. *Energy Conversion and Management*, 90, pp.121–127.

Liu, Y.H. et al., 2016. A novel maximum power point tracker for thermoelectric generation system. *Renewable Energy*, 97, pp.306–318. Available at: http://dx.doi.org/10.1016/j.renene.2016.05.001.

Lu, H. et al., 2013. Experiment on thermal uniformity and pressure drop of exhaust heat exchanger for automotive thermoelectric generator. *Energy*, 54, pp.372–377. Available at: http://dx.doi.org/10.1016/j.energy.2013.02.067.

Lv, S. et al., 2016. Design, fabrication and feasibility analysis of a thermo-electric wearable helmet. *Applied Thermal Engineering*, 109, pp.138–146. Available at: http://dx.doi.org/10.1016/j.applthermaleng.2016.08.057.

Ma, H.-K. et al., 2014. Waste heat recovery using a thermoelectric power generation system in a biomass gasifier. *Applied Thermal Engineering*, pp.1–6. Available at: http://linkinghub.elsevier.com/retrieve/pii/S1359431114008424.

Ma, T. et al., 2015. Simulation of thermoelectric-hydraulic performance of a thermoelectric power generator with longitudinal vortex generators. *Energy*, 84, pp.695–703. Available at: http://linkinghub.elsevier.com/retrieve/pii/S0360544215003278.

Mal, R., Prasad, R. & Vijay, V.K., 2016. Multi-functionality clean biomass cookstove for off-grid areas. *Process Safety and Environmental*

Protection, 104, pp.85–94. Available at: http://dx.doi.org/10.1016/j.psep.2016.08.003.

Malek, H., 2016. Extremum Seeking Control (ESC) for Maximum Power Point Tracking (MPPT) of Photo-Voltaic system. Available at: https://uk.mathworks.com/matlabcentral/fileexchange/56545-extremum-seeking-control--esc--for-maximum-power-point-tracking--mppt--of-photo-voltaic-system [Accessed January 22, 2017].

Malek, H., Dadras, S. & Chen, Y., 2016. Performance analysis of fractional order extremum seeking control. *ISA Transactions*, 63(3), pp.281–287. Available at: http://linkinghub.elsevier.com/retrieve/pii/S0019057816300234.

Manikandan, S. & Kaushik, S.C., 2015. Thermodynamic studies and maximum power point tracking in thermoelectric generator-thermoelectric cooler combined system. *Cryogenics*, 67, pp.52–62. Available at: http://dx.doi.org/10.1016/j.cryogenics.2015.01.008.

Martínez, a., Astrain, D. & Rodríguez, a., 2011. Experimental and analytical study on thermoelectric self cooling of devices. *Energy*, 36(8), pp.5250–5260. Available at: http://dx.doi.org/10.1016/j.energy.2011.06.029.

Massaguer, E. et al., 2014. Development and validation of a new TRNSYS type for the simulation of thermoelectric generators. *Applied Energy*, 134, pp.65–74. Available at: http://www.sciencedirect.com/science/article/pii/S0306261914008137.

Massaguer, E. et al., 2015. Modeling analysis of longitudinal thermoelectric energy harvester in low temperature waste heat recovery applications. *Applied Energy*, 140, pp.184–195. Available at: http://linkinghub.elsevier.com/retrieve/pii/S0306261914012549.

Meng, F. et al., 2014. Thermoelectric power generation driven by blast furnace slag flushing water. *Energy*, 66, pp.965–972. Available at: http://dx.doi.org/10.1016/j.energy.2014.02.018.

Meng, J.-H., Wang, X.-D. & Chen, W.-H., 2016. Performance investigation and design optimization of a thermoelectric generator applied in automobile exhaust waste heat recovery. *Energy Conversion and Management*, 120, pp.71–80. Available at: http://www.sciencedirect.com/science/article/pii/S0196890416303296.

Meng, J.H., Wang, X.D. & Zhang, X.X., 2013. Transient modeling and dynamic characteristics of thermoelectric cooler. *Applied Energy*, 108, pp.340–348. Available at: http://dx.doi.org/10.1016/j.apenergy.2013.03.051.

Microchip, MCP1663. Available at: http://www.microchip.com/wwwproducts/en/MCP1663 [Accessed August 4, 2017a].

Microchip, MCP1663 9V/12V/24V Output Boost Regulator Evaluation Board. Available at: http://www.microchip.com/DevelopmentTools/ProductDetails.aspx?PartNO=ADM00664 [Accessed August 4, 2017b].

Mikkenie, R. et al., 2012. A quick method to determine the capacitance characteristics of thin layer X5R multilayer capacitors. *Journal of the European Ceramic Society*, 32(1), pp.167–173. Available at: http://dx.doi.org/10.1016/j.jeurceramsoc.2011.08.003.

Miranda, Á.G., Chen, T.S. & Hong, C.W., 2013. Feasibility study of a green energy powered thermoelectric chip based air conditioner for electric vehicles. *Energy*, 59, pp.633–641. Available at: http://linkinghub.elsevier.com/retrieve/pii/S0360544213006002.

Montecucco, a., Buckle, J.R. & Knox, a. R., 2012. Solution to the 1-D unsteady heat conduction equation with internal Joule heat generation for thermoelectric devices. *Applied Thermal Engineering*, 35(1), pp.177–184. Available at: http://dx.doi.org/10.1016/j.applthermaleng.2011.10.026.

Morini, M. et al., 2013. Optimal allocation of thermal, electric and cooling loads among generation technologies in household applications. *Applied Energy*, 112, pp.205–214. Available at: http://dx.doi.org/10.1016/j.apenergy.2013.05.078.

Mozharivskyj, Y. et al., 2004. Promising thermoelectric material: Zn4Sb3 or Zn6-delta Sb5. Its composition, structure, stability, and polymorphs. Structure and stability of Zn1-delta Sb. *Chemistry of Materials*, 16(8), pp.1580–1589.

Najjar, Y.S.H. & Kseibi, M.M., 2017. Thermoelectric stoves for poor deprived regions – A review. *Renewable and Sustainable Energy Reviews*, 80(January 2016), pp.597–602. Available at: http://linkinghub.elsevier.com/retrieve/pii/S1364032117308444.

Nguyen, N.Q. & Pochiraju, K. V., 2013. Behavior of thermoelectric generators exposed to transient heat sources. *Applied Thermal Engineering*, 51(1–2), pp.1–9. Available at: http://dx.doi.org/10.1016/j.applthermaleng.2012.08.050.

Niu, Z. et al., 2015. Elucidating modeling aspects of thermoelectric generator. *International Journal of Heat and Mass Transfer*, 85, pp.12–32. Available at: http://linkinghub.elsevier.com/retrieve/pii/S0017931015001258.

Noori, M., Gardner, S. & Tatari, O., 2015. Electric vehicle cost, emissions, and water footprint in the United States: Development of a regional optimization model. *Energy*, 89, pp.610–625. Available at: http://linkinghub.elsevier.com/retrieve/pii/S0360544215007811.

Ohta, H. et al., 2007. Giant thermoelectric Seebeck coefficient of a two-dimensional electron gas in SrTiO3. *Nature materials*, 6(2), pp.129–134.

Orr, B. et al., 2016. A review of car waste heat recovery systems utilising thermoelectric generators and heat pipes. *Applied Thermal Engineering*, 101, pp.490–495. Available at: http://dx.doi.org/10.1016/j.applthermaleng.2015.10.081.

Orr, B. et al., 2014. Electricity generation from an exhaust heat recovery system utilising thermoelectric cells and heat pipes. *Applied Thermal Engineering*, 73(1), pp.588–597. Available at:

http://linkinghub.elsevier.com/retrieve/pii/S1359431114006322.
Paraskevas, A. & Koutroulis, E., 2016. A simple maximum power point tracker for thermoelectric generators. *Energy Conversion and Management*, 108, pp.355–365. Available at: http://dx.doi.org/10.1016/j.enconman.2015.11.027.
Park, J.-D., Lee, H. & Bond, M., 2014. Uninterrupted thermoelectric energy harvesting using temperature-sensor-based maximum power point tracking system. *Energy Conversion and Management*, 86, pp.233–240. Available at: http://www.sciencedirect.com/science/article/pii/S0196890414004385.
Park, K. et al., 2013. Enhanced high-temperature thermoelectric properties of Ce- and Dy-doped ZnO for power generation. *Energy*, 54, pp.139–145. Available at: http://dx.doi.org/10.1016/j.energy.2013.03.023.
Qiu, K. & Hayden, a. C.S., 2012. Development of a novel cascading TPV and TE power generation system. *Applied Energy*, 91(1), pp.304–308. Available at: http://dx.doi.org/10.1016/j.apenergy.2011.09.041.
Rabari, R., Mahmud, S. & Dutta, A., 2014. Numerical simulation of nanostructured thermoelectric generator considering surface to surrounding convection. *International Communications in Heat and Mass Transfer*, 56, pp.146–151. Available at: http://dx.doi.org/10.1016/j.icheatmasstransfer.2014.06.006.
Raj, A., 2010. *Calculating Efficiency*, Available at: http://www.ti.com/lit/an/slva390/slva390.pdf.
Ramli, M.A.M. et al., 2016. A review on maximum power point tracking for photovoltaic systems with and without shading conditions. *Renewable and Sustainable Energy Reviews*, 67, pp.144–159.
Ramli, M.A.M. et al., 2017. A review on maximum power point tracking for photovoltaic systems with and without shading conditions. *Renewable and Sustainable Energy Reviews*, 67, pp.144–159.
Rathi, N., Ahmed, A. & Kumar, R., 2011. Comparative Study of Soft Switching and Hard Switching For Brushless DC Motor. *International Journal of Recent Trends in Electrical & Electronics Engineering*, 1(1), pp.1–5.
Rattner, A.S. & Garimella, S., 2011. Energy harvesting, reuse and upgrade to reduce primary energy usage in the USA. *Energy*, 36(10), pp.6172–6183. Available at: http://dx.doi.org/10.1016/j.energy.2011.07.047.
Ravi, 2016. DC to DC (Buck/Boost/Buck Boost/SEPIC/CUK) converters. *mathworks.com*. Available at: https://uk.mathworks.com/matlabcentral/fileexchange/60167-dc-to-dc--buck-boost-buck-boost-sepic-cuk--converters [Accessed January 1, 2017].
Ravi Chandran, K.S., 2015. Transient Joule heating of graphene, nanowires and filaments: Analytical model for current-induced temperature evolution including substrate and end effects. *International Journal of Heat and Mass Transfer*, 88, pp.14–19. Available at:

http://linkinghub.elsevier.com/retrieve/pii/S0017931015003749.
Reddy, B.V.K. et al., 2012. A fluid-thermo-electric coupled field analysis of a novel integrated thermoelectric device. *Energy Procedia*, 14(December 2011), pp.2088–2095. Available at: http://dx.doi.org/10.1016/j.egypro.2011.12.1212.
Reddy, B.V.K. et al., 2013. Mathematical modeling and numerical characterization of composite thermoelectric devices. *International Journal of Thermal Sciences*, 67, pp.53–63. Available at: http://dx.doi.org/10.1016/j.ijthermalsci.2012.11.004.
Reddy, B.V.K. et al., 2014. Thermoelectric-hydraulic performance of a multistage integrated thermoelectric power generator. *Energy Conversion and Management*, 77, pp.458–468. Available at: http://dx.doi.org/10.1016/j.enconman.2013.09.040.
Redmond, M. et al., 2013. Hotspot cooling in stacked chips using thermoelectric coolers. *IEEE Transactions on Components, Packaging and Manufacturing Technology*, 3(5), pp.759–767.
Remeli, M.F. et al., 2015. Simultaneous power generation and heat recovery using a heat pipe assisted thermoelectric generator system. *Energy Conversion and Management*, 91, pp.110–119. Available at: http://linkinghub.elsevier.com/retrieve/pii/S0196890414010309.
Rosas-Caro, J.C. et al., 2016. A novel DC-DC multilevel SEPIC converter for PEMFC systems. *International Journal of Hydrogen Energy*, 41(48), pp.23401–23408. Available at: http://dx.doi.org/10.1016/j.ijhydene.2016.06.042.
Roshan, Y.M. & Moallem, M., 2013. Maximum power point estimation and tracking using power converter input resistance control. *Solar Energy*, 96, pp.177–186. Available at: http://dx.doi.org/10.1016/j.solener.2013.07.020.
Royale, A. & Simic, M., 2015. Research in Vehicles With Thermal Energy Recovery Systems. *Procedia Computer Science*, 60, pp.1443–1452. Available at: http://linkinghub.elsevier.com/retrieve/pii/S1877050915023480.
Sahin, A.Z. & Yilbas, B.S., 2013. Thermodynamic irreversibility and performance characteristics of thermoelectric power generator. *Energy*, 55, pp.899–904. Available at: http://dx.doi.org/10.1016/j.energy.2013.03.064.
Seetawan, T., Singsoog, K. & Srichai, S., 2014. Thermoelectric Energy Conversion of p-Ca3Co4O9/n-CaMnO3 Module. In *The 6th International Conference on Applied Energy – ICAE2014*. pp. 2–5.
Sellitto, a., 2014. Frequency dependent figure-of-merit in cylindrical thermoelectric nanodevices. *Physica B: Condensed Matter*, 456, pp.57–65. Available at: http://www.sciencedirect.com/science/article/pii/S0921452614006784.
Shang, F., Krishnamurthy, M. & Isurin, A., 2016. A Novel High Gain Step-Up Resonant DC-DC Converter for Automotive Application. , pp.880–885.

Shawwaf, A., 2010. *Optimization of the electric properties of thermoelectric generators*, Available at: http://www.control.lth.se/Publication/5873.html.

Shi, Y. et al., 2015. Design and performance of compact thermoelectric generators based on the extended three-dimensional thermal contact interface. *Energy Conversion and Management*, 106, pp.110–117. Available at: http://dx.doi.org/10.1016/j.enconman.2015.09.031.

Snarskii, a. a. & Bezsudnov, I.V., 2015. Rotating thermoelectric device in periodic steady state. *Energy Conversion and Management*, 94, pp.103–111. Available at: http://linkinghub.elsevier.com/retrieve/pii/S0196890415000709.

Snyder, G.J. et al., 2004. Disordered zinc in Zn4Sb3 with phonon-glass and electron-crystal thermoelectric properties. *Nature materials*, 3(7), pp.458–463.

Snyder, G.J. et al., 2003. Thermoelectric microdevice fabricated by a MEMS-like electrochemical process. *Nature materials*, 2(8), pp.528–531.

Snyder, G.J. & Toberer, E.S., 2008. Complex thermoelectric materials. *Nature materials*, 7(2), pp.105–114.

Stevens, R.J., Weinstein, S.J. & Koppula, K.S., 2014. Theoretical limits of thermoelectric power generation from exhaust gases. *Applied Energy*, 133, pp.80–88. Available at: http://dx.doi.org/10.1016/j.apenergy.2014.07.075.

Su, G.J. & Peng, F.Z., 2005. A low cost, triple-voltage bus dc-dc converter for automotive applications. *Conference Proceedings - IEEE Applied Power Electronics Conference and Exposition - APEC*, 2, pp.1015–1021.

Suh, I.-S., Cho, H. & Lee, M., 2014. Feasibility study on thermoelectric device to energy storage system of an electric vehicle. *Energy*, 76, pp.436–444. Available at: http://linkinghub.elsevier.com/retrieve/pii/S0360544214009761.

Taghvaee, M.H. et al., 2013. A current and future study on non-isolated DC – DC converters for photovoltaic applications. *Renewable and Sustainable Energy Reviews*, 17, pp.216–227. Available at: http://dx.doi.org/10.1016/j.rser.2012.09.023.

Tan, M. et al., 2011. Oriented growth of A2Te3 (A = Sb, Bi) films and their devices with enhanced thermoelectric performance. *Sensors and Actuators, A: Physical*, 171(2), pp.252–259. Available at: http://dx.doi.org/10.1016/j.sna.2011.09.020.

Tan, M., Deng, Y. & Hao, Y., 2014. Improved thermoelectric performance of a film device induced by densely columnar Cu electrode. *Energy*, 70, pp.143–148. Available at: http://dx.doi.org/10.1016/j.energy.2014.03.099.

TECTEG MFR, TEG1-PB-12611-6.0. Available at: http://thermoelectric-generator.com/product/teg1-pb-12611-6-0/ [Accessed December 22, 2017].

Texas Instruments, TPS63060 2.5V to 12V input voltage, 93% Efficient, 2.25A Switch Current Limit, Buck-Boost Converter. Available at:

http://www.ti.com/product/TPS63060 [Accessed August 4, 2017].
Tie, S.F. & Tan, C.W., 2013. A review of energy sources and energy management system in electric vehicles. *Renewable and Sustainable Energy Reviews*, 20, pp.82–102. Available at: http://dx.doi.org/10.1016/j.rser.2012.11.077.
Twaha, S. et al., 2016. A comprehensive review of thermoelectric technology: Materials, applications, modelling and performance improvement. *Renewable and Sustainable Energy Reviews*, 65, pp.698–726.
Twaha, S. et al., 2017. Parameter analysis of thermoelectric generator/dc-dc converter system with maximum power point tracking. *Energy for Sustainable Development*, 41, pp.49–60.
Twaha, S. et al., 2017. Performance analysis of thermoelectric generator using dc-dc converter with incremental conductance based maximum power point tracking. *Energy for Sustainable Development*, 37, pp.86–98.
Tzeng, S.C., Jeng, T.M. & Lin, Y.L., 2014. Parametric study of heat-transfer design on the thermoelectric generator system. *International Communications in Heat and Mass Transfer*, 52, pp.97–105. Available at: http://dx.doi.org/10.1016/j.icheatmasstransfer.2014.01.021.
Uddin, K. et al., 2016. The effects of high frequency current ripple on electric vehicle battery performance. *Applied Energy*, 178, pp.142–154. Available at: http://dx.doi.org/10.1016/j.apenergy.2016.06.033.
Varnhagen, S. et al., 2011. A numerical investigation on the efficiency of range extending systems using Advanced Vehicle Simulator. *Journal of Power Sources*, 196(6), pp.3360–3370. Available at: http://dx.doi.org/10.1016/j.jpowsour.2010.10.086.
Veerachary, M., Mohan, M.M. & Reddy, B.A., 2013. Centralized digital controller for two-input integrated DC-DC converter. *Proceedings of the International Conference on Power Electronics and Drive Systems*, pp.244–249.
Walker, G.R. & Sernia, P.C., 2004. Cascaded DC–DC Converter Connection of Photovoltaic Modules. *IEEE Transactions on Power Electronics*, 53(4), pp.1002–1016.
Wang, F., Cao, Y. & Wang, G., 2015. Thermoelectric generation coupling methanol steam reforming characteristic in microreactor. *Energy*, 80, pp.642–653. Available at: http://linkinghub.elsevier.com/retrieve/pii/S0360544214013772.
Wang, J.L., Wu, J.Y. & Zheng, C.Y., 2014. Simulation and evaluation of a CCHP system with exhaust gas deep-recovery and thermoelectric generator. *Energy Conversion and Management*, 86, pp.992–1000. Available at: http://linkinghub.elsevier.com/retrieve/pii/S0196890414005615.
Wang, N., Li, X. & Mao, J., 2015. Improvement of Thermal Environment by Thermoelectric Coolers and Numerical Optimization of Thermal Performance. , 62(8), pp.2579–2586.

Wang, Q. et al., 2016. A critical review of thermal management models and solutions of lithium-ion batteries for the development of pure electric vehicles. *Renewable and Sustainable Energy Reviews*, 64, pp.106–128.

Wang, X. et al., 2016. A study on heat transfer enhancement in the radial direction of gas flow for thermoelectric power generation. *Applied Thermal Engineering*, 102, pp.176–183.

Wang, X.D. et al., 2012. A three-dimensional numerical modeling of thermoelectric device with consideration of coupling of temperature field and electric potential field. *Energy*, 47(1), pp.488–497. Available at: http://dx.doi.org/10.1016/j.energy.2012.09.019.

Wang, Y., Dai, C. & Wang, S., 2013. Theoretical analysis of a thermoelectric generator using exhaust gas of vehicles as heat source. *Applied Energy*, 112, pp.1171–1180. Available at: http://dx.doi.org/10.1016/j.apenergy.2013.01.018.

Weng, C.-C. & Huang, M.-J., 2014. A study of using a thermoelectric generator to harvest energy from a table lamp. *Energy*, 76, pp.788–798. Available at: http://linkinghub.elsevier.com/retrieve/pii/S0360544214010329.

wikipedia, Thermoelectric effect. Available at: https://en.wikipedia.org/wiki/Thermoelectric_effect#Thomson_effect [Accessed August 28, 2015].

Van De Wouw, N., Haring, M. & Nesic, D., 2012. Extremum-seeking control for periodic steady-state response optimization. In *Proceedings of the IEEE Conference on Decision and Control*. pp. 1603–1608.

Wu, G. & Yu, X., 2014. A holistic 3D finite element simulation model for thermoelectric power generator element. *Energy Conversion and Management*, 86, pp.99–110. Available at: http://dx.doi.org/10.1016/j.enconman.2014.04.040.

Wu, Y. et al., 2014. Numerical simulations on the temperature gradient and thermal stress of a thermoelectric power generator. *Energy Conversion and Management*, 88, pp.915–927. Available at: http://linkinghub.elsevier.com/retrieve/pii/S0196890414008085.

Yang, B., Wang, P. & Bar-Cohen, A., 2007. Mini-contact enhanced thermoelectric cooling of hot spots in high power devices. *IEEE Transactions on Components and Packaging Technologies*, 30(3), pp.432–438.

Yap, Y.Z., Naayagi, R.T. & Woo, W.L., 2017. Thermoelectric energy harvesting for mobile phone charging application. *IEEE Region 10 Annual International Conference, Proceedings/TENCON*, pp.3241–3245.

Yilbas, B.S. & Sahin, A.Z., 2014. Thermal characteristics of combined thermoelectric generator and refrigeration cycle. *Energy Conversion and Management*, 83, pp.42–47. Available at: http://dx.doi.org/10.1016/j.enconman.2014.02.067.

Yu, C. & Chau, K.T., 2009. Thermoelectric automotive waste heat energy recovery using maximum power point tracking. *Energy Conversion and*

Management, 50(6), pp.1506–1512. Available at: http://dx.doi.org/10.1016/j.enconman.2009.02.015.

Yu, S. et al., 2015a. Effect of vehicle driving conditions on the performance of thermoelectric generator. *Energy Conversion and Management*, 96, pp.363–376. Available at: http://linkinghub.elsevier.com/retrieve/pii/S019689041500206X.

Yu, S. et al., 2015b. Start-up modes of thermoelectric generator based on vehicle exhaust waste heat recovery. *Applied Energy*, 138, pp.276–290. Available at: http://linkinghub.elsevier.com/retrieve/pii/S030626191401112X.

Yusop, A.M., Mohamed, R. & Mohamed, A., 2016. Inverse dynamic analysis type of MPPT control strategy in a thermoelectric-solar hybrid energy harvesting system. *Renewable Energy*, 86, pp.682–692. Available at: http://dx.doi.org/10.1016/j.renene.2015.08.071.

Zachár, A. et al., Application of Thermopile Technology in the Automotive Industry.

Zhao, C.H., Round, S.D. & Kolar, J.W., 2008. An Isolated Three-Port Biodirectional DC-DC Converter With Decoupled Power Flow Management. *Ieee Transactions on Power Electronics*, 23(5), pp.2443–2453.

Zheng, X.F., Liu, C.X., Yan, Y.Y., et al., 2014. A review of thermoelectrics research - Recent developments and potentials for sustainable and renewable energy applications. *Renewable and Sustainable Energy Reviews*, 32, pp.486–503. Available at: http://dx.doi.org/10.1016/j.rser.2013.12.053.

Zheng, X.F., Liu, C.X., Boukhanouf, R., et al., 2014. Experimental study of a domestic thermoelectric cogeneration system. *Applied Thermal Engineering*, 62(1), pp.69–79.

Zheng, X.F., Yan, Y.Y. & Simpson, K., 2012. A potential candidate for the sustainable and reliable domestic energy generation-Thermoelectric cogeneration system. *Applied Thermal Engineering*, 53(2), pp.305–311. Available at: http://dx.doi.org/10.1016/j.applthermaleng.2012.03.020.

Zolriasatein, a. et al., 2015. Influence of PCA on thermoelectric properties and hardness of nanostructured Ba–Cu–Si clathrates. *Materials & Design*, 87, pp.883–890. Available at: http://linkinghub.elsevier.com/retrieve/pii/S0264127515303452.

Appendices

Appendix 1

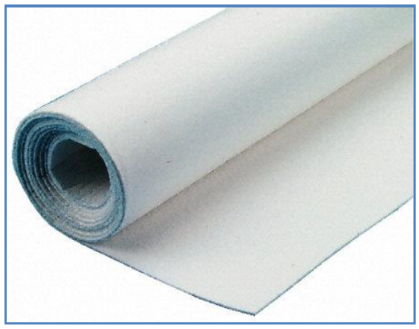
EN

Professionally approved products.

Datasheet

Calcium-Magnesium Silicate Thermal Insulating Sheet, 2.8m x 0.61m x 2mm

RS Stock number 724-8906



Description:

Superwool 607 HT Paper is made of Superwool 607 MAX fibres bonded with a low percentage of organic binder. It has excellent thermal insulation characteristics and exceptional handling properties. Very flexible and resistant to tearing, Superwool 607 MAX paper is particularly suited to all applications requiring further processing (laminated composites, die-cutting, rolling and folding). The organic binder burns out cleanly on the first firing at approximately 300 °C, with ignition starting at 180 °C.

- Paper manufactured from high temperature insulation wool
- Classification Temperature 1300 °C (ENV 1094-3)
- Good resistance to tearing
- High flexibility
- Low shot content
- Precise thickness
- Smooth on both sides
- Resistant to thermal shock
- Very low thermal conductivity
- Not affected by the presence of molten aluminium
- No reaction with alumina based bricks in application in the range of the typical use temperature.